MECHANICAL BEHAVIOR AND RECOVERY OF FIBER REINFORCED CONCRETE AFTER HIGH TEMPERATURE EXPOSURE

by

Abdullah Huzeyfe Akca

B.S., Civil Engineering, Yıldız Technical University, 2009

M.S., Civil Engineering, Boğaziçi University, 2011

Submitted to the Institute for Graduate Studies in
Science and Engineering in partial fulfillment of
the requirements for the degree of
Doctor of Philosophy

Graduate Program in Civil Engineering

Boğaziçi University

2017

ACKNOWLEDGEMENTS

Firstly, I would like to express my sincere gratitude and regards to my thesis supervisor Assoc. Prof. Nilüfer Özyurt Zihnioğlu for her invaluable support and guidance. I have learnt so much from her and still have so much to learn as an academician.

I would like to thank to my co-supervisor Dr. Ahmet Gökçe for his advices and interest during my Phd study.

I would like to thank to my thesis committee members Prof. Turan Özturan and Assist. Prof. Özgür Bezgin for their support and suggestions and I would also like to thank to Assist. Prof. Ahmet Beşer Kızılkanat and Assist. Prof. Serdar Selamet for their interest and sparing time in examining my thesis and taking part in my thesis jury.

I am grateful to TÜBİTAK - Turkish Technological and Scientific Research Institute - for their financial support during my PhD education. I am also thankful to Boğaziçi University BAP - Scientific Research Projects for their financial support (Project ID: 14A04D2).

I also gratefully acknowledge the Koç University Chemical Engineering Departments for providing necessary materials and services. I would like to show my gratitude to AKÇANSA, BOĞAZİÇİ BETON and BASF-YKS for their supports.

I would like to thank my colleagues and friends Ahmet Onur Pehlivan, Dr. Anıl Niş, Hasan Yıldırım who helped and encouraged me to complete all of the experiments which were necessary for my project.

I would like to express my deepest thanks to Ümit Melep for his technical assistance and labor during every stage of my study. I am also thankful to Melike Babucci, Dr. Bilge Gedik Uluocak, Hasan Şenel, Hamdi Ayar and Yener Aydın for their help.

Finally, I would like to express my deepest gratitude to my beloved wife Sema and my lovely daughter Ahu Sevde for their love and understanding. At last but not the least, I am indebted to my dear parents Ali Rıza and Süreyya, my brothers Ubeyde and Mücahid and also my parents in-law, Yusuf and Melahat whose love, trust and support made this possible. I would like to express how I am fortunate to have them.

ABSTRACT

MECHANICAL BEHAVIOR AND RECOVERY OF FIBER REINFORCED CONCRETE AFTER HIGH TEMPERATURE EXPOSURE

In spite of the importance of strength regain of fire damaged concrete in terms of repair and rehabilitation, very few studies had been conducted. Most of the available data are in qualitative form and restricted to strength recovery only. In this study, rehydration and deterioration processes of concrete after high temperature exposure were investigated in details. Therefore, air and water re-curing methods were applied to air entrained fiber reinforced concrete incorporating different type of cementitious materials. Before and after re-curing processes, compression tests were conducted to determine mechanical properties and SEM, XRD and TG analyses were carried out to determine the morphological changes in concrete. Moreover, heated surfaces of concrete were monitored during air-recuring period and the relation between crack growth rate and compressive strength reduction were investigated. Deterioration in mechanical properties and changes in microstructure of concrete were observed after heating and these deterioration and changes continued during air re-curing period. On the other hand, recovery in mechanical properties and morphology of concrete were observed after water re-curing period. And finally, similar tests were conducted on reinforced concrete beams and prominent effects of air and water re-curing were also observed in these specimens.

ÖZET

YÜKSEK SICAKLIK UYGULAMASI SONRASI LİFLİ BETONUN MEKANİK DAVRANIŞI VE İYİLEŞMESİ

Yangında zarar görmüş betonların eski özelliklerini geri kazanması onarım ve iyileştirme açısından önem arz etmektedir, buna karşın bu konuda yapılan çalışmalar sayıca çok azdır. Sonuçların çoğu genellikle betonun dayanım kazanması ile ilgili verilerle sınırlı kalmıştır. Bu çalışmada yüksek sıcaklık etkisinde zarar görmüş betonda soğuma sonrasındaki rehidrasyon ve bozulma süreci daha kapsamlı incelenmiştir. Bu sebeple, yüksek sıcaklıklara maruz bırakılmış farklı tiplerdeki hava sürüklenmiş lifli betonlara hava ve su kürü uygulanmıştır. Kür öncesi ve sonrası mekanik özellikler basınç testleriyle, morfolojik özellikler SEM, XRD ve TG analizlerle incelenmiş ve değerlendirilmiştir. Ayrıca hava kürü sırasındaki bozulma süreci fotoğraflanarak takip edilmiş ve oluşan çatlakların beton dayanımı ile ilişkisi araştırılmıştır. Sonuç olarak yüksek sıcaklığa maruz kalan betonlarda ciddi mekanik kayıplar ve morfolojik değişimler görülmekte ve bu kayıplar hava kürü sırasında devam etmektedir. Su kürü sırasında ise yüksek sıcaklık etkisiyle kötüleşen mekanik özellikler geri kazanılmaktadır. Çalışma sonunda seçilen beton grupları ile üretilen betonarme kirişlerde yapılan benzer incelemelerde de hava ve su kürünün belirgin etkileri gözlemlenmiştir.

TABLE OF CONTENTS

ACKNOWLEDGEMENTS iii
ABSTRACT v
ÖZET vi
LIST OF FIGURES xi
LIST OF TABLES xxv
LIST OF SYMBOLS xxxiv
LIST OF ACRONYMS/ABBREVIATIONS xxxv
1. INTRODUCTION 1
2. LITERATURE REVIEW 5
2.1. Fire 5
2.1.1. Class A 6
2.1.2. Class B 6
2.1.3. Class C 6
2.1.4. Class D 6
2.1.5. Class K 6
2.2. Fire Testing 7
2.2.1. The Cellulosic Fire Curve (ISO 834) 7
2.2.2. The Hydrocarbon Curve 7
2.2.3. The RABT Curve 8
2.2.4. The RWS Curve 9
2.3. Temperature Monitoring 9
2.3.1. Thermoscopes and Thermometers 9
2.3.2. Thermocouples 10
2.4. Concrete at Elevated Temperatures 10
2.4.1. Maximum Temperature 11
2.4.1.1. Effects on Compressive Strength of Concrete 12
2.4.1.2. Effects on Modulus of Elasticity of Concrete 19
2.4.2. Exposure Time 24
2.4.3. Heating Rate 26

2.4.4. Water to Cementitious Ratio 26
2.4.5. Moisture Content 27
2.4.6. Type of Cement and Aggregate 27
2.5. Improving Fire Performance of Concrete 28
2.5.1. Mineral Admixtures 28
2.5.2. Fibers 29
2.5.3. Chemical Admixtures 31
2.6. Post Fire Behavior 31
2.6.1. Disintegration 32
2.6.2. Recovery 34
2.7. Fire Tests on Structural Elements 36
2.7.1. Fire Tests on Structural Beams 38
2.7.2. Fire Tests on Structural Slabs 39
2.7.3. Fire Tests on Structural Columns 39
3. EXPERIMENTAL STUDY 40
3.1. Materials 40
3.1.1. Cement 40
3.1.2. Ground Granulated Blast Furnace Slag 40
3.1.3. Pulverized Fly Ash 42
3.1.4. Aggregates 43
3.1.5. Fibers 43
3.1.6. Chemical Admixtures 43
3.2. Mix Proportions 44
3.3. Concrete Groups 46
3.4. Tests on Small Sized Specimens 47
3.4.1. Heating Procedure 47
3.4.2. Re-curing Processes 49
3.4.3. Macroscopic and Microscopic Observations 49
3.4.3.1. Mass Change Measurements 50
3.4.3.2. Black Pixel Analysis 50
3.4.3.3. SEM/EDAX Observations 50

3.4.3.4. XRD Analysis 50
3.4.3.5. Thermogravimetric Analysis 52
3.4.4. Residual Compressive Strength and Modulus of Elasticity Measurements 52
3.5. Tests on Reinforced Concrete Beams 52
3.5.1. Heating Procedure 55
3.5.2. Re-curing Processes 55
3.5.3. SEM/EDAX Observations 57
3.5.4. Residual Flexural Load Capacity and Flexural Rigidity Measurements 57
4. TEST RESULTS OF SMALL SIZED SPECIMENS 58
4.1. Fresh State Properties 59
4.2. Thermocouple Monitoring 59
4.3. Spalling of Concrete 66
4.4. Mass Change of Concrete 69
4.5. Surface Crack Monitoring 69
4.6. XRD Results 74
4.7. SEM Observations 75
4.7.1. Changes in C-S-H After Heating 76
4.7.2. Morphology of Concrete After Re-curing Periods 78
4.7.3. Changes of Center of Concrete Specimens 78
4.8. TGA Results 84
4.9. Residual Mechanical Properties of Concrete 90
4.9.1. Effect of Re-curing 94
4.9.1.1. Long Term Effect of Re-curing 95
4.9.2. Effect of Mineral Admixtures 97
4.9.3. Effect of Air Entrainment 98
4.9.4. Effect of Fiber Reinforcement 99
4.10. Results of Black Pixel Analyses 100
5. TEST RESULTS OF REINFORCED CONCRETE BEAMS 105
5.1. SEM Observations 105

5.2. Residual Flexural Load Capacity and Flexural Rigidity Measurements . 109
6. CONCLUSION 120
6.1. Tests on Small Sized Concrete Specimens 120
6.1.1. After Cooling 123
6.1.2. After Air Re-curing 124
6.1.3. After Water Re-curing 126
6.2. Tests on Reinforced Concrete Beams 127
6.3. Recommendations 128
REFERENCES 129
APPENDIX A: MASS CHANGE TABLES 138
APPENDIX B: SEM IMAGES 151
APPENDIX C: TGA DIAGRAMS 170
APPENDIX D: STRESS & STRAIN DIAGRAMS 181
APPENDIX E: COMPRESSIVE STRENGTH TABLES 194
APPENDIX F: MODULUS OF ELASTICITY TABLES 201
APPENDIX G: BPA IMAGES AND GRAPHS 208

LIST OF FIGURES

Figure 2.1. Fire classification. 5

Figure 2.2. Fire curves. 8

Figure 2.3. Calibration curves of widely used thermocouple types. 11

Figure 2.4. Changes in concrete during heating. 12

Figure 2.5. Coefficient $k_{c\theta}$ allowing for decrease of characteristic strength (f_{ck}) of concrete, Eurocode 2. 13

Figure 2.6. Mathematical model for stress-strain relationships of concrete under compression at elevated temperatures, Eurocode 2. 23

Figure 2.7. Thermogravimetric analysis (TGA) curves of polypropylene (PP) and the PP/sisal fibre composites. 29

Figure 2.8. Polypropylene fiber bed. 30

Figure 2.9. Disintegration of a concrete specimen. a) just after cooling period b) 7 days after cooling period. 33

Figure 2.10. Disintegration of pastes. 33

Figure 2.11. SEM pictures of a) a disintegrated and b) a 7 days water re-cured concrete. 36

Figure 2.12. Decrease of characteristic strength of tension and compression reinforcement. 38

Figure 3.1. Heating scenario. 48

Figure 3.2. a) Heat insulation of concrete specimens in electrical furnace, b) positions of the K-type thermocouples used to monitor temperature change. 49

Figure 3.3. Crack growth monitoring on black and white images captured from C0P specimen during air re-curing. 51

Figure 3.4. BPA value of C0P specimen. 51

Figure 3.5. Compression test setup. 53

Figure 3.6. Reinforcing bar configuration. 53

Figure 3.7. Minimum dimensions and axis distances for simply supported beams made with reinforced and prestressed concrete. 54

Figure 3.8. Schematized front view of fire test set up. 55

Figure 3.9. Schematized side view of fire test set up. 56

Figure 3.10. Heating scenario of reinforced concrete beams according to ISO-834 cellulosic fire. 56

Figure 3.11. Schematized four point bending test set up. 57

Figure 4.1. Flow chart of the study. 58

Figure 4.2. Survival frequencies of heated concrete groups produced by using a) only PC, b) PC+GGBFS and c) PC+PFA. 68

Figure 4.3. Initial and final crack pictures of air re-cured specimens a) F0H, b) FAP, c) FAH. 71

Figure 4.4. Initial and final crack pictures of water re-cured specimens a) F0H, b) FAP, c) FAH. 72

Figure 4.5. TGA and DTA diagrams of dust obtained from air re-cured concrete surface. 73

Figure 4.6. TGA and DTA diagrams of dust obtained from water re-cured concrete surface. 74

Figure 4.7. XRD results of samples obtained from CAP group. 75

Figure 4.8. SEM pictures obtained from CAP a) before heating b) after heating and cooling. 76

Figure 4.9. SEM pictures obtained from SAP a) before heating b) after heating and cooling. 77

Figure 4.10. SEM pictures obtained from FAP a) before heating b) after heating and cooling. 77

Figure 4.11. SEM pictures obtained from CAP after a) air re-curing b) water re-curing. 79

Figure 4.12. SEM pictures obtained from SAP after a) air re-curing b) water re-curing. 79

Figure 4.13. SEM pictures obtained from FAP after a) air re-curing b) water re-curing. 80

Figure 4.14. Cracks filled with $CaCO_3$ after water re-curing. 80

Figure 4.15. Microstructure of the center of concretes after cooling a) CAP, b) SAP, c) FAP. 81

Figure 4.16. Microstructure of the center of air re-cured concrete a) CAP, b) SAP, c) FAP. 82

Figure 4.17. Microstructure of the center of water re-cured concrete a) CAP, b) SAP, c) FAP. 83

Figure 4.18. TGA results of Portland cement concrete. 84

Figure 4.19. TGA results of concrete incorporating GGBFS. 85

Figure 4.20. TGA results of concrete incorporating PFA. 85

Figure 4.21. DTA diagrams of Portland cement concrete. 86

Figure 4.22. DTA diagrams of concrete incorporating GGBFS. 86

Figure 4.23. DTA diagrams of concrete incorporating PFA. 87

Figure 4.24. Residual compressive strength percentages of Portland cement concrete groups. 91

Figure 4.25. Residual compressive strength percentages of concrete groups incorporating GGBFS. (* many of the heated specimens of SA0 group spalled during heating and survived specimens had severe cracks and damage after heating). 92

Figure 4.26. Residual compressive strength percentages of concrete groups incorporating PFA. (Since all of the specimens of F00, F0S, FA0 and FAS groups spalled during heating residual properties of these groups could not be evaluated.) 92

Figure 4.27. Residual modulus of elasticity percentages of Portland cement concrete groups. 93

Figure 4.28. Residual modulus of elasticity percentages of concrete groups incorporating GGBFS. (* many of the heated specimens of SA0 group spalled during heating and survived specimens had severe cracks and damage after heating). 93

Figure 4.29. Residual modulus of elasticity percentages of concrete groups incorporating PFA. (Since all of the specimens of F00, F0S, FA0 and FAS groups spalled during heating residual properties of these groups could not be evaluated.) 94

Figure 4.30. Black pixel analyses results of all groups. 103

Figure 4.31. Black pixel analyses results of all groups without air entrainment. 103

Figure 4.32. Black pixel analyses results of all air entrained groups. 104

Figure 5.1. SEM pictures obtained from heated surface of CAP a) before heating b) after cooling c) after air re-curing d) after water re-curing. . 107

Figure 5.2. SEM pictures obtained from heated surface of SAP a) before heating b) after cooling c) after air re-curing d) after water re-curing. . 108

Figure 5.3. SEM pictures obtained from reinforcing bar level of CAP a) before heating b) after cooling c) after air re-curing d) after water re-curing.109

Figure 5.4. SEM pictures obtained from reinforcing bar level of SAP a) before heating b) after cooling c) after air re-curing d) after water re-curing.110

Figure 5.5. Load & deflection curves of CAP group. 111

Figure 5.6. Load & deflection curves of CAH group. 112

Figure 5.7. Load & deflection curves of SAP group. 112

Figure 5.8. Load & deflection curves of SAH group. 113

Figure 5.9. Calculation of area under the curve. 115

Figure 5.10. Calculation of instantaneous flexural rigidity (EI) values. 117

Figure 5.11. Flexural rigidity & deflection curves of CAP group. 117

Figure 5.12. Flexural rigidity & deflection curves of CAH group. 118

Figure 5.13. Flexural rigidity & deflection curves of SAP group. 118

Figure 5.14. Flexural rigidity & deflection curves of SAH group. 119

Figure B.1. Figure 4.8.a at lower magnification. 151

Figure B.2. Figure 4.8.b at lower magnification. 152

Figure B.3. Figure 4.9.a at lower magnification. 152

Figure B.4. Figure 4.9.b at lower magnification. 153

Figure B.5. Figure 4.10.a at lower magnification. 153

Figure B.6. Figure 4.10.b at lower magnification. 154

Figure B.7. Figure 4.11.a at lower magnification. 154

Figure B.8. Figure 4.11.b at lower magnification. 155

Figure B.9. Figure 4.12.a at lower magnification. 155

Figure B.10. Figure 4.12.b at lower magnification. 156

Figure B.11. Figure 4.13.a at lower magnification. 156

Figure B.12. Figure 4.13.b at lower magnification. 157

Figure B.13. Figure 4.15.a at lower magnification. 157

Figure B.14. Figure 4.15.b at lower magnification. 158

Figure B.15. Figure 4.15.c at lower magnification. 158

Figure B.16. Figure 4.16.a at lower magnification. 159

Figure B.17. Figure 4.16.b at lower magnification. 159

Figure B.18. Figure 4.16.c at lower magnification. 160

Figure B.19. Figure 4.17.a at lower magnification. 160

Figure B.20. Figure 4.17.b at lower magnification. 161

Figure B.21. Figure 4.17.c at lower magnification. 161

Figure B.22. Figure 5.1.a at lower magnification. 162

Figure B.23. Figure 5.1.b at lower magnification. 162

Figure B.24. Figure 5.1.c at lower magnification. 163

Figure B.25. Figure 5.1.d at lower magnification. 163

Figure B.26. Figure 5.2.a at lower magnification. 164

Figure B.27. Figure 5.2.b at lower magnification. 164

Figure B.28. Figure 5.2.c at lower magnification. 165

Figure B.29. Figure 5.2.d at lower magnification. 165

Figure B.30. Figure 5.3.a at lower magnification. 166

Figure B.31. Figure 5.3.b at lower magnification. 166

Figure B.32. Figure 5.3.c at lower magnification. 167

Figure B.33. Figure 5.3.d at lower magnification. 167

Figure B.34. Figure 5.4.a at lower magnification. 168

Figure B.35. Figure 5.4.b at lower magnification. 168

Figure B.36. Figure 5.4.c at lower magnification. 169

Figure B.37. Figure 5.4.d at lower magnification. 169

Figure C.1. TGA and DTA diagrams of CAP concrete before heating. 170

Figure C.2. TGA and DTA diagrams of CAP concrete after cooling (Surface). 171

Figure C.3. TGA and DTA diagrams of CAP concrete after cooling (Center). . 171

Figure C.4. TGA and DTA diagrams of air re-cured CAP concrete (Surface). . 172

Figure C.5. TGA and DTA diagrams of air re-cured CAP concrete (Center). . 172

Figure C.6. TGA and DTA diagrams of water re-cured CAP concrete (Surface). 173

Figure C.7. TGA and DTA diagrams of water re-cured CAP concrete (Center). 173

Figure C.8. TGA and DTA diagrams of SAP concrete before heating. 174

Figure C.9. TGA and DTA diagrams of SAP concrete after cooling (Surface). 174

Figure C.10. TGA and DTA diagrams of SAP concrete after cooling (Center). . 175

Figure C.11. TGA and DTA diagrams of air re-cured SAP concrete (Surface). . 175

Figure C.12. TGA and DTA diagrams of air re-cured SAP concrete (Center). . 176

Figure C.13. TGA and DTA diagrams of water re-cured SAP concrete (Surface). 176

Figure C.14. TGA and DTA diagrams of water re-cured SAP concrete (Center). 177

Figure C.15. TGA and DTA diagrams of FAP concrete before heating. 177

Figure C.16. TGA and DTA diagrams of FAP concrete after cooling (Surface). 178

Figure C.17. TGA and DTA diagrams of FAP concrete after cooling (Center). . 178

Figure C.18. TGA and DTA diagrams of air re-cured FAP concrete (Surface). . 179

Figure C.19. TGA and DTA diagrams of air re-cured FAP concrete (Center). . 179

Figure C.20. TGA and DTA diagrams of water re-cured FAP concrete (Surface). 180

Figure C.21. TGA and DTA diagrams of water re-cured FAP concrete (Center). 180

Figure D.1. Stress and strain diagrams of C00 concrete. 181

Figure D.2. Stress and strain diagrams of C0S concrete. 182

Figure D.3. Stress and strain diagrams of C0P concrete. 182

Figure D.4. Stress and strain diagrams of C0H concrete. 183

Figure D.5. Stress and strain diagrams of CA0 concrete. 183

Figure D.6. Stress and strain diagrams of CAS concrete. 184

Figure D.7. Stress and strain diagrams of CAP concrete. 184

Figure D.8. Stress and strain diagrams of CAH concrete. 185

Figure D.9. Stress and strain diagrams of S00 concrete. 185

Figure D.10. Stress and strain diagrams of S0S concrete. 186

Figure D.11. Stress and strain diagrams of S0P concrete. 186

Figure D.12. Stress and strain diagrams of S0H concrete. 187

Figure D.13. Stress and strain diagrams of SA0 concrete. 187

Figure D.14. Stress and strain diagrams of SAS concrete. 188

Figure D.15. Stress and strain diagrams of SAP concrete. 188

Figure D.16. Stress and strain diagrams of SAH concrete. 189

Figure D.17. Stress and strain diagrams of F00 concrete. 189

Figure D.18. Stress and strain diagrams of F0S concrete. 190

Figure D.19. Stress and strain diagrams of F0P concrete. 190

Figure D.20. Stress and strain diagrams of F0H concrete. 191

Figure D.21. Stress and strain diagrams of FA0 concrete. 191

Figure D.22. Stress and strain diagrams of FAS concrete. 192

Figure D.23. Stress and strain diagrams of FAP concrete. 192

Figure D.24. Stress and strain diagrams of FAH concrete. 193

Figure G.1. BPA images of a C0P specimen and corresponding normalized area (N.A.) values. 209

Figure G.2. BPA images of a C0H specimen and corresponding normalized area (N.A.) values. 210

Figure G.3. BPA images of a CA0 specimen and corresponding normalized area (N.A.) values. 211

Figure G.4. BPA images of a CAS specimen and corresponding normalized area (N.A.) values. 212

Figure G.5. BPA images of a CAP specimen and corresponding normalized area (N.A.) values. 213

Figure G.6. BPA images of a CAH specimen and corresponding normalized area (N.A.) values. 214

Figure G.7. BPA images of a S0P specimen and corresponding normalized area (N.A.) values. 215

Figure G.8. BPA images of a S0H specimen and corresponding normalized area (N.A.) values. 216

Figure G.9. BPA images of a SAS specimen and corresponding normalized area (N.A.) values. 217

Figure G.10. BPA images of a SAP specimen and corresponding normalized area (N.A.) values. 218

Figure G.11. BPA images of a SAH specimen and corresponding normalized area (N.A.) values. 219

Figure G.12. BPA images of a F0P specimen and corresponding normalized area (N.A.) values. 220

Figure G.13. BPA images of a F0H specimen and corresponding normalized area (N.A.) values. 221

Figure G.14. BPA images of a FAP specimen and corresponding normalized area (N.A.) values. 222

Figure G.15. BPA images of a FAH specimen and corresponding normalized area (N.A.) values. 223

Figure G.16. Graph obtained after BPA on a C0P specimen. 224

Figure G.17. Graph obtained after BPA on a C0H specimen. 224

Figure G.18. Graph obtained after BPA on a CA0 specimen. 225

Figure G.19. Graph obtained after BPA on a CAS specimen. 225

Figure G.20. Graph obtained after BPA on a CAP specimen. 226

Figure G.21. Graph obtained after BPA on a CAH specimen. 226

Figure G.22. Graph obtained after BPA on a S0P specimen. 227

Figure G.23. Graph obtained after BPA on a S0H specimen. 227

Figure G.24. Graph obtained after BPA on a SAS specimen. 228

Figure G.25. Graph obtained after BPA on a SAP specimen. 228

Figure G.26. Graph obtained after BPA on a SAH specimen. 229

Figure G.27. Graph obtained after BPA on a F0P specimen. 229

Figure G.28. Graph obtained after BPA on a F0H specimen. 230

Figure G.29. Graph obtained after BPA on a FAP specimen. 230

Figure G.30. Graph obtained after BPA on a FAH specimen. 231

LIST OF TABLES

Table 2.1. Reduction in residual compressive strength of concrete incorporating fillers. 15

Table 2.2. Reduction in residual compressive strength of normal strength concrete incorporating pozzolanic materials. 16

Table 2.3. Reduction in residual compressive strength of high strength concrete incorporating pozzolanic materials. 17

Table 2.4. Reduction in residual compressive strength of fiber reinforced concrete. 20

Table 2.5. Reduction in residual compressive strength of air entrained concrete. 20

Table 2.6. Stress-strain relationships of concrete with siliceous aggregates and concrete with calcareous aggregates at high temperatures, Eurocode 2. 22

Table 2.7. Reduction in modulus of elasticity of concrete incorporating fly ash. 22

Table 2.8. Reduction in modulus of elasticity of concrete incorporating GGBFS. 24

Table 2.9. Reduction in modulus of elasticity of fiber reinforced concrete. . . 25

Table 2.10. Reduction in residual mechanical properties after extended heat exposure. 26

Table 2.11. Changes in compressive strength of HSC and NSC. 27

Table 2.12. Residual compressive strength of air/water re-cured concrete. . . . 35

Table 3.1. Mechanical properties of Portland cement. 41

Table 3.2. Chemical properties of Portland cement. 41

Table 3.3. Chemical properties of ground granulated blast furnace slag. 41

Table 3.4. Physical properties of ground granulated blast furnace slag. 42

Table 3.5. Chemical properties of pulverized fly ash. 42

Table 3.6. Physical properties of pulverized fly ash. 42

Table 3.7. Properties of fibers. 43

Table 3.8. Mix proportions of Portland cement concrete groups. 44

Table 3.9. Mix proportions of ground granulated blast furnace slag concrete groups. 45

Table 3.10. Mix proportions of pulverized fly ash concrete groups. 45

Table 3.11. Portland cement groups and designations. 46

Table 3.12. Ground granulated blast furnace slag groups and designations. . . 46

Table 3.13. Pulverized fly ash groups and designations. 47

Table 4.1. Fresh state properties of PC groups. 59

Table 4.2. Fresh state properties of PC+GGBFS groups. 60

Table 4.3. Fresh state properties of PC+PFA groups. 60

Table 4.4. Maximum temperatures at predefined depths from the surface after 200 minutes of heating, PC Groups. 61

Table 4.5. Maximum temperatures at predefined depths from the surface after 200 minutes of heating, PC+GGBFS Groups. 62

Table 4.6. Maximum temperatures at predefined depths from the surface after 200 minutes of heating, PC+PFA Groups. 62

Table 4.7. Average temperature values at predefined depths from the surface (at the end of the 200 minutes heating period). 63

Table 4.8. Maximum temperatures at predefined depths from the surface during total heating and cooling processes (200 minutes of heating and 150 minutes of cooling), PC Groups. 64

Table 4.9. Maximum temperatures at predefined depths from the surface during total heating and cooling processes (200 minutes of heating and 150 minutes of cooling), PC+GGBFS Groups. 64

Table 4.10. Maximum temperatures at predefined depths from the surface during total heating and cooling processes (200 minutes of heating and 150 minutes of cooling), PC+PFA Groups. 65

Table 4.11. Average temperature values at predefined depths from the surface (During 200 minutes heating and 150 minutes of cooling). 65

Table 4.12. Survival frequencies of PC Groups. 66

Table 4.13. Survival frequencies of PC+GGBFS Groups. 67

Table 4.14. Survival frequencies of PC+PFA Groups. 67

Table 4.15. Residual masses of PC Groups. 70

Table 4.16. Residual masses of PC+GGBFS Groups. 70

Table 4.17. Residual masses of PC+PFA Groups. 71

Table 4.18. Calculated $Ca(OH)_2$ and $CaCO_3$ percentages in concrete samples before heating. 88

Table 4.19. Calculated $Ca(OH)_2$ and $CaCO_3$ percentages in concrete samples after cooling. 88

Table 4.20. Calculated $Ca(OH)_2$ and $CaCO_3$ percentages in air re-cured concrete samples. 89

Table 4.21. Calculated $Ca(OH)_2$ and $CaCO_3$ percentages in water re-cured concrete samples. 89

Table 4.22. Average residual compressive strength and modulus of elasticity percentages of all concrete groups. 95

Table 4.23. Long term residual compressive strength percentages. 96

Table 4.24. Long term residual modulus of elasticity percentages. 96

Table 4.25. Average residual compressive strength and modulus of elasticity percentages of PP fiber added concrete categories. 97

Table 4.26. Average residual compressive strength and modulus of elasticity percentages of concrete categories with and without air entrainment. 98

Table 4.27. Average residual compressive strength and modulus of elasticity percentages of plain, steel fiber reinforced, PP fiber reinforced and hybrid fiber reinforced concrete categories. 99

Table 4.28. Residual compressive strength and BPA values of Portland cement concrete. 101

Table 4.29. Residual compressive strength and BPA values of concrete incorporating GGBFS. 102

Table 4.30. Residual compressive strength and BPA values of concrete incorporating PFA. 102

Table 5.1. Initial and residual load bearing capacities of RC beams. 114

Table 5.2. Initial and residual toughness values. 115

Table 5.3. Average flexural rigidities calculated from EI vs deflection curves. . 119

Table 6.1. Summary of the first stage of the study. 121

Table 6.2. Summary of the second stage of the study. 122

Table A.1. Mass changes of C00 concrete. 138

Table A.2. Mass changes of C0S concrete. 139

Table A.3. Mass changes of C0P concrete. 139

Table A.4. Mass changes of C0H concrete. 140

Table A.5. Mass changes of CA0 concrete. 140

Table A.6. Mass changes of CAS concrete. 141

Table A.7. Mass changes of CAP concrete. 141

Table A.8. Mass changes of CAH concrete. 142

Table A.9. Mass changes of S00 concrete. 142

Table A.10. Mass changes of S0S concrete. 143

Table A.11. Mass changes of S0P concrete. 143

Table A.12. Mass changes of S0H concrete. 144

Table A.13. Mass changes of SA0 concrete. 144

Table A.14. Mass changes of SAS concrete. 145

Table A.15. Mass changes of SAP concrete. 145

Table A.16. Mass changes of SAH concrete. 146

Table A.17. Mass changes of F00 concrete. 146

Table A.18. Mass changes of F0S concrete. 147

Table A.19. Mass changes of F0P concrete. 147

Table A.20. Mass changes of F0H concrete. 148

Table A.21. Mass changes of FA0 concrete. 148

Table A.22. Mass changes of FAS concrete. 149

Table A.23. Mass changes of FAP concrete. 149

Table A.24. Mass changes of FAH concrete. 150

Table E.1. Compressive strength test results of Portland cement concrete groups before heating. 194

Table E.2. Compressive strength test results of Portland cement concrete groups after cooling. 195

Table E.3. Compressive strength test results of air re-cured Portland cement concrete groups. 195

Table E.4. Compressive strength test results of water re-cured Portland cement concrete groups. 196

Table E.5. Compressive strength test results of concrete groups incorporating GGBFS before heating. 196

Table E.6. Compressive strength test results of concrete groups incorporating GGBFS after cooling. 197

Table E.7. Compressive strength test results of air re-cured concrete groups incorporating GGBFS. 197

Table E.8. Compressive strength test results of water re-cured concrete groups incorporating GGBFS. 198

Table E.9. Compressive strength test results of concrete groups incorporating PFA before heating. 198

Table E.10. Compressive strength test results of concrete groups incorporating PFA after cooling. 199

Table E.11. Compressive strength test results of air re-cured concrete groups incorporating PFA. 199

Table E.12. Compressive strength test results of water re-cured concrete groups incorporating PFA. 200

Table F.1. Modulus of elasticity test results of Portland cement concrete groups before heating. 201

Table F.2. Modulus of elasticity test results of Portland cement concrete groups after cooling. 202

Table F.3. Modulus of elasticity test results of air re-cured Portland cement concrete groups. 202

Table F.4. Modulus of elasticity test results of water re-cured Portland cement concrete groups. 203

Table F.5. Modulus of elasticity test results of concrete groups incorporating GGBFS before heating. 203

Table F.6. Modulus of elasticity test results of concrete groups incorporating GGBFS after cooling. 204

Table F.7. Modulus of elasticity test results of air re-cured concrete groups incorporating GGBFS. 204

Table F.8. Modulus of elasticity test results of water re-cured concrete groups incorporating GGBFS. 205

Table F.9. Modulus of elasticity test results of concrete groups incorporating PFA before heating. 205

Table F.10. Modulus of elasticity test results of concrete groups incorporating PFA after cooling. 206

Table F.11. Modulus of elasticity test results of air re-cured concrete groups incorporating PFA. 206

Table F.12. Modulus of elasticity test results of water re-cured concrete groups incorporating PFA. 207

LIST OF SYMBOLS

a	Axis distance of reinforcing steel from the nearest exposed surface
a_{sd}	Axis distance to the side of beam for the corner bars (or tendon or wire) of beams
b_{min}	Minimum width of beam recommended by Eurocode 2
b_w	Width of beam
EI	Flexural rigidity
f_{ck}	Characteristic strength
f_c, θ	Characteristic value of compressive strength of concrete at temperature θ for a specified strain
h	Height of beam
i	Data number
$k_c\theta$	Strength reduction coefficient
m	Mass
n	Total number of data
P_i	i_{th} data of load
Δ_i	i_{th} data of deflection
Δ_m	Mass change
ε	Strain of concrete
ε_{c1}, θ	Thermal peak strain of concrete
$\varepsilon_{cu1}, \theta$	Thermal ultimate strain of concrete
$\varepsilon_{s,fi}$	Strain of the reinforcing steel at temperature θ
θ	Temperature

LIST OF ACRONYMS/ABBREVIATIONS

AEA	Air Entraining Admixture
BPA	Black Pixel Analysis
CBC	Cement Based Composite
CH	Calcium Hydroxide
CS	Calcium Silicates
CSF	Condensed Silica Fume
CSH	Calcium Silicate Hydrate
DSLR	Digital Single Lens Reflex Camera
DTA	Differential Thermal Analysis
EDX	Energy Dispersive X-ray Analysis
FA	Fly Ash
GGBFS	Ground Granulated Blast Furnace Slag
HCM	Hydrocarbon Curve-Modified
HPC	High Performance Concrete
HSC	High Strength Concrete
LSF	Lime Saturation Factor
LVDT	Linear Variable Differential Transformer
NA	Normalized Area
NSC	Normal Strength Concrete
PC	Portland Cement
PP	Poly Propylene
PFA	Pulverized Fly Ash
RC	Reinforced Concrete
SE	Secondary Electron
SEM	Scanning Electron Microscopy
TC	Thermocouple
TG	Thermogravimetry
TGA	Thermogravimetric Analysis

WD	Work Distance
XRD	X-Ray Diffaction

1. INTRODUCTION

As a widely used material, concrete also is used in different kinds of structures such as foundations, dams, bridges, highways, tunnels, nuclear plants, etc. Special properties and different degrees of durability of concrete depending on the environmental conditions can be desired for these kinds of structures. Therefore, determining ingredients of concrete and investigating their effects on concrete properties, especially for supplementary materials, is very important by means of durability.

In terms of durability, the effects of high temperatures and also fire flame exposure on concrete have been investigated. Results showed that, in terms of fire resistance concrete has superior properties since concrete is an incombustible material, it can preserve its properties relatively longer than other structural materials during fire and released gases and fumes from the heated concrete are not toxic [1]. However, various kinds of deteriorations were observed on the concrete specimens which were subjected to fire or high temperatures such as spalling, crazing, cracking, color changes, mass and strength losses [2, 3].

The deteriorations depend on two factors. The first one is internal factor which covers all the intrinsic parameters of concrete, water to cementitious ratio, aggregate and cement types, inclusion of fibers and pozzolanas etc. For instance, concrete with river sand experiences a color change to pink/red after 300°C due to the iron oxide content of sand and concrete incorporating silica fume more than 10% of its binder amount is more prone to spalling than concrete with no silica fume due to increased impermeability of concrete. And secondly, external factors such as heating temperature, heating rate, exposure time at the maximum temperature and cooling conditions etc. influence the respond of concrete subjected to fire. For example, residual strength of the concrete decreases as the maximum temperature exposed to concrete increases and also concrete becomes more prone to spalling when it is subjected to higher heating rates.

Limiting the deteriorations occurred in concrete at elevated temperatures can be possible by improving the fire performance of concrete. Therefore, researchers used various kinds of materials in concrete to improve the fire performance of concrete. Poon *et al.* [4] investigated the contribution of pozzolanic materials; silica fume, pulverized fly ash (PFA) and ground granulated blast furnace slag (GGBFS) and they observed positive effects of these pozzolanic materials (except silica fume) on the fire performance of high strength concrete (HSC). According to many studies, inclusion of silica fume caused reduction in residual strength and spalling of concrete by densifiying microstructure. On the contrary, addition of fly ash or slag showed better performance and also in some studies, strength gain observed at temperatures ranged from 200°C to 300°C because of tobermorite formation [3].

Otherwise, some researchers focused on the contribution of fibers to increase the fire resistance of concrete. Kalifa *et al.* [5] studied the effect of polypropylene (PP) fiber addition into high performance concrete (HPC) exposed to 800°C and the results of the study showed that addition of PP fiber reduced the risk of spalling of HPC. Polymer based fibers have low melting points approximately 170°C. Above this point PP fibers melt and after 450°C they completely disappear by forming microchannels which contribute to outward migration of gases and water vapor from concrete pores [2, 6]. Similarly, the improving effect of PP fibers was also confirmed by Han *et al.* [7]. Moreover, Chen and Liu [8] investigated the residual strength properties of steel, carbon, PP and hybrid fiber reinforced HSC exposed up to 800°C and they observed the favorable effect of existence of a high melting point fiber like steel or carbon fiber together with a low melting point fiber like PP fiber in HSC [3].

Akca and Özyurt Zihnioğlu [2] conducted a study which investigated the contribution of air entraining admixture (AEA) to fire performance of cement based composites (CBC) and also used AEA and PP fibers together in CBC so as to create more permeable network in concrete. These CBC specimens were heated to elevated temperatures (300°C, 600°C and 900°C) with a heating rate of 10°C/min and subjected to the maximum temperatures for one hour in an electrical furnace. Results showed that addition of AEA diminished the decrease in residual strength but this result was found to be

irregular after 300°C for thick specimens. The collaboration of AEA and PP fibers decreased the risk of spalling of CBC.

Concrete undergoes changes in its morphology and physical structure during high temperature exposure and loses its strength and durability. Dehydration of hydrates starts after 400°C and continues until the complete decomposition of calcium silicate hydrate (C-S-H) gels. [9]. Therefore, a detailed repairing process such as replacing damaged layer of concrete with fresh concrete can be essential after fire. On the other hand, after cooling, these dehydrated components rehydrate if they come in contact with water molecules diffused in concrete and fire damaged concrete may regain its strength. Some studies reported this phenomenon and inferred that concrete could regain most of its original strength if concrete was subjected to water re-curing or concrete was kept in a moist environment properly [10–12]. Rehydration products fill the capillaries occurred due to fire exposure and reduce the porosity of concrete resulting in strength regain. But the behavior of rehydration reactions is vital because in some cases, expanded rehydration products may result in disintegration of concrete such as CaO expansion. In order to compensate this effect, calcium hydroxide (CH) content of concrete can be reduced by using some mineral admixtures in concrete or high melting point fibers can be used in concrete [13].

Studies conducted on recovery and rehabilitation of fire damaged concrete are very limited in literature. Generally, strength regain of concrete was investigated in these studies. On the other hand, microstructural changes in concrete after high temperature exposure have important effects on residual mechanical and physical properties of concrete. Moreover, effects of today's widely used materials in concrete such as fibers, mineral and chemical admixtures on disintegration and recovery of concrete are needed to be evaluated. Therefore, an experimental study which had two stages was designed and additional materials used in concrete; mineral admixtures, different types of fibers and air entraining admixtures and re-curing methods following the cooling of concrete were chosen as test parameters. In the presents research, effects of these parameters on post heating mechanical behavior of concrete and microstructural changes in concrete were evaluated. At the first stage, small sized cubic specimens were used

and mechanical tests were conducted on them. Also, XRD, TGA and SEM investigation were conducted on these small sized specimens in order to understand changes in morphology of concrete after heating and re-curing. After all the tests and evaluations were completed on small sized specimens, reinforced concrete beams were produced by using selected concrete groups and they were subjected to ISO-834 fire scenario to investigate disintegration and recovery processes on full sized structural members.

2. LITERATURE REVIEW

Fires have been in nature since the creation of Earth due to the volcanic activity, thunderbolts etc. Earliest human species found the ways to control the fire and that allowed to cook food and to obtain warmth and protection [14]. Also fire was used in daily activities to form new tools and weapons. Occasionally, mistakes in making fire resulted in disaster and fire damaged the places where they lived affected human life. Since then, structural fires have been observed and the prevention techniques have been investigated.

2.1. Fire

Fuels are the main parameter when fires are classified, Figure 2.1 [15]. Maximum temperatures experienced during a fire depend on the fuel burnt and also environmental conditions such as open area, ventilated room etc.

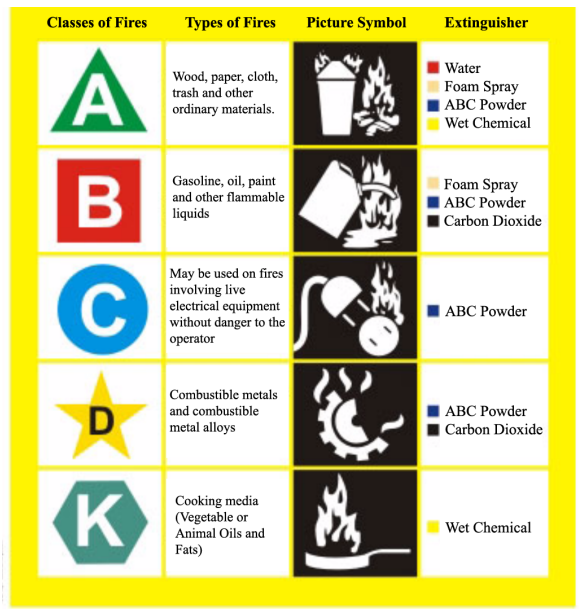

Figure 2.1. Fire classification [15].

2.1.1. Class A

The most commonly encountered fire type is Class A fires since they occur as a result of burning of widely used combustible materials such as paper, textile and wood. In order to extinguish a Class A type of fire water can be used [14].

2.1.2. Class B

Class B fires occur as a result of ignition of flammable materials which contains petrochemical materials. In order to extinguish a Class B type of fire, burning materials can be suppressed by a suitable cover or foam which deplete oxygen supply [14].

2.1.3. Class C

Class C fires cover fires occurred due to electrical problems. In order to extinguish a Class C type of fire, firstly electrical circuit must be deactivated and then carbon dioxide gas which is heavier than air can be used [14].

2.1.4. Class D

There are some combustible metals such as magnesium and titanium which may give a rise to fires called Class D. In this class of fire water should not be used since water can react with these kind of materials and trigger the fire. On the other hand, some powder agents can be used in order to extinguish a Class D fire [14].

2.1.5. Class K

Class K fires occur as a result of burning of organic fat and oils. In order to extinguish a Class K type of fire, Purple K agent which contains high amount of potassium bicarbonate can be used [14].

2.2. Fire Testing

Each country develops its own fire tests in accordance with its national building codes and regulations. In a real fire, the reactions of a material to fire are very important hence, fire tests gives information about how a material influences the growth of fire in a testing room from origin to the time when flashover takes place. The data obtained from a specific fire test is evaluated and results give information about the fire performance of tested material [16, 17].

Moreover, this kind of fire tests provide information about the fire performance of protection systems and structural members since the performance of them will directly affects the stability of the structure [16].

Non combustibility is an important property for a material and an incombustible material can be used without restriction anywhere in a building. However, non-combustibility is not adequate for the materials used in structural load bearing members. The materials such as concrete and steel have to preserve their strength and stability during and after fire. Therefore, some fire scenarios were designed to test the fire performance of materials, Figure 2.2 [16].

2.2.1. The Cellulosic Fire Curve (ISO 834)

The cellulosic fire curve is an ISO-based fire scenario which is widely used in the world, including BS 476, AS 1530, DIN 4102, ASTM and the new European Norm (BS EN 1363-1). This scenario represents a ventilated controlled fire for example residential fires and therefore it is not representative of most tunnel fires [16]. In this fire scenario temperature reaches 800°C in 25 minutes.

2.2.2. The Hydrocarbon Curve

The Hydrocarbon curve is a simulation of a ventilated oil fire and the temperature reaches to 1110°C after 30 minutes. In this fire scenario petrochemical materials

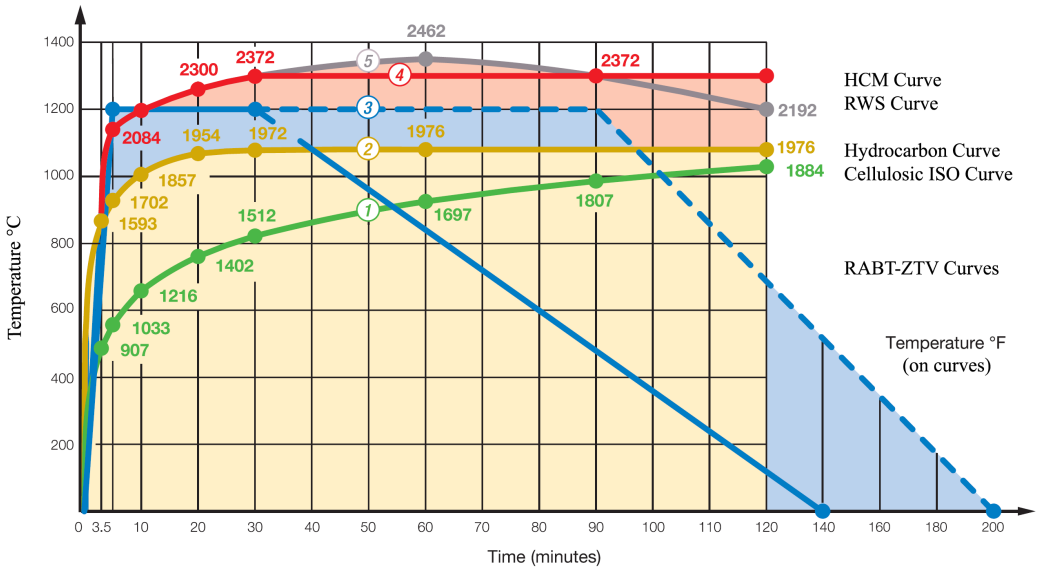

Figure 2.2. Fire curves [16].

are considered as fuels and therefore it is a model of an oil tank fire or a petroleum fire. Since energy capacity of petrochemical materials varies there are some other hydrocarbon fire curves in order to model fires which use them as fuels. In some cases duration of tests is limited in seconds and in some other cases duration of tests are limited in days [16]. For instance, HCM curve (Modified Hydrocarbon Curve) can also be seen in 2.2.

2.2.3. The RABT Curve

This curve was developed after Eureka project in Germany and covers vehicle fires. Temperature increases suddenly after flashover and the rate of increase is 240°C/minute in the RABT curve (car) for the first 5 minutes. The duration at the maximum temperature is relatively shorter than other curves [16]. The RABT curve (train) can also be seen in Figure 2.2.

2.2.4. The RWS Curve

It is a specific petroleum fire scenario since fire load was determined as 300MW and the fire occurs in an enclosed area such as tunnels. Although this scenario was developed in Netherlands for the tunnel fire tests it is also approved internationally [16]. In this fire scenario temperature reaches to 1300°C after 30 minutes.

2.3. Temperature Monitoring

The speeds and motion of atoms in a material determine the range of energy among the molecules. Temperature is the average of this thermal energy and temperature does not depend on the size or type of object. Due to some internal or external factors, energy stored in a material changes thereby temperature of the material can change. The changes in temperature can be measured by some special devices such as thermometers, thermocouples etc. depending on heat transfer rules.

During standard fire tests temperature monitoring is essential either in the furnace or in test specimens. Burners of the furnace work regarding the data from temperature monitoring systems in order to keep the temperature in the furnace between the given limits of standards. Moreover, temperature monitoring devices placed in test specimens give information about the risk of failure, explosion etc. Most common temperature monitoring devices especially used in fire tests on concrete members are thermocouples and infrared thermometers.

2.3.1. Thermoscopes and Thermometers

Thermoscope is a kind of primitive temperature measuring devices. They have a cylindrical container or tube in which the position of liquid changes depending on temperature changes. Thereafter, a scale bar was placed on surface of the container and the early thermometer was formed. During a century it evolved by the use of suitable and standardized materials. Finally, melting and boiling points of water were chosen as fixed points on scale bars in order to have a universal scale. Today with the

help of wireless technologies, temperature of materials can be measured by infrared thermometers. Infrared thermometers or thermal cameras can be used in a wide range of areas. Fire extinguishers use this kind of thermal scanners to be able to find their way in the event of fire. However, non-contact temperature measuring devices are not as useful as thermocouples when internal temperature changes are the main concern.

2.3.2. Thermocouples

Thermocouples are commonly used temperature monitoring devices. They have a basic electrical configuration depending on a voltage change on the junction between two different wires. As the temperature of the wires from different materials changes the wires experience different amount of volume change due to thermal expansion or contraction. Therefore, the strain at the junction changes and a temperature-dependent voltage is created. Eventually, this voltage can be measured by a calibrated electronic device according to thermocouple type and change in temperature can be obtained. There are two kinds of thermocouples depending on material type. J, K, T and E types of thermocouples are the most known types of "base metal" thermocouples and R, S, and B types are commonly used types of "noble metal" thermocouples. Figure 2.3 represents calibration curves and maximum working temperatures of various types of thermocouples [18].

2.4. Concrete at Elevated Temperatures

Mostly, concrete is accidentally subjected to high temperature due to fire conditions and the properties of concrete are affected. Apart from structural fires, concrete resists the effects of artificially induced high temperatures such as out of furnaces and atomic reactors, in pavements subjected to jet engine blast. However, in some applications such as landing pads for missiles and in nuclear power plants and during structural fires concrete experiences extremely high temperatures and then concrete may deteriorate and lose its durability [17].

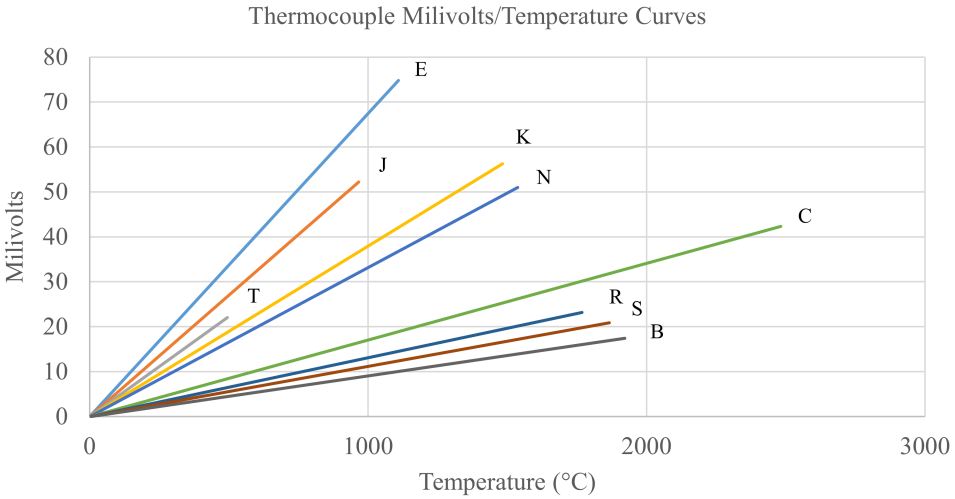

Figure 2.3. Calibration curves of widely used thermocouple types [18].

The reason of deterioration of concrete is not only the maximum temperature reached during a fire because other external factors and some internal parameters also affect the behavior of concrete under elevated temperatures. The external factors include also the followings: length of exposure, rate of temperature rise, temperature of concrete at initiation of exposure to high temperature. The intrinsic parameters can be listed as water to cementitious ratio, moisture content of the concrete, concrete age, type of aggregate and cement used. Therefore in literature, the results of the same fire tests conducted on similar concretes are almost different [1].

2.4.1. Maximum Temperature

The reaction of ordinary concrete to high temperatures varies and the changes are interrelated to other factors but the maximum temperature of concrete experienced can be considered as a dominant factor.

Physicochemical changes occurred in concrete during heating can be seen in Figure 2.4 [13]. After 100°C evaporation of free moisture in concrete begins, hot permeability of concrete increases and loss of chemical water of weaker bonds especially dissociation of ettringite starts. At the temperatures around 300°C concrete incorpo-

rating siliceous aggregates starts to lose its strength, after 400°C calcium hydroxide starts to decompose and concrete shrinks. Quartz particles exhibit phase changes, α to β, and expand at 573°C. Total loss of chemically bond water occurs at the range of 800°C and 1000°C and then concrete melts.

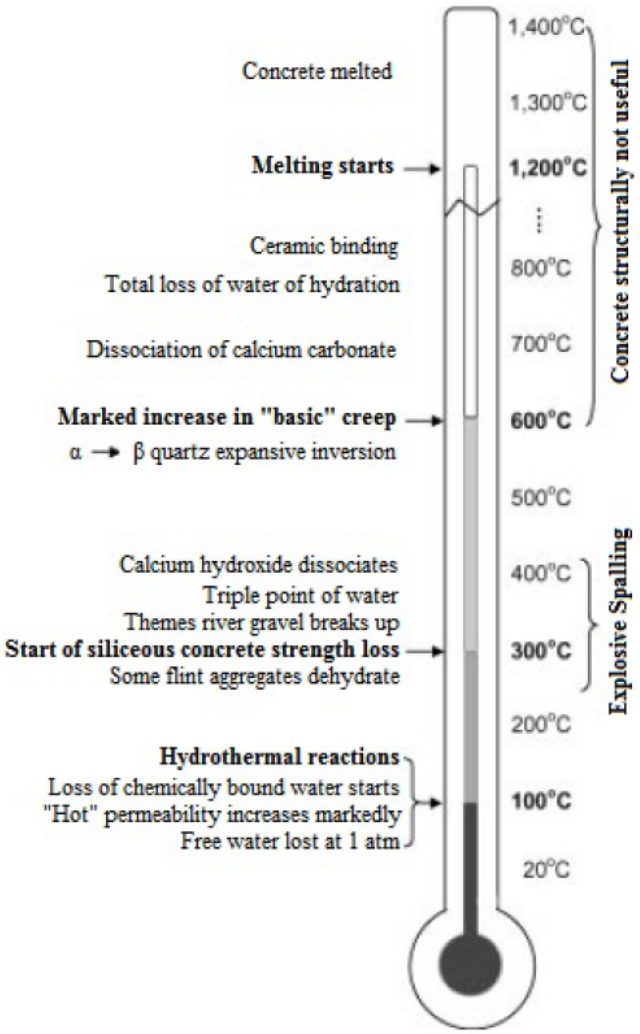

Figure 2.4. Changes in concrete during heating [13].

2.4.1.1. Effects on Compressive Strength of Concrete. These physicochemical changes cause deteriorations in mechanical and durability properties of concrete. Strength of concrete decreases gradually and concrete loses its original strength after 1200°C. The temperature of structural materials experienced in the event of fire is important while the post fire behavior of whole structure is being evaluated. Because of the fact that

reduction in mechanical properties of concrete decrease depending on the magnitude of internal temperature and the amount of reduction must be known during structural analyses. Therefore, standards and regulations recommend various decreasing factors in order to predict residual mechanical properties of fire damaged structural materials. For example, Eurocode 2 recommends decreasing factors to calculate allowable strength of concrete at various temperatures as given in Figure 2.5 [19].

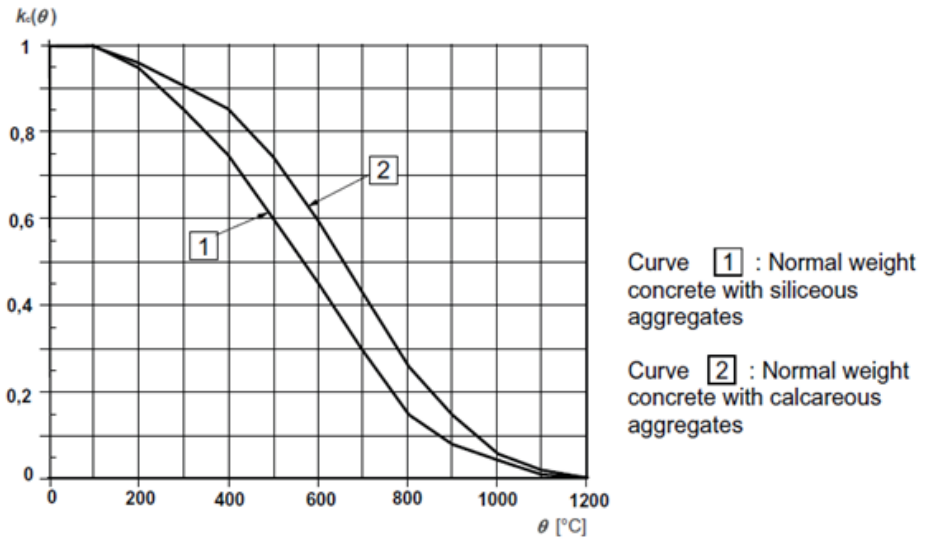

Figure 2.5. Coefficient $k_{c\theta}$ allowing for decrease of characteristic strength (f_{ck}) of concrete, Eurocode 2 [19].

Since the deterioration observed in concrete changes depending on the ingredients of concrete, present standards and recommendations can not cover all types of concrete used in structures today. Therefore, some researches about residual properties of concrete after a fire or high temperature exposure focused on changes in mechanical properties of different kind of concretes such as, ultra high strength concrete, reactive powder concrete, pozzolanic concrete, fiber reinforced concrete, air entrained concrete, autoclaved concrete etc.

When the changes in compressive strength of concrete are evaluated it can be seen that concrete preserves its original compressive strength up to 300°C and in some cases compressive strength of concrete can slightly increase after heating. In the range

of 300°C-800°C prominent decreases can be seen in residual compressive strength of concrete. After 800°C compressive strength of concrete decreases to insignificant levels [20].

Increase in residual compressive strength below 300°C was frequently reported in literature [2, 21–23]. The reason of increase in compressive strength was attributed to tobermorite formation in some researches [2, 24]. Benhood and Ziari stated that this strength gaining around 200°C could be the result of changes in Van der Walls forces due to evaporation of water [25]. Another explanation of strength gain can be the hydration of unhydrated cement particles since evaporated water molecules change their positions in concrete and they can come in contact with unhydrated cement particles in heated concrete [22]. Similar explanations were given by Khoury and he inferred that breaking of bonds occurred in silicon-water compounds below 300°C [23]. Therefore, new bonds were created between the silicon and oxygen atoms which is relatively stronger than previous compound and this may cause improvement in residual compressive strength of concrete [23].

Severe deteriorations in residual compressive strength of concrete heated more than 300°C were reported in literature [2, 21, 22, 26–28]. According to Chan *et al.* compressive strength of normal strength plain concrete decreased 25%, 60% and 80% at 400°C, 600°C and 800°C, respectively [26]. Li *et al.* reported in their study that residual compressive strength of normal strength plain concrete decreased 29%, 42% and 62% at 400°C, 600°C and 800°C,respectively [27].

Inclusion of mineral admixtures influences the changes in residual properties of concrete after a fire or high temperature exposure. Anwar Hossain used volcanic ash in concrete and cement replacement ratio of volcanic ash was 20% [28]. Results showed that concrete incorporating volcanic ash lost 5%, 45% and 70% of initial compressive strength after heating to 400°C, 600°C and 800°C,respectively [28]. Uysal used different fillers such as limestone powder, basalt powder and marble powder in concrete mixes in his study [21]. Similar to other studies concrete specimens were heated up to 800°C and residual mechanical properties were determined after cooling. When the results

of the study were evaluated it can be seen that using high amount of filler in concrete instead of cement (30% of total cementitious amount in the mix) may result in further reduction in residual compressive strength of concrete after 400°C. Because of the fact that materials used in concrete finer than cement particles densify concrete matrix by filling pores of concrete. This dense matrix hinders evacuation of water vapour resulting in cracks and spalling which further reduce the mechanical properties of concrete. Table 2.1 shows residual compressive strength percentages of Portland cement concrete group and concrete groups incorporating various filler materials.

Table 2.1. Reduction in residual compressive strength of concrete incorporating fillers [21].

Concrete Group	**Reduction in Compressive Strength (%)**		
	200°C	**400°C**	**600°C**
Control Concrete	18	50	76
Concrete with limestone powder	23	53	81
Concrete with basalt powder	20	49	79
Concrete with marble powder	22	49	83

On the other hand, using today's widely used mineral admixtures such as pulverized fly ash (PFA), ground granulated blast furnace slag (GGBFS) and condensed silica fume (CSF) in concrete may results in better residual compressive strength after heating [4]. However the effects of silica fume are limited since it has a very fine particle distribution similar to fillers. This may cause densification of concrete and eventually spalling of concrete can be observed during heating [4]. Poon *et al.* used these 3 pozzolanic materials in high strength concrete (HSC) and 2 of them (PFA and GGBFS) in normal strength concrete (NSC) and they heated concrete specimens up

to 800°C, [4]. Test results showed that using PFA and GGBFS in concrete gave better results in NSC groups as can be seen in Table 2.2. If the average values of PFA groups and GGBFS groups are calculated it can be seen that reduction in compressive strength of NSC with PFA were 15%, 59% and 83% at 400°C, 600°C and 800°C, respectively and reduction in compressive strength of NSC with GGBFS were 17%, 48% and 80% at 400°C, 600°C and 800°C, respectively. On the other hand, reduction in compressive strength of Portland cement NSC were higher than these values and 26%, 70% and 90% at 400°C, 600°C and 800°C, respectively. Moreover, according to the results it can be concluded that 30% PFA replacement and 40% GGBFS replacement in normal strength concrete are optimum ratios in terms of high temperature performance of concrete.

Table 2.2. Reduction in residual compressive strength of normal strength concrete incorporating pozzolanic materials [4].

Concrete Group	**Reduction in Compressive Strength (%)**		
	400°C	**600°C**	**800°C**
Portland Cement Concrete	26	70	90
Concrete with PFA (30% of cement replacement)	14	63	84
Concrete with PFA (40% of cement replacement)	16	55	82
Concrete with GGBFS (30% of cement replacement)	15	49	79
Concrete with GGBFS (40%of cement replacement)	19	46	80

Similar results were obtained in HSC groups as can be seen in Table 2.3. Additionally the effects of CSF on residual compressive strength of HSC after heat exposure were evaluated and Poon *et al.* found that 10% CSF replacement had a positive effect

on residual compressive strength at 400°C while it had a negative effect on residual compressive strength after 600°C [4]. HSC groups incorporating PFA or GGBFS showed better performance than Portland cement HSC before 800°C while they had higher reduction in residual compressive strength than Portland cement HSC at 800°C. When the overall results of HSC groups were evaluated it can be considered that 30% PFA replacement and 40% GGBFS replacement in also high strength concrete are optimum ratios in terms of high temperature performance of concrete.

Table 2.3. Reduction in residual compressive strength of high strength concrete incorporating pozzolanic materials [4].

Concrete Group	**Reduction in Compressive Strength (%)**		
	400°C	**600°C**	**800°C**
Portland Cement Concrete	11	42	76
Concrete with CSF (5% of cement replacement)	7	48	79
Concrete with PFA (30% of cement replacement)	2	33	68
Concrete with PFA (40% of cement replacement)	-4	43	70
Concrete with GGBFS (30% of cement replacement)	3	47	73
Concrete with GGBFS (40%of cement replacement)	0	39	71

Some other studies also pointed out the positive effects of replacement or addition of pozzolanic materials in concrete on residual compressive strength at high temperatures. Seleem *et al.* used metakaolin, silica fume, fly ash and ground granulated blast furnace slag in their study and reported that if such pozzolanic materials were added in different concrete groups at the amount of 10% of cement content residual

compressive strength values of these groups were always higher than Portland cement concrete group up to 800°C [29]. When the addition ratio raised to 20% similar results were obtained. In other case, the pozzolanic materials used in concrete were replaced with 10% or 20% of cement. Results showed that only 20% of silica fume replaced concrete showed higher reduction in residual compressive strength than Portland cement concrete. Therefore, pozzolanic materials can be used in concrete by replacing with predetermined amount of cement in order to obtain an economical solution for high temperature conditions.

Recent studies about fiber reinforced concrete at high temperatures mostly investigated effects of polypropylene fiber reinforcement on residual mechanical properties of concrete since polyproylene fibers melt after 170°C and form micro channels in concrete which facilitate evacuation of water vapor [2,13,30–32]. By the way spalling risk of concrete decreases but porosity of concrete increases [2,33]. Sideris *et al.* used 5 kilograms polypropylene fibers in both 1 m^3 of normal strength concrete and high performance concrete and they heated concrete specimens up to 700°C [34]. They reported that plain normal strength concrete lost 23% and 54% of its initial compressive strength at 500°C and 700°C, respectively. Polypropylene fiber reinforced ones lost 35% and 58% of initial compressive strength at 500°C and 700°C, respectively. However, almost all the plain high performance concrete specimens spalled after 500°C. On the other hand, all the polypropylene fiber reinforced high performance concrete specimens kept their stabilities at any temperature level. Therefore, using polypropylene fibers in concrete is important if concrete has a high risk of spalling. But amount of polypropylene fiber should be determined properly since it has negative effects on residual compressive strength.

Using high melting point fiber like steel fibers can be considered as an alternative way to avoid concrete from spalling. After heating they can survive in concrete and porosity of concrete may not increase so much. Poon *et al.* used steel fibers in concrete at a volume ratio of 1% and they heated concrete specimens up to 800°C [35]. No spalling was observed during heating processes. According to the results, reductions in compressive strength of steel fiber reinforced concrete were 45% and 67% at 600°C

and 800°C, respectively while reductions in plain concrete were 53% and 75% at 600°C and 800°C, respectively. Sideris *et al.* produced also steel fiber reinforced concrete in their aforementioned study and 40 kilograms of steel fibers were used in both 1 m^3 of normal strength concrete and high performance concrete [34]. Almost all of their plain high performance concrete specimens spalled during heating on the other hand most of the steel fiber reinforced high performance concrete specimens survived.

Peng *et al.* also investigated the effects of fiber reinforcement on mechanical properties of concrete at high temperatures. They used polypropylene fibers, steel fibers and hybrid fibers (mix of polypropylene and steel fibers) in different concrete mixes [36]. Their results showed that steel fiber reinforced group had lower strength reduction after heating when it was compared to other groups as can be seen in Table 2.4 but high amount of spalling was observed in steel fiber reinforced group. Polypropylene fiber reinforced concrete lost its compressive strength higher than plain concrete after heating. Compressive strength loss of hybrid fiber reinforced group was less than polypropylene fiber reinforced concrete and was higher than steel fiber reinforced concrete. Therefore, using hybrid fibers in concrete reduces the risk of spalling during heating and also decreases reduction in compressive strength after heating.

There are also widely used chemical materials which can effect the fire behavior of concrete such as air entraining admixtures. On the other hand, there is a limited number of study which focused on effects of air entrainment on concrete subjected to high temperatures or fire in literature. In a research concrete groups were designed depending on air entraining agent content and these concrete specimens were subjected to high temperatures [37]. Results of the study can be seen in Table 2.5 and further decreases in residual compressive strength of air entrained groups were observed at 500°C. However, air entrained concrete groups performed slightly better than concrete without air entrainment at 700°C.

2.4.1.2. Effects on Modulus of Elasticity of Concrete. High temperatures affect not only compressive strength but also modulus of elasticity of concrete since increased

Table 2.4. Reduction in residual compressive strength of fiber reinforced concrete [36].

Concrete Group	**Reduction in Compressive Strength (%)**	
	600°C	**800°C**
Plain concrete	24	71
Polypropylene fiber reinforced concrete	25	75
Steel fiber reinforced concrete	11	61
Hybrid fiber reinforced concrete	25	64

Table 2.5. Reduction in residual compressive strength of air entrained concrete [37].

Concrete Group	**Reduction in Compressive Strength (%)**	
	500°C	**700°C**
Concrete without air entrainment	25	75
Air entrained concrete (4%)	36	71
Air entrained concrete (6%)	43	73
Air entrained concrete (8%)	52	73

number of cracks in concrete results in high amount of volume change under loading conditions. Therefore, stress-strain relationship of concrete changes prominently during and after high temperature exposure. This means further deflection, twist and contraction of structural elements under different loading conditions. On the other hand, these deformations must be lower than serviceability limits given in national or international codes. To be able to predict the behavior of a fire damaged structural element load-deformation relation of structural materials should be well known. Consequently, standards and regulations provide some stress-strain curves of structural materials at various temperatures. Table 2.6 represents the changes in peak strains of concrete with siliceous aggregate and concrete with calcareous aggregates at high temperatures and Figure 2.6 explains parameters stated in Table 2.6 as given in Eurocode 2, [19]. As a result, modulus of elasticity which strongly affects the behavior of a structure also decreases with increased temperature. After 500°C, modulus of elasticity of concrete decreases the half of the initial value [1].

Savva *et al.* investigated the effects of fly ash (FA) on modulus of elasticity of concrete at 300°C and 750°C and they used two different FA contents [38]. As can be seen in Table 2.7 residual modulus of elasticity of Portland cement concrete was lower than the half of initial modulus of elasticity at 300°C and almost negligible modulus of elasticity was retained at 750°C. Using FA in concrete at a 10% cement replacement ratio resulted in an improvement in residual modulus of elasticity value while using FA in concrete with a 30% cement replacement ratio resulted in further reduction in residual modulus of elasticity at 300°C. At 750°C residual modulus of elasticity values of concrete groups incorporating FA can also be considered negligible.

Effects of ground granulated blast furnace slag (GGBFS) on residual modulus of elasticity of concrete were investigated by Li *et al.* [39]. Similar to aforementioned study, Li *et al.* used GGBFS in concrete with cement replacement ratios of 10% and 30% and concrete specimens were heated up to 700°C. They obtained less amount of modulus of elasticity reduction when the results of two studies were compared. Table 2.8 shows reduction in modulus of elasticity of concrete incorporating GGBFS at various temperatures. According to results it can be concluded that as the content

Table 2.6. Stress-strain relationships of concrete with siliceous aggregates and concrete with calcareous aggregates at high temperatures, Eurocode 2 [19].

Concrete	**Siliceous aggregates**			**Calcareous aggregates**		
Temperature,teta	$f_{c,\theta}/fck$	$\varepsilon_{c1,\theta}$	$\varepsilon_{cu1,\theta}$	$f_{c,\theta}/fck$	$\varepsilon_{c1,\theta}$	$\varepsilon_{cu1,\theta}$
[°C]	[-]	[-]	[-]	[-]	[-]	[-]
20	1.00	0.0025	0.0200	1.00	0.0025	0.0200
100	1.00	0.0040	0.0225	1.00	0.0040	0.0225
200	0.95	0.0055	0.0250	0.97	0.0055	0.0250
300	0.85	0.0070	0.0275	0.91	0.0070	0.0275
400	0.75	0.0100	0.0300	0.85	0.0100	0.0300
500	0.60	0.0150	0.0325	0.74	0.0150	0.0325
600	0.45	0.0250	0.0350	0.60	0.0250	0.0350
700	0.30	0.0250	0.0375	0.43	0.0250	0.0375
800	0.15	0.0250	0.0400	0.27	0.0250	0.0400
900	0.08	0.0250	0.0425	0.15	0.0250	0.0425
1000	0.04	0.0250	0.0450	0.06	0.0250	0.0450
1100	0.01	0.0250	0.0475	0.02	0.0250	0.0475
1200	0.00	-	-	0.00	-	-

Table 2.7. Reduction in modulus of elasticity of concrete incorporating fly ash [38].

Concrete Group	**Reduction in Modulus of Elasticity (%)**	
	300°C	**700°C**
Portland cement concrete	59	95
Concrete with PFA (%10 cement replacement)	46	96
Concrete with PFA (%30 cement replacement)	70	98

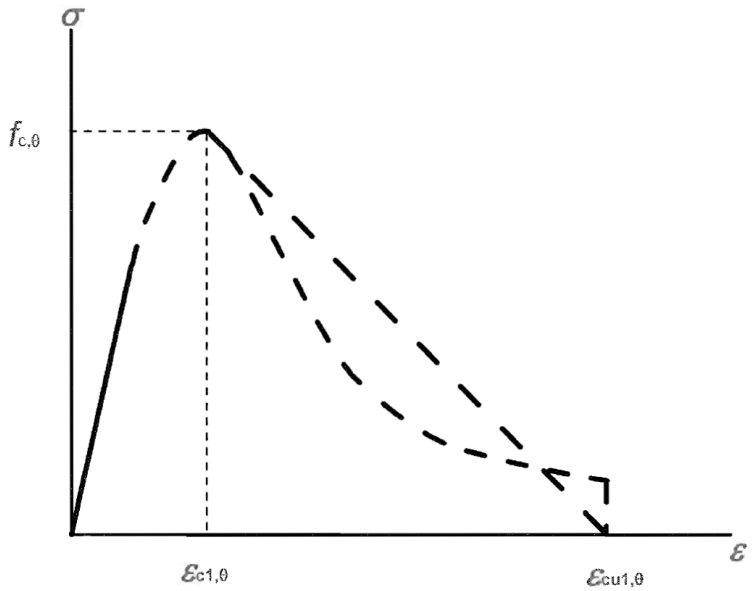

Range	Stress $\sigma(\theta)$
$\varepsilon \leq \varepsilon_{c1,\theta}$	$\frac{3\varepsilon f_{c,\theta}}{\varepsilon_{c1,\theta}\left(2+\left(\frac{\varepsilon}{\varepsilon_{c1,\theta}}\right)^3\right)}$
$\varepsilon_{c1(\theta)} < \varepsilon \leq \varepsilon_{cu1,\theta}$	For numerical purposes a descending branch should be adopted. Linear or non-linear models are permitted.

Figure 2.6. Mathematical model for stress-strain relationships of concrete under compression at elevated temperatures, Eurocode 2 [19].

of GGBFS increased in concrete, reduction in modulus of elasticity also increases at high temperatures.

Table 2.8. Reduction in modulus of elasticity of concrete incorporating GGBFS [39].

Concrete Group	**Reduction in Modulus of Elasticity (%)**		
	300°C	**500°C**	**700°C**
Portland cement concrete	45	70	93
Concrete with GGBFS (%10 cement replacement)	46	72	94
Concrete with GGBFS (%30 cement replacement)	48	75	93

Using high melting point fibers in concrete can be beneficial since they survive after heating and can resist to new cracks occurred during loading. On the other hand, low melting point fibers like polypropylene fibers may result in additional deformation during loading since they disappear after heating and increase porosity of concrete. Sideris *et al.* also investigated changes in modulus of elasticity of fiber reinforced concrete and their results were given in Table 2.9 [34]. According to the results polypropylene fiber reinforced concrete lost higher modulus of elasticity than plain concrete and steel fiber reinforced concrete and steel fiber reinforced concrete retained higher modulus of elasticity than polypropylene fiber reinforced concrete and plain concrete at high temperatures.

2.4.2. Exposure Time

In general concrete has good properties with respect to fire resistance because of the fact that it is an incombustible material and it has low thermal conductivity. The period of time which concrete resists the severe fire conditions is higher than most of the structural materials [1]. Unfortunately, high temperature exposure has always had some adverse effects on concrete. Therefore, duration of concrete in a fire or a

Table 2.9. Reduction in modulus of elasticity of fiber reinforced concrete [34].

Concrete Group	**Reduction in Modulus of Elasticity (%)**		
	300°C	**500°C**	**700°C**
Plain concrete	22	71	89
Polypropylene fiber reinforced concrete	40	62	93
Steel fiber reinforced concrete	19	63	88

high temperature supply is an important factor which determines the deterioration occurred in concrete. Cülfik and Özturan conducted a study on high-performance mortar at elevated temperatures and they also investigated the effects of duration of heat exposure on the residual mechanical properties [40].

Different mortar specimens were subjected to 300°C, 600°C and 900°C in an electrical furnace. First group of specimens were kept in the furnace at the maximum temperature for an hour and the second group were kept at the maximum temperature level for 10 hours. In order to understand the changes in mechanical properties they conducted compression tests and flexural bending tests on heated specimens. Their results showed that the specimens exposed to maximum heating temperatures for 10 hours showed much more deteriorations in compressive strength, modulus of rupture and modulus of elasticity than the specimens exposed to same maximum heating temperatures for an hour [40]. Table 2.10 shows the reduction in residual mechanical properties of specimens after extended heat exposure in the study of Cülfik and Özturan.

Table 2.10. Reduction in residual mechanical properties after extended heat exposure [40].

Maximum Temperature (°C)	**Compressive Strength (%)**	**Modulus of Rupture (%)**	**Modulus of Elasticity (%)**
300	9	10	3
600	15	27	17
900	21	-	-

2.4.3. Heating Rate

The rate of heating has an important influence on how the physical properties of the concrete are affected. Rapid heating causes a temperature difference between the outer surfaces of concrete member and its deeper part. This situation results in high thermal gradients in concrete and therefore spalling may occur. In a cellulosic fire temperature can reach 600°C in 10 minutes which corresponds to a heating rate of 60°C/min and in a hydrocarbon fire temperature can exceed 1000°C in 10 minutes which corresponds to a heating rate of 100°C/min.

2.4.4. Water to Cementitious Ratio

This ratio is the most important parameter in determining the strength of concrete. In the event of fire, concretes with lower water to cementitious ratios show higher residual strengths but they generally lose their strength at higher rates. Chan *et al.* compared high strength concrete and normal strength concrete which had 0.32 and 0.80 water to cementitious ratios, respectively [41]. The comparison of control series of HSC and NSC can be seen in Table 2.11 [41]. According to the study, normal strength concrete preserved 45% of its initial compressive strength after exposure to 800°C. On the other hand, high strength concrete groups retained 28% of their initial compressive strength in average.

Table 2.11. Changes in compressive strength of HSC and NSC [41].

Mix	**Compressive Strength (MPa)**	
	20°C	**800°C**
NSC	34.9	15.8 (45%)
HSC-1	97.3	24.9 (26%)
HSC-2	113.5	38.7 (34%)
HSC-3	99.1	23.9 (24%)

High amount of cementitious material in concrete densifies its microstructure and reduces the porosity of concrete. By the way, vapor diffusivity of concrete increases and during heat exposure this can limit the evacuation of water vapor ensuing from evaporation of free water and crystal water in concrete due to temperature increase. If the pore pressure in concrete exceeds the tensile strength of concrete spalling may occur. Therefore, spalling can be observed in high strength concrete members more frequently than normal strength concrete members.

2.4.5. Moisture Content

After 100°C free water in concrete evaporates and therefore vapor pressure increases in the pores and results in moisture gradients in concrete. Especially, moisture gradients are the main factor of the spalling of concrete. High temperature increases the pressure of water vapor entrapped in concrete pores and when the stresses around the pores exceed the tensile strength of concrete spalling occurs. Above 3% moisture by weight, traditional concrete is more prone to spalling. However, even the zero moisture may cause spalling of dense concrete [30].

2.4.6. Type of Cement and Aggregate

Concrete with higher calcium hydroxide content is more prone to strength loss due to the fact that calcium hydroxide dehydrates and shrinks approximately 33% after

400°C. Therefore, using blended cement may improve fire performance of concrete [13].

When concrete is considered as a whole, aggregates occupy approximately 70% of concrete in volume. Therefore, thermal properties of aggregates strongly influence the resulting thermal properties of concrete. Aggregates with low thermal expansion coefficients are preferable to those with high coefficients because when concrete shrinks after 400°C high amount of expansion of aggregates may result in disruption of cement matrix. On the other hand, lightweight concrete which incorporates lightweight aggregates has lower thermal conductivity coefficient and is less prone to deterioration during fire [1].

2.5. Improving Fire Performance of Concrete

There are number of studies which investigated the methods to improve the fire performance of concrete. Results of the studies showed that using mineral and chemical admixtures and adding various fibers in concrete may enhance the residual properties of concrete.

2.5.1. Mineral Admixtures

As aforementioned, it was reported that concrete which had lower calcium hydroxide content showed better performance after high temperature exposure [13]. Hence, using mineral admixture such as slag and fly ash in concrete improves fire resistance of concrete by reducing calcium hydroxide amount via pozzolanic reactions. However, positive effect of silica fume is limited due to its small particle sizes. Silica fume particles fill the small voids and pores in concrete and densify it and therefore probability of spalling of concrete increases at high temperatures [42].

Poon *et al.* [4] conducted a research on the effects of pozzolonic materials in residual mechanical properties and durability performance of concrete at elevated temperatures. They used silica fume, fly ash and ground granulated blast furnace slag in different concrete mixes with various cement replacement ratios. Specimens were

heated up to 800°C. According to their conclusions, concrete groups incorporating puzzolonic admixtures performed better at high temperatures than Portland cement concrete groups with the exception of concrete group incorporating silica fume. And this positive effect was due to secondary reaction of free lime with pozzolanic materials used in concrete mixes.

2.5.2. Fibers

Using polypropylene fibers in concrete is the best known way to increase the spalling resistance of concrete at elevated temperatures. Polypropylene fibers melt after 170°C and completely disappear after 450°C heating as can be seen in thermogravimetric analysis curve, Figure 2.7 [6]. Therefore, melted PP fibers form microchannels in concrete matrix which permit the evacuation of water vapor and help to reduce vapor pressure in concrete [2]. Figure 2.8 shows PP fiber bed formed after melting.

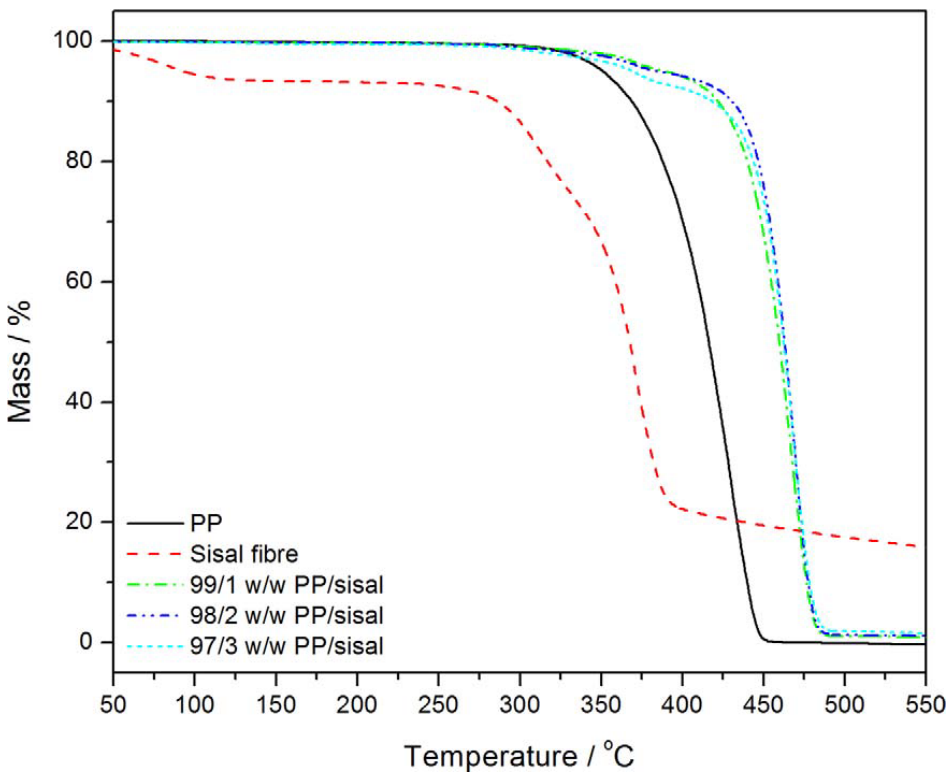

Figure 2.7. Thermogravimetric analysis (TGA) curves of polypropylene (PP) and the PP/sisal fibre composites [6].

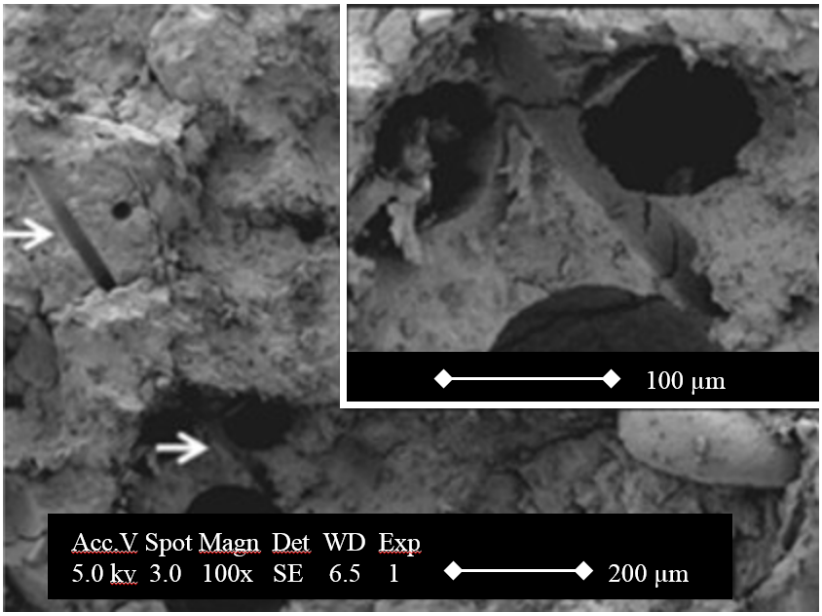

Figure 2.8. Polypropylene fiber bed [2].

Addition of high melting point fibers is also useful in slow heating conditions [43]. In the case of rapid heating, high melting point fibers such as steel fibers increase the spalling temperature up to 800°C but mostly it cannot prevent concrete from spalling [8]. Literature results about the effects of steel fibers on spalling of concrete were contradictory [44]. Because of the fact that, Peng *et al.* inferred that steel fiber reinforced concrete increased the fracture energy of concrete resulting in higher spalling resistance of concrete [36].

Hybrid fiber reinforced concrete which contains both steel and polypropylene fibers can be a good way to improve fire performance and spalling resistance of concrete [35]. Poon *et al.* used steel fibers and polypropylene fibers together and they suggested that steel fibers increased the performance of polypropylene fibers by improving resistance against spalling [35].

2.5.3. Chemical Admixtures

Chemical admixtures especially air entrained admixtures also influence the behavior of concrete both during heating and after cooling. Because of the fact that thermal properties of air entrained concrete are different from thermal properties of concrete produced with the same ingredients except air entraining agents. Air voids in concrete decrease thermal conductivity of concrete and temperature distribution in concrete during heating changes. For example, temperature of inner parts of air entrained concrete can be less than temperatures of inner parts of concrete without air entrainment while temperature at the heated surfaces of the air entrained concrete can be higher than heated surface temperature of concrete without air entrainment. Therefore, inner part of air entrained concrete experiences relatively lower temperatures than concrete without air entrainment and because of this deterioration in mechanical properties of air entrained concrete can be lower. Nevertheless, maximum temperature and also duration of heating process are important because temperatures in air entrained concrete and concrete without air entrainment can get closer after a period of time.

Akca and Özyurt Zihnioğlu reported that positive effect of air entrainment on residual compressive strength of concrete was observed in some groups however they inferred that this effect was limited and could not be valid for high strength concrete [2]. Due to the dense microstructure of HPC water vapor occurred in entrained and entrapped air voids cannot diffuse easily in cement matrix and hence vapor pressure in the voids increases dramatically. In order to eliminate this negative effect, polypropylene fibers can be used in HPC and after fibers melt and produce interconnected permeable network with air voids in concrete [2]. By the way the risk of spalling of air entrained concrete can be reduced.

2.6. Post Fire Behavior

The effects of high temperatures on residual properties of concrete continue in subsequent days of cooling. Dehydration products especially CaO and calcium silicates produced during heating are chemically active and may give reactions with water and

carbon dioxide in air. These newly formed rehydration products can have detrimental effects or improving effects on concrete so these new formations affect the post fire behavior of concrete. Therefore, response of concrete depends on initial ingredients, heating and cooling methods and post fire environmental conditions.

2.6.1. Disintegration

Disintegration of concrete occurs in subsequent days of cooling and there are several studies in literature which reported disintegration of concrete specimens after heating [2,40,45–48]. The reason of disintegration is not fully understood but according to the recent researches $CaO/Ca(OH)_2$ phase changes occurred after heating can be one of the main factors [2, 45–47]. Because of the fact that, as the temperature in concrete increases $Ca(OH)_2$ loses its water content and turns to CaO, moreover it shrinks and results in cracks in concrete, Figure 2.9 [45–47]. Therefore, concrete preserves its stability if the concrete heated below 400°C since dehydration of $Ca(OH)_2$ starts above this temperature. On the other hand, if concrete experiences temperatures higher than 400°C disintegration of concrete is frequently observed after cooling [22, 49]. Post fire effect of this phenomenon on concrete is the rehydration of CaO, because of the fact that CaO expands approximately 44% by volume and this expansion may cause further deterioration of concrete [47, 50].

Mendes *et al.* produced both Portland cement and ground granulated blast furnace slag pastes (GGBFS pastes include also Portland cement) and heated them up to 800°C [45]. Following the cooling period severe cracks occurred on Portland cement pastes which heated higher than 400°C, Figure 2.10. Compression tests showed that these specimens had almost no strength. On the other hand, Portland cement paste specimens experienced less than 400°C kept their physical stability and also maintained their compressive strength. Also Mendes *et al.* inferred that these dehydration and rehydration processes of $Ca(OH)_2$ had no severe impact in pastes where Portland cement and GGBFS were used together [45]. Owing to the fact that, using GGBFS reduces initial content of $Ca(OH)_2$ in paste and this can eliminate the negative effect of $CaO/Ca(OH)_2$ phase transformation following to cooling.

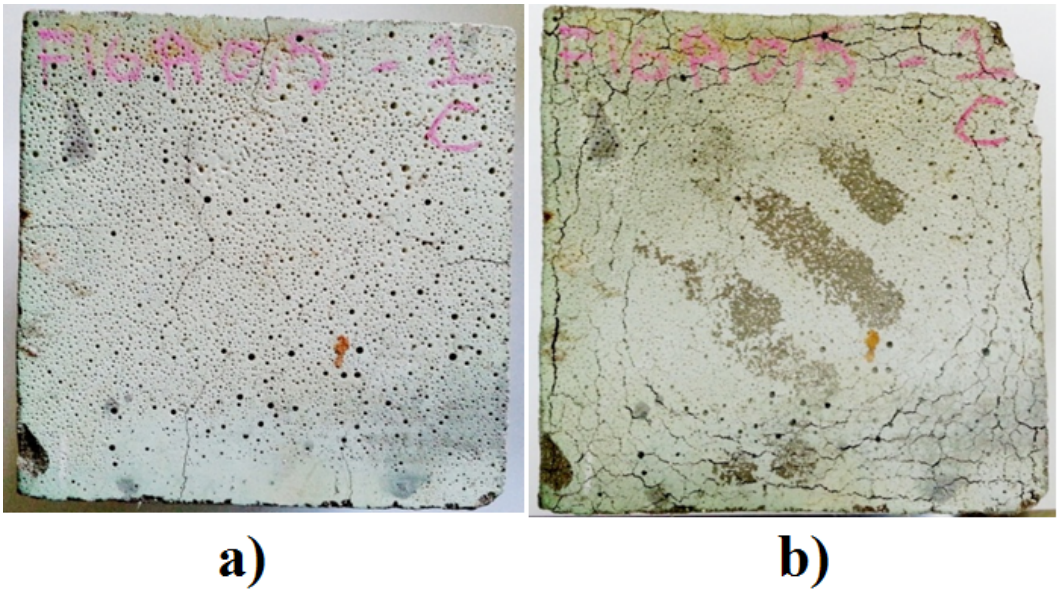

Figure 2.9. Disintegration of a concrete specimen. a) just after cooling period b) 7 days after cooling period [51].

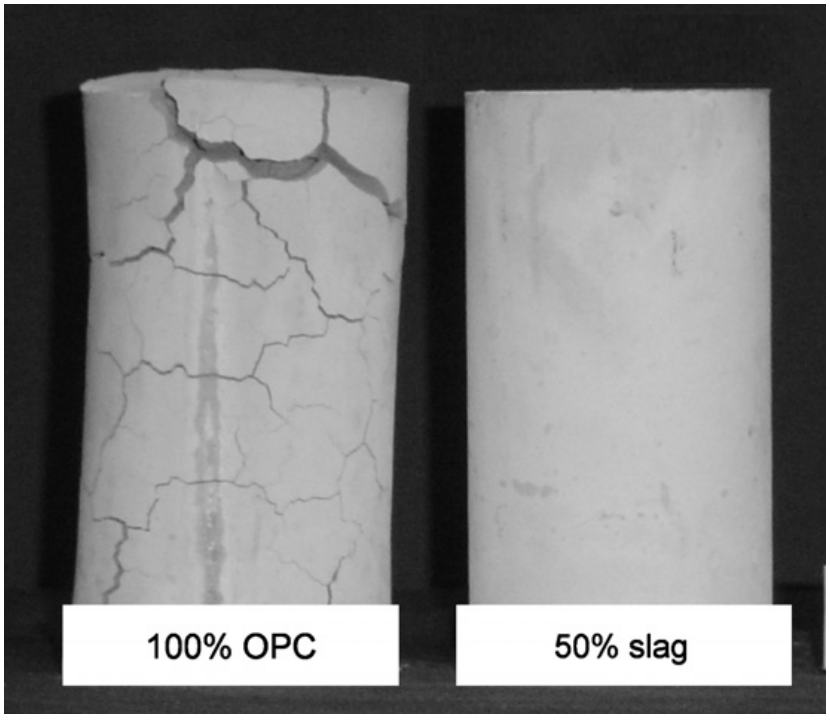

Figure 2.10. Disintegration of pastes [45].

However, in some cases, disintegration of concrete incorporating GGBFS can be observed due the decomposition of C-S-H in concrete during fire [2, 52]. Additionally, the amount of GGBFS used with Portland cement is important. Akca and Özyurt Zihnioğlu produced cement based composites (CBC) incorporating GGBFS and they heated the composite specimens up to 900°C [2]. They reported that specimens which heated to 300°C or 600°C preserved their physical stabilities. On the other hand specimens which heated to 900°C completely disintegrated after a period of time of cooling since at 700°C decomposition of C-S-H is almost completed [52].

2.6.2. Recovery

High temperature exposure causes to open new capillaries in concrete therefore strength of concrete reduces and concrete becomes less durable after cooling. As aforementioned before, chemical reactions occur in concrete during heating. These reactions can be detrimental for concrete at post heating stage and sometimes it is very hard to obtain reverse reactions.

Recovery of mechanical properties and durability of concrete begins with rehydration process which includes the followings: partial rehydration of newly formed calcium silicates, hydration of unhydrated cement particles, rehydration of CaO, secondary reaction between unhydrated pozzolans and the newly produced calcium hydroxide and carbonation of CaO [12]. Therefore, if suitable method is applied recovery of concrete can be obtained after every temperature level of heating.

Although sustainability is one of the main concerns for the world there are very limited studies in literature about the rehydration process which may result in an improvement in concrete after a fire or high temperature exposure [12, 53, 54]. Alonso and Fernandez produced Portland cement pastes and they heated their specimens up to 750°C [54]. After cooling specimens were sealed and kept in a saturated chamber for three and a half months. According to their results C-S-H was formed after rehydration of nesosilicate which was dehydrated C-S-H with a molar ratio of $Ca/Si \approx 2$ and portlandite was formed after rehydration of CaO. Also calcite formation was observed

in sealed specimens. However Alonso and Fernandez inferred that after rehydration severe cracks occurred on specimens.

On the other hand Poon *et al.* conducted a comprehensive study on post fire recovery of normal strength concrete and high strength concrete incorporating mineral admixtures [12]. Specimens were heated to 800°C and were cooled naturally. Then, some specimens were placed in water tank for water 28 days of re-curing. Remaining specimens were submerged in water for 2 hours then placed in a moist environment for 28 days of air re-curing. Results showed that mechanical properties of concrete groups increased after both air and water re-curing as can be seen in Table 2.12. However, regained compressive strength was higher in water re-cured concrete groups. Poon *et al.* concluded that permanent moisture or water supply were needed in order to obtained improved recovery.

Table 2.12. Residual compressive strength of air/water re-cured concrete [12].

		Residual Compressive Strength (%)		
	Group	**After cooling**	**28 days of re-curing**	
			Air	**Water**
NSC	Portland cement	10	31	47
	Fly ash	16	32	44
	GGBFS	20	35	41
HSC	Portland cement	24	37	61
	Fly ash	32	47	69
	GGBFS	29	36	55

During re-curing process, water re-cured concrete preserves its stability and does not disintegrate, moreover cracks in concrete are almost filled by rehydration products [2]. The size of those rehydration products is relatively smaller than the initial hydration products. Therefore a finer pore structure is formed and concrete regains its strength partially [12]. SEM pictures also show the filling effect of rehydration process in Figure 2.11. Figure 2.11.a presents the crack pattern of a disintegrated concrete. On

the other hand, as can be seen in Figure 2.11.b, the surface of 7 days water re-cured concrete looks like an undamaged concrete surface [2].

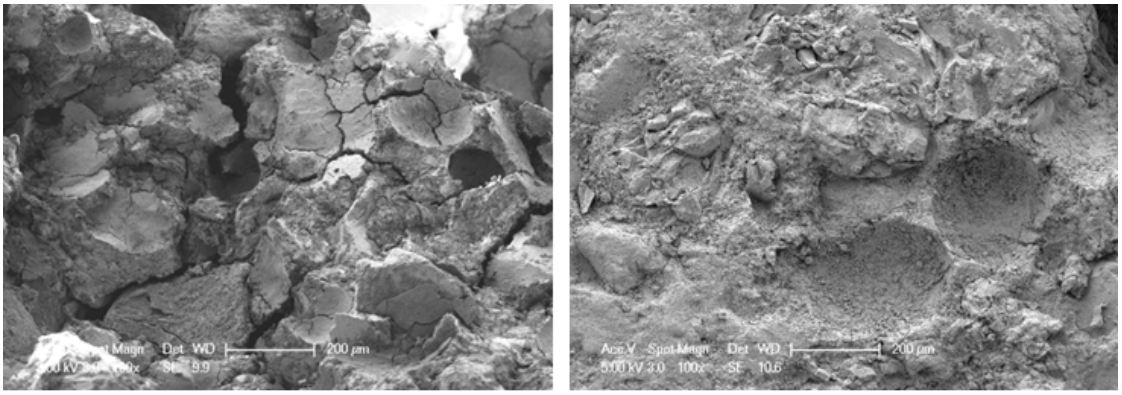

Figure 2.11. SEM pictures of a) a disintegrated and b) a 7 days water re-cured concrete. [51]

Limited number of studies on the post fire disintegration and recovery of concrete showed that concrete exposed to temperatures higher than 800°C may disintegrate after cooling period and in order to eliminate this negative effect, re-curing of concrete can be beneficial. In terms of recovery, the balance between the deteriorative effect of expansion of CaO rehydration and the production of new CSH gels is very important. Therefore, pozzolans and their amounts in concrete are the determinative parameters in the extent of recovery. On the other hand, the expansion of CaO after high temperature exposure causes tensile stresses in concrete and this may be balanced by high melting point fibers such as steel fibers. However, there is not any investigation on the effects of high melting point fibers on the post fire recovery of concrete in literature.

2.7. Fire Tests on Structural Elements

In literature, most of the studies focused on effects of high temperatures or fire on concrete used small sized specimens. On the other hand, there are few works concerning the effects of high temperature or fire on real structural members or even real structural systems. Because of the fact that, fire tests on full scale structural

members are expensive and need professional workmanship and technical assistance. Moreover, this kind of equipped laboratories are not common and it is generally not easy to find an available fire laboratory. Nevertheless, tests on full-sized structural members can better simulate the behavior of real structure in the event of fire.

Generally cylinders, cubes and prism beams are used in laboratories as small sized specimens. If all of the faces of specimens are subjected to heating temperature inside them can rapidly increase. Therefore, smaller specimens experience higher temperatures than bigger specimens under same heating conditions. As aforementioned, as the temperature monitored in concrete reaches higher levels deterioration in the properties of concrete is observed [2, 4].

In the event of fire, structural beams and slabs are more prone to experience higher temperatures [55]. Moreover, tension zones of these members are directly subjected to heating and combination of these tensile stresses and thermal stresses can reach tensile strength capacity of concrete and member may eventually fail during heating. Therefore, beams and slabs were mostly used in recent studies and they were generally subjected to ISO-834 fire scenario which can better simulate a fire in building. Application of severe fire scenarios in a furnace recommends high capacity ventilation systems and also special heating systems such as gas jets and burners etc. Many of the furnaces use propane gases instead hydrocarbon fuel since hydrocarbon fuel releases visible smokes.

Design rules of structural elements are given in standards and recommendations. In terms of fire, dimensional parameters especially cover thickness change significantly to preserve reinforcing elements. Because of the fact that reinforcing steel which is also an incombustible material is not as resistant as concrete at high temperatures. Figure 2.12 shows reduction of compressive and tensile strength of hot rolled reinforcement at high temperatures as given in Eurocode 2 [19]. As can be seen from the graph 400°C is a critical temperature at the reinforcing bar level since reduction in compressive and tensile strength of reinforcing steel begins at this temperature. Therefore, concrete cover plays an important role in the event of fire. Generally, 25 mm of cover thickness

is used for the conventional structural application. In terms of structural fire design 25 mm of concrete cover means low level of protection and structural element needs special insulation application.

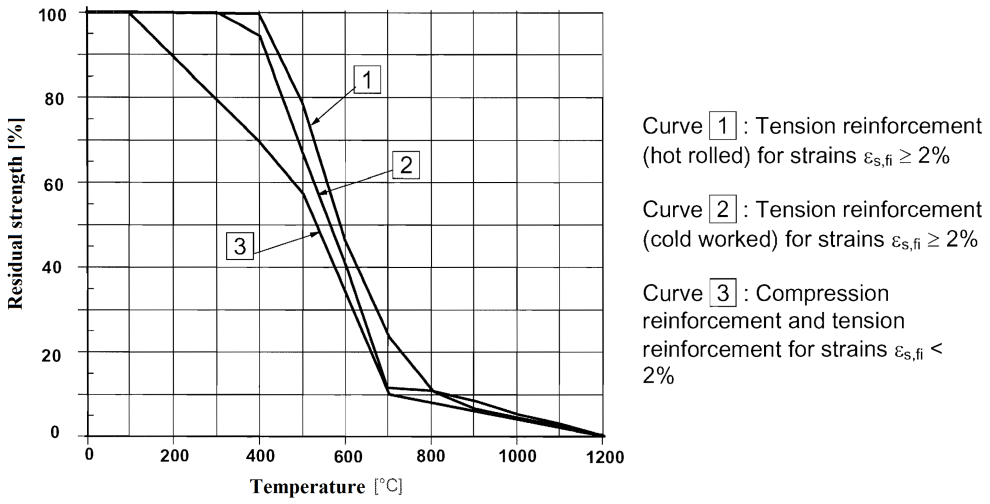

Figure 2.12. Decrease of characteristic strength of tension and compression reinforcement [19].

2.7.1. Fire Tests on Structural Beams

As it was mentioned before, risk of having damage of beams and slabs during fire is relatively higher. Therefore, most of the researches on structural elements under fire conditions focused on structural beams and slabs. Although, beams and slabs are mostly fixed and continuous elements in structures, frequently simply supported beams and slabs are used in fire tests due to furnace sizes and capacity. Loaded elements can also be subjected to high temperatures since they can give more realistic results.

Recent results showed that if reinforcing bar had no damage after fire exposure maximum load bearing capacity of the beam did not change significantly. Jiangtaoa *et al.* found that only 10% of reduction was observed in the peak load of continuous beams after heating [55]. On the other hand, more than 100% of increases at mid-point deflection were measured after heat exposure because earlier cracks occurred at the maximum moment zone (Ellingwood and Lin that reported these earlier cracks

occurred 30 minutes after ignition [56].). Due to excessive amount of cracks on the structural elements residual flexural rigidity changes drastically.

2.7.2. Fire Tests on Structural Slabs

There are very few studies on fire tests on structural slabs in literature since the sizes of slabs are relatively larger than beams and columns. Researches showed that conventional yield line pattern was followed during fire tests on simply supported two-way slabs in the case of no spalling [57, 58]. Thickness of slabs is smaller than other dimensions therefore well designed and preserved reinforcement is vital to be able to carry loads under severe conditions. In case of spalling of concrete cover sudden temperature increase in lower reinforcement can be seen and this may change failure mechanisms [59]. On the other hand, research showed that the risk of spalling in restrained slabs surrounded by cooler structural elements was lower [59]. Because of the fact that restrained points produce compression zone under the slabs and therefore pore pressure is needed to be higher than the absolute combination of existing compressive stress and tensile stress corresponding to tensile strength of concrete.

2.7.3. Fire Tests on Structural Columns

Generally fire tests on structural columns are easier to do than fire tests on other structural elements. Because of their position in structural systems columns are less prone to experience high temperatures. Additionally, width and depth of columns are relatively larger and this may result in lower temperatures experienced at the inner parts of structural element. Therefore, main core of columns generally preserves its mechanical properties after a fire. Important thing is to preserve reinforcement during fire as such in reinforced beams and reinforced slabs. On the other hand risk of spalling is lower since columns work under compression in structural systems. In a study conducted by Chen *et al.* load bearing capacity of columns which were subjected to ISO-834 fire scenario for 2 hours decreased 20% in average under eccentric loading conditions [60]. Stiffness of columns decreased 50% in average since less amount of cracks occur in columns with respect to beams and slabs [60].

3. EXPERIMENTAL STUDY

In this study, the post fire behavior of concrete was investigated. For this purpose, 24 types of concrete were produced and two different types of re-curing methods were applied after cooling. Residual mechanical properties of concretes were determined. Microstructural investigations were conducted on the samples obtained from concrete specimens. According to tests results obtained from small sized concrete specimens 4 types of concrete were chosen in order to produce reinforced concrete beams. These beams were subjected to ISO-834 fire scenario for 120 minutes in a fire testing room. Moreover, similar tests and evaluations were applied on reinforced concrete in order to determine residual mechanical properties of reinforced concrete beams and residual morphology of concretes.

3.1. Materials

CEM I type Portland cement (PC), ground granulated blast furnace slag (GGBFS) and F type pulverized fly ash (PFA) were used in concrete groups as cementitious materials. Crushed stone and river sand were used as aggregates and steel and polypropylene fibers were used as reinforcing elements. Air entraining admixture and superplasticizer were used as chemical admixtures.

3.1.1. Cement

CEM I 42.5 R type Portland cement was used in this study and mechanical properties of cement was given in Table 3.1 and chemical properties of cement was given in Table 3.2.

3.1.2. Ground Granulated Blast Furnace Slag

Chemical properties of ground granulated blast furnace slag (GGBFS) were given in Table 3.3 and physical properties of GGBFS were given in Table 3.4

Table 3.1. Mechanical properties of Portland cement.

Mechanical Characteristic	**Day**	**Standards**	**Test Results**
Early Strength	2	>20.0 MPa	28.3 MPa
Early Strength	7	———	42.1 MPa
Standard Strength	28	>42.5 MPa	54.8 MPa
		<62.5 MPa	

Table 3.2. Chemical properties of Portland cement.

Composition	(%)	**Composition**	(%)
SiO_2	19.63	SO_3	3.23
Insoluble residue	0.28	Loss on ignition	2.03
Al_2O_3	5.58	Cl^-	0.04
Fe_2O_3	3.32	Na_2O	0.21
CaO	63.67	K_2O	0.68
MgO	1.25	Unknown	0.36
LSF	0.96	Free lime	2.00
Mineralogical Compounds		C_3S	50.36
		C_2S	18.37
		C_3A	9.18
		C_4AF	10.10

Table 3.3. Chemical properties of ground granulated blast furnace slag.

Composition	(%)	**Composition**	(%)
SiO_2	40.95	Na_2O	0.56
Al_2O_3	12.10	K_2O	0.36
Fe_2O_3	1.28	Cl^-	0.02
CaO	36.63	SO_3	0.16
MgO	5.48	Loss on ignition	0.11

Table 3.4. Physical properties of ground granulated blast furnace slag.

Physical Property	**Test Result**
Density	2920 (kg/m^3)
Pozzolanic Activity Index 7 day	52.3 (%)
Pozzolanic Activity Index 28 day	74.4 (%)
Residue on 45μm sieve	1.1 (%)

3.1.3. Pulverized Fly Ash

F type pulverized fly ash was used in concrete groups incorporating PFA. Chemical properties of pulverized fly as were given in Table 3.5 and physical properties of pulverized fly ash were given in Table 3.6

Table 3.5. Chemical properties of pulverized fly ash.

Composition	**(%)**	**Composition**	**(%)**
SiO_2	54.57	SO_3	0.20
Free lime	0.02	Loss on ignition	3.30
Al_2O_3	25.26	Cl^-	0.004
Fe_2O_3	6.28	Na_2O	0.38
CaO	2.10	K_2O	4.04
MgO	2.08	Unknown	0.36

Table 3.6. Physical properties of pulverized fly ash.

Physical Property	**Test Result**
Density	2130 (kg/m^3)
Pozzolanic Activity Index 28 day	83 (%)
Pozzolanic Activity Index 90 day	97 (%)
Residue on 45μm sieve	29.4 (%)

3.1.4. Aggregates

Siliceous crushed stone and siliceous river sand were used as coarse and fine aggregates in concrete mixes. Specific gravities of crushed stone and river sand were 2.70 and 2.65, respectively.

3.1.5. Fibers

Multi filament polypropylene fibers and hooked end steel fibers were used in this study. Properties of fibers were given in Table 3.7.

Table 3.7. Properties of fibers.

Properties	**Unit**	**Fiber**	
		Polypropylene	**Steel**
Length	(mm)	12	35
Diameter	(μm)	32	550
Aspect ratio	-	375	65
Tensile strength	MPa	250	1345
Modulus of elasticity	GPa	3.5	210
Specific gravity	-	0.9	7.8
Melting Point	(°C)	165	

3.1.6. Chemical Admixtures

Oil alcohol and ammonium salt based air entraining admixture (AEA) and modified polycarboxylate based superplasticizer were used in concrete mixes. Specific gravities of air entraining admixture and superplasticizer were 1.02 and 1.21, respectively.

3.2. Mix Proportions

Cement replacement ratios of GGBFS and PFA were 40% and 30%, respectively since these ratios were found to be optimum in some previous researches [4, 61]. Total amount of cementitious materials in 1 m^3 of concrete was 450 kg in every concrete groups and all concrete groups had 0.45 water to cementitious ratio. Water contents were determined according to TS EN 206-1 and TS 13515 since cement equivalence factors for GGBFS and PFA are 0.8 and 0.4, respectively. Table 3.8, Table 3.9 and Table 3.10 show mix proportions of concrete groups. As chemical admixtures, oil alcohol and ammonium salt based air entraining admixture (AEA) and modified polycarboxylate based superplasticizer were used in concrete mixes. Steel fibers were used as high melting point fibers and PP fibers were used as low melting point fibers to reinforce concrete groups. In PP fiber reinforced groups PP fibers were used 0.2% of volume of concrete and in steel fiber reinforced groups steel fibers were used 0.5% of volume of concrete. PP fibers and steel fibers were added at contents of 0.25% and 0.1% per volume in hybrid fiber reinforced concrete groups, respectively. River sand and siliceous gravel were used in all concrete groups as aggregates.

Table 3.8. Mix proportions of Portland cement concrete groups.

Materials	**PC Groups** (kg/m^3)
Portland Cement	450
Water	203
Aggregate No1	484
Aggregate No2	484
Crushed Sand	564
River Sand	225
Super Plasticizer (min-max)	5.3 - 6.7
In Polyproylene fiber reinforced groups PP fiber amount	1.8
In Steel fiber reinforced groups Steel fiber amount	40
In Hybrid fiber reinforced groups PP fiber amount/Steel fiber amount	0.9 / 21
In air entrained groups AEA amount	0.3

Table 3.9. Mix proportions of ground granulated blast furnace slag concrete groups.

Materials	**PC+GGBFS Groups** (kg/m^3)
Portland Cement	270
GGBFS	180
Water	186
Aggregate No1	493
Aggregate No2	493
Crushed Sand	574
River Sand	229
Super Plasticizer (min-max)	6.9 - 8.3
In Polyproylene fiber reinforced groups PP fiber amount	1.8
In Steel fiber reinforced groups Steel fiber amount	40
In Hybrid fiber reinforced groups PP fiber amount/Steel fiber amount	0.9 / 21
In air entrained groups AEA amount	0.3

Table 3.10. Mix proportions of pulverized fly ash concrete groups.

Materials	**PC+PFA Groups** (kg/m^3)
Portland Cement	315
PFA	135
Water	167
Aggregate No1	496
Aggregate No2	496
Crushed Sand	577
River Sand	230
Super Plasticizer (min-max)	8.6 - 10.4
In Polyproylene fiber reinforced groups PP fiber amount	1.8
In Steel fiber reinforced groups Steel fiber amount	40
In Hybrid fiber reinforced groups PP fiber amount/Steel fiber amount	0.9 / 21
In air entrained groups AEA amount	0.3

3.3. Concrete Groups

There are 24 types of concrete and two re-curing methods. Table 3.11, Table 3.12 and Table 3.13 present the concrete groups and their designations. C represents Portland cement concrete, S represents concrete incorporating GGBS and F represents concrete incorporating PFA. S and P represent steel and polypropylene fibers reinforcement, respectively and H represents the use of hybrid fiber (steel and polypropylene reinforcement). And finally, A represents air entrainment.

Table 3.11. Portland cement groups and designations.

Portland Cement - C							
Air Entrained - A				Without Air Entrainment - 0			
Steel Fiber S	PP Fiber P	Hybrid Fiber H	Without Fibers 0	Steel Fiber S	PP Fiber P	Hybrid Fiber H	Without Fibers 0
CAS	CAP	CAH	CA0	C0S	C0P	C0H	C00

Table 3.12. Ground granulated blast furnace slag groups and designations.

Ground Granulated Blast Furnace Slag - S							
Air Entrained - A				Without Air Entrainment - 0			
Steel Fiber S	PP Fiber P	Hybrid Fiber H	Without Fibers 0	Steel Fiber S	PP Fiber P	Hybrid Fiber H	Without Fibers 0
SAS	SAP	SAH	SA0	S0S	S0P	S0H	S00

Concrete specimens were tested before heating (control series), just after cooling, and after water and air re-curing. Therefore, these 24 groups expanded to 96 series. 0 and X represent control series and series tested just after cooling, respectively. Also, W and Z represent water re-curing in water and air re-curing in laboratory environment,

Table 3.13. Pulverized fly ash groups and designations.

Pulverized Fly Ash - F							
Air Entrained - A				Without Air Entrainment - 0			
Steel Fiber S	PP Fiber P	Hybrid Fiber H	Without Fibers 0	Steel Fiber S	PP Fiber P	Hybrid Fiber H	Without Fibers 0
FAS	FAP	FAH	FA0	F0S	F0P	F0H	F00

respectively. For example, FAPW represents the water re-cured air entrained PP fiber reinforced concrete incorporating pulverized fly ash.

3.4. Tests on Small Sized Specimens

15 cubic specimens with dimensions of 15x15x15 cm were produced for every concrete groups. One day after production, specimens were demolded and placed in curing water for 27 days. Then they were conditioned in laboratory environment for additional 2 months before tests [4, 26, 62]. 3 cubic specimens were used to determine initial properties of concrete before heating. Remaining 12 cubic specimens were heated to 1000°C. 3 of them were used to monitor temperature pattern in concrete cubes during heating, 3 of them were tested to determine properties after cooling and remaining 6 cubic specimens were subjected to air and water re-curing. Additionally, 6 more cube specimens were produced by using CAH, SAH and FAH concrete groups in order to see the long term effect of re-curing. Finally, CAH, SAH and FAH groups had 21 and remaining groups had 15 specimens to test and therefore total number of cube specimens was 378 (21 specimens x 3 groups + 15 specimens x 21 groups).

3.4.1. Heating Procedure

An electrical furnace which has a 1250°C maximum operation temperature was used in this study. Two stages of heating were determined and during the first stage

specimens were heated to 1000°C and during the second stage specimens were kept at this temperature until the end of the total heating time (200 minutes). Figure 3.1 represents the heating procedure. Electrical furnace was operated at full power and temperature inside the furnace reached 1000°C in approximately 120 minutes. Since furnace heating capacity was limited, heating rate was 20°C/min at the beginning but the rate decreased to 5°C/min at the end of the first stage of heating. After the second stage completed, hot concrete specimens were not taken out until the furnace cooled down to 100°C.

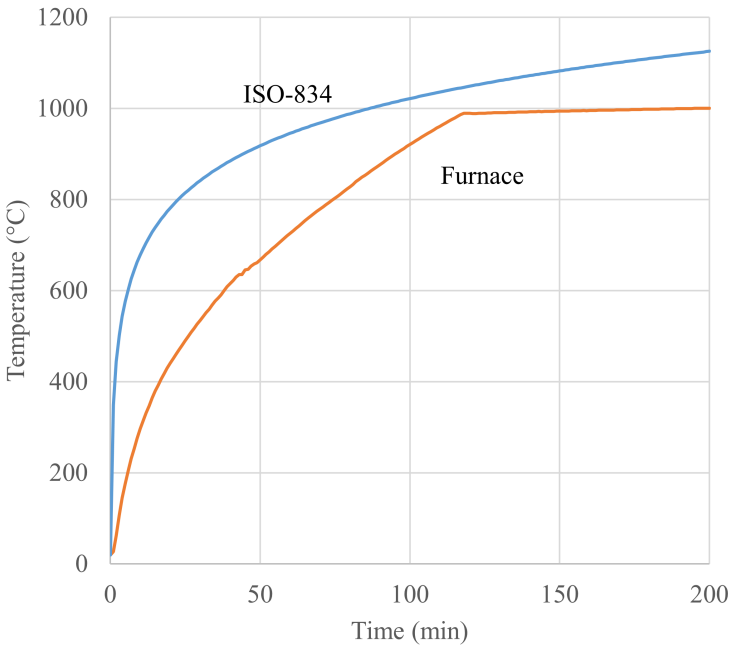

Figure 3.1. Heating scenario.

Four concrete cubes were placed together in the electrical furnace and in order to simulate one face heating conditions they were insulated with aerated concrete blocks as shown in Figure 3.2. For temperature monitoring K-Type thermocouples were placed in a concrete at hardened state before heating. Thermocouple holes were drilled and thermocouples were placed in these holes. Then holes were filled with concrete powder obtained from the same concrete specimen during drilling. Thermocouple wires were high temperature resistant therefore they could survive after multiple uses.

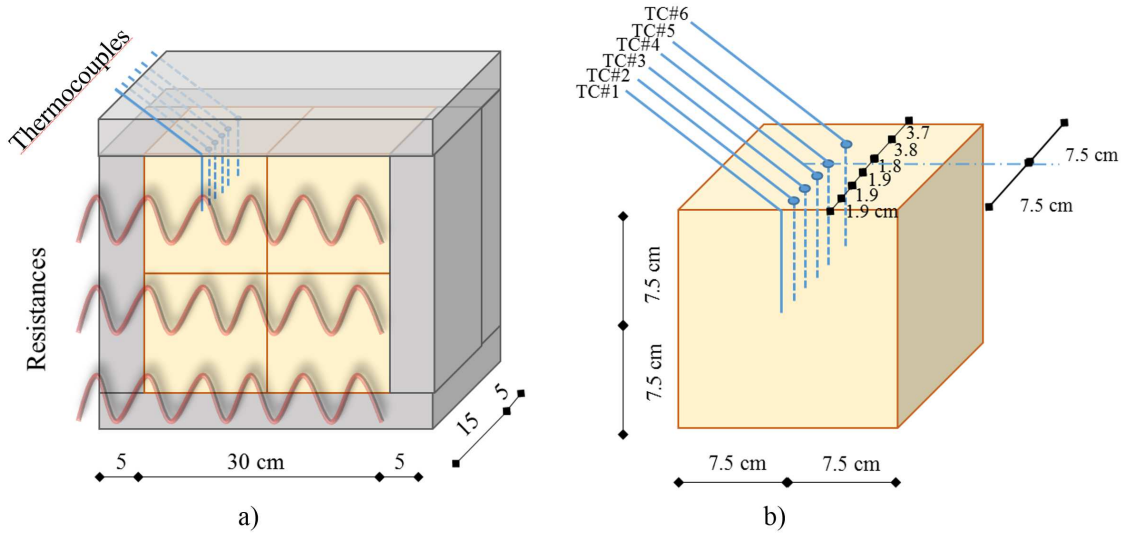

Figure 3.2. a) Heat insulation of concrete specimens in electrical furnace, b) positions of the K-type thermocouples used to monitor temperature change.

3.4.2. Re-curing Processes

After heating and cooling processes 3 specimens were subjected to air re-curing and 3 specimens were subjected to water re-curing for 28 days. Only the heated faces of water re-cured specimens were subjected to tap water. Air re-cured specimens were kept in laboratory environment which has a relative humidity of 65±10% and temperature of 20±2°C during re-curing period.

3.4.3. Macroscopic and Microscopic Observations

Visual changes on heated or fire exposed concrete give information about maximum temperature experienced and amount of deterioration of concrete [2, 63, 64]. In this study, spalling frequencies of heated specimens were examined, black pixel analyses were applied on air re-cured concrete cubes. Mass changes of concrete specimens were monitored at every stage after heating. Moreover, SEM/EDAX observations and TGA and XRD analyses were conducted on powder samples obtained from concrete cubes. The details will be given below.

3.4.3.1. Mass Change Measurements. Cubic concrete specimens were initially weighted before heating and the specimens were weighted again after heating and cooling process and following the water and air re-curing processes.

3.4.3.2. Black Pixel Analysis. Crack development during air re-curing was monitored by taking photos of heated surfaces at every hour for a week. A high resolution DSLR camera and a 100 mm macro lens were used in order to obtain detailed images. As can be seen in Figure 3.3, these images were converted to 8-bit black and white images by using an image processing software called ImageJ and black pixel analyses (BPA) were conducted on them. Black pixels represent cracks, air voids, surface delamination and shadow (due to positions of spotlights) on the heated surfaces of specimens. Total areas of black pixels were calculated for every images separately. Then these calculated values were divided to black pixel area of first image in order to obtain normalized area values. Finally, normalized area-time graphs were drawn for all concrete groups except the groups experienced spalling during heating and trend lines were fitted on the graphs as shown in Figure 3.4. These curves were used to monitor deterioration of concrete for 7 days. The slopes of fitted trend lines were called BPA rates and they were compared to compressive strength reduction ratios of air re-cured concrete groups.

3.4.3.3. SEM/EDAX Observations. In this study, only cementitious type was chosen as a parameter during micro level investigations since properties of microstructure mostly depend on types of cementitious materials and aggregates used in concrete mixes. Therefore, SEM investigations were conducted on air entrained PP fiber reinforced concrete groups (CAP, SAP and FAP). Samples were obtained from the heated surface and center of concrete cubes. An environmental scanning electron microscope (Philips XL30 ESEM-FEG/EDAX) was used to understand the morphological changes in concrete.

3.4.3.4. XRD Analysis. XRD analyses were conducted on air entrained PP fiber reinforced Portland cement concrete. Samples were obtained from the surface of a specimen before heating and heated surfaces of specimens after heating. Unfortunately, further

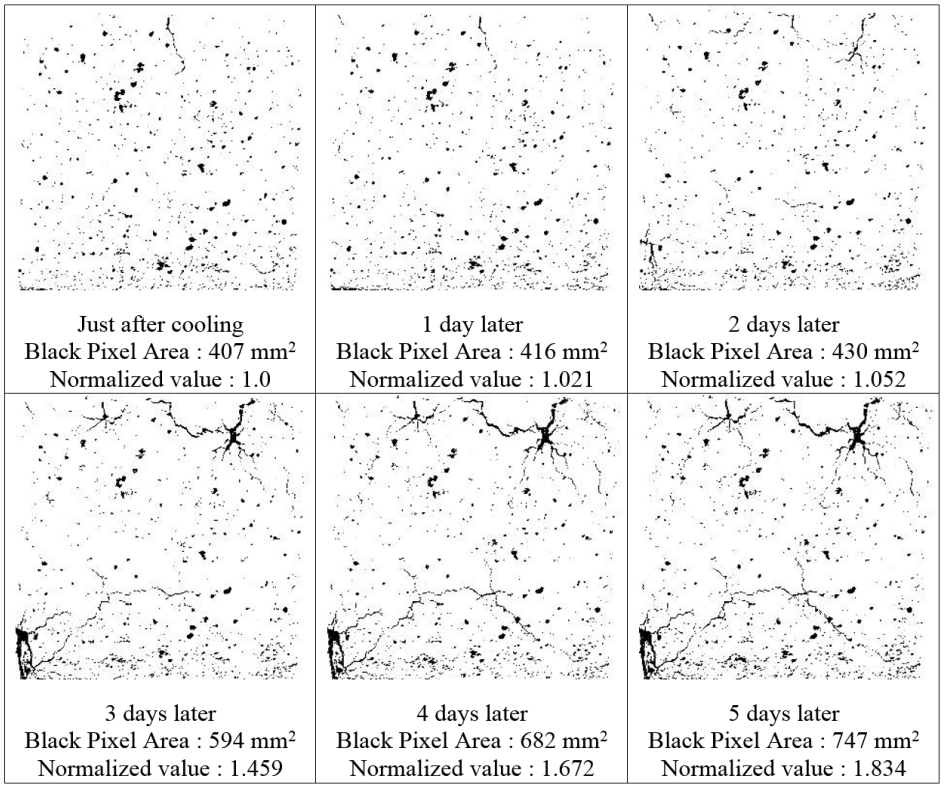

Figure 3.3. Crack growth monitoring on black and white images captured from C0P specimen during air re-curing.

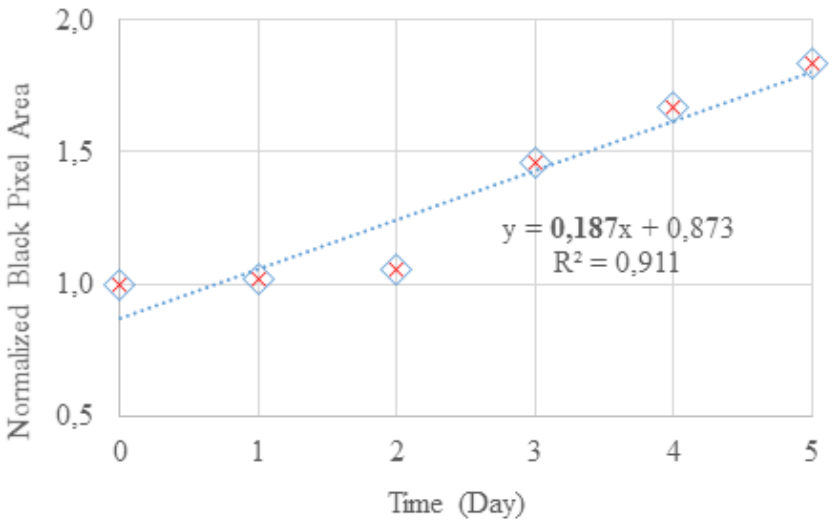

Figure 3.4. BPA value of C0P specimen.

investigations could not be done on other types of cementitious concrete groups. Because of the fact that, XRD analyses were suspended in Advanced Technologies Research and Development Center for long period of time since XRD specialist quitted ATRD center.

3.4.3.5. Thermogravimetric Analysis. In order to determine phase changes such as $CaO/Ca(OH)_2$ and $CaO/CaCO_3$ conversions in concrete after heating and re-curing periods, thermogravimetric analyses were also conducted on powder samples. Similar to SEM analyses, TGAs were conducted on air entrained PP fiber reinforced concrete groups (CAP, SAP and FAP). Samples were obtained from the heated surface and center of concrete cubes. After analyses, TGA curves and differential thermal analysis curves were obtained.

3.4.4. Residual Compressive Strength and Modulus of Elasticity Measurements

Compression tests were carried out on cubic concrete specimens before heating, after cooling and after re-curing periods in order to evaluate changes in mechanical properties of concrete. During tests, a compression press which has 3000 kN of maximum loading capacity was used and loading rate was set as 0.6 MPa/s. Also, a compressometer frame which includes two LVDTs was used on cubic concrete specimens to be able to measure length changes and to determine modulus of elasticity, as seen in Figure 3.5. The compressometer frame was removed after 40% of ultimate strength of concrete specimens was reached and tests continued until failure occurred to determine compressive strength values.

3.5. Tests on Reinforced Concrete Beams

Disintegration and recovery of concretes were also investigated on reinforced concrete (RC) beams. Therefore, 4 different concrete groups were chosen according to results of small sized concrete groups. These groups were CAP, CAH, SAP and SAH

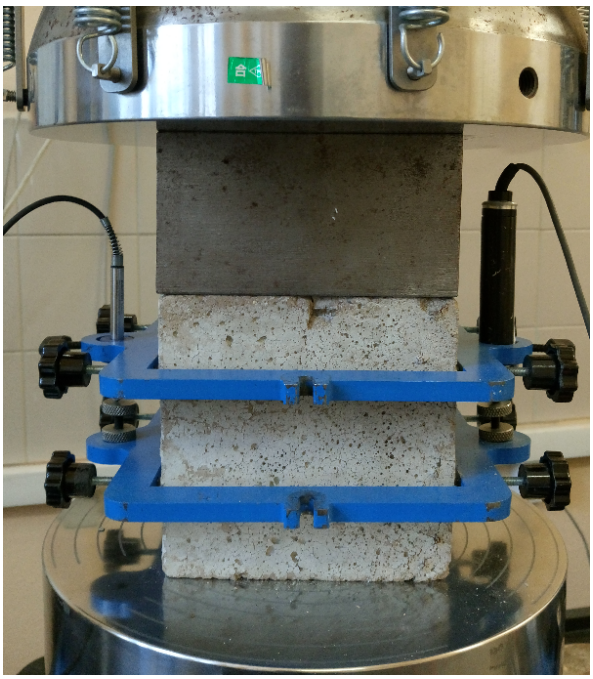

Figure 3.5. Compression test setup.

since they had less probabilities of spalling during heating. 4 RC beams were produced for each of concrete group. Totaly 16 RC beams with dimensions of 20x25x180cm were produced. 4 of them were used to determine initial properties before heating, remaining 12 beams were subjected to heating. After heating 4 of heated beams were used to determine the properties at after cooling stage and remaining 8 beams were subjected to re-curing (4 beams for water re-curing and 4 beams for air re-curing). S420 ribbed steel bars were used in RC beams as can be seen in Figure 3.6. Minimum cover thicknesses were determined according to Eurocode 2 as shown in Figure 3.7 [19].

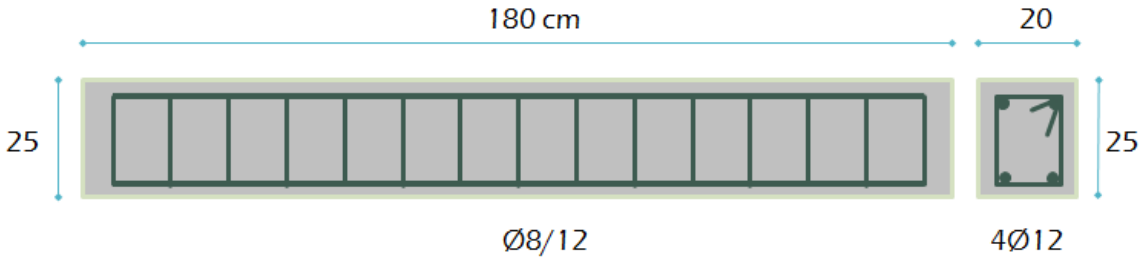

Figure 3.6. Reinforcing bar configuration.

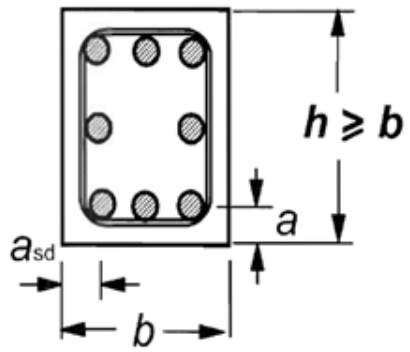

Standard fire resistance	Minimum dimensions (mm)						
	Possible combinations of a and b_{min} where a is the average axis distance and b_{min} is the width of beam				Web thickness b_w		
					Class WA	Class WB	Class WC
1	2	3	4	5	6	7	8
R 120	b_{min}= 200 a = 65	240 60	300 55	500 50	130	120	120
$a_{sd} = a + 10mm$							

Figure 3.7. Minimum dimensions and axis distances for simply supported beams made with reinforced and prestressed concrete [19].

3.5.1. Heating Procedure

Fire test was done in Efectis Era Laboratories in Tuzla/İstanbul. Two aerated concrete beams were used as supports in order to obtain simply supported beam structure. 12 reinforced concrete beams were placed on these supports and clear span length was 140 cm. Before heating reinforced concrete beams were insulated with ceramic fiber blanket. The front view of test set up was schematized in Figure 3.8 and the side view of test set up was schematized in Figure 3.9. Temperature of testing room was increased according to IS0-834 cellulosic fire scenario for 120 minutes as can be seen in Figure 3.10.

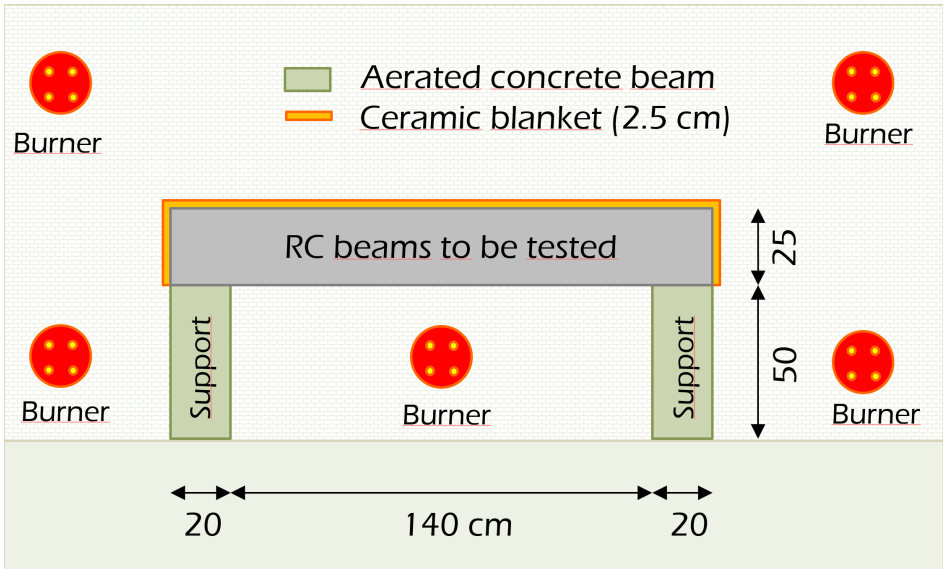

Figure 3.8. Schematized front view of fire test set up.

3.5.2. Re-curing Processes

After heating beams were transferred to Structure Laboratory in Boğaziçi University. 4 beams were tested to determine properties at the after cooling stage and remaining 8 beams were subjected to re-curing. Air re-cured beams were kept in laboratory environment and water re-cured beams were placed on two supports had a thickness of 1cm in a water pool which had a water level of 3cm.

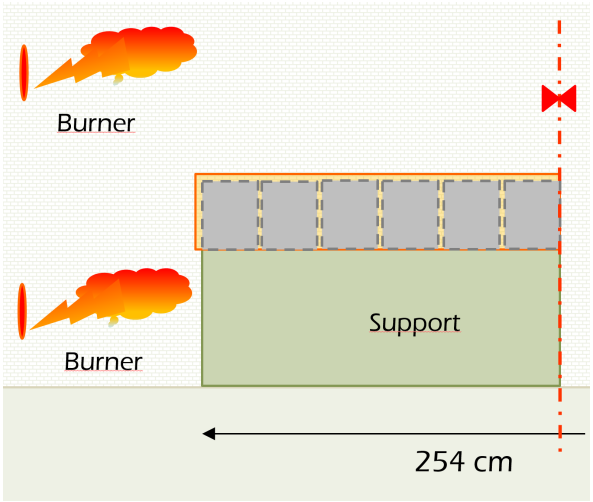

Figure 3.9. Schematized side view of fire test set up.

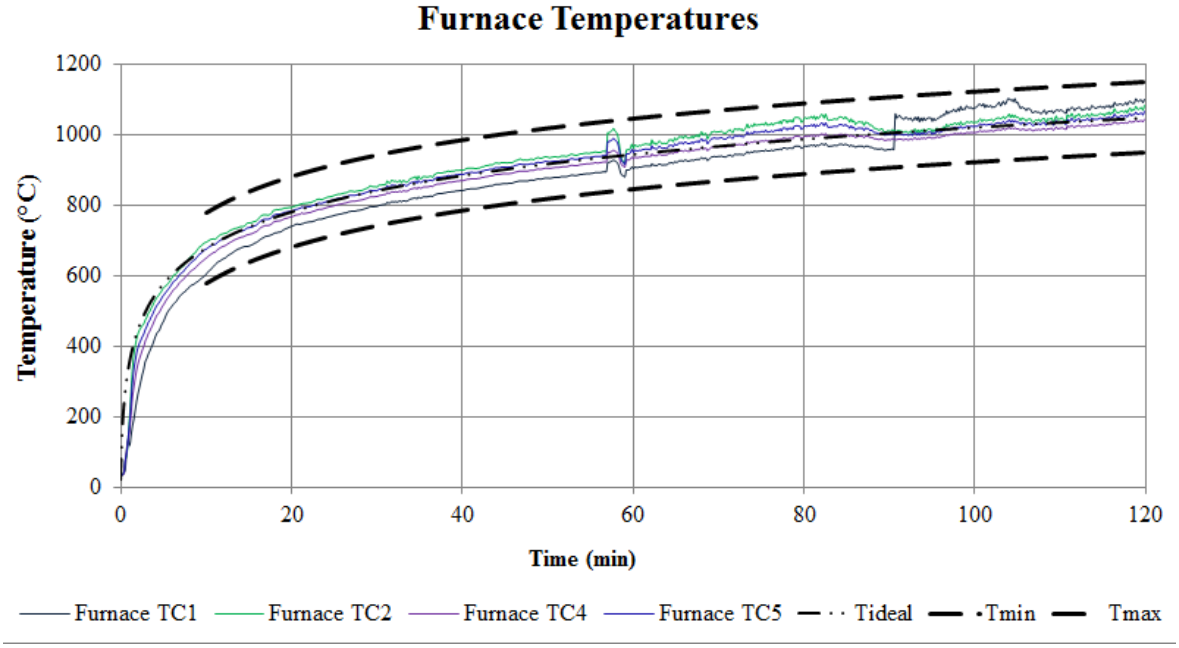

Figure 3.10. Heating scenario of reinforced concrete beams according to ISO-834 cellulosic fire.

3.5.3. SEM/EDAX Observations

As aforementioned before, only cementitious material type was chosen as a parameter during micro level investigations since properties of microstructure mostly depend on types of cementitious materials and aggregates used in concrete mixes. Similar to SEM investigations of small sized concrete groups, SEM investigations of reinforced concrete beams were conducted on air entrained PP fiber reinforced concrete groups (CAP and SAP). Samples were taken from the bottom surface of beams and from the level of lower longitudinal reinforcing bar in order to conduct SEM investigation on them.

3.5.4. Residual Flexural Load Capacity and Flexural Rigidity Measurements

Four point bending tests were conducted on RC beams before heating, after cooling and at the end of air and water re-curing periods and load deformation graphs were drawn. During tests, incremental load was applied and 500kg was loaded on beam specimens in a minute. 2 LVDTs collected mid-span deflection data in millimeter at 8Hz. Loading set up of beam specimens was schematized in Figure 3.11.

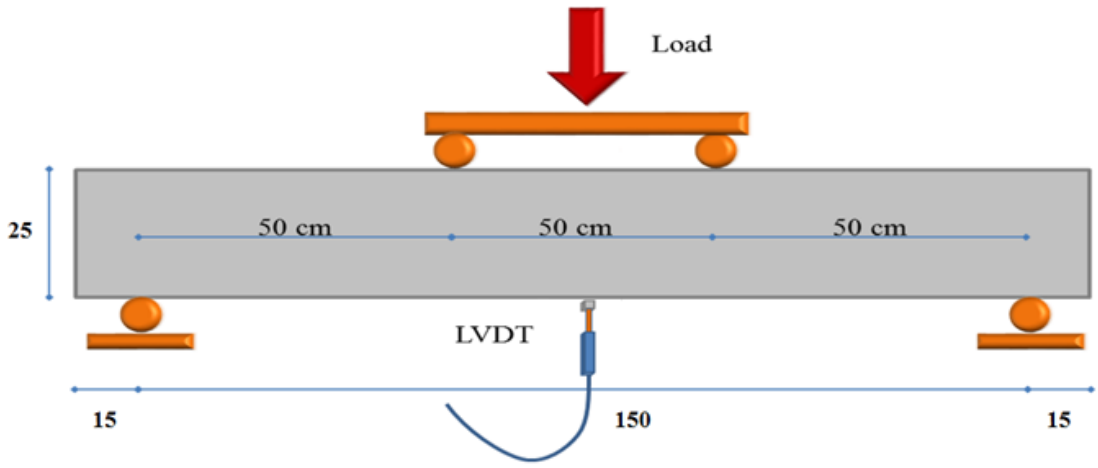

Figure 3.11. Schematized four point bending test set up.

4. TEST RESULTS OF SMALL SIZED SPECIMENS

In this study, the post fire behavior of concrete was investigated. For this purpose, 24 types of concrete were produced and two different types of re-curing methods were applied after cooling. 15 cubic specimens with dimensions of 15x15x15 cm were produced for every concrete groups. One day after production, specimens were demolded and placed in curing water for 27 days. Then they were conditioned in laboratory environment for additional 2 months before tests [4, 26, 62]. 3 cubic specimens were used to determine initial properties of concrete before heating. Remaining 12 cubic specimens were heated to 1000°C. 3 of them were used to monitor temperatures in concrete cubes during heating, 3 of them were tested to determine properties after cooling and remaining 6 cubic specimens were subjected to air and water re-curing. Additionally, 6 more cube specimens were produced by using CAH, SAH and FAH concrete groups in order to see the long term effect of re-curing. Finally, CAH, SAH and FAH groups had 21 and remaining groups had 15 specimens to test and therefore total number of cube specimens was 378. Flow chart of the study can be seen in Figure 4.1.

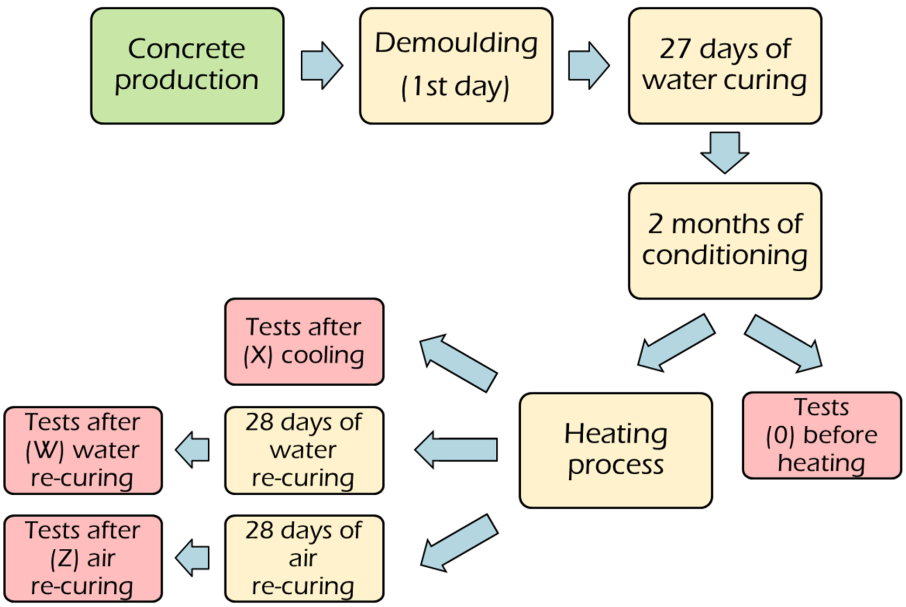

Figure 4.1. Flow chart of the study.

Crack development and mass changes of concrete specimens were monitored at every stage after heating. Microstructural changes in different concrete types were also investigated. For this purpose, small samples were taken from the concrete specimens before heating, after cooling, after air re-curing and after water re-curing. SEM/EDX, XRD and TGA investigations were conducted on these samples.

4.1. Fresh State Properties

After mixing of materials slump tests and unit weight measurement were conducted on fresh concrete. Slump tests results and unit weights of fresh concrete can be seen in Table 4.1, Table 4.2 and Table 4.3.

Table 4.1. Fresh state properties of PC groups.

Group	**Slump (cm)**	**Unit Weight** (kg/m^3)
C00	20	2.397
C0S	18	2.424
C0P	20	2.366
C0H	20	2.415
CA0	19	2.342
CAS	19	2.343
CAP	20	2.292
CAH	20	2.317
Average	19.5	2.362

4.2. Thermocouple Monitoring

4 concrete cubes were used during each set of heating and K-Type thermocouples were placed in one of them. Temperatures at the surface and inside of the concrete were monitored during both heating and cooling period. Maximum temperatures measured during heating part (first 200 minutes of heating) and measured during heating and cooling parts (first 200 minutes and 150 minutes of cooling in furnace) were determined

Table 4.2. Fresh state properties of PC+GGBFS groups.

Group	**Slump (cm)**	**Unit Weight** (kg/m^3)
S00	19	2.382
S0S	19	2.404
S0P	19	2.390
S0H	19	2.373
SA0	21	2.320
SAS	20	2.294
SAP	21	2.281
SAH	20	2.273
Average	19.8	2.340

Table 4.3. Fresh state properties of PC+PFA groups.

Group	**Slump (cm)**	**Unit Weight** (kg/m^3)
F00	20	2.411
F0S	19	2.437
F0P	19	2.380
F0H	19	2.412
FA0	20	2.335
FAS	19	2.374
FAP	20	2.301
FAH	20	2.324
Average	19.5	2.372

for every set of heating. Since every concrete groups had 3 sets of heating finally 3 maximum data for the heating parts and 3 maximum data for the total heating and cooling parts were obtained for one concrete group. In order to have a one single value at every parts of heating average of these 3 data obtained during heating and average of other 3 data obtained during both heating and cooling were calculated. Monitored temperatures during heating part at various depths of Portland cement concrete, concrete incorporating GGBFS and concrete incorporating PFA can be seen in Table 4.4, Table 4.5 and Table 4.6, respectively.

Table 4.4. Maximum temperatures at predefined depths from the surface after 200 minutes of heating, PC Groups.

Thermocouple No#	**TC#1**	**TC#2**	**TC#3**	**TC#4**	**TC#5**	**TC#6**
Depth (mm)	0	19	38	57	75	113
C00 (°C)	1000	761	581	483	398	358
C0S (°C)	1000	781	608	496	417	380
C0P (°C)	1000	756	584	471	393	353
C0H (°C)	1000	762	589	468	408	364
CA0 (°C)	1000	735	526	432	362	316
CAS (°C)	1000	743	575	441	368	334
CAP (°C)	1000	754	605	477	386	344
CAH (°C)	1000	778	617	491	397	335

According to the results surface temperatures reached 1000°C in all the concrete groups after 200 minutes of heating and monitored temperatures decreased as the depth of measurement increased since one face heating conditions were simulated in the electrical furnace. Moreover, concrete groups without air entrainment experienced at least 353°C and concrete groups with air entrainment experienced at least 313°C at the inner parts after 200 minutes of heating. Overall results showed that air entrained groups experienced less temperatures than concrete groups without air entrainment. In order to understand better the effect of air entrainment, average values of all concrete groups without air entrainment and average values of all concrete groups with air

Table 4.5. Maximum temperatures at predefined depths from the surface after 200 minutes of heating, PC+GGBFS Groups.

Thermocouple No#	**TC#1**	**TC#2**	**TC#3**	**TC#4**	**TC#5**	**TC#6**
Depth (mm)	0	19	38	57	75	113
S00 (°C)	1000	-	-	-	-	-
S0S (°C)	1000	781	609	516	452	389
S0P (°C)	1000	788	580	503	429	378
S0H (°C)	1000	773	594	502	438	374
SA0 (°C)	1000	-	-	-	-	-
SAS (°C)	1000	757	568	469	387	318
SAP (°C)	1000	751	559	470	377	313
SAH (°C)	1000	732	550	435	363	319

Table 4.6. Maximum temperatures at predefined depths from the surface after 200 minutes of heating, PC+PFA Groups.

Thermocouple No#	**TC#1**	**TC#2**	**TC#3**	**TC#4**	**TC#5**	**TC#6**
Depth (mm)	0	19	38	57	75	113
F00 (°C)	1000	-	-	-	-	-
F0S (°C)	1000	-	-	-	-	-
F0P (°C)	1000	735	620	533	452	425
F0H (°C)	1000	759	631	551	478	454
FA0 (°C)	1000	-	-	-	-	-
FAS (°C)	1000	-	-	-	-	-
FAP (°C)	1000	761	605	527	445	394
FAH (°C)	1000	722	599	535	452	425

entrainment were calculated and were given Table 4.7 for the first 200 minutes of heating. When the temperature data at various depths were compared it can be seen that differences between concrete without air entrainment and air entrained concrete increase as the depth of measurement increases.

Table 4.7. Average temperature values at predefined depths from the surface (at the end of the 200 minutes heating period).

Thermocouple No#	**TC#1**	**TC#2**	**TC#3**	**TC#4**	**TC#5**	**TC#6**
Depth (mm)	0	19	38	57	75	113
Concrete Groups Without AEA (°C)	1000	764	603	509	436	395
Concrete Groups With AEA (°C)	1000	747	581	483	401	353
Difference (°C)	0	17	22	26	35	42

However, temperature of the inner parts of concrete continued to increase for a while during cooling of the furnace since temperature of the furnace was higher than inner parts of concrete. Therefore, measured maximum temperatures after both heating and cooling (200 minutes of heating and 150 minutes of cooling) increased at various depths of PC concrete, concrete incorporating GGBFS and concrete incorporating PFA as given in Table 4.8, Table 4.9 and Table 4.10, respectively. Moreover, concrete groups without air entrainment experienced at least 578°C and concrete groups with air entrainment experienced at least 534°C at the inner parts after both heating and cooling periods. When the whole of heating and cooling periods was considered it can be seen that concrete groups experienced at least 534°C which may result in severe strength losses [2, 4, 13]. Similarly, average temperature values of all the concrete groups without air entrainment and all the air entrained concrete groups at various depths were calculated and they were given in Table 4.11. When the total heating and cooling period was examined it can bee seen that difference (25°C) between concrete without air entrainment and air entrained concrete decreased at the deepest part when it was compared to difference (42°C) obtained after first part of heating.

Table 4.8. Maximum temperatures at predefined depths from the surface during total heating and cooling processes (200 minutes of heating and 150 minutes of cooling), PC Groups.

Thermocouple No#	**TC#1**	**TC#2**	**TC#3**	**TC#4**	**TC#5**	**TC#6**
Depth (mm)	0	19	38	57	75	113
C00 (°C)	1000	814	697	650	634	584
C0S (°C)	1000	817	713	668	644	602
C0P (°C)	1000	818	697	644	620	599
C0H (°C)	1000	799	670	617	600	578
CA0 (°C)	1000	782	625	579	559	534
CAS (°C)	1000	773	666	619	602	583
CAP (°C)	1000	770	659	614	590	564
CAH (°C)	1000	797	677	635	620	579

Table 4.9. Maximum temperatures at predefined depths from the surface during total heating and cooling processes (200 minutes of heating and 150 minutes of cooling), PC+GGBFS Groups.

Thermocouple No#	**TC#1**	**TC#2**	**TC#3**	**TC#4**	**TC#5**	**TC#6**
Depth (mm)	0	19	38	57	75	113
S00 (°C)	1000	-	-	-	-	-
S0S (°C)	1000	806	673	636	617	584
S0P (°C)	1000	821	672	641	623	591
S0H (°C)	1000	808	678	638	626	592
SA0 (°C)	1000	-	-	-	-	-
SAS (°C)	1000	798	651	617	600	569
SAP (°C)	1000	801	647	619	600	570
SAH (°C)	1000	780	645	611	599	572

Table 4.10. Maximum temperatures at predefined depths from the surface during total heating and cooling processes (200 minutes of heating and 150 minutes of cooling), PC+PFA Groups.

Thermocouple No#	**TC#1**	**TC#2**	**TC#3**	**TC#4**	**TC#5**	**TC#6**
Depth (mm)	0	19	38	57	75	113
F00 (°C)	1000	-	-	-	-	-
F0S (°C)	1000	-	-	-	-	-
F0P (°C)	1000	780	708	683	662	645
F0H (°C)	1000	801	704	693	660	644
FA0 (°C)	1000	-	-	-	-	-
FAS (°C)	1000	-	-	-	-	-
FAP (°C)	1000	791	676	649	620	607
FAH (°C)	1000	766	685	659	640	621

Table 4.11. Average temperature values at predefined depths from the surface (During 200 minutes heating and 150 minutes of cooling).

Thermocouple No#	**TC#1**	**TC#2**	**TC#3**	**TC#4**	**TC#5**	**TC#6**
Depth (mm)	0	19	38	57	75	113
Concrete Groups Without AEA (°C)	1000	805	691	657	636	608
Concrete Groups With AEA (°C)	1000	784	662	627	608	583
Difference (°C)	0	21	29	30	28	25

4.3. Spalling of Concrete

During heating, explosive spalling was observed in some concrete groups. If a concrete specimen preserved its integrity after heating it was counted as a survived specimen. Then survival frequencies of each concrete group were calculated as given in Table 4.12, Table 4.13 and Table 4.14. Moreover Figure 4.2 represents survival frequencies of all of the heated concrete groups. Results showed that plain concrete groups have higher tendency to spall during heat exposure.

Table 4.12. Survival frequencies of PC Groups.

PC Groups	**Number of Heated Specimens**	**Number of Spalling**	**Survival Frequency [%]**
C00	9	3	67
C0S	9	2	78
C0P	9	-	100
C0H	9	-	100
CA0	9	-	100
CAS	9	-	100
CAP	9	-	100
CAH	9	-	100

Usage of mineral admixtures increases the spalling risk of concrete [34]. Survival frequency was 67% in plain Portland cement concrete group (C00) on the other hand, all the specimens of plain concrete groups incorporating mineral admixtures (S00 and F00) spalled during heating. Moreover, all of the non-fibrous air entrained Portland cement concrete (CA0) specimens kept their stabilities during heating but survival frequencies of SA0 and FA0 were 44% and 0%, respectively. When all the heated specimens were considered, 7% of specimens of Portland cement concrete, 21% of specimens of concrete with GGBFS and 50% of concrete with PFA spalled during heating. This result was expected since using mineral admixture densifies microstructure and reduces permeability of concrete preventing evacuation of water vapour.

Table 4.13. Survival frequencies of PC+GGBFS Groups.

PC+GGBFS Groups	**Number of Heated Specimens**	**Number of Spalling**	**Survival Frequency [%]**
S00	9	9	0
S0S	9	1	89
S0P	9	-	100
S0H	9	-	100
SA0	9	5	44
SAS	9	-	100
SAP	9	-	100
SAH	9	-	100

Table 4.14. Survival frequencies of PC+PFA Groups.

PC+PFA Groups	**Number of Heated Specimens**	**Number of Spalling**	**Survival Frequency [%]**
F00	9	9	0
F0S	9	9	0
F0P	9	-	100
F0H	9	-	100
FA0	9	9	0
FAS	9	9	0
FAP	9	-	100
FAH	9	-	100

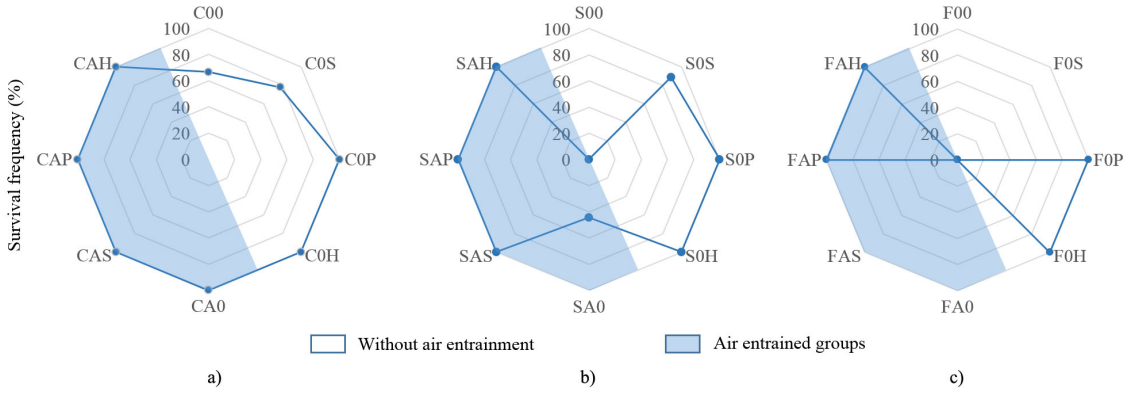

Figure 4.2. Survival frequencies of heated concrete groups produced by using a) only PC, b) PC+GGBFS and c) PC+PFA.

Effect of fiber addition on spalling resistance of concrete was also examined. None of the PP fiber and hybrid fiber reinforced concrete specimens spalled but spalling was observed in steel fiber reinforced concrete groups. 78% and 89% of steel fiber reinforced specimens of Portland cement group (C0S) and concrete group incorporating GGBFS (S0S) survived after heating, respectively. However, all the steel fiber reinforced specimens spalled during heating in concrete groups incorporating PFA (F0S and FAS). Another observation on steel fiber reinforced concrete is that spalling occurred at higher temperatures when it is compared to plain concrete groups. Temperature monitoring results showed that spalling started when the surface temperature of concrete was approximately 550°C in plain concrete groups while in steel fiber reinforced groups spalling started at the surface temperature around 650°C. Steel fibers may survive during heating and preserve some amount of tensile strength capacity of concrete [35]. However, continuous temperature rise in concrete results in higher pore pressure and thermal gradients. Finally, these stresses might exceed the tensile strength of concrete and some of concrete specimens eventually may fail. Therefore, using only steel fibers may not be considered as an effective way in terms of spalling.

4.4. Mass Change of Concrete

First free water in concrete evaporates then the chemically bonded water evaporates during heating. Carbon dioxide release of concrete starts due to the beginning of decarbonation of carbonates in concrete at around 600°C [2, 45, 46]. Therefore, total mass of a concrete specimen decreases prominently during heating to 1000°C. Also mass of concrete changes following to cooling since chemical reactions occur in concrete and moisture content of concrete increases. Table 4.15, Table 4.16 and Table 4.17 show the average residual mass percentages of Portland cement concrete groups, concrete groups incorporating GGBFS and concrete groups incorporating PFA, respectively. In this study, according to after cooling period mass loss measurements, specimens retained 92% of their initial masses in average. And at the end of air re-curing period, masses of the air re-cured specimens slightly increased and reached to 93% of their initial values. On the other hand, masses of water re-cured specimens exceeded their initial masses and reached to 100.5% of their initial values. This is probably due to the fact that, water could easily diffuse in concrete from the submerged face of the specimen due to increased porosity and permeability after heating. TGA results which will be given in the upcoming sections represent that significant part of this increase is chemically bonded water and carbon dioxide.

4.5. Surface Crack Monitoring

Heated surfaces of concrete specimens were evaluated after cooling in concrete groups incorporating PFA and specific cracks were chosen to monitor by using a light microscope. Firstly initial crack pictures were captured after cooling then specimens were placed their re-curing environment. Cracks were monitored once a week under a light microscope. Initial and final crack pictures of air re-cured specimens and water re-cured specimens were given in Figure 4.3 and Figure 4.4, respectively.

Crack numbers and size of existing cracks increased in monitored crack areas during air re-curing period. During air re-curing, a whitish dusty layer covered heated surface. Powder sample was taken from this layer and TGA was applied on powder

Table 4.15. Residual masses of PC Groups.

Groups	**After Cooling X (%)**	**Air Re-cured Z (%)**	**Water Re-cured W (%)**
C00	92.2	92.9	100.5
C0S	92.4	94.1	99.6
C0P	91.9	92.1	101.0
C0H	92.4	93.2	100.5
CA0	92.2	93.3	100.2
CAS	92.0	93.5	101.0
CAP	91.7	93.1	101.2
CAH	91.6	93.0	100.9
Average	92.1	93.2	100.6

Table 4.16. Residual masses of PC+GGBFS Groups.

Groups	**After Cooling X (%)**	**Air Re-cured Z (%)**	**Water Re-cured W (%)**
S00	-	-	-
S0S	91.6	92.4	100.6
S0P	91.3	91.7	100.9
S0H	91.3	92.1	100.5
SA0	89.6	91.0	100.1
SAS	91.1	91.9	100.6
SAP	90.7	91.7	101.2
SAH	90.9	91.8	101.3
Average	91.2	91.9	100.9

Table 4.17. Residual masses of PC+PFA Groups.

Groups	**After Cooling X (%)**	**Air Re-cured Z (%)**	**Water Re-cured W (%)**
F00	-	-	-
F0S	-	-	-
F0P	92.7	93.4	100.6
F0H	92.7	93.2	100.3
FA0	-	-	-
FAS	-	-	-
FAP	91.7	92.5	100.7
FAH	92.1	92.6	101.1
Average	92.3	92.9	100.7

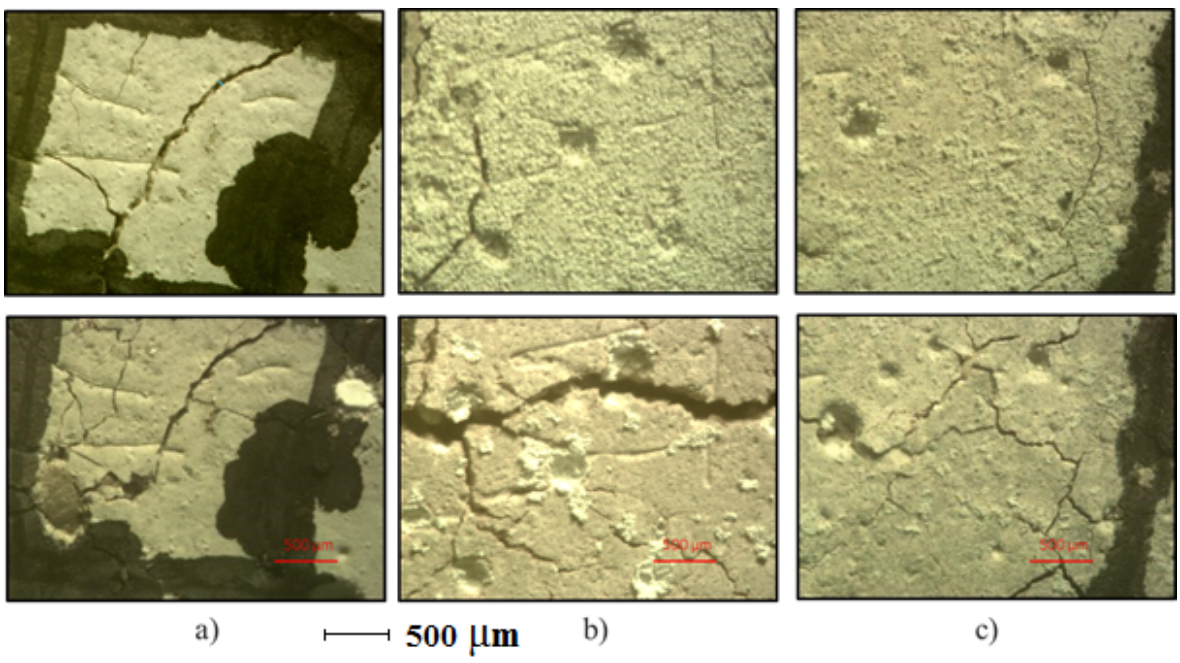

Figure 4.3. Initial and final crack pictures of air re-cured specimens a) F0H, b) FAP, c) FAH.

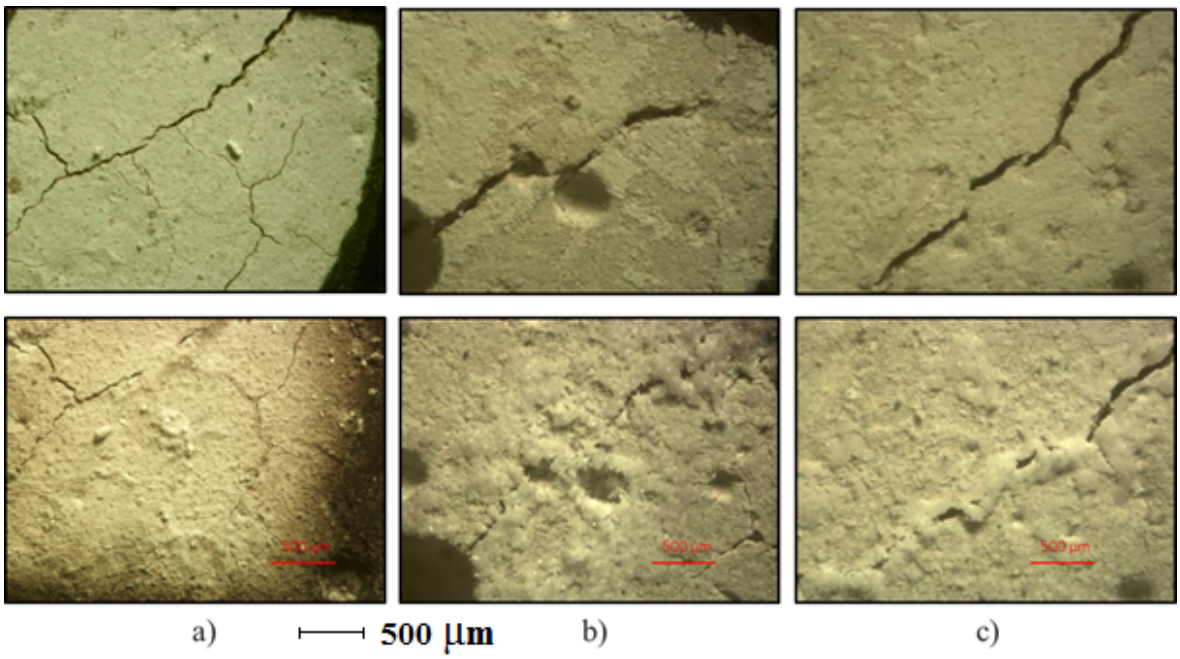

Figure 4.4. Initial and final crack pictures of water re-cured specimens a) F0H, b) FAP, c) FAH.

sample. TGA and differential thermal analysis (DTA) results can be seen in Figure 4.5. Peaks in DTA diagrams give information about the phase changes and transformations. DTA peaks of a concrete sample around 450°C represent $Ca(OH)_2$ dehydration and around 700°C represent $CaCO_3$ decarbonation [65–67]. Both peaks were observed on DTA diagram of air re-cured specimen. Measured mass loss around $Ca(OH)_2$ peak represents evaporated water and was shown as Δm_{CH} in Equation 4.1. Measured mass loss around $CaCO_3$ peak represents released carbon dioxide and was shown as Δm_{CC} in Equation 4.2. According to Equation 4.3 and Equation 4.4, the ratios between measured mass loses around $Ca(OH)_2$ and $CaCO_3$ peaks and actual amounts of $Ca(OH)_2$ and $CaCO_3$ can be calculated [68]. Based on this and by using given equations, the ratios between measured mass loses around $Ca(OH)_2$ and $CaCO_3$ peaks and actual amounts of $Ca(OH)_2$ and $CaCO_3$ can be calculated.

After calculations it was found that 42% of the sample was $Ca(OH)_2$ and 35% of the sample was $CaCO_3$. The critical thing is the presence of $Ca(OH)_2$ because of the

fact that $Ca(OH)_2$ is produced after rehydration of CaO with a 44% of volume increase which may give rise to disintegration of concrete [2, 40, 45]. Therefore, rehydration of CaO can be the reason of crack development on the heated surfaces of air re-cured specimens.

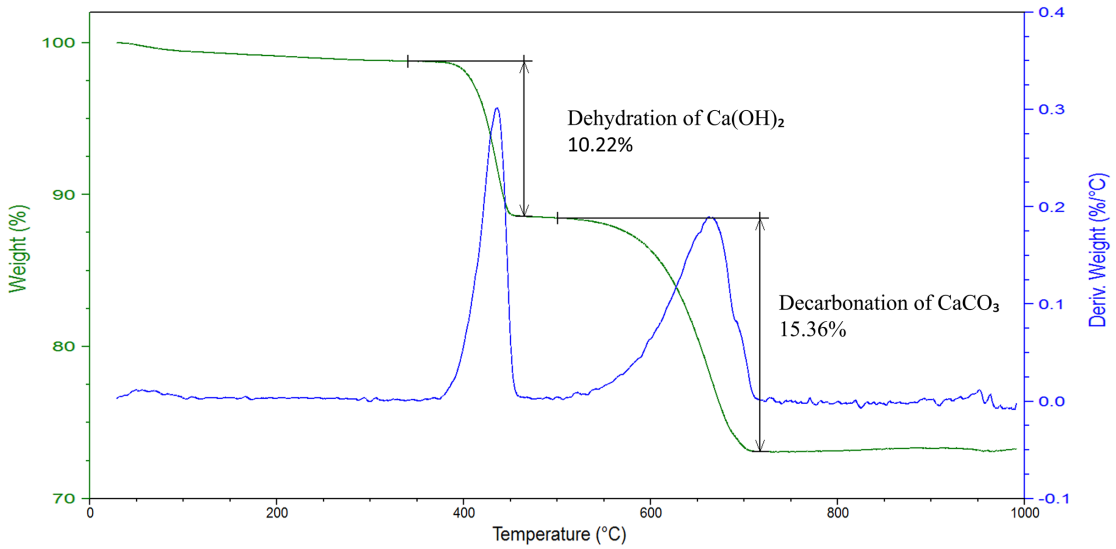

Figure 4.5. TGA and DTA diagrams of dust obtained from air re-cured concrete surface.

$$\underbrace{Ca(OH)_2}_{m_{CH}} \quad = \quad CaO \quad + \quad \underbrace{H_2O}_{\text{Measured mass change } \Delta m_{CH}} \tag{4.1}$$

$$\underbrace{CaCO_3}_{m_{CC}} \quad = \quad CaO \quad + \quad \underbrace{CO_2}_{\text{Measured mass change } \Delta m_{CC}} \tag{4.2}$$

$$m_{CH} = \Delta m_{CH} \times \frac{74g/mol}{18g/mol} \tag{4.3}$$

$$m_{CC} = \Delta m_{CC} \times \frac{100g/mol}{44g/mol} \tag{4.4}$$

On the other hand, some of the smaller cracks (smaller than 10 μm in width) disappeared after water re-curing period. Similar to air re-cured samples another whitish

layers were formed along the cracks which might fill the smaller cracks. Powder sample was also taken from this layer and TGA was applied on powder sample. TGA and differential thermal analysis (DTA) results can be seen in Figure 4.6. Only $CaCO_3$ peak was observed on DTA diagram and according to Equation 4.2 and Equation 4.4, $CaCO_3$ content was 94% of total mass of the sample. Since $Ca(OH)_2$ is soluable in water almost no $Ca(OH)_2$ precipitated on water re-cured surface of concrete. Therefore, further deterioration was stopped and specimens kept their stabilities during water re-curing period.

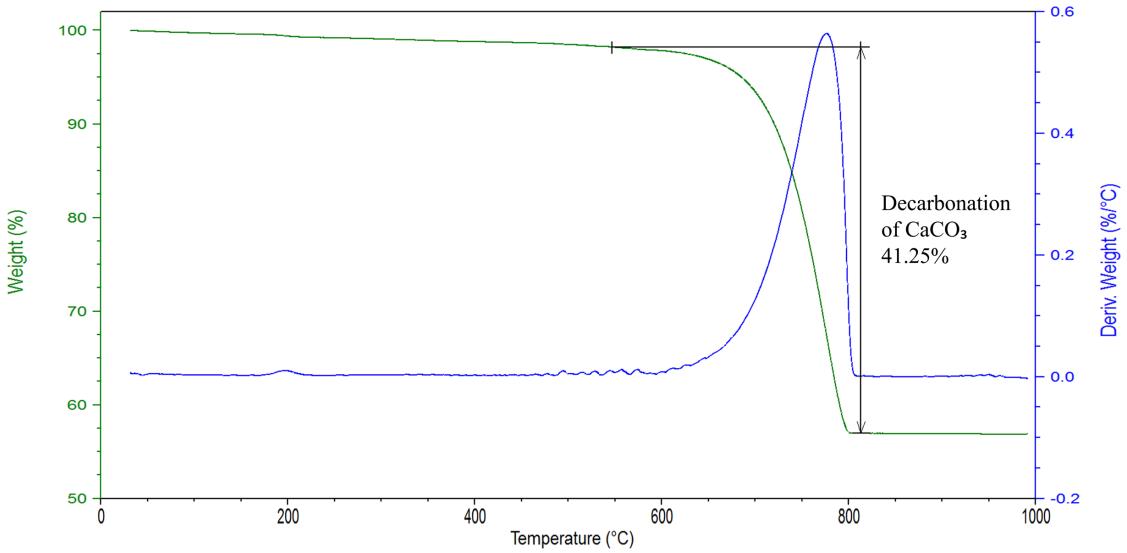

Figure 4.6. TGA and DTA diagrams of dust obtained from water re-cured concrete surface.

4.6. XRD Results

XRD results give information about the presence of phases and compounds in sample. XRD results of samples obtained from CAP group can be seen in Figure 4.7. According to results, C-S-H and $Ca(OH)_2$, (CH) disappeared after heating and calcium silicate, (CS) formations were observed on the heated surface. After air re-curing period, similar to TGA results $CaCO_3$, (calcite) and $Ca(OH)_2$, (CH) formations were observed on the surface. On the other hand, $CaCO_3$, (calcite) and C-S-H peaks can be seen on XRD diagram of sample obtained from water re-cured specimen. Also

the intensity of calcium silicate peak decreased after water re-curing since a part of them formed C-S-H after rehydration. As aforementioned, $Ca(OH)_2$, (CH) dissolved in curing water and its negative effect on heated surface due to expansion after rehydration was eliminated.

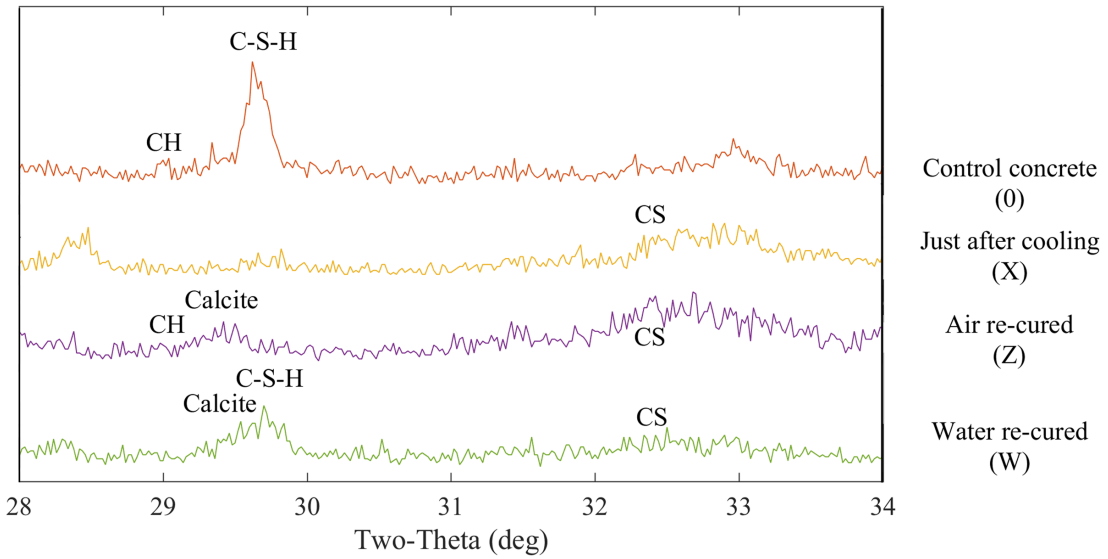

Figure 4.7. XRD results of samples obtained from CAP group.

4.7. SEM Observations

Changes in microstructure of concrete due to thermal applications determine the behavior of macroscopic material under specific conditions [69, 70]. Bonds between molecules can be broken with a temperature increase and breaking of most of the bonds occurs after 750°C [52,54]. Therefore, residual mechanical properties of concrete drastically decrease after 750°C [2,4,13,26,40,64]. In this study, only cementitious material type was chosen as a parameter during SEM investigation since properties of microstructure mostly depend on types of cementitious materials and aggregates used in concrete mixes. Therefore, samples were only taken from the air entrained PP fiber reinforced concrete groups (CAP, SAP and FAP). In order to understand morphological changes SEM/EDX and TGA were carried out on these samples. Conventional high vacuum scanning electron microscope was used to investigate surface morphol-

ogy. Therefore, secondary electrons (SE) were measured on platinum coated samples to obtain pure images and applied accelerating voltage (Acc V) and working distance (WD) were in the range of 12 kV–20 kV and 9.4 mm–13.3 mm, respectively. Since water re-cured samples were saturated before SEM, they were dried at 40°C in an oven for two hours not to have a vacuum problem.

4.7.1. Changes in C-S-H After Heating

During SEM investigations, C-S-H gels were traced via EDX analyses since the molar ratio of Ca/Si gives information about the existence and types of C-S-H [69, 71]. In literature it is reported that if C-S-H gel has a loose fibril-like morphology Ca/Si ratios up to a minimum of 0.6 can be measured. On the other hand, if C-S-H loses its extensions by forming dense granular-like morphology, measured Ca/Si values reported to be around 2.0 [71]. Evaluated SEM pictures of Portland cement concrete, concrete incorporating GGBFS and concrete incorporating PFA before heating and after cooling were given in Figure 4.8, Figure 4.9 and Figure 4.10, respectively.

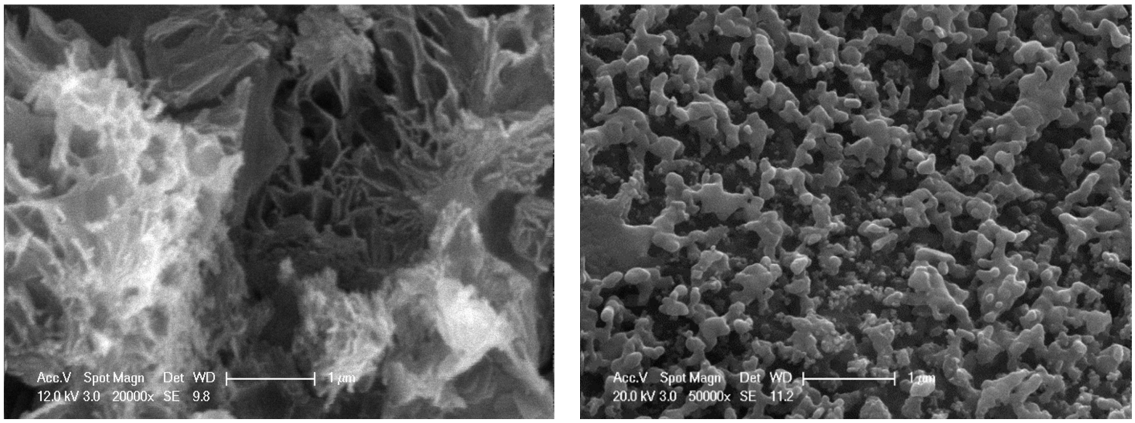

Figure 4.8. SEM pictures obtained from CAP a) before heating b) after heating and cooling.

When the specimens produced for this study was examined, initially, C-S-H gels were found to have sharp extensions in PC concrete and Ca/Si ratios were around

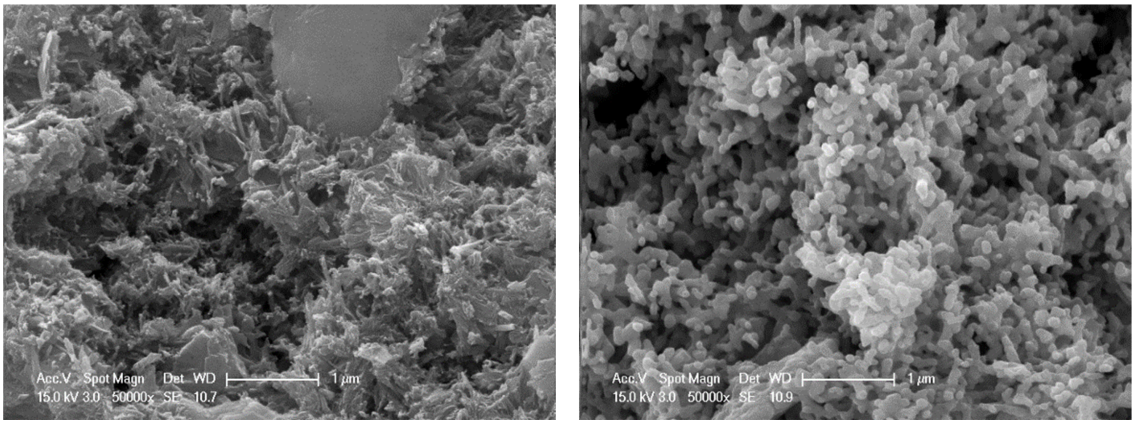

Figure 4.9. SEM pictures obtained from SAP a) before heating b) after heating and cooling.

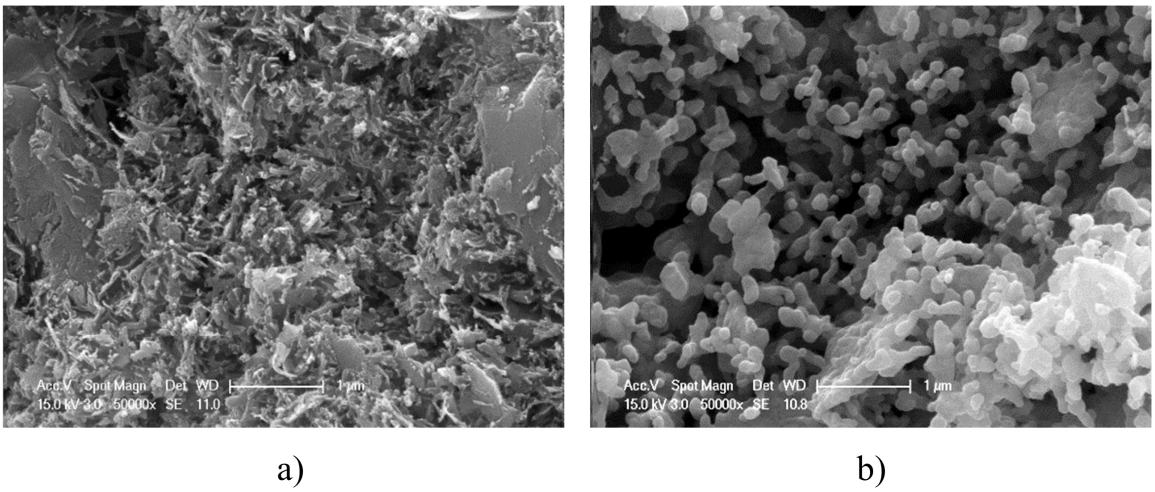

Figure 4.10. SEM pictures obtained from FAP a) before heating b) after heating and cooling.

1.3. On the other hand, in mineral added concrete groups, C-S-H gels were like dense granular particles and the molar ratios of Ca/Si of concrete incorporating GGBFS and concrete incorporating PFA were around 1.7 and 1.6, respectively. After heating, C-S-H gels shrank and densified and represented a granular form as can be seen in Figure 4.8.(b), Figure 4.9.(b) and Figure 4.10.(b) [69]. Lin *et al.* reported that C-S-H turned to C_2S (belite) and C_3S (alite) by losing its water molecules [52]. Also Ca/Si ratio has a tendency to increase after heating as Taylor stated in her book [72]. In this study, Ca/Si ratios increased and measured around 1.9, 1.9 and 1.7 in PC concrete, concrete with GGBFS and concrete with PFA, respectively.

4.7.2. Morphology of Concrete After Re-curing Periods

SEM investigations were conducted on samples obtained from heated surfaces of air re-cured and water re-cured concretes, Figure 4.11, Figure 4.12 and Figure 4.13. As can be seen in SEM pictures of air re-cured samples, after air re-curing period, forms of dehydrated C-S-H particles remained almost same for all concrete groups. On the other hand, prominent changes were observed in microstructures of water re-cured concrete. Mainly, granular formations seen after heating disappeared and new formations which have sharp extensions were observed in all concrete samples. These extensions probably occurred due to rehydration and carbonation and may play a role in recovery of concrete after water re-curing. For instance, one of the reason of this recovery was probably due to filling of cracks with $CaCO_3$ as monitored during SEM investigations, as seen in Figure 4.14.

4.7.3. Changes of Center of Concrete Specimens

SEM pictures obtained from the center of concretes after cooling can be seen in Figure 4.15. When monitored temperatures at the center (75 mm depth) of CAP, SAP and FAP were examined it can be understood that temperature at the center of concrete were around 600°C. Therefore, C-S-H gels lost high amount of water and shrank similar to surface level investigations. Measured molar ratios of Ca/Si values were around 1.5, 1.7 and 1.7 for CAP, SAP and FAP, respectively.

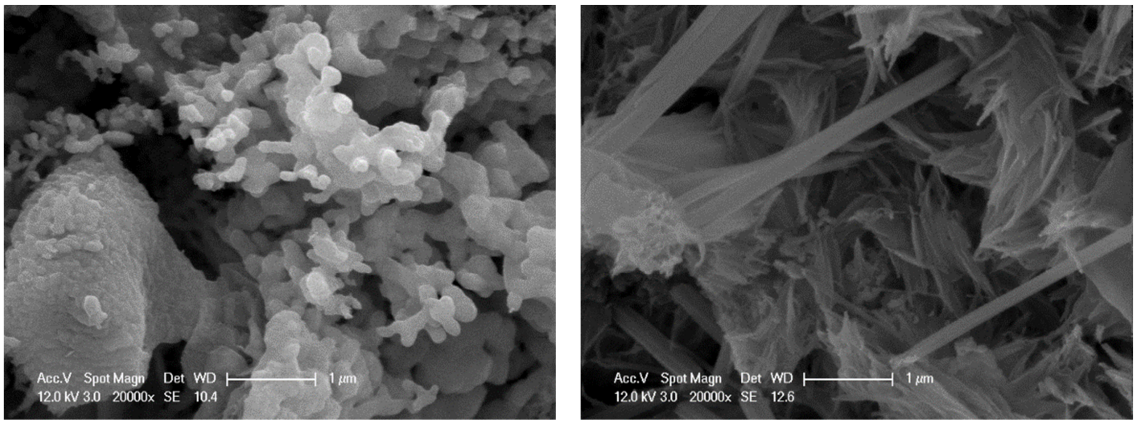

Figure 4.11. SEM pictures obtained from CAP after a) air re-curing b) water re-curing.

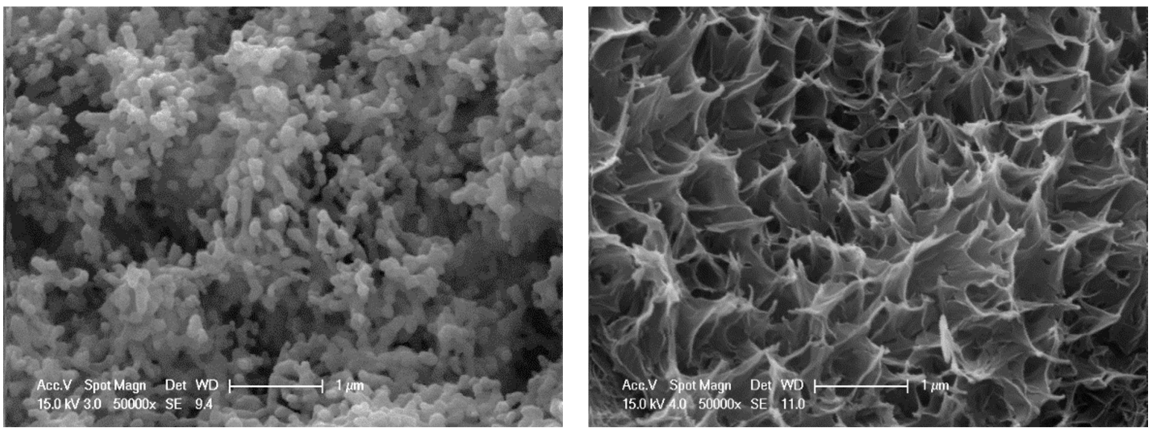

Figure 4.12. SEM pictures obtained from SAP after a) air re-curing b) water re-curing.

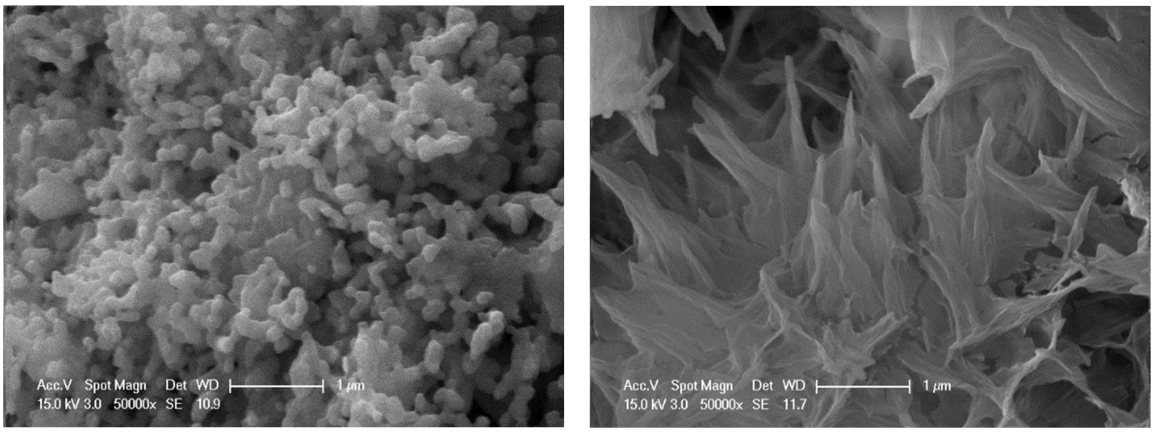

a) b)

Figure 4.13. SEM pictures obtained from FAP after a) air re-curing b) water re-curing.

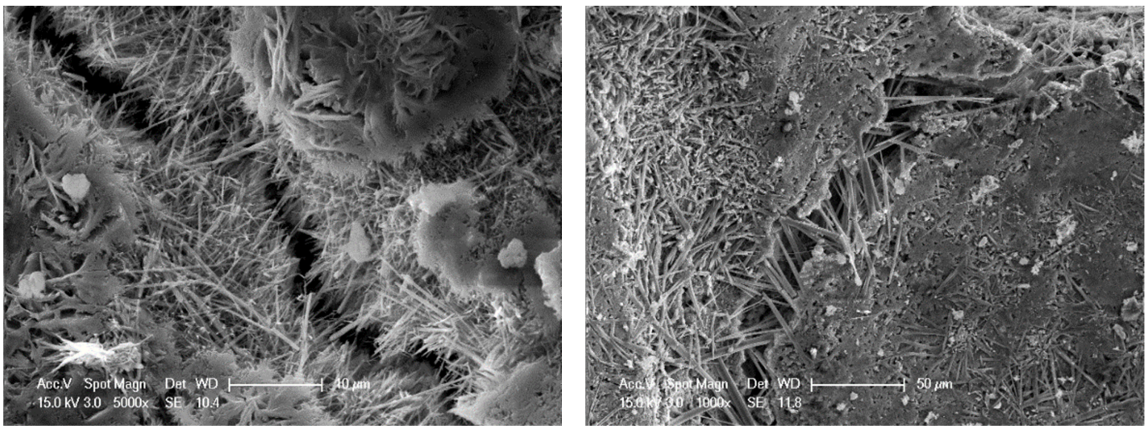

a) b)

Figure 4.14. Cracks filled with $CaCO_3$ after water re-curing.

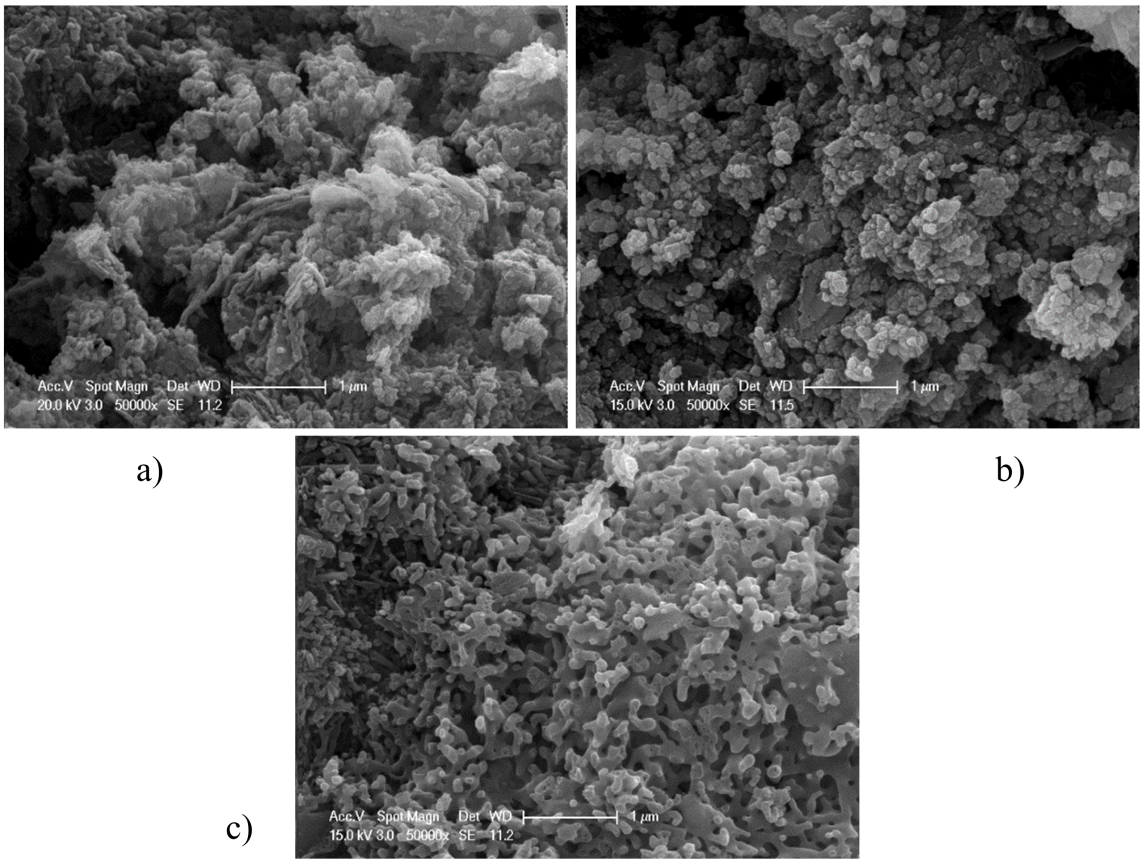

Figure 4.15. Microstructure of the center of concretes after cooling a) CAP, b) SAP, c) FAP.

After air re-curing period microstructure of concrete did not change prominently as can be seen in Figure 4.16. During SEM investigations almost no $Ca(OH)_2$ were observed on the samples obtained from the center of the air re-cured concrete specimens. On the other hand, new formations were observed on water re-cured samples. Newly formed C-S-H and $Ca(OH)_2$ crystals can be seen in Figure 4.17. This means that, although only the heated faces were subjected to water re-curing water molecules were able to diffuse in concrete via capillary action. At the surface level $Ca(OH)_2$ crystals were not common in water re-cured concrete since most of them dissolved in curing water.

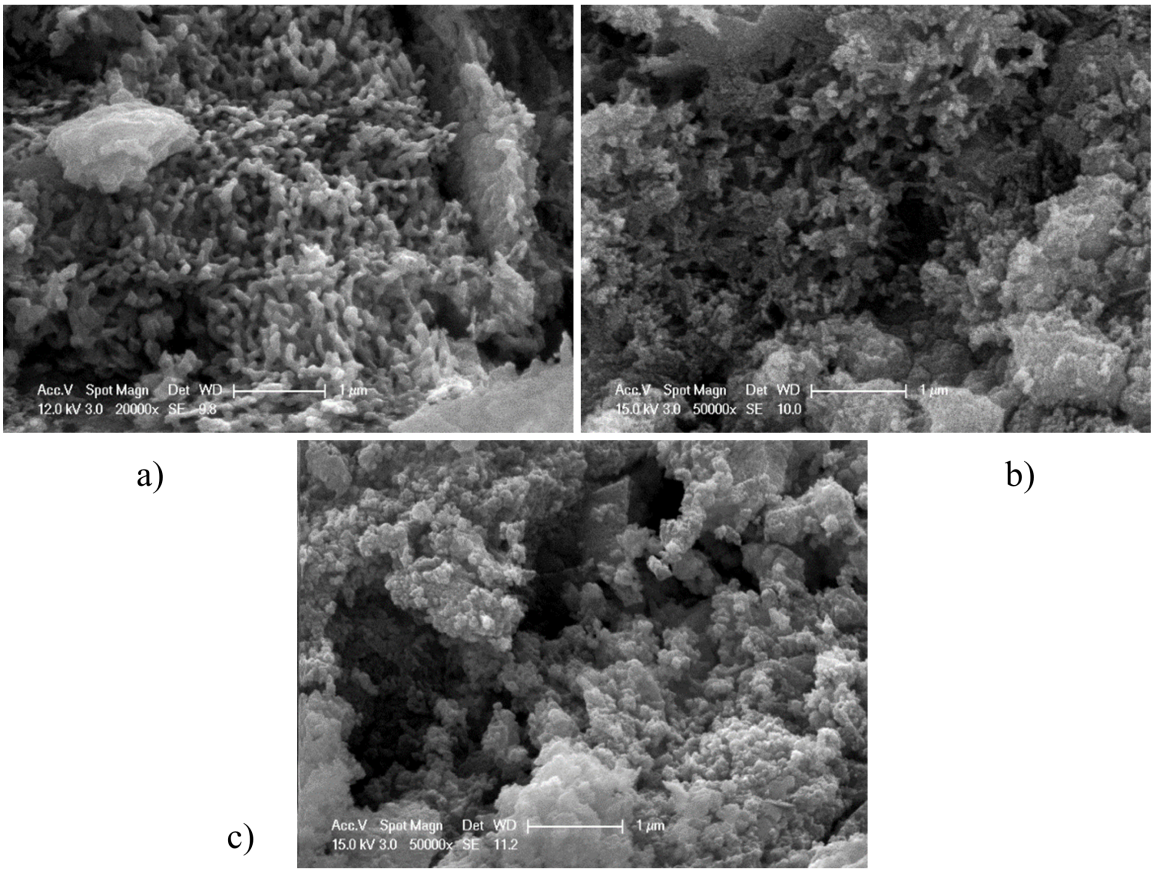

Figure 4.16. Microstructure of the center of air re-cured concrete a) CAP, b) SAP, c) FAP.

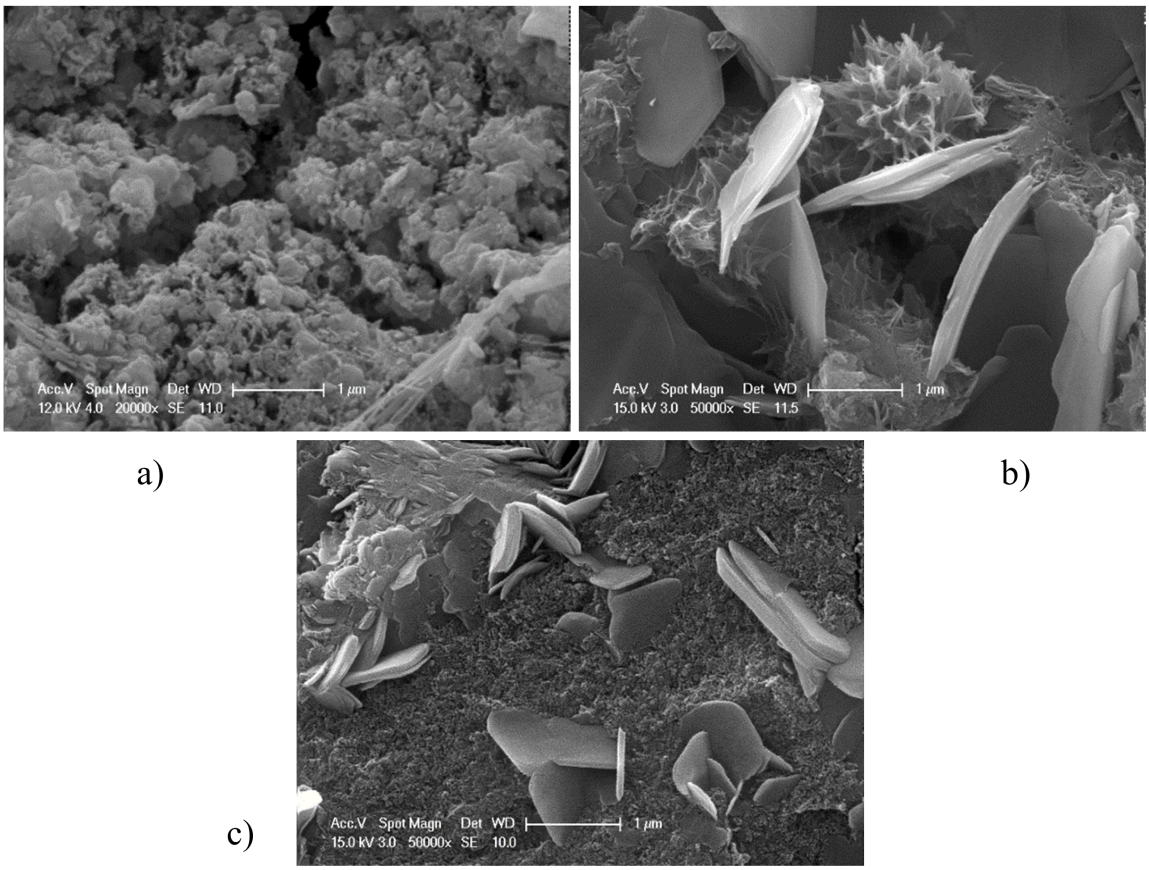

Figure 4.17. Microstructure of the center of water re-cured concrete a) CAP, b) SAP, c) FAP.

4.8. TGA Results

Concrete pieces were taken from the heated surfaces of specimens and they were pounded in a steel bowl in order to obtain powder samples. Thermogravimetric analyses were conducted on 15 mg of powder samples. Heating rate was 20°C/min and samples were heated to 800°C in Nitrogen atmosphere with a purge rate of 60 mL/min. Results of thermogravimetric analyses of Portland cement concrete, concrete incorporating GGBFS and concrete incorporating PFA were given in Figure 4.18, Figure 4.19 and Figure 4.20, respectively.

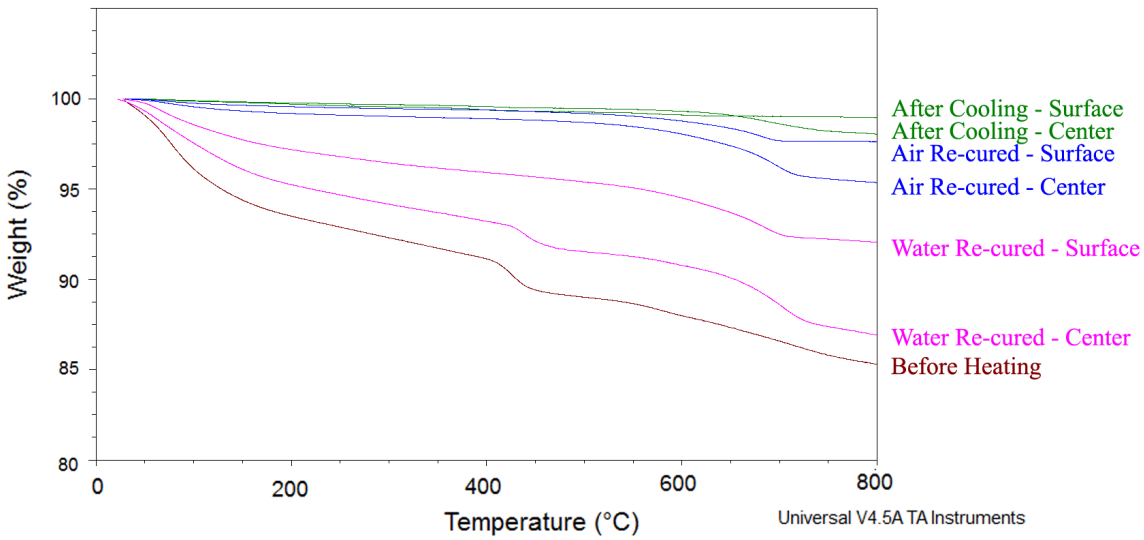

Figure 4.18. TGA results of Portland cement concrete.

After thermogravimetric measurements differential thermal analysis (DTA) diagrams of Portland cement concrete, concrete incorporating GGBFS and concrete incorporating PFA were drawn as can be seen in Figure 4.21, Figure 4.22 and Figure 4.23, respectively. Peaks in DTA diagrams give information about the phase changes and transformations. DTA peaks of a concrete sample around 450°C represent $Ca(OH)_2$ dehydration and around 700°C represent $CaCO_3$ decarbonation [65–67].

$Ca(OH)_2$ and $CaCO_3$ contents can be calculated by using mass loss data. Measured mass loss around $Ca(OH)_2$ peak represents evaporated water and measured mass

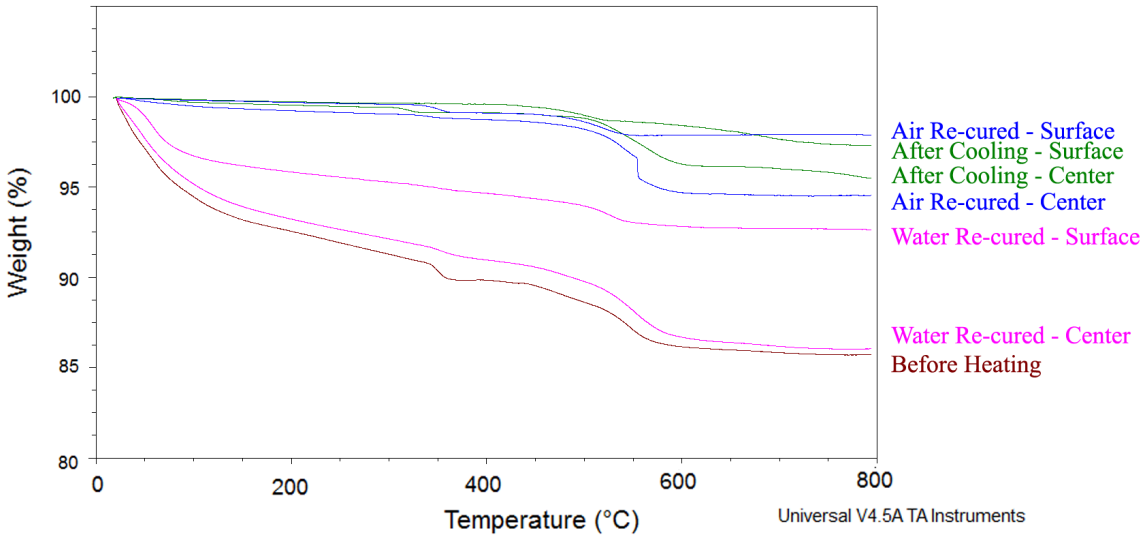

Figure 4.19. TGA results of concrete incorporating GGBFS.

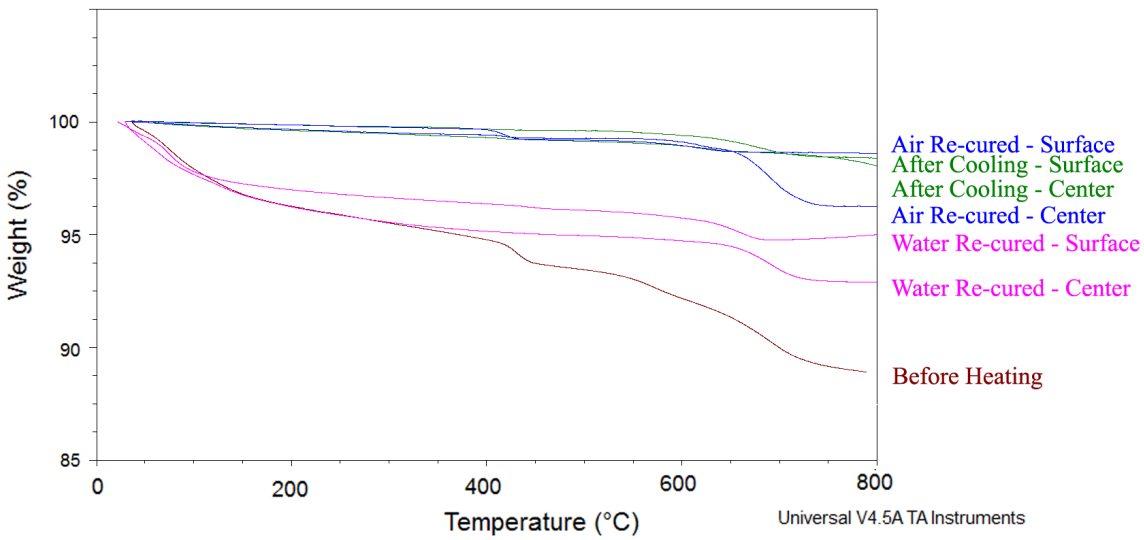

Figure 4.20. TGA results of concrete incorporating PFA.

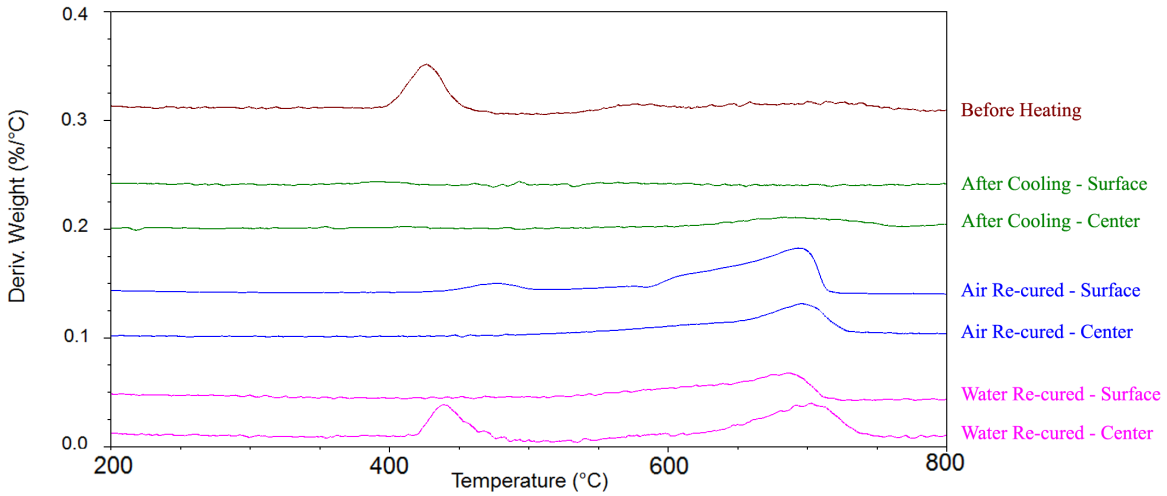

Figure 4.21. DTA diagrams of Portland cement concrete.

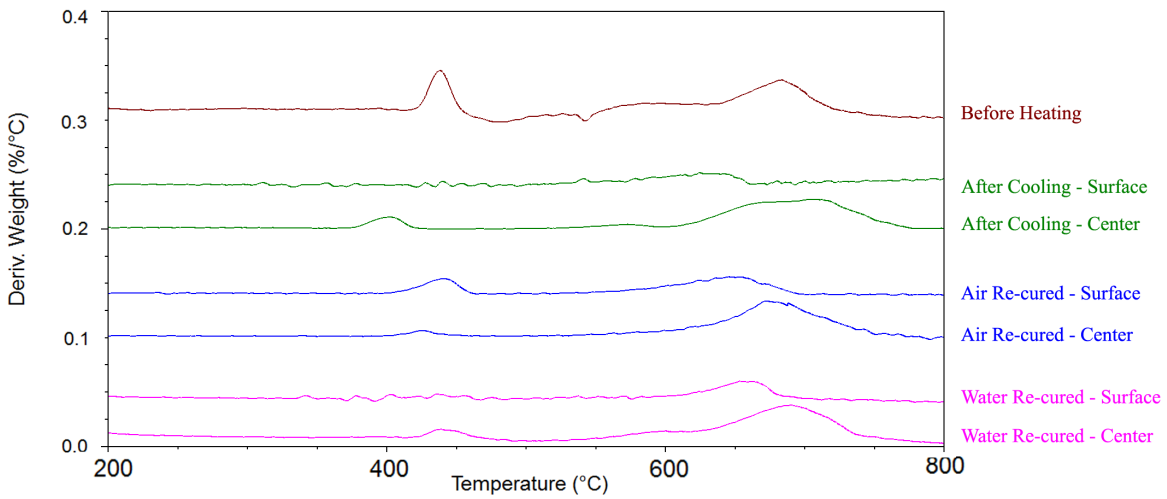

Figure 4.22. DTA diagrams of concrete incorporating GGBFS.

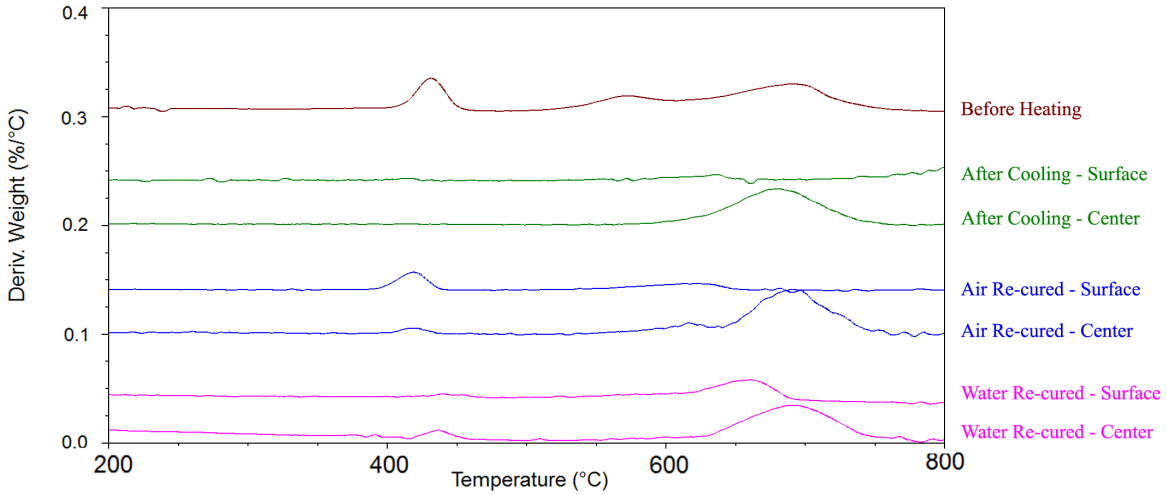

Figure 4.23. DTA diagrams of concrete incorporating PFA.

loss around $CaCO_3$ peak represents released carbon dioxide. According to Equation 4.1, Equation 4.2, Equation 4.3 and Equation 4.4 the ratios between measured mass loses around $Ca(OH)_2$ and $CaCO_3$ peaks and actual amounts of $Ca(OH)_2$ and $CaCO_3$ can be calculated.

Table 4.18 shows calculated $Ca(OH)_2$ and $CaCO_3$ contents of concrete samples before heating. According to the results, there were initially $Ca(OH)_2$ and $CaCO_3$ in all non-heated samples. Moreover, amount of $Ca(OH)_2$ measured in mineral added concrete samples is approximately 50% less than the measured amount of $Ca(OH)_2$ in Portland cement concrete. Table 4.19, Table 4.20 and Table 4.21 show calculated $Ca(OH)_2$ and $CaCO_3$ contents of concrete samples after cooling, after air re-curing and after water re-curing, respectively.

After cooling DTA diagrams showed that there were no $Ca(OH)_2$ and $CaCO_3$ in samples obtained from heated surfaces because of the fact that most of the crystals and gels deteriorated during heating. Since maximum temperature at the center of concrete specimens were around 600°C, at this part of concrete $CaCO_3$ did not totally decarbonated. Most of $Ca(OH)_2$ crystals dehydrated at this part of concrete. After air re-curing period both $Ca(OH)_2$ and $CaCO_3$ peaks reappeared. The presence of

Table 4.18. Calculated $Ca(OH)_2$ and $CaCO_3$ percentages in concrete samples before heating.

	Sample from	**Before Heating - 0**	
		$Ca(OH)_2$ (%)	$CaCO_3$ (%)
Portland Cement	Surface	8.3	5.8
	Center		
PC+GGBFS	Surface	4.3	6.4
	Center		
PC+PFA	Surface	4.5	7.1
	Center		

Table 4.19. Calculated $Ca(OH)_2$ and $CaCO_3$ percentages in concrete samples after cooling.

	Sample from	**After Cooling - X**	
		$Ca(OH)_2$ (%)	$CaCO_3$ (%)
Portland Cement	Surface	0.5	0.3
	Center	0.4	2.7
PC+GGBFS	Surface	0.1	1.6
	Center	1.2	6.2
PC+PFA	Surface	0.3	0.8
	Center	0.2	6.0

Table 4.20. Calculated $Ca(OH)_2$ and $CaCO_3$ percentages in air re-cured concrete samples.

	Sample from	**Air Re-cured - Z**	
		$Ca(OH)_2$ (%)	$CaCO_3$ (%)
Portland Cement	Surface	2.5	7.5
	Center	0.2	6.4
PC+GGBFS	Surface	2.0	2.7
	Center	0.9	5.7
PC+PFA	Surface	1.9	1.1
	Center	0.6	6.7

Table 4.21. Calculated $Ca(OH)_2$ and $CaCO_3$ percentages in water re-cured concrete samples.

	Sample from	**Water Re-cured - W**	
		$Ca(OH)_2$ (%)	$CaCO_3$ (%)
Portland Cement	Surface	0.1	7.0
	Center	6.1	8.0
PC+GGBFS	Surface	0.4	3.1
	Center	3.3	7.6
PC+PFA	Surface	0.1	2.9
	Center	1.4	6.2

$Ca(OH)_2$ on the surface of the heated specimen is hypothesized to be the reason of newly formed cracks due to its expansion history during air re-curing. Because of the fact that surface level of a concrete specimen was the weakest part of it after heating since surface of the specimens experienced 1000°C during heating. 2.5% of $Ca(OH)_2$ was found in sample obtained from Portland cement concrete surface and 2% of $Ca(OH)_2$ were found in samples obtained from mineral added concrete surfaces. $CaCO_3$ ratio reached 7.5% at the surface level of Portland cement concrete while less amount of carbonation was observed in mineral added concrete groups.

On the other hand, there were no $Ca(OH)_2$ peaks on DTA diagrams of water re-cured concrete samples obtained from surface level. Since $Ca(OH)_2$ is a soluble crystal in water [73], newly formed $Ca(OH)_2$ crystals can be dissolved in curing water. Absence of $Ca(OH)_2$ on the heated surfaces of concrete can result in a slowdown of new crack formation. Moreover, C-S-H formation was observed on water re-cured surface of concrete specimens via XRD analysis. Therefore, after water re-curing period specimens kept their stabilities and the numbers and sizes of existing cracks did not change. When centroidal part of water re-cured concrete specimens were evaluated $Ca(OH)_2$ peaks were observed similar to SEM investigation results. On the other hand, presence of $Ca(OH)_2$ at the inner parts of concrete is not severe as it is found on the surface level. Because, inner part of concrete is stronger than its surface level after heating and also expansion of CaO can be 3 dimensionally restrained by concrete itself. Contents of $Ca(OH)_2$ increased to 6.1% in Portland cement concrete while they were 3.3% and 1.4% in concrete incorporating GGBFS and concrete incorporating PFA, respectively. Less amount of $Ca(OH)_2$ in mineral added concrete groups can be the result of pozzolonic activity.

4.9. Residual Mechanical Properties of Concrete

Changes in morphology of concrete affect its mechanical properties [52, 74, 75], therefore compressive strength tests were conducted on concrete specimens before heating, after cooling and after re-curing processes. Mechanical properties of concrete groups deteriorated after heating. Residual compressive strength and modulus of elas-

ticity percentages were calculated by dividing the measured values after heating and re-curing to initial values measured before heating. Figure 4.24, Figure 4.25 and Figure 4.26 represent residual compressive strength percentages of all concrete types. During compression tests modulus of elasticity values of concrete groups were also determined and residual modulus of elasticity percentages of all concrete types were given in Figure 4.27, Figure 4.28 and Figure 4.29. Compression tests could not be done after heating in five groups (S00, F00, F0S, FA0 and FAS) since all of the specimens of these groups spalled during heating processes. Moreover, survived specimens of SA0 group had severe damage since many of the specimens of this group spalled during heating. Therefore, relatively lower mechanical properties were measured in SA0 group.

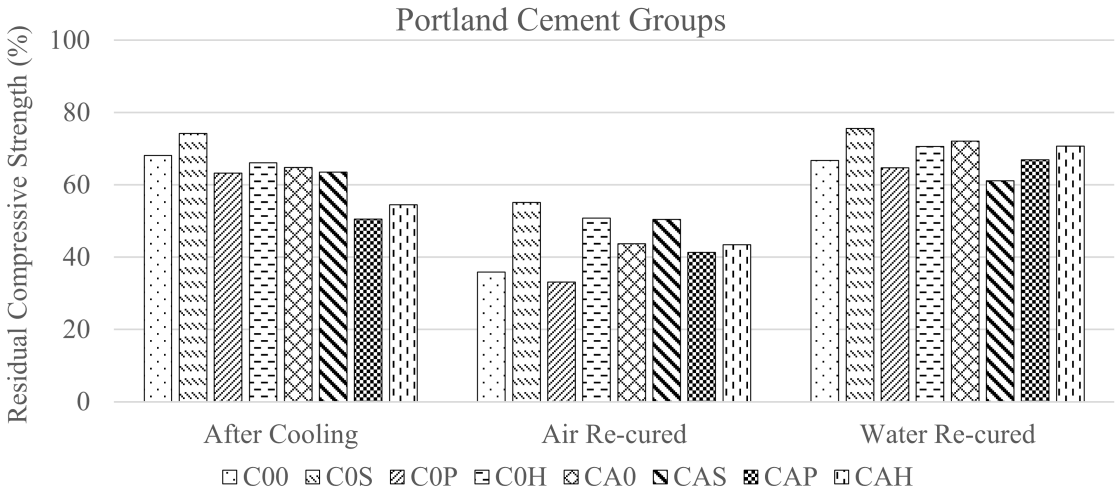

Figure 4.24. Residual compressive strength percentages of Portland cement concrete groups.

According to the results, it is clear to see that mechanical properties of concrete following to cooling period are influenced by the environmental conditions. Because of the fact that, further deteriorations were observed in air re-cured concrete groups in both compressive strength and modulus of elasticity values. And this can be explained by the monitored cracks occurred on the surface of concrete during air re-curing period due to CaO rehydration since surface level which was the weakest part of concrete after heating could not be able to resist stresses resulting from this expansion. On the other hand, compressive strength of concrete increased slightly and modulus of elasticity

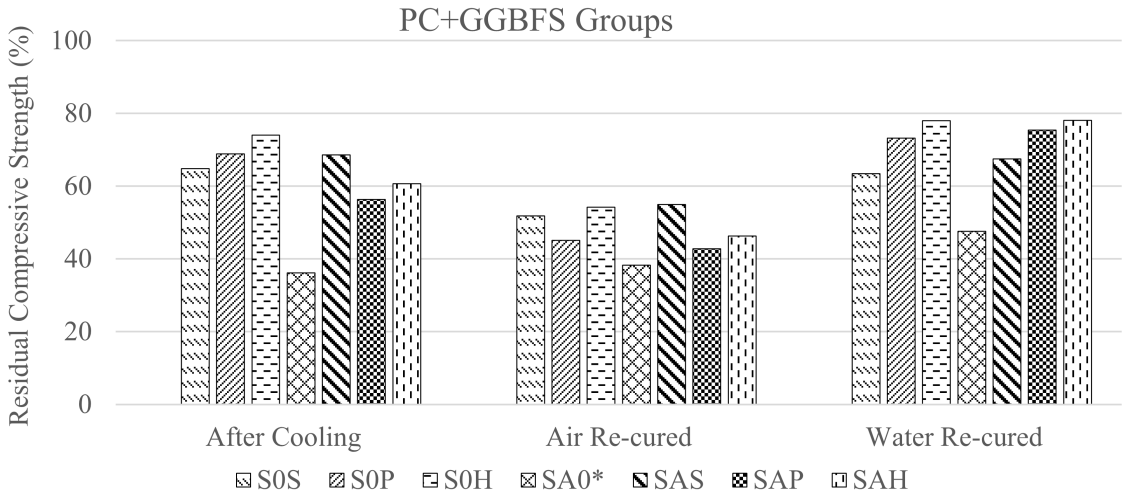

Figure 4.25. Residual compressive strength percentages of concrete groups incorporating GGBFS. (* many of the heated specimens of SA0 group spalled during heating and survived specimens had severe cracks and damage after heating).

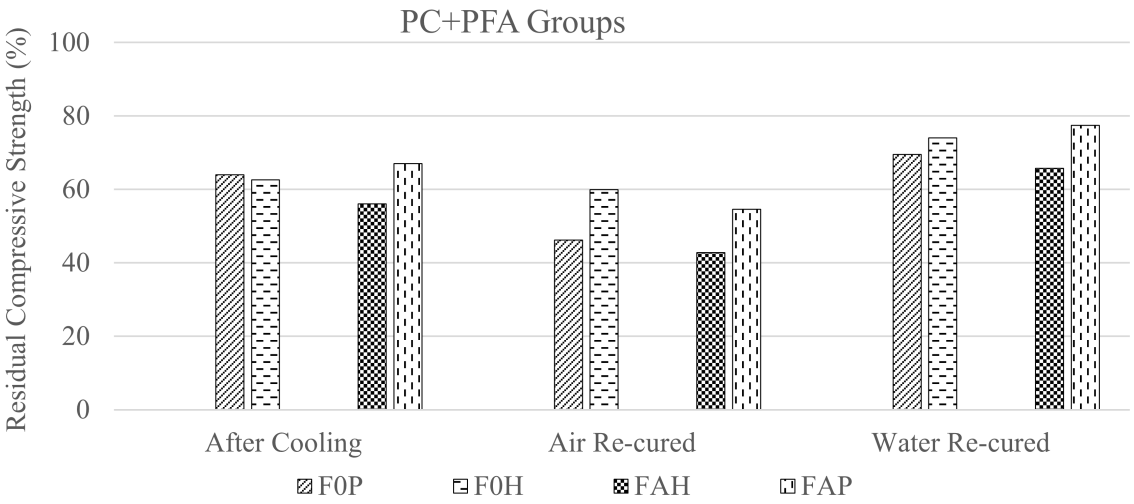

Figure 4.26. Residual compressive strength percentages of concrete groups incorporating PFA. (Since all of the specimens of F00, F0S, FA0 and FAS groups spalled during heating residual properties of these groups could not be evaluated.)

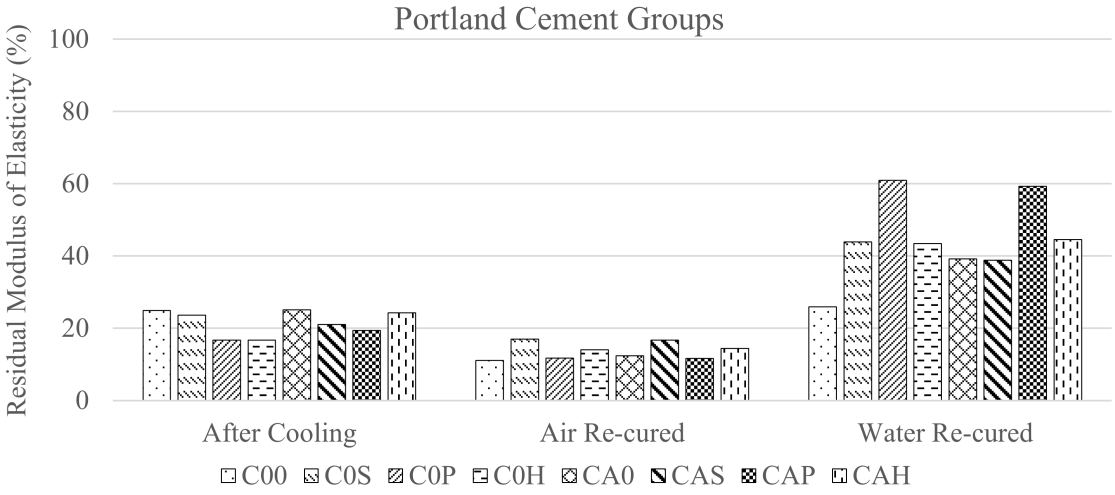

Figure 4.27. Residual modulus of elasticity percentages of Portland cement concrete groups.

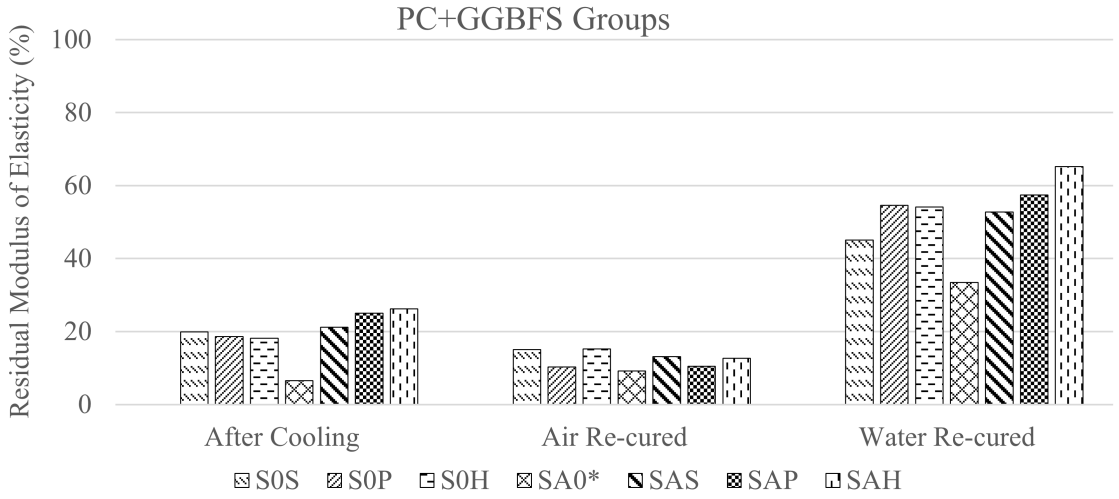

Figure 4.28. Residual modulus of elasticity percentages of concrete groups incorporating GGBFS. (* many of the heated specimens of SA0 group spalled during heating and survived specimens had severe cracks and damage after heating).

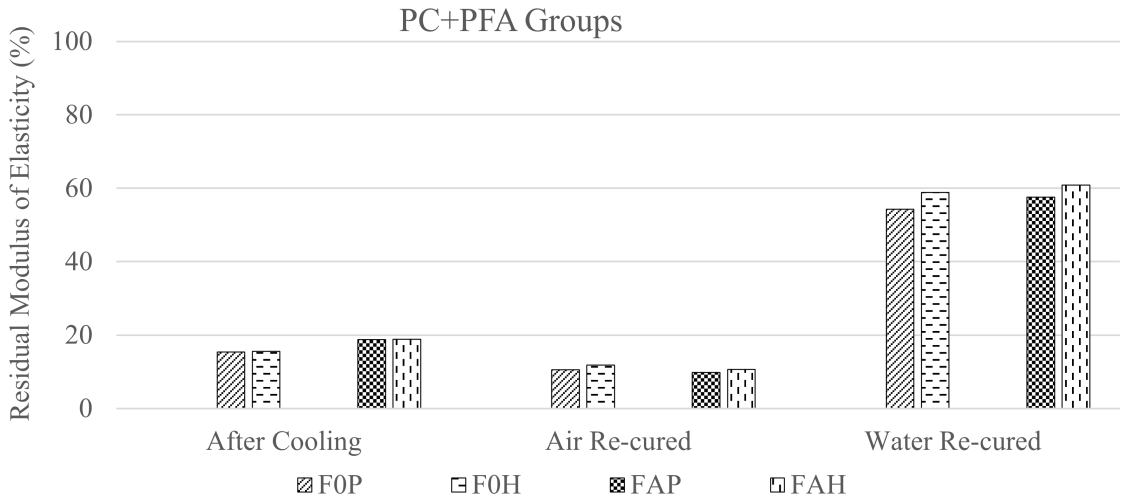

Figure 4.29. Residual modulus of elasticity percentages of concrete groups incorporating PFA. (Since all of the specimens of F00, F0S, FA0 and FAS groups spalled during heating residual properties of these groups could not be evaluated.)

values increased significantly after water re-curing period. Owing to the fact that, C-S-H and $CaCO_3$ formations were observed in concrete matrix at the surface level while there was no $Ca(OH)_2$ formation on the re-cured surface. Also cracks partially filled with $CaCO_3$ were monitored after water re-curing. Changes in residual mechanical properties were further evaluated below depending on re-curing types and materials used in concrete.

4.9.1. Effect of Re-curing

Average residual compressive strength and modulus of elasticity percentages of all the groups were calculated in order to see overall effects of re-curing on mechanical properties and results can be seen in Table 4.22. Average residual compressive strength and modulus of elasticity percentages of all the groups tested after cooling were 64% and 21%, respectively. It is clear to see that modulus of elasticity of concrete deteriorated higher than compressive strength since concrete softened due to the cracks resulting in higher contraction during loading [35, 62]. Newly formed cracks in concrete after

air re-curing period resulted in higher degradation in mechanical properties. Average residual compressive strength and modulus of elasticity percentages of all the air re-cured concrete groups dropped to 47% and 13%, respectively. On the other hand, important amount of strength and modulus of elasticity recovery were observed in water re-cured groups. In these groups, residual compressive strength and modulus of elasticity percentages increased to 71% and 51% (on average), respectively. As aforementioned in crack monitoring part, some of the cracks were filled during water re-curing period and therefore higher recovery was observed in modulus of elasticity of concrete than compressive strength of concrete.

Table 4.22. Average residual compressive strength and modulus of elasticity percentages of all concrete groups.

Category	**Residual Compressive Strength (%)**			**Residual Modulus of Elasticity (%)**		
	X	**Z**	**W**	**X**	**Z**	**W**
All Groups	64	47	71	21	13	51

4.9.1.1. Long Term Effect of Re-curing. Six concrete specimens of CAH, SAH and FAH groups were subjected to long term re-curing for 3 months. Then residual mechanical properties of these specimens were determined. Table 4.23 and Table 4.24 exhibit long terms residual compressive strength and long term modulus of elasticity percentages of CAH, SAH and FAH groups, respectively. When the concrete groups were evaluated separately it can be seen that long term effects of air and water re-curing were controversial. However, if averages of all concrete groups were calculated it can be concluded that long term air re-curing has a negative effect on mechanical properties of concrete while water re-curing has a positive effect on mechanical properties of concrete. On the other hand, the extent of these effects was not prominent.

Table 4.23. Long term residual compressive strength percentages.

Groups	**Residual Compressive Strength [%]**			
	28 days of re-curing		**90 days of re-curing**	
	Z	**W**	**Z**	**W**
CAH	43.5	70.8	44.3	72.6
SAH	46.3	78.1	41.9	83.1
FAH	54.6	77.5	53.2	77.0
Average	48.1	75.5	46.5	77.6

Table 4.24. Long term residual modulus of elasticity percentages.

Groups	**Residual Modulus of Elasticity [%]**			
	28 days of re-curing		**90 days of re-curing**	
	Z	**W**	**Z**	**W**
CAH	14.4	44.5	13.7	52.5
SAH	12.7	65.2	10.6	65.0
FAH	10.6	60.8	12.2	62.9
Average	12.6	56.8	12.2	60.1

4.9.2. Effect of Mineral Admixtures

Residual properties of Portland cement concrete groups and mineral added concrete groups after heating were very close but in general mineral added groups had slightly higher values. Since all the specimens of F00, F0S, FA0 and FAS spalled and residual mechanical properties of them could not be determined, only test results of PP fiber added concrete categories (CP, SP and FP) were compared as can be seen in Table 4.25 in order to understand the effect of mineral admixtures.

Table 4.25. Average residual compressive strength and modulus of elasticity percentages of PP fiber added concrete categories.

Category	**Residual Compressive Strength (%)**			**Residual Modulus of Elasticity (%)**		
	X	**Z**	**W**	**X**	**Z**	**W**
CP[1]	59	42	68	19	13	52
SP[2]	65	47	76	22	12	58
FP[3]	62	51	72	17	11	58

Average residual compressive strength and modulus of elasticity percentages of CP concrete groups after cooling were 59% and 19%, respectively. On the other hand, average residual compressive strength and modulus of elasticity percentages of SP and FP groups were 65%, 62% and 22%, 17%, respectively. At the just after cooling stage, concrete with GGBFS preserved its mechanical properties better than other types of concrete. After air re-curing period, lesser decrease was observed in compressive strength but higher decrease was observed in modulus of elasticity of concrete with PFA than other types of concrete. Average residual compressive strength and modulus of elasticity percentages of CP, SP and FP groups were 42%, 47%, 51% and 13%, 12%, 11%, respectively. Positive effect of mineral admixtures in mechanical properties

[1]CP stands for average residual mechanical properties of C0P, C0H, CAP and CAH groups.
[2]SP stands for average residual mechanical properties of S0P, S0H, SAP and SAH groups.
[3]FP stands for average residual mechanical properties of F0P, F0H, FAP and FAH groups.

can be seen better in water re-cured concrete groups, especially in concrete groups incorporating GGBFS because, average residual compressive strength and modulus of elasticity percentages of CP, SP and FP groups were 68%, 76%, 72% and 52%, 58%, 58%, respectively.

4.9.3. Effect of Air Entrainment

All concrete groups were gathered under two categories depending on use of AEA in concrete mixes in order to see the effects of air entrainment on mechanical properties of concrete after heating and re-curing processes. Average residual mechanical properties of all concrete groups without AEA and all concrete groups with AEA were given in Table 4.26. Residual compressive strength percentages of air entrained category were lower than that of concrete category without air entrainment after heating. But this difference disappeared after re-curing periods and almost same average values were obtained after air re-curing and after water re-curing. On the contrary, residual modulus of elasticity percentages of air entrained concrete category were higher than that of concrete groups without air entrainment.

Table 4.26. Average residual compressive strength and modulus of elasticity percentages of concrete categories with and without air entrainment.

Category	**Residual Compressive Strength (%)**			**Residual Modulus of Elasticity (%)**		
	X	**Z**	**W**	**X**	**Z**	**W**
Without AEA[4]	67	48	71	19	13	49
With AEA[5]	60	47	71	22	12	53

[4]Without AEA stands for all concrete groups without air entrainment.

[5]With AEA stands for all concrete groups with air entrainment.

4.9.4. Effect of Fiber Reinforcement

Finally, all concrete groups were gathered under four different categories depending on fiber types in order to evaluate the effects of fiber reinforcement on mechanical properties of concrete after heating and re-curing processes. Average residual mechanical properties of all non-fibrous (plain) concrete, all steel fiber reinforced concrete, all PP fiber reinforced concrete and all hybrid fiber reinforced categories were shown in Table 4.27.

Table 4.27. Average residual compressive strength and modulus of elasticity percentages of plain, steel fiber reinforced, PP fiber reinforced and hybrid fiber reinforced concrete categories.

Category	**Residual Compressive Strength (%)**			**Residual Modulus of Elasticity (%)**		
	X	**Z**	**W**	**X**	**Z**	**W**
Plain[6]	66	40	69	25	12	33
Steel[7]	68	53	67	21	15	45
PP[8]	60	42	69	19	11	57
Hybrid[9]	64	52	75	20	13	55

Average residual compressive strength and modulus of elasticity percentages of PP fiber reinforced concrete category after heating and after air re-curing were 60%, 42% and 19% 11%, respectively. These ratios (except 42% residual compressive strength after heating) were the lowest values obtained after compression tests. Based on this result it can be concluded that mechanical degradation was higher in PP fiber reinforced groups after heating and air re-curing. Because, micro channels were formed in concrete due to melting of PP fibers during heating. Combination of micro channels and cracks occurring during heating and air re-curing period may influence the

[6]Plain stands for average residual mechanical properties of non-fibrous groups.

[7]Steel stands for average residual mechanical properties of all steel fiber reinforced groups.

[8]PP stands for average residual mechanical properties of all PP fiber reinforced groups.

[9]Hybrid stands for average residual mechanical properties of all hybrid fiber reinforced groups.

amount of deterioration in PP fiber reinforced concrete. The highest residual mechanical property values were measured in steel fiber reinforced concrete among all the fiber reinforced concrete groups after heating and after air re-curing. Steel fibers survived during heating and they probably prevented concrete from excessive cracking during heating and air re-curing period. Results of compression tests conducted after heating and after air re-curing also showed that residual mechanical property values of hybrid fiber reinforced concrete were between the results of PP fiber reinforced and steel fiber reinforced concrete categories. Results of fiber reinforced concrete categories obtained after water re-curing were better than that of plain concrete category. The highest amount of recovery of compressive strength was obtained in hybrid fiber reinforced category with a residual compressive strength ratio of 75% and the highest amount of modulus of elasticity recovery was observed in PP fiber reinforced category with a residual modulus of elasticity ratio of 57% after water re-curing.

4.10. Results of Black Pixel Analyses

Surface pictures of specimens were captured during the first week of air re-curing and these pictures were evaluated in an image analysis software. Then, BPA rates of air re-cured concrete specimens were calculated to monitor damage development and these values were compared to differences in compressive strength values after air re-curing period as shown in Table 4.28, Table 4.29 and Table 4.30. Individual compressive strength value of monitored specimen (air re-cured for 28 days following cooling period and tested at the end of this 28 day period) and average compressive strength value of 3 specimens tested after cooling (as an initial strength value before air re-curing period) were used to calculate the change in compressive strength during air re-curing period. After comparison a scattergram was obtained as shown in Figure 4.30 and it showed that there was a logarithmic relation between changes in compressive strength and BPA rates. Calculated R^2 value for all set of data was 0.71. This rate can be increased by using advanced photographing techniques, by analyzing in a specific software, by increasing sample size etc. For example, air voids on the surface of the specimens influence the total amount of black pixels. If the effect of air voids are somehow

eliminated more accurate BPA rates can be obtained. Therefore, the scattergrams of air entrained concrete groups and concrete groups without air entrainment were drawn separately as shown in Figure 4.31 and Figure 4.32. And as expected, a higher R^2 value (0.97) was obtained in concrete groups without air entrainment.

Table 4.28. Residual compressive strength and BPA values of Portland cement concrete.

Group	**X-Group (MPa)**	**Z-Individual (MPa)**	**(Z-X)/X (%)**	**BPA Rate (Day)**
C00	Spalling was observed, (Not examined)			
C0S	Spalling was observed, (Not examined)			
C0P	36.9	20.1	-45.5	0.187
C0H	36.7	24.6	-32.8	0.056
CA0	35.5	22.2	-37.5	0.087
CAS	34.9	25.6	-26.9	0.087
CAP	25.3	21.2	-16.1	0.007
CAH	27.2	24.3	-10.5	0.019

Table 4.29. Residual compressive strength and BPA values of concrete incorporating GGBFS.

Group	**X-Group (MPa)**	**Z-Individual (MPa)**	**(Z-X)/X (%)**	**BPA Rate (Day)**
S00	Spalling was observed, (Not examined)			
S0S	Spalling was observed, (Not examined)			
S0P	43.8	29.1	-33.6	0.075
S0H	44.6	29.5	-33.8	0.059
SA0	Spalling was observed, (Not examined)			
SAS	34.2	26	-24.1	0.079
SAP	28.2	23.8	-15.7	0.025
SAH	29.6	22.3	-24.7	0.021

Table 4.30. Residual compressive strength and BPA values of concrete incorporating PFA.

Group	**X-Group (MPa)**	**Z-Individual (MPa)**	**(Z-X)/X (%)**	**BPA Rate (Day)**
F00	Spalling was observed, (Not examined)			
F0S	Spalling was observed, (Not examined)			
F0P	45.5	30.3	-33.5	0.071
F0H	44.2	37.3	-15.6	0.019
FA0	Spalling was observed, (Not examined)			
FAS	Spalling was observed, (Not examined)			
FAP	33.3	22.3	-32.9	0.067
FAH	39.3	28.6	-27.2	0.055

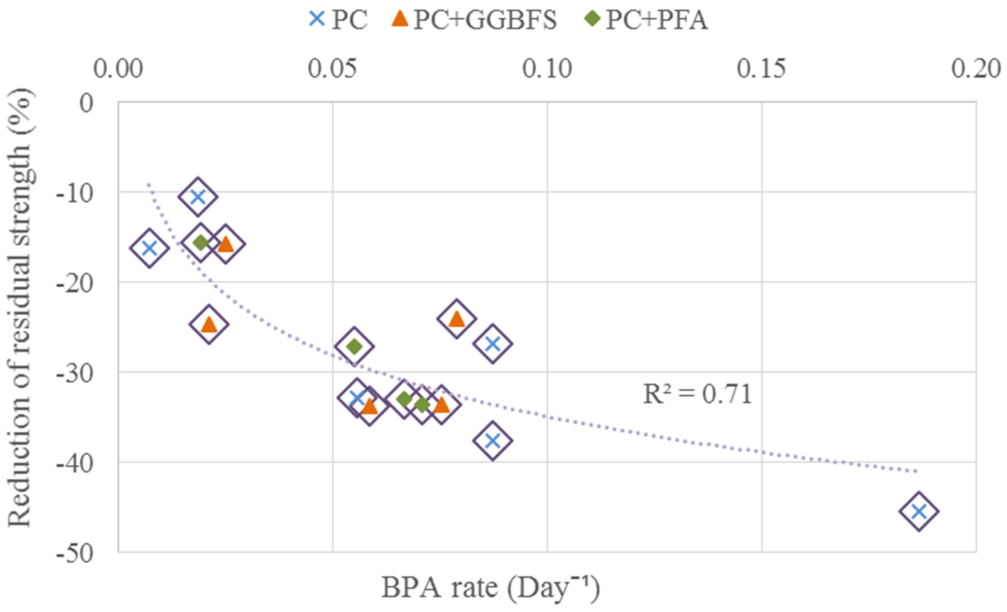

Figure 4.30. Black pixel analyses results of all groups.

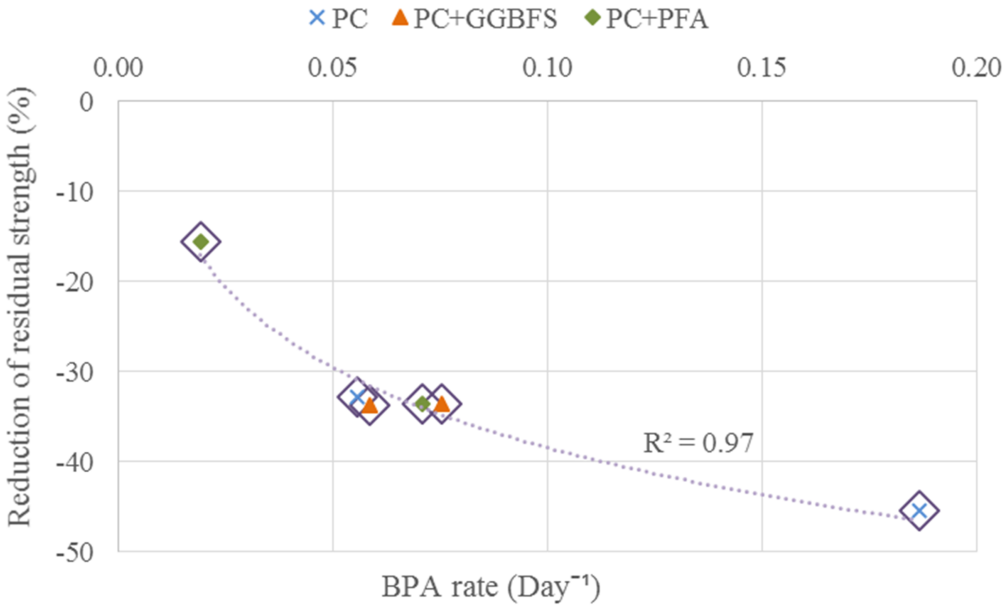

Figure 4.31. Black pixel analyses results of all groups without air entrainment.

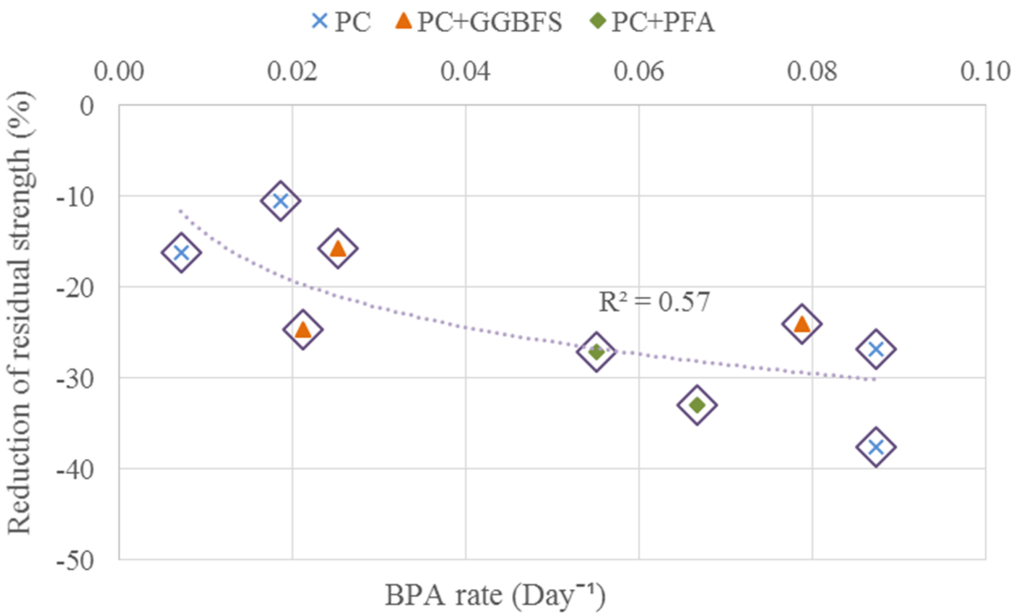

Figure 4.32. Black pixel analyses results of all air entrained groups.

5. TEST RESULTS OF REINFORCED CONCRETE BEAMS

In this chapter, disintegration and recovery of concrete were investigated on reinforced concrete beams. After tests completed on small sized specimens possible concrete groups were determined to use in production of reinforced concrete beams. In order to reduce risk of spalling, firstly concrete groups including PP fibers were chosen (C0P, C0H, CAP, CAH, S0P, S0H, SAP, SAH, F0P, F0H, FAP, FAH). Since positive effect of air entrainment on spalling resistance of concrete was seen during small sized specimens tests air entrained concrete groups (CAP, CAH, SAP, SAH, FAP, FAH) were selected among chosen groups at the first elimination. Concrete groups incorporating pulverized fly ash groups had higher risk of spalling than other concrete types according to results of small sized specimen tests. Therefore, at the final stage concrete groups incorporating PFA were eliminated and finally 4 different concrete groups were left. These concrete groups were CAP, CAH, SAP and SAH since they had less probabilities of spalling during heating.

4 reinforced concrete beams were produced for each of concrete group. Totaly 16 reinforced concrete beams had a dimensions of 20x25x180cm were produced. 4 of them were used to determine initial properties before heating, remaining 12 beams were subjected to heating. After heating 4 of heated beams were used to determine the properties at after cooling stage and remaining 8 beams were subjected to re-curing (4 beams for water re-curing and 4 beams for air re-curing). S420 ribbed steel bars were used in reinforced concrete beams and minimum cover thicknesses were determined according to Eurocode 2 [19].

5.1. SEM Observations

Similar to SEM observations on small sized concrete specimens only cementitious type was chosen as a parameter. Therefore samples were obtained from PP fiber

reinforced concrete beams (RC beam made with CAP concrete and RC beam made with SAP concrete) before heating, after cooling, after air re-curing and after water re-curing. Samples were taken from heated surface and lower reinforcing bar level of a RC beam. Conventional high vacuum scanning electron microscope was used to investigate surface morphology. Therefore, secondary electrons (SE) were measured on platinum coated samples to obtain pure images. Applied accelerating voltage (Acc V) was 15 kV and working distance (WD) were in the range of 10.2 mm–11.7 mm, respectively. Since water re-cured samples were saturated before SEM, they were dried at 40°C in an oven for two hours not to have a vacuum problem.

SEM pictures obtained from heated surface of CAP concrete before heating, after cooling, after air re-curing and after water re-curing can be seen in Figure 5.1 and SEM pictures obtained from heated surface of SAP concrete before heating, after cooling, after air re-curing and after water re-curing can be seen in Figure 5.2. Since concrete surfaces experienced more than 1000°C during heating microstructure of concrete at surface level significantly changed. C-S-H gel lost its water content and turned to a granular and amorphous form after cooling. Calcium hydroxide disappeared after cooling at the surface level. Since similar morphological changes occurred on the heated surfaces of RC beams with the heated surfaces of small sized concrete cubes, cracks and crazing were also observed on the heated surfaces of RC beams after cooling. After air re-curing period, newly formed calcium hydroxide crystals were observed on the heated surfaces especially in Portland cement concrete. Overall morphology of concrete changed and granular formations disappeared after water re-curing.

Samples were taken from the lower bar level of RC beams and SEM observations were conducted on them. SEM pictures obtained from lower bar level of CAP and SAP beams were given in Figure 5.3 and Figure 5.4, respectively. As can be seen in SEM pictures, there were still calcium hydroxide plates at lower bar level after heating. Because of the fact that distance between the heated surface and axis of lower bars was determined according to Eurocode 2, (a=65 mm), in order to preserve reinforcing steel during 120 minutes of heating [19]. According to this design it is expected that temperature at the reinforcing bar level does not exceed 400°C during

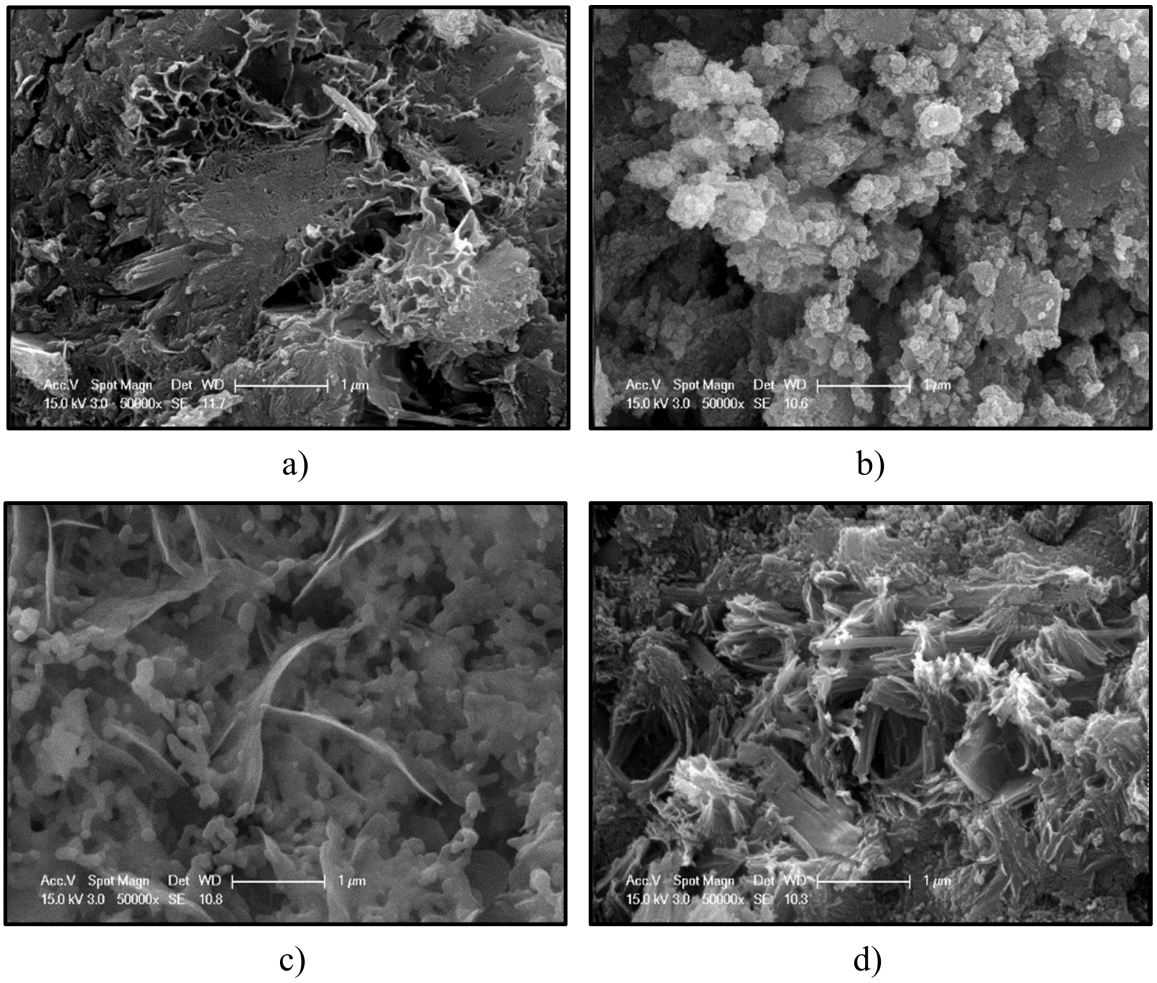

Figure 5.1. SEM pictures obtained from heated surface of CAP a) before heating b) after cooling c) after air re-curing d) after water re-curing.

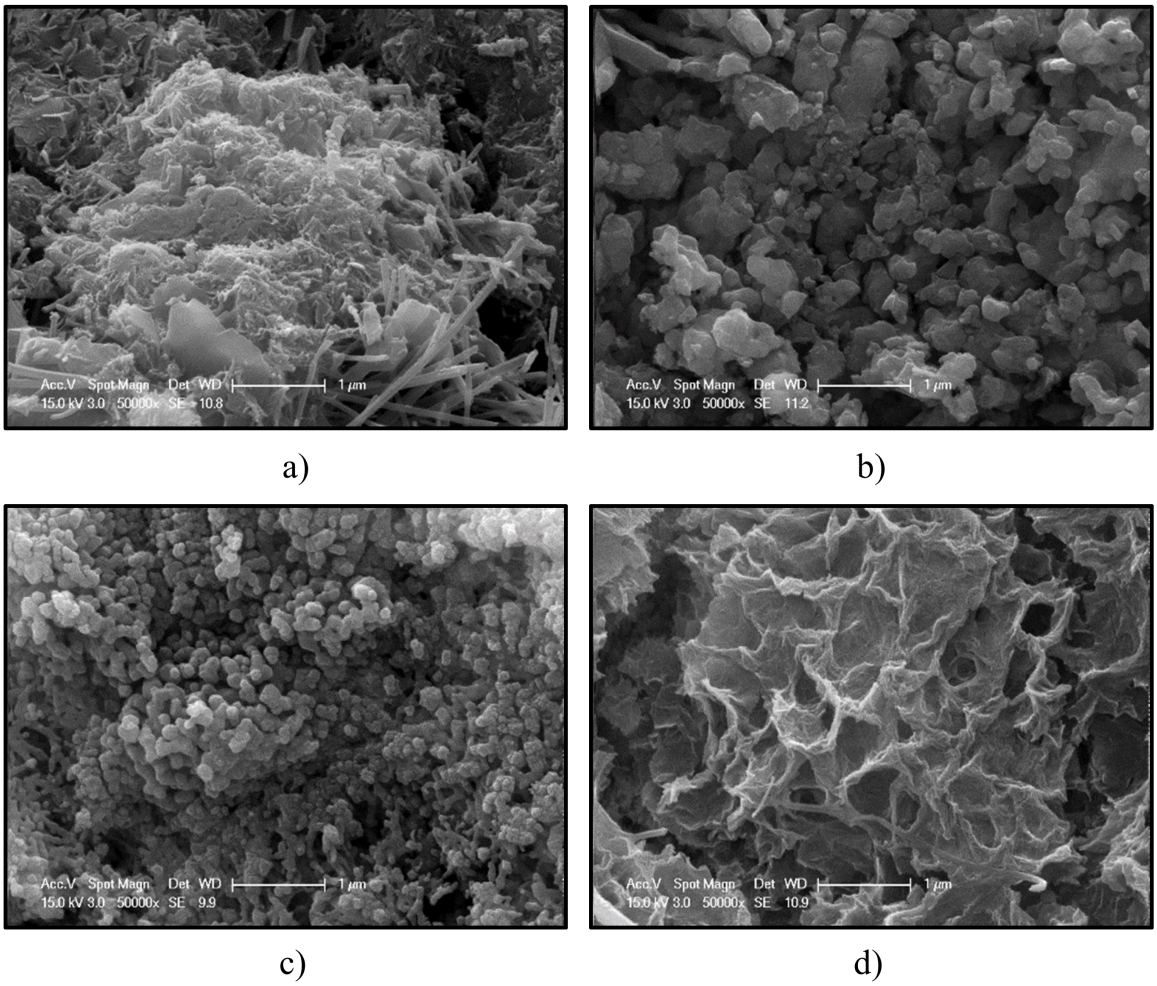

Figure 5.2. SEM pictures obtained from heated surface of SAP a) before heating b) after cooling c) after air re-curing d) after water re-curing.

heating. Therefore, most probably temperature around lower bar did not exceed 400°C during our fire test and there was no prominent change among SEM pictures obtained from lower bar level at any stage.

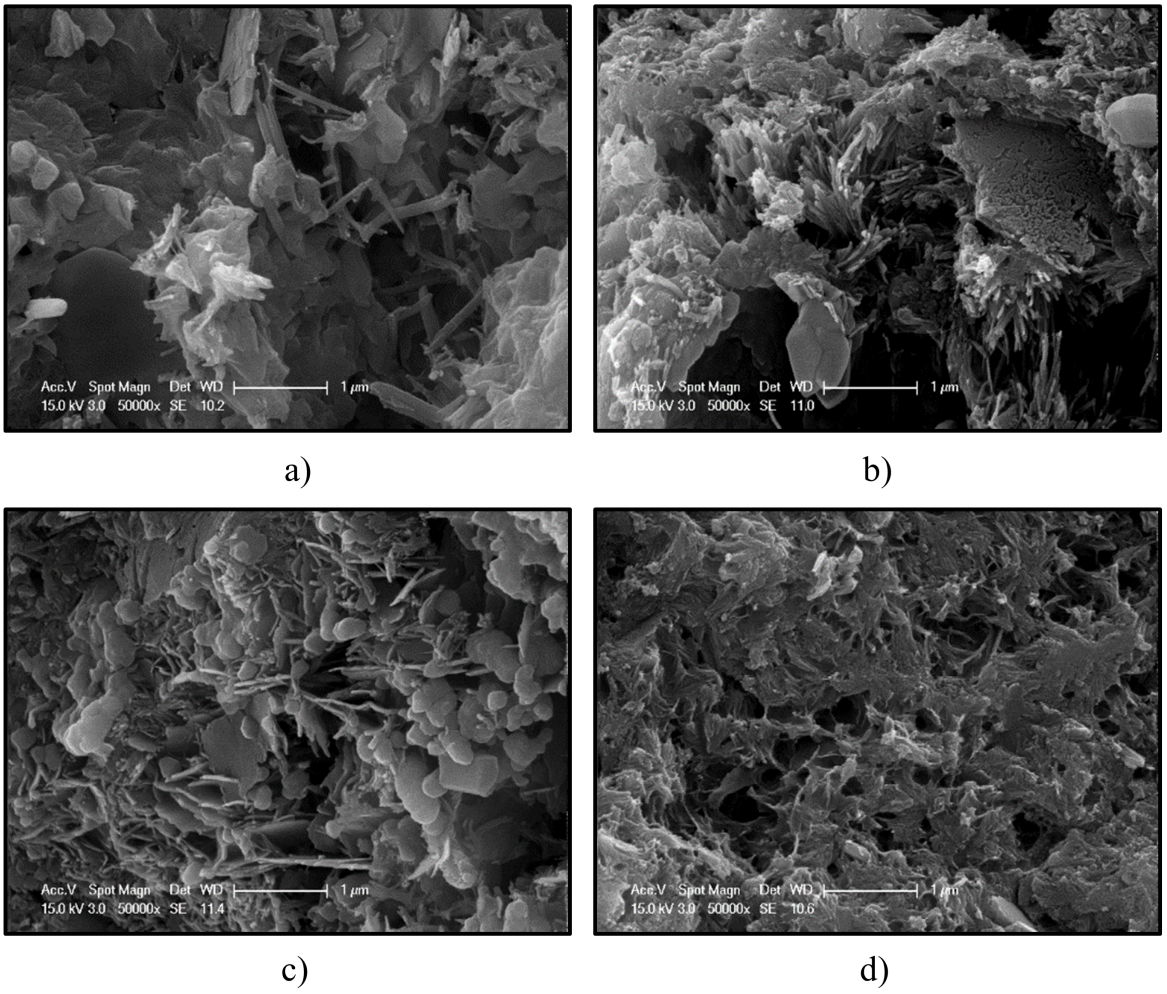

Figure 5.3. SEM pictures obtained from reinforcing bar level of CAP a) before heating b) after cooling c) after air re-curing d) after water re-curing.

5.2. Residual Flexural Load Capacity and Flexural Rigidity Measurements

Four point bending tests were conducted on 4 RC beams before heating. Remaining 12 beams were subjected to 120 minutes of fire tests. Four point bending tests were conducted on 4 RC beams after cooling and remaining 8 RC beams were subjected to air and water re-curing. At the end of air and water re-curing periods four point

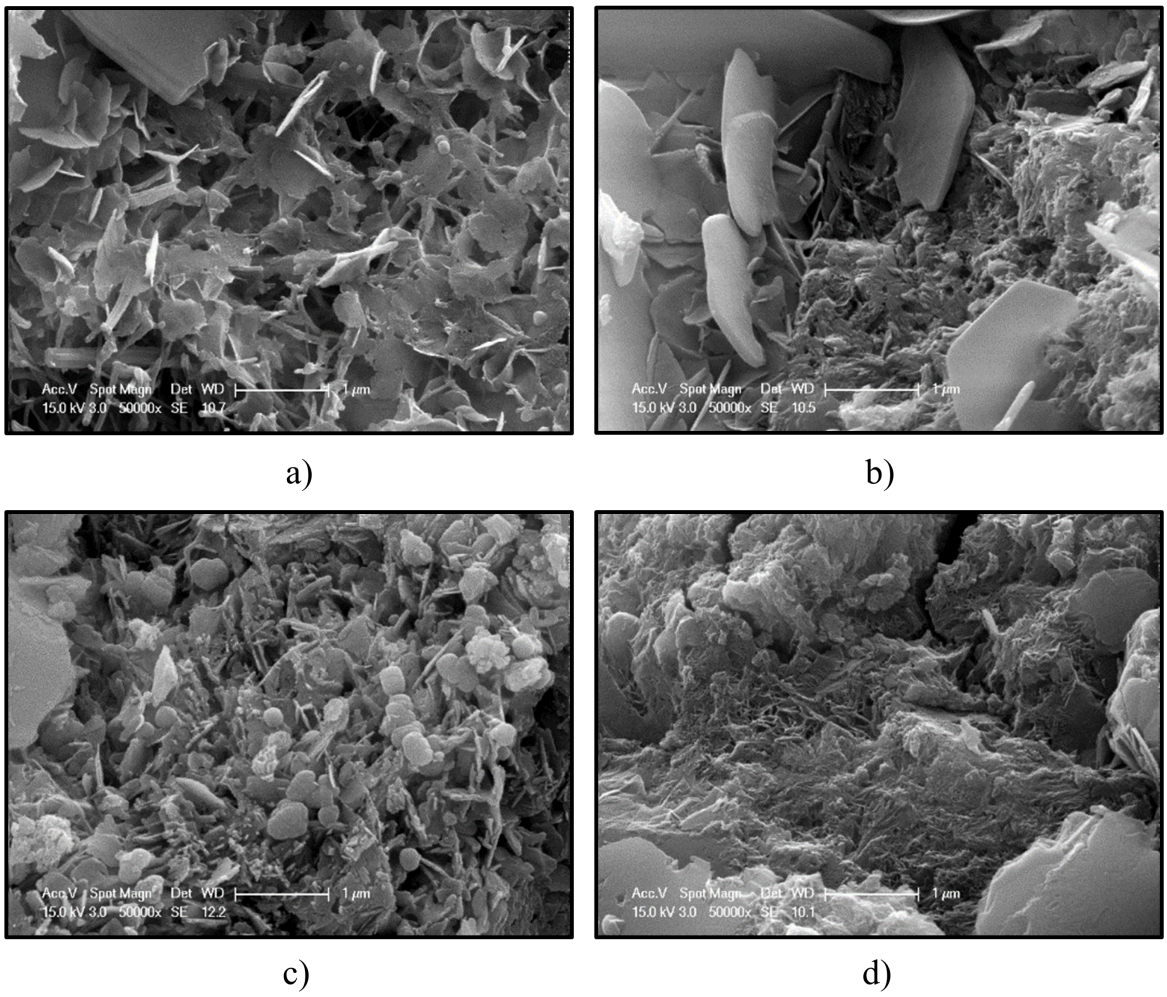

Figure 5.4. SEM pictures obtained from reinforcing bar level of SAP a) before heating b) after cooling c) after air re-curing d) after water re-curing.

bending tests were conducted on 8 RC beams. During each tests, incremental load was applied and 500kg was loaded on beam specimens in a minute. 2 LVDTs collected mid-span deflection data in millimeter at 8Hz. After bending tests load deformation graphs were drawn.

Load-deflection curves of CAP and CAH groups were given in Figure 5.5 and 5.6, respectively. Also, load-deflection curves of SAP and SAH groups were given in Figure 5.7 and 5.8, respectively. When the resulting graphs were evaluated elasto-plastic behavior of RC beams under for point loading conditions was observed. Load bearing capacities decreased after heating in all concrete types. Curves obtained from beams tested after cooling and curves obtained from beams tested after air re-curing were very similar. Plastic deformation parts of curves obtained from water re-cured RC beams were also similar to curves obtained after cooling and after air re-curing. On the other hand, linear elastic part of curves obtained from water re-cured RC beams were different than other curves.

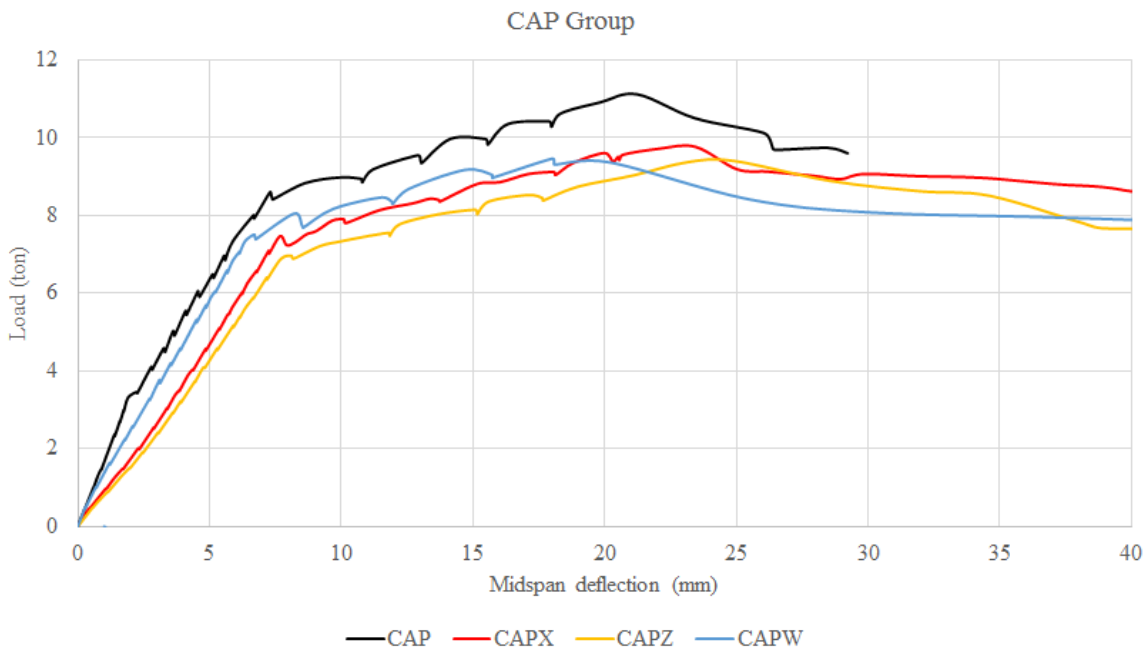

Figure 5.5. Load & deflection curves of CAP group.

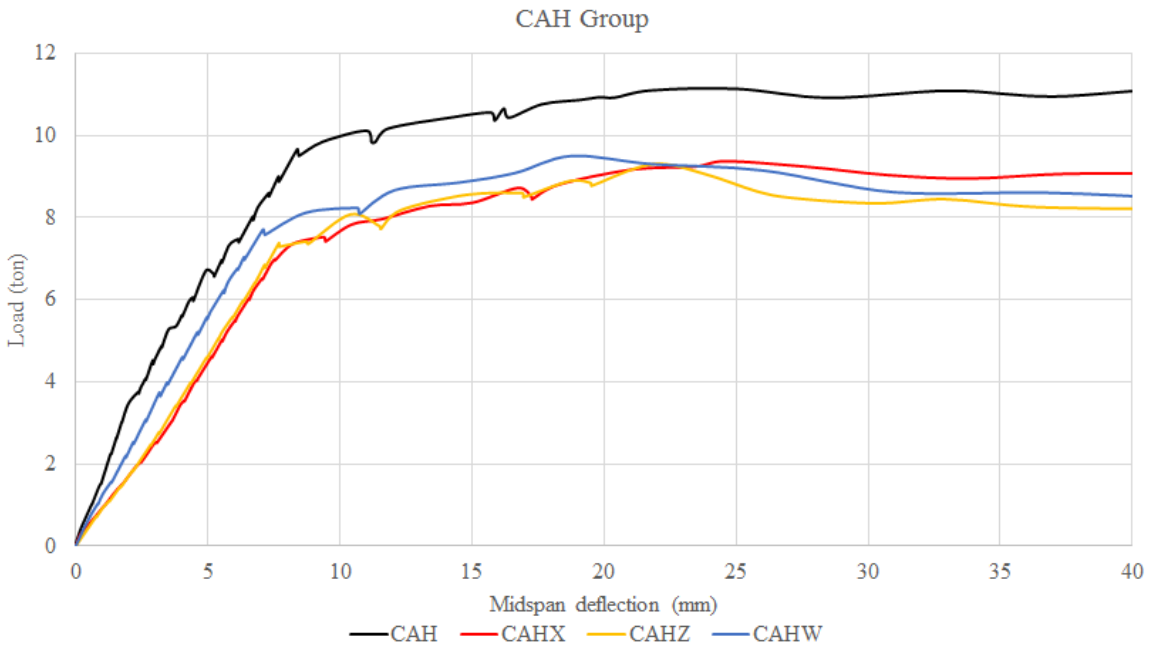

Figure 5.6. Load & deflection curves of CAH group.

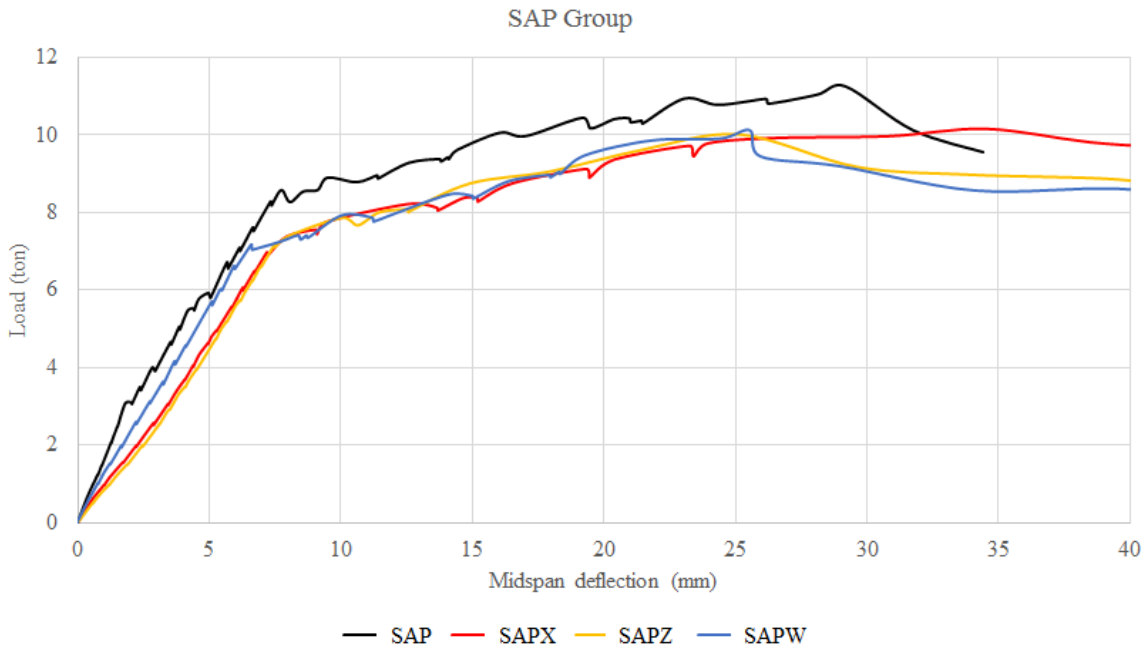

Figure 5.7. Load & deflection curves of SAP group.

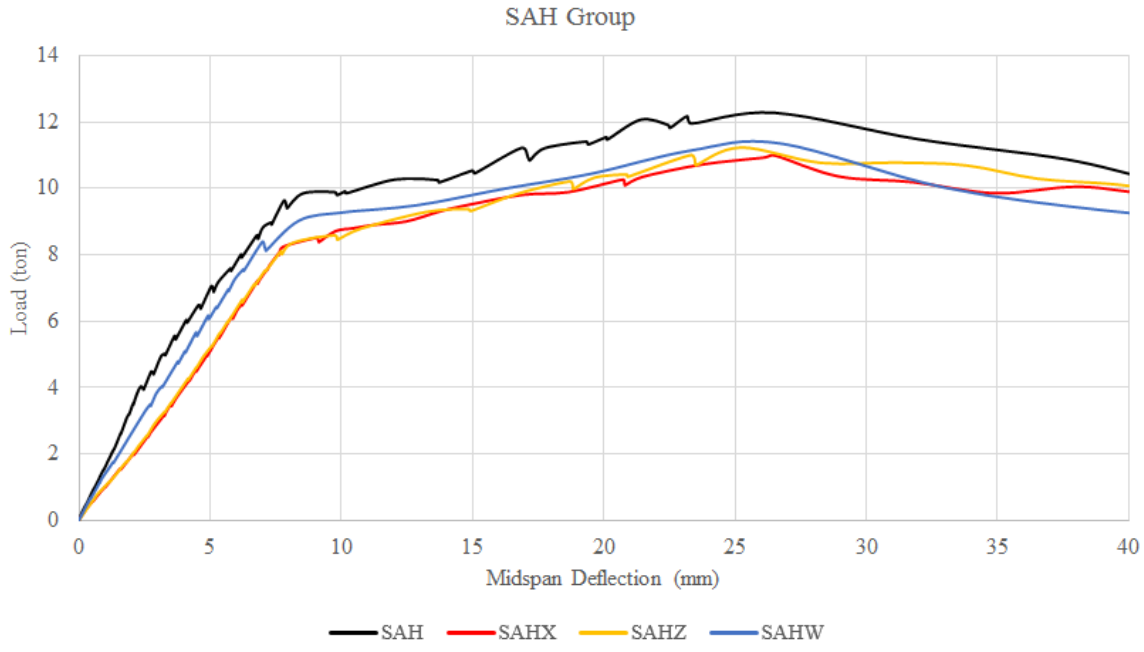

Figure 5.8. Load & deflection curves of SAH group.

In order to compare maximum load bearing capacities peak loads of the curves were determined. Firstly, load bearing capacities of non-heated RC beams were determined. Then, residual load bearing capacities of heated beams were determined. Table 5.1 represents residual load bearing capacities of RC beams. Residual load bearing capacities of RC beams produced with SAP and SAH concrete groups were higher than residual load bearing capacities of RC beams produced with CAP and CAH groups. After air re-curing period RC beams produced with SAP and SAH concrete groups preserved their load bearing capacities better than air re-cured RC beams produced with CAP and CAH concrete groups. Reduction in load bearing capacities was observed in water re-cured RC beams produced with PP fiber reinforced concrete groups (CAP and SAP) while increase in load bearing capacities was observed in water re-cured RC beams produced with hybrid fiber reinforced concrete groups (CAH and SAH). Although there were differences among residual load bearing capacities measured after cooling, after air re-curing and after water re-curing these differences were relatively small when they compared to reduction in mechanical properties of small sized concrete specimens.

Table 5.1. Initial and residual load bearing capacities of RC beams.

	Initial Load Bearing Capacitiy	**Residual Load Bearing Capacity**					
Concrete Group	**Before Heating**	**After Cooling**		**Air Re-cured**		**Water Re-cured**	
	(tons)	**(tons)**	**(%)**	**(tons)**	**(%)**	**(tons)**	**(%)**
CAP	11.1	9.8	87.8	9.4	84.6	9.5	85.1
CAH	11.1	9.4	84.1	9.3	83.5	9.5	85.3
SAP	11.3	10.2	90.3	10	89	10.1	89.9
SAH	12.3	11	89.6	11.2	91.5	11.3	92.5
		Avg.	88.0	Avg.	87.2	Avg.	88.2

The area under load-deflection curves represents toughness which is the energy absorption capacity of a material. To be able to see the changes in toughness after heating and after re-curing areas under the load-deflection curves were calculated. Area under a curve was calculated by applying the method given in Figure 5.9. Area was calculated between zero deflection and 10 mm of midspan deflection since around 10 mm of deflection yielding of reinforcing steel occurred and high amount of energy was absorbed by reinforcing steel beyond 10 mm of deflection. Table 5.2 shows initial and residual toughness values of each concrete groups. Toughness values decreased 23.3% in average after cooling. Toughness of concrete groups incorporating GGBFS groups (SAP and SAH) decreased less than Portland cement concrete groups (CAP and CAH) at this stage. When the after cooling results were evaluated regarding the effect of fiber types it can be seen that deterioration in toughness of PP fiber reinforced concrete groups (CAP and SAP) was less than hybrid fiber reinforced concrete groups (CAH and SAH).

After air re-curing period reduction in average residual toughness value raised to 25%. In this case, increase in residual toughness of hybrid fiber reinforced groups (CAH and SAH) was observed. Therefore, using steel fibers in concrete can be beneficial to

preserve energy absorbtion capacity of structural element following to cooling period. On the other hand, after water re-curing period recovery in residual toughness values was obtained. Reduction in average residual toughness value decreased to 12.2% after water re-curing. Hybrid fiber reinforced groups (CAH and SAH)showed higher amount of recovery in toughness than only PP fiber reinforced concrete groups (CAP and SAP).

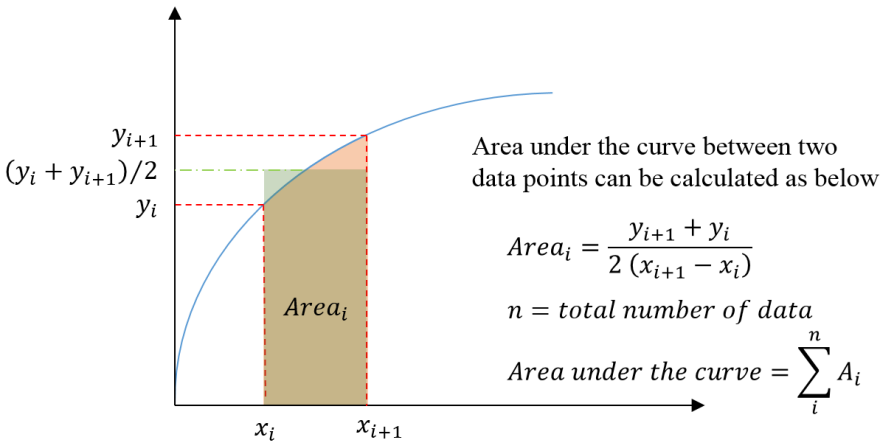

Figure 5.9. Calculation of area under the curve.

Table 5.2. Initial and residual toughness values.

	Initial Toughness	**Residual Toughness**					
Concrete Group	**Before Heating**	**After Cooling**		**Air Re-cured**		**Water Re-cured**	
	(tmm)	**(tmm)**	**(%)**	**(tmm)**	**(%)**	**(tmm)**	**(%)**
CAP	58.7	45.2	77.0	41.5	70.7	52.5	89.4
CAH	61.6	43.7	70.9	44.7	72.6	51.5	83.6
SAP	56.4	45.2	80.1	44.0	78.0	49.6	87.9
SAH	63.4	49.8	78.5	50.0	78.9	57.1	90.1
		Avg.	76.7	Avg.	75.0	Avg.	87.8

Range of the area under the ascending part of load deformation curve depends on the slope of the curve. Flexural rigidity of the beam (EI) which corresponds to slope of load deformation curve can be considered as an important parameter when evaluating

toughness of a material in the ascending region. Therefore, instantaneous EI values were calculated by following the procedure given in Figure 5.10. Then, flexural rigidity (EI) and deflection curves were drawn for all reinforced concrete beams. Figure 5.11 and Figure 5.12 represent flexural rigidity and deflection curves of RC beams produced by using CAP and CAH groups, respectively. Figure 5.13 and Figure 5.14 represent flexural rigidity and deflection curves of RC beams produced by using SAP and SAH groups, respectively. Residual flexural rigidity values decreased after heating for all concrete groups. Before heating curves and water re-cured curves were distinguished among all the curves since very similar flexural rigidity curves were obtained in RC beams tested after cooling and RC beams tested after air re-curing. The positive effect of water re-curing on flexural rigidity can be explained by two factors. The first one is recovery in modulus of elasticity of concrete after water re-curing and the second one can be the filling effect of newly formed crystals and gels during water re-curing which increases uncracked cross sectional area.

To be able to compare the rate of deterioration and recovery in residual flexural rigidities, average flexural rigidities of each curves were calculated and they were given in Table 5.3 for all concrete groups. According to table, flexural rigidities decreased 33.5% in average after cooling and further decrease was seen in residual flexural rigidities after air re-curing period. On the other hand, recovery in residual flexural rigidities of water re-cured RC beams was obtained and average residual flexural rigidity of water re-cured RC beams raised to 82.7%.

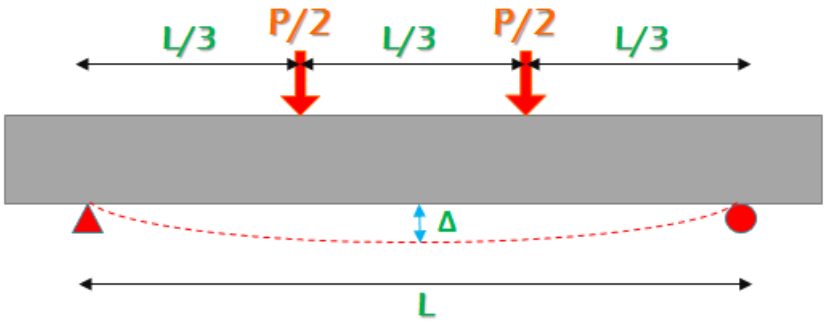

$$i = data\ number$$

$$\Delta_i = \frac{23P_iL^3}{1296[EI]_i} \quad \Rightarrow \quad [EI]_i = \frac{23P_iL^3}{1296\Delta_i}$$

Figure 5.10. Calculation of instantaneous flexural rigidity (EI) values.

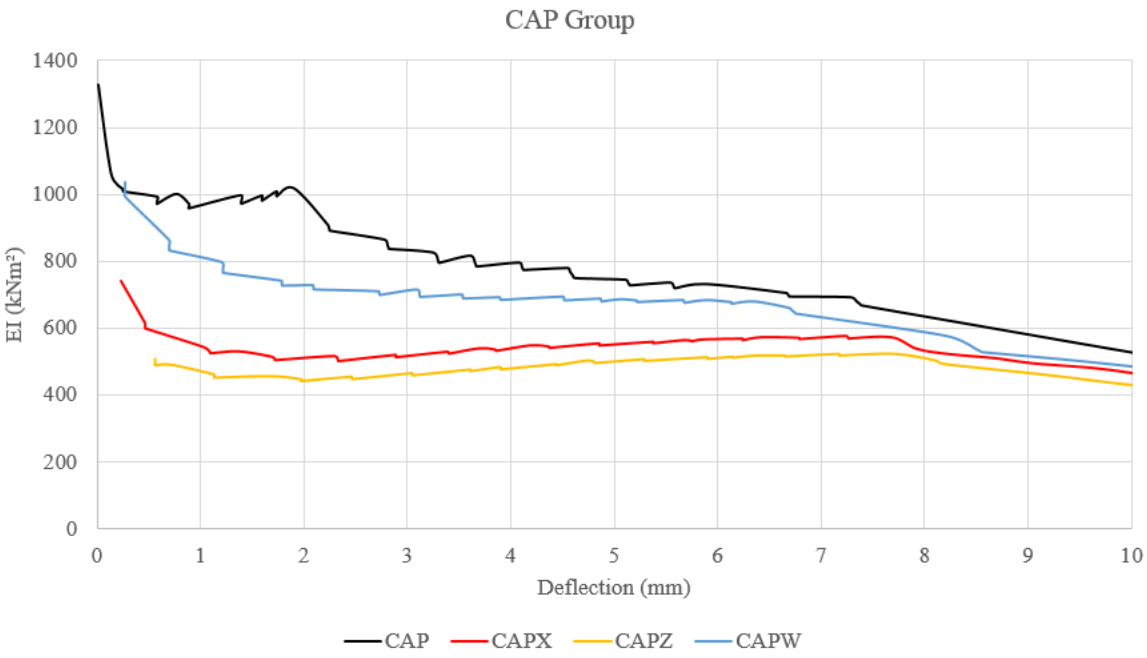

Figure 5.11. Flexural rigidity & deflection curves of CAP group.

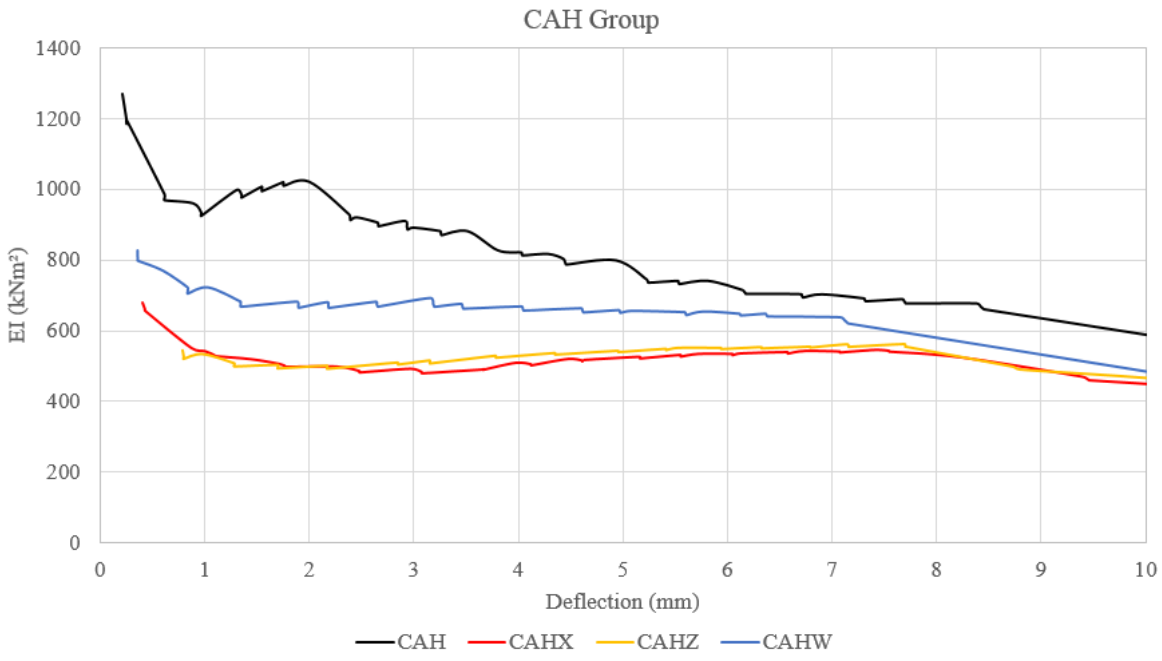

Figure 5.12. Flexural rigidity & deflection curves of CAH group.

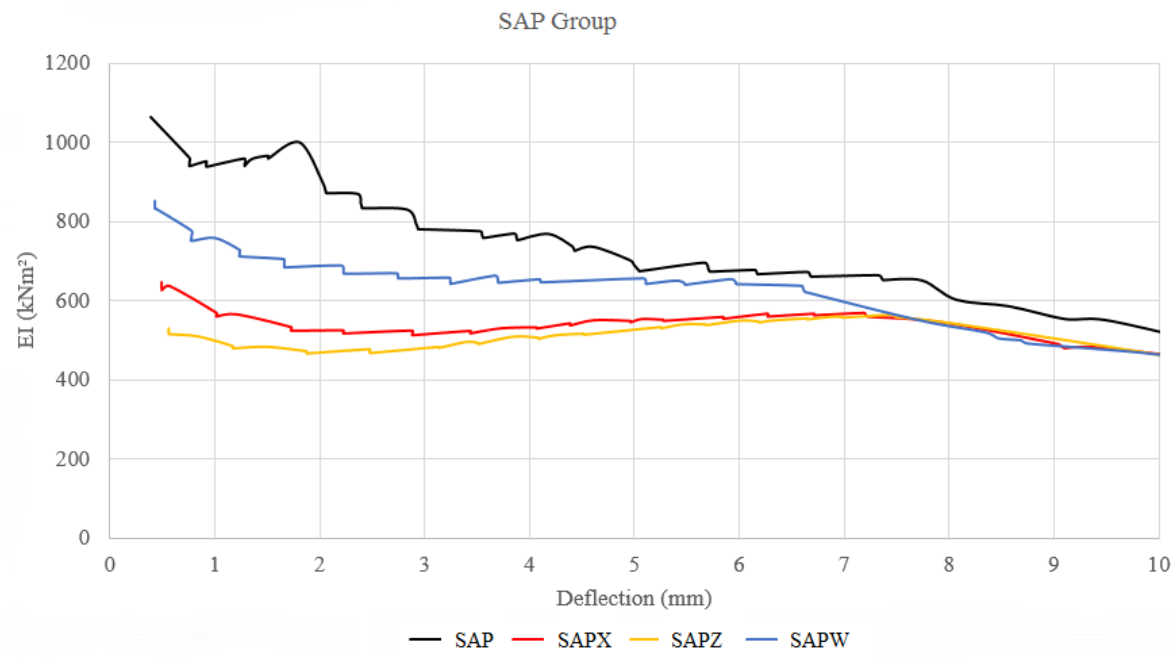

Figure 5.13. Flexural rigidity & deflection curves of SAP group.

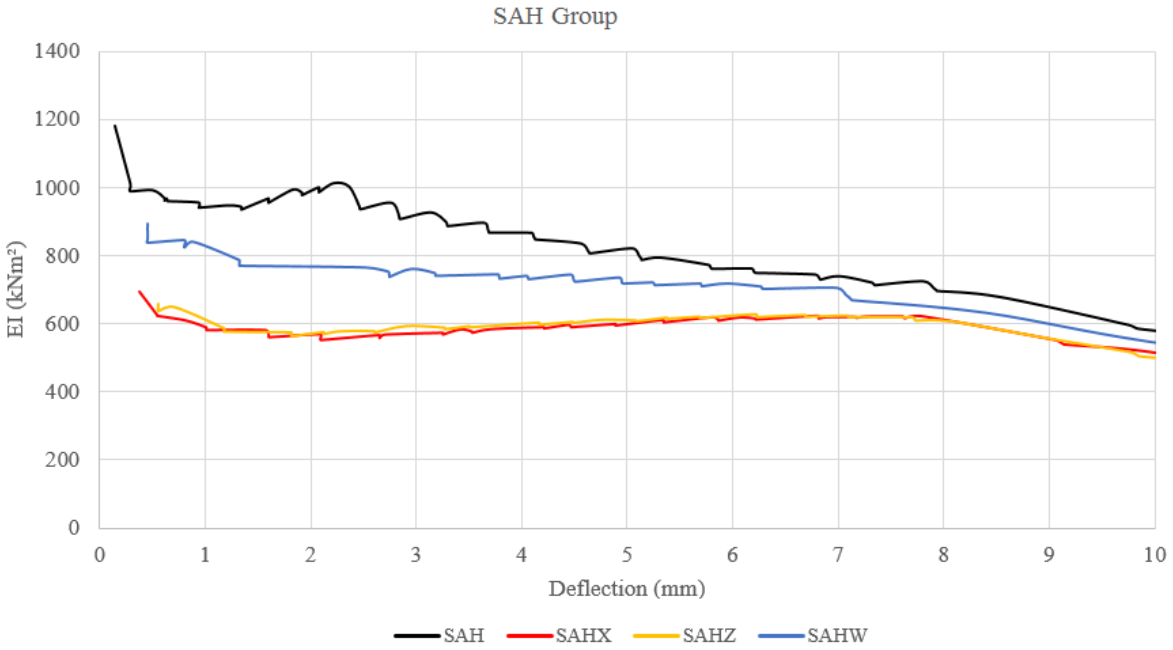

Figure 5.14. Flexural rigidity & deflection curves of SAH group.

Table 5.3. Average flexural rigidities calculated from EI vs deflection curves.

	Initial Flexural Rigidity (EI)	**Residual Flexural Rigidity (EI)**					
Concrete Group	**Before Heating**	**After Cooling**		**Air Re-cured**		**Water Re-cured**	
	(kNm^2)	(kNm^2)	(%)	(kNm^2)	(%)	(kNm^2)	(%)
CAP	816	538	65.9	487	59.7	684	83.8
CAH	826	514	62.2	529	64.0	657	79.5
SAP	786	538	68.4	515	65.5	645	82.1
SAH	847	587	69.3	595	70.2	724	85.5
	Avg.	544	66.5	532	64.9	678	82.7

6. CONCLUSION

In this study, deterioration and recovery of mechanical properties of various kinds of concrete under air and water re-curing regimes were investigated. Moreover, effects of widely used materials in concrete such as fibers, mineral and chemical admixtures on disintegration and recovery of concrete were evaluated. Therefore, an experimental study which had two stages was designed. For the first stage of the study 15x15x15cm cubic concrete specimens were produced and these specimens were subjected to 1000°C in an electrical furnace under one face heating conditions. Experimental procedure of the first stage of the study was summarized in Table 6.1.

At the second stage of the study post fire behavior of reinforced concrete was investigated. After evaluation of the results of first part of the study was completed 4 concrete groups were determined. By using selected concrete groups reinforced concrete beams were cast and these RC beams were subjected to ISO-834 cellulosic fire scenario in a full sized fire room. Experimental procedure of the second part of the study was summarized in Table 6.2.

6.1. Tests on Small Sized Concrete Specimens

Physical and mechanical properties of concrete were determined before heating, after cooling and after re-curing processes. And also morphological changes were monitored at every stages. During heating processes temperatures inside concrete specimens were measured.

Mix properties of concrete groups without air entrainment were determined in order to obtain 50 MPa of compressive strength at 28 day. However, initial mechanical properties of every concrete group were determined before heating which corresponds to 3 months after concrete production. Therefore, there were prominent differences in mechanical properties of concrete groups due to puzzolanic effects. Also air entrainment caused decreases in mechanical properties. Before heating, Portland cement concrete

Table 6.1. Summary of the first stage of the study.

Concrete dimensions	15x15x15 cm cubes
Water to cement ratio	0.45
Cementitious	Portland cement Pulvarized fly ash Graund granulated blast furnace slag
Total cement content for $1m^3$ concrete	450 kg
Maximum aggregate size	22 mm
Fibers	Multi-filament polypropylene Hooked end steel
Chemical admixture	Air entraining admixture
Heating procedure	One face heating
Maximum heating temperature	1000°C
Total duration of heating	200 minutes
Cooling method	Natural in furnace
Re-curing method	28 days of air re-curing 28 days of water re-curing
Tests and investigations	Spalling statistics Mass loss monitoring Compression tests X-Ray diffraction analyses SEM investigations Thermogravimetric analyses Black pixel analyses

Table 6.2. Summary of the second stage of the study.

Reinforced concrete beam dimensions	180x25x20 cm beams
Water to cement ratio	0.45
Concrete groups	CAP, CAH, SAP, SAH
Maximum aggregate size	22 mm
Reinforcing elements	$2\phi12+2\phi12$ S420 $8\phi/15$ S420
Heating procedure	ISO-834
Total duration of heating	120 minutes
Cooling method	Air cooling in furnace
Re-curing method	28 days of air re-curing 28 days of water re-curing
Tests and investigations	Flexural bending tests SEM investigations

groups without air entrainment had compressive strength in the range of 55 MPa - 64 MPa while compressive strength of air entrained Portland cement groups were in the range of 50 MPa - 55 MPa. GGBFS concrete groups without air entrainment had compressive strength in the range of 60 MPa - 63 MPa while compressive strength of air entrained GGBFS groups were in the range of 49 MPa - 57 MPa. PFA concrete groups without air entrainment had compressive strength in the range of 69 MPa - 71 MPa while compressive strength of air entrained PFA groups were in the range of 59 MPa - 62 MPa.

Before heating, Portland cement concrete groups without air entrainment had modulus of elasticity in the range of 28.7 GPa - 30.3 GPa while modulus of elasticity of air entrained Portland cement groups were in the range of 27.2 GPa - 29.4 GPa. GGBFS concrete groups without air entrainment had modulus of elasticity in the range of 29.3 GPa - 31.8 GPa while modulus of elasticity of air entrained GGBFS groups were in the range of 26.9 GPa - 28.8 GPa. PFA concrete groups without air entrainment had

modulus of elasticity in the range of 30.8 GPa - 33.5 GPa while modulus of elasticity of air entrained PFA groups were in the range of 28.5 GPa - 30.7 GPa.

Using air entraining admixtures in concrete groups influenced firstly the densities of concrete. Before heating, densities of concrete groups without air entrainment at hardened state were similar and around 2.40 gr/cm^3 and densities of air entrained concrete groups at hardened state were very close and around 2.31 gr/cm^3. Entrained air voids affect thermal properties of concrete and therefore during heating air entrained concrete specimens experienced lower temperatures than concrete groups without air entrainment.

6.1.1. After Cooling

Temperature monitoring data showed that inner parts of concrete experienced lower temperatures than surface of concrete. On the other hand, concrete groups without air entrainment experienced at least 578°C while air entrained concrete groups experienced at least 534°C (According to data collected by thermocouples placed 113mm below the heated surface.). Therefore, severe deteriorations in all concrete groups were expected after heating.

First indication of this deterioration was the sound of spalling of concrete in furnace during heating. Spalling was observed especially in non-fibrous concrete groups. Risk of spalling of fiber reinforced concrete especially PP fiber reinforced ones was significantly lower than other groups. Addition of air entraining admixture was also found beneficial in order to improve spalling resistance of concrete. On the other hand using mineral admixtures increased the risk of spalling especially addition of pulverized fly ash since half of the PFA groups experienced spalling during heating.

After heating mass losses of concrete specimens were observed and mass losses were approximately 8% after heating. Because of the fact that free water evaporates after 100°C, chemically bonded water also evaporates and after 600°C calcite formations in concrete release carbon dioxide. By the way concrete shrinks with an increasing tem-

perature and cracks occur in concrete. Morphological changes due to chemical activity were monitored after heating and SEM investigations showed that overall morphology of concrete turned to a granular and amorphous form after heating. C-S-H gel lost its extensions and densified after heating hence molar ratio of C-S-H increased and was measured around 1.8. Moreover, ettringite and $Ca(OH)_2$ crystals disappeared after heating. XRD results sowed that calcium silicates appeared after heating since C-S-H lost its water content. Additionally, this results were confirmed by TGA analysis since no peaks representing $Ca(OH)_2$ and $CaCO_3$ decomposition were observed on DTA results of concrete groups tested after cooling.

Survived specimens had existing cracks after heating which resulted in mechanical degradation especially in modulus of elasticity of concrete. Compression tests results revealed that reductions in modulus of elasticities were approximately 81% and higher than reductions in compressive strength of concrete which was around 36.2% after heating. When mineral added concrete groups are evaluated separately it can be seen that concrete groups incorporating GGBFS and concrete groups incorporating PFA retained their mechanical properties slightly higher than Portland cement concrete groups. Effect of air entrainment was found negative since 10% higher reduction was observed in residual compressive strength of air entrained concrete groups but spalling tendencies of air entrained concrete specimens decreased.

Although polypropylene fibers have positive effect on spalling resistance of concrete polypropylene fiber reinforced concrete groups exhibited higher reduction in both residual compressive strength and residual modulus of elasticity. This negative effect was also observed in hybrid fiber reinforced groups since hybrid fiber groups include polypropylene fibers also.

6.1.2. After Air Re-curing

Cracks on the air re-cured concrete specimens increased day by day after cooling. To be able to understand crack occurring rate after cooling heated surfaces of concrete specimens were monitored by using a DSLR camera for a period of time. Captured pho-

tos were uploaded to an image analysis software called ImageJ and black pixel analyses were conducted on them. BPA results showed that there was a relation between crack occurring rate which was also called BPA rate and reduction in compressive strength of concrete. As the BPA rate of a concrete group increased reduction in compressive strength increased during air re-curing.

SEM investigations showed that overall morphology of concrete especially calcium silicate formations remained almost same after air re-curing. TGA and XRD analyses revealed that $Ca(OH)_2$ and $CaCO_3$ were formed in air re-cured concrete samples. The reason of further cracking and mechanical degradation was considered as phase change of CaO to $Ca(OH)_2$ with an excessive volume increase. This expansive reaction resulted in extra cracking on the heated surface which experienced higher temperatures during heating and was damaged higher than other parts of concrete.

Due to this continuous deteriorations in concrete during air re-curing mechanical properties of concrete continued to decrease in this period. Reduction in compressive strength increased from 36.2% to 52.6% in average and reduction in modulus of elasticity increased from 81% to 88% in average. Retrogression in residual compressive strength was again higher in Portland cement concrete groups than mineral added concrete groups. In this period there were no prominent effect of air entrainment on residual mechanical properties of concrete. Similar to after cooling compression test results reduction in polypropylene fiber reinforced concrete groups was higher than other concrete groups. Because, melted polypropylene fiber channels may combine with new cracks during air re-curing. On the other hand, reduction in mechanical properties of steel fiber reinforced group was limited and lower than other groups. Survived steel fibers probably prevented concrete from further cracking in this period.

Moreover, long term effects of air re-curing on residual mechanical properties of concrete were investigated and it was found that average mechanical properties of concrete groups which were subjected to long term air re-curing continued to decrease slowly.

6.1.3. After Water Re-curing

Water re-cured concrete specimens kept their physical stabilities and disintegration was not observed in water re-cured specimens. Also mass of concrete specimens prominently increased and was around 100.6% of initial value (before heating) since they absorbed curing water in this period. According to TGA results, at least half of the increase was chemically bonded water and carbon dioxide. Microstructure of concrete prominently changed after water re-curing, granular formations and porous structure disappeared in this period. TGA and XRD results also revealed that there was no $Ca(OH)_2$ on the heated and water re-cured surface of specimens since $Ca(OH)_2$ is a soluble compound in water. Therefore, no additional cracks were observed on water re-cured concrete specimens. On the other hand, some of the small cracks on the water re-cured surface were filled by $CaCO_3$ formations. $Ca(OH)_2$ formations were found at the inner part of concrete via TGA and $Ca(OH)_2$ content was higher than air re-cured concrete in this part of concrete. Since C-S-H formation was observed in water re-cured sample via XRD analyses it can be concluded that concrete regained or at least preserved its residual strength and some of the internal and external cracks were filled with hydration products like $Ca(OH)_2$ and carbonation products $CaCO_3$ resulting in recovery in modulus of elasticity of concrete.

Reduction in residual compressive strength of water re-cured concrete specimens decreased from 36.2% to 29.4%. Recovery in modulus of elasticity was more pronounced and reduction in residual modulus of elasticity of water re-cured concrete specimens decreased from 81% to 49%. Higher amount of recovery in both compressive strength and modulus of elasticity was obtained in mineral added concrete groups. While there was no prominent effect of air entrainment in residual compressive strength, higher recovery was obtained in modulus of elasticity of air re-cured concrete groups than concrete groups without air entrainment. Although, polypropylene fiber reinforcement had negative effects on residual mechanical properties of concrete after heating and during air re-curing, polypropylene fiber reinforced concrete showed higher recovery since micro channels formed after heating in these concrete groups probably increased water diffusion rate.

Additionally, long term effects of water re-curing on residual mechanical properties of concrete were investigated and it was found that average mechanical properties of concrete groups which were subjected to long term water re-curing continued to increase slowly.

6.2. Tests on Reinforced Concrete Beams

Four concrete groups were selected regarding the results of tests on small sized concrete specimens. By using these concrete groups 16 reinforced concrete beams were cast. 12 of the beams were subjected to ISO-834 cellulosic fire scenario for 120 minutes. Then, four point flexural bending tests and SEM investigations were conducted on these reinforced concrete beams before heating, after cooling and after re-curing processes.

Similar results to SEM observations on small sized specimens were obtained during SEM investigations on reinforced concrete beams especially at the surface level. After heating overall morphology of concrete samples turned to a granular and porous form at surface level. On the other hand, $Ca(OH)_2$ crystals were observed in lower bar level samples which means that concrete experienced less than 450°C at lower bar level. It was expected because concrete cover thickness was determined according to recommendations (a=65mm) in order to preserve reinforcing steel during 120 minutes of heating. After air re-curing period $Ca(OH)_2$ formations were observed on heated surfaces also. On the other hand, after water re-curing overall morphology changed again and granular and porous microstructure of concrete disappeared.

Four point bending test results showed that residual load bearing capacities of reinforced beams decreased approximately 12% after cooling. After air and water re-curing periods load bearing capacities remained almost same. Then, areas under load-deformation curves were calculated in order to obtained flexural toughness values. After air re-curing flexural toughness values slightly diminished while increases were observed in flexural toughness of water re-cured reinforced concrete beams. The reason of this recovery was the increase in flexural rigidities of water re-cured reinforced concrete beams. Therefore, instantaneous flexural rigidities were obtained by using the load-

deflection formulas for every single load-deflection data collected during bending tests. Flexural rigidity of beams increased to 82.7% of initial value after water re-curing while it was 66.5% of initial value after cooling.

6.3. Recommendations

Taking actions in subsequent days of heating or a fire is vital since chemical changes continue in this period and determine fate of concrete. Water re-curing can be considered as one of the proper way to preserve concrete from further cracking and mechanical deterioration. If water re-curing will not be applicable for a structure some precautions can be taken such as using high melting point fibers in concrete because of the fact that in the event of fire they can survive and limit the crack formation at the post fire stage. In general, use of PP fibers, steel fibers and air entraining admixtures is suggested to prevent and/or delay spalling. Though PP fibers result in higher deteriorations in the after cooling period they showed better performance by means of regain in mechanical properties after water re-curing. Although using mineral admixtures is an economical and environmentally friendly solution to obtain a durable concrete they should be carefully used since their use in a non-fibrous concrete can increase risk of spalling during heating.

According to the results of this study it is clear to see that $Ca(OH)_2$ content in concrete decreases during water re-curing period while there is an increase in the amount of $CaCO_3$ in concrete cover. This may result in reduction in Ph level of concrete at the reinforcing bar level and therefore corrosion of reinforcing bar may occur due to higher carbonation in concrete cover. Additionally, there can be cracks on the heated concrete surface which may accelerate corrosion of steel reinforcement. Therefore, corrosion of reinforcing steel in water re-cured concrete can be further investigated.

REFERENCES

1. Neville, A. M., *Properties of Concrete*, Longman Scientific and Technical, New York, NY, USA, 2000.

2. Akca, A. H. and N. Özyurt Zihnioğlu, "High Performance Concrete under Elevated Temperatures", *Construction and Building Materials*, Vol. 44, pp. 317–328, 2013.

3. Akca, A. H., "The effects of polypropylene fiber and air entraining admixture addition on high performance concrete exposed to elevated temperatures", *Dissertation*, p. 135, 2011.

4. Poon, C. S., S. Azhar, M. Anson and Y. K. Wong, "Comparison of the Strength and Durability Performance of Normal and High Strength Pozzolanic Concretes at Elevated Temperatures", *Cement and Concrete Research*, Vol. 31, pp. 1291–1300, 2001.

5. Kalifa, P., F. D. Menneteau and D. Quenard, "Spalling and Pore Pressure in HPC at High Temperature", *Cement and Concrete Research*, Vol. 30, pp. 1915–1927, 2000.

6. Mofokeng, J. P., A. S. Luyt, T. Tabi and J. Kovacs, "Comparison of injection moulded, natural fibre-reinforced composites with PP and PLA as matrices", *Journal of Thermoplastic Composite*, Vol. 25, pp. 927–948, 2011.

7. Han, C. G., Y. S. Hwang, S. H. Yang and N. Gowripalan, "Performance of Spalling Resistance of High Performance Concrete with Polypropylene Fiber Contents and Lateral Confinement", *Cement and Concrete Research*, Vol. 35, pp. 1747–1753, 2005.

8. Chen, B. and J. Liu, "Residual Strength of Hybrid-Fiber-Reinforced High-Strength Concrete after Exposure to High Temperatures", *Cement and Concrete Research*,

Vol. 34, pp. 1065–1069, 2004.

9. Bazant, Z. P. and M. F. Kaplan, *Concrete at High Temperatures: Material Properties and Mathematical Models*, Longman Group Ltd., Harlow, England, 1996.

10. Crook, D. N. and M. J. Murray, "Regain of Strength and Firing of Concrete", *Magazine of Concrete Research*, Vol. 22, pp. 149–154, 1970.

11. Sarshar, R. and G. A. Khoury, "Material and Environmental Factors Influencing the Compressive Strength of Unsealed Cement Paste and Concrete at High Temperatures", *Magazine and Concrete Research*, Vol. 45, pp. 51–61, 1993.

12. Poon, C. H., S. Azhar, M. Anson and Y. Wong, "Strength and Durability Recovery of Fire-Damaged Concrete After Post-Fire-Curing", *Cement and Concrete Research*, Vol. 31, pp. 1307–1318, 2001.

13. Khoury, G. A., "Effect of Fire on Concrete and Concrete Structures", *Structural Engineering Materials*, Vol. 22, pp. 429–447, 2000.

14. Falck Productions, *Classes of Fire*, 2017, http://www.falckproductions.com/resources/fire-safety-and-firewatch/classes-of-fire-a-b-c-d-and-k/, accessed at September 2017.

15. Safety Poster Shop, *Fire extinguisher USA classification*, 2012, https://www.safetypostershop.com/industrial-safety-posters/fire-classification-usa-and-canada/, accessed at September 2017.

16. Promat, *Tunnel Fire Protection of Tunnel Structures and Services*, 2008, http://www.promat-tunnel.com/downloads/get/en/def78d67-8ac7-43fa-943e-5ede00cc648e, accessed at September 2017.

17. Concrete Construction, *Effect of High Temperature on Hardened Concrete*, 1971, http://www.concreteconstruction.net/how-to/materials/effect-of-high-

temperature-on-hardened-concrete_o, accessed at September 2017.

18. REOTEMP Instrument Corporation, *Thermocouple Info*, 2011, http://www.thermocoupleinfo.com/thermocouple-types.htm, accessed at September 2017.

19. The European Union Per Regulation, *Eurocode 2: Design of concrete structures - Part 1-2: General rules - Structural fire design*, European Committee for Standardization, Brussels, Belgium, 1992.

20. Ma, Q., R. Guo, Z. Zhao, Z. Lin and K. He, "Mechanical properties of concrete at high temperature—A review", *Construction and Building Materials*, Vol. 93, pp. 371–383, 2015.

21. Uysal, M., "Self-compacting concrete incorporating filler additives: Performance at high temperatures", *Construction and Building Materials*, Vol. 26, pp. 701–706, 2012.

22. Dias, W., G. Khoury and P. Sullivan, "Self-compacting concrete incorporating filler additives: Performance at high temperatures", *Construction and Building Materials*, Vol. 87, pp. 160–166, 1990.

23. Khoury, G., "Compressive strength of concrete at high temperature: a reassessment", *Magazine of concrete research*, Vol. 44, pp. 291–309, 1992.

24. Tanyildizi, H. and A. Coskun, "The effect of high temperature on compressive strength and splitting tensile strength of structural lightweight concrete containing fly ash", *Construction and Building Materials*, Vol. 22, pp. 2269–2275, 2008.

25. Behnood, A. and H. Ziari, "Effects of silica fume addition and water to cement ratio on the properties of high-strength concrete after exposure to high temperatures", *Cement and concrete composites*, Vol. 30, pp. 106–112, 2008.

26. Chan, Y., G. F. Peng and M. Anson, "Residual strength and pore structure of high-strength concrete and normal strength concrete after exposure to high temperatures", *Cement and Concrete Composites*, Vol. 21, pp. 23–27, 1999.

27. Li, M., C. Qian and W. Sun, "Mechanical properties of high-strength concrete after fire", *Cement and Concrete Research*, Vol. 34, pp. 1001–1005, 2004.

28. Hossain, K. M. A., "High strength blended cement concrete incorporating volcanic ash: Performance at high temperatures", *Cement and Concrete Composites*, Vol. 28, pp. 535–545, 2006.

29. Seleem, H. H., A. M. Rashad and T. Elsokary, "Effect of elevated temperature on physico-mechanical properties of blended cement concrete", *Construction and Building Materials*, Vol. 25, pp. 1009–1107, 2011.

30. Hertz, K. D., "Limits of Spalling of Fire Exposed Concrete", *Fire Safety Journal*, Vol. 38, p. 1, 2003.

31. Kodur, V. K. R., F. Cheng, T. Wang and M. A. Sultan, "Effect of strength and fiber reinforcement on fire resistance of high-strength concrete columns", *Journal of Structural Engineering*, Vol. 129, pp. 253–259, 2003.

32. Wu, B., E. S. Lam, Q. Liu, W. Y. Chung and F. Ho, "Creep behavior of high-strength concrete with polypropylene fibers at elevated temperatures", *ACI Materials Journal*, Vol. 107, pp. 176–184, 2010.

33. Komonen, J. and V. Penttala, "Effects of High Temperature on the Pore Structure and Strength of Plain and Polypropylene Fiber Reinforced Cement Pastes", *Fire Technology*, Vol. 39, pp. 23–34, 2003.

34. Sideris, K. K., P. Manita and E. Chaniotakis, "Performance of thermally damaged fibre reinforced concretes", *Construction and Building Materials*, Vol. 23, pp. 1232–1239, 2009.

35. Poon, C. S., Z. H. Shui and L. Lam, "Compressive behavior of fiber reinforced high-performance concrete subjected to elevated temperatures", *Cement and Concrete Research*, Vol. 34, pp. 2215–2222, 2004.

36. Peng, G., W. Yang, J. Zhao, Y. Liu, S. Bian and L. Zhao, "Explosive spalling and residual mechanical properties of fiber-toughened high-performance concrete subjected to high temperatures", *Cement and Concrete Research*, Vol. 36, pp. 723–727, 2006.

37. Seçer, O., "Strength properties of concretes with fiber, entrained air and expanded perlite aggregates after exposure to high temperatures and confinement with GFRP", *Dissertation*, p. 117, 2008.

38. Savva, A., P. Manita and K. K. Sideris, "Influence of elevated temperatures on the mechanical properties of blended cement concretes prepared with limestone and siliceous aggregates", *Cement and Concrete Composites*, Vol. 27, pp. 239–248, 2005.

39. Li, Q., Z. Li and G. Yuan, "Effects of elevated temperatures on properties of concrete containing ground granulated blast furnace slag as cementitious material", *Construction and Building Materials*, Vol. 35, pp. 687–692, 2012.

40. Culfik, M. S. and T. Ozturan, "Effect on elevated temperatures on the Residual Mechanical Properties of High-Performance Mortar", *Cement and Concrete Research*, Vol. 32, pp. 809–816, 2002.

41. Chan, Y. N., X. Luo and W. Sun, "Compressive strength and pore structure of high-performance concrete after exposure to high temperature up to 800 degrees C", *Cement and Concrete Research*, Vol. 30, pp. 247–251, 2000.

42. Aydın, S., "Development of a High-Temperature-Resistant Mortar by Using Slag and Pumice", *Fire Safety Journal*, Vol. 43, pp. 610–617, 2008.

43. Lau, A. and M. Anson, "Effect of High Temperatures on High Performance Steel Fibre Reinforced Concrete", *Cement and Concrete Research*, Vol. 36, pp. 1698–1707, 2006.

44. Yermak, N., P. Pliya, A. L. Beaucour, A. Simon and A. Noumowe, "Influence of steel and/or polypropylene fibres on the behaviour of concrete at high temperature: Spalling, transfer and mechanical properties", *Construction and Building Materials*, Vol. 132, pp. 240–250, 2017.

45. Mendes, A., J. Sanjayan and F. Collins, "Long-Term Progressive Deterioration Following Fire Exposure of OPC versus Slag Blended Cement Pastes", *Materials and Structures*, Vol. 42, pp. 95–101, 2009.

46. Mendes, A., J. Sanjayan and F. Collins, "Effects of slag and cooling method on the progressive deterioration of concrete after exposure to elevated temperatures as in a fire event", *Materials and Structures*, Vol. 44, pp. 709–718, 2011.

47. Mendes, A., J. G. Sanjayan, W. P. Gates and F. Collins, "The Influence of Water Absorption and Porosity on the Deterioration of Cement Paste and Concrete Exposed to Elevated Temperatures, as in a Fire Event", *Cement and Concrete Composites*, Vol. 34, pp. 1067–1074, 2012.

48. Arioz, O., "Effects of elevated temperatures on properties of concrete", *Fire Safety Journal*, Vol. 42, pp. 516–522, 2007.

49. Mendes, A., J. Sanjayan and F. Collins, "Phase transformations and mechanical strength of OPC/Slag pastes submitted to high temperatures", *Materials and Structures*, Vol. 41, pp. 345–350, 2008.

50. Petzold, A. and M. Rohrs, *Concrete for High Temperatures*, Maclaren and Sons Ltd., London, England, 1970.

51. Akca, A. H. and N. Özyurt Zihnioğlu, "Effects of Post-Fire Curing on the Proper-

ties of HPCC", *Cementürk*, Vol. 30, pp. 58–65, 2013.

52. Lin, W. M., T. Lin and L. J. Powers-Couche, "Microstructures of Fire-Damaged Concrete", *ACI Materials Journal*, Vol. 93, pp. 199–205, 1996.

53. Horiguchi, T. and S. L. Suhaendi, "Recovery Behavior of Hybrid Fiber Reinforced High Strength Concrete After Fire Exposure", *Journal of Structural Fire Engineering*, Vol. 1, pp. 219–229, 2010.

54. Alonso, C. and L. Fernandez, "Dehydration and rehydration processes of cement paste exposed to high temperature environments", *Journal of Materials Science*, Vol. 39, pp. 3015–3024, 2004.

55. Jiangtaoa, Y., L. Zhaoudaoa and X. Kaib, "Experimental Study on the Performance of RC Continuous", *Procedia Engineering*, Vol. 14, pp. 821–829, 2011.

56. Ellingwood, B. and T. D. Lin, "Flexural and Shear Behavior of Concrete Beams During Fires", *Journal of Structural Engineering*, Vol. 117, pp. 440–458, 1991.

57. Zhang, D., Y. Fang and Y. Dong, "Behaviour of full-scale two-way simply supported concrete slabs in fire", *Magazine of Concrete Research*, Vol. 66, pp. 836–844, 2014.

58. Bailey, C. G. and W. S. Toh, "Behaviour of concrete floor slabs at ambient and elevated temperatures", *Fire Safety Journal*, Vol. 42, pp. 425–436, 2007.

59. Huang, Z., "The behaviour of reinforced concrete slabs in fire", *Fire Safety Journal*, Vol. 45, pp. 271–282, 2010.

60. Chen, Y., Y. Chang, G. YTao and M. Sheu, "Experimental research on post-fire behaviour of reinforced concrete columns", *Fire Safety Journal*, Vol. 44, pp. 741–748, 2009.

61. Lee, H. S., X. Y. Wang, L. N. Zhang and K. T. Koh, "Analysis of the Optimum

Usage of Slag for the Compressive Strength of Concrete", *Materials*, Vol. 8, pp. 1213–1229, 2015.

62. Chang, Y. F., Y. H. Chen, M. S. Sheu and G. C. Yao, "Residual stress-strain relationship for concrete after exposure to high temperatures", *Cement and Concrete Research*, Vol. 36, pp. 1999–2005, 2006.

63. Ingham, J. P., "Application of petrographic examination techniques to the assessment of fire-damaged concrete and masonry structures", *Materials Characterization*, Vol. 21, pp. 23–27, 2009.

64. Yüzer, N., F. Aköz and L. D. Öztürk, "Compressive strength–color change relation in mortars at high temperature", *Cement and Concrete Research*, Vol. 34, pp. 1803–1807, 2004.

65. Menendez, E. and L. Vega, "Analysis of the behaviour of the structural concrete after the fire at the Windsor Building in Madrid", *Fire and Materials*, Vol. 34, pp. 95–107, 2010.

66. Branda, F., G. Luciani, A. Costantini and C. Piccioli, "Interpretation of the thermogravimetric curves of ancient pozzolanic concretes", *Archaeometry*, Vol. 43, pp. 447–453, 2001.

67. Villain, G., M. Thiery and G. Platret, "Measurement methods of carbonation profiles in concrete: Thermogravimetry, chemical analysis and gammadensimetry", *Cement and Concrete Research*, Vol. 37, pp. 1182–1192, 2007.

68. Shen, Q., B. Bao and G. Pan, "Influence of CSH carbonation on the porosity of cement paste", *Magazine of Concrete Research*, Vol. 68, pp. 504–514, 2016.

69. Djaknoun, S., E. Quedraogo and A. A. Benyahia, "Characterization of the behavior of high performance mortar subjected to high temperatures", *Construction and Building Materials*, Vol. 28, pp. 176–186, 2012.

70. Akca, A. H. and N. Özyurt Zihnioğlu, "Mechanical behavior and recovery of FRC after high temperature exposure", *Key Engineering Materials*, Vol. 711, pp. 457–464, 2016.

71. Hou, D., Z. Li and H. Ma, "Morphology of calcium silicate hydrate (C-S-H) gel: a molecular dynamic study", *Advances in Cement Research*, Vol. 27, pp. 135–146, 2015.

72. Taylor, H. F. W., *Cement chemistry*, , Academic Press Limited, London, England, 1992.

73. Reardon, E. J. and R. Fagan, "The calcite/portlandite phase boundary: enhanced calcite solubility at high pH", *Applied Geochemistry*, Vol. 15, pp. 327–335, 2000.

74. Palardy, D., M. Onofrei and G. Ballivy, "Microstructural changes due to elevated temperature in cement based grouts", *Advanced Cement Based Materials*, Vol. 8, pp. 132–138, 1998.

75. Peng, G. and Z. Huang, "Change in microstructure of hardened cement paste subjected to elevated temperatures", *Construction and Building Materials*, Vol. 22, pp. 593–599, 2008.

APPENDIX A: MASS CHANGE TABLES

Masses of the specimens before heating, after cooling, after air re-curing and after water re-curing were given in following tables. "0" sign represents the specimen before heating, "X" represents the specimen tested just after cooling. "Z" and "W" represent air re-cured specimen and water re-cured specimen, respectively.

Table A.1. Mass changes of C00 concrete.

C00 (#)	**0** (g)	**X** (g)	**(X-0)/0** (%)	**Z** (g)	**(Z-0)/0** (%)	**W** (g)	**(W-0)/0** (%)
1	7989	7341	-8.1				
2	8069	7460	-7.5				
3	8034	7451	-7.3				
4	8102	7471	-7.8	7514	-7.3		
5	8171	7520	-8.0	7601	-7.0		
6	8108	Spalled					
7	8059	7416	-8.0			8096	0.5
8	8008	Spalled					
9	8017	Spalled					
AVG	8062	7443	-7.8	7558	-7.1	8096	0.5

Table A.2. Mass changes of C0S concrete.

C0S (#)	**0** (g)	**X** (g)	**(X-0)/0** (%)	**Z** (g)	**(Z-0)/0** (%)	**W** (g)	**(W-0)/0** (%)
1	8260	7542	-8.7				
2	8200	7616	-7.1				
3	8180	7523	-8.0				
4	8170	7542	-7.7	7727	-5.4		
5	8049	7531	-6.4			7978	-0.9
6	8140	Spalled					
7	8040	7452	-7.3	7531	-6.3		
8	8131	Spalled					
9	8096	7438	-8.1			8103	0.1
AVG	8141	7521	-7.6	7629	-5.9	8041	-0.4

Table A.3. Mass changes of C0P concrete.

C0P (#)	**0** (g)	**X** (g)	**(X-0)/0** (%)	**Z** (g)	**(Z-0)/0** (%)	**W** (g)	**(W-0)/0** (%)
1	8040	7413	-7.8				
2	8068	7447	-7.7				
3	7803	7151	-8.4				
4	8122	7469	-8.0	7491	-7.8		
5	8034	7375	-8.2	7409	-7.8		
6	8037	7376	-8.2	7378	-8.2		
7	8100	7450	-8.0			8180	1.0
8	7830	7210	-7.9			7916	1.1
9	7860	7190	-8.5			7933	0.9
AVG	7988	7342	-8.1	7426	-7.9	8010	1.0

Table A.4. Mass changes of C0H concrete.

C0H (#)	**0** (g)	**X** (g)	**(X-0)/0** (%)	**Z** (g)	**(Z-0)/0** (%)	**W** (g)	**(W-0)/0** (%)
1	8020	7488	-6.6	7488	-6.6		
2	8110	7579	-6.5	7579	-6.5		
3	8030	7446	-7.3	7446	-7.3		
4	8072	7445	-7.8			8120	0.6
5	8058	7423	-7.9			8051	-0.1
6	8053	7381	-8.3			8137	1.0
7	8090	7460	-7.8				
8	8060	7440	-7.7				
9	8100	7430	-8.3				
AVG	8066	7455	-7.6	7504	-6.8	8103	0.5

Table A.5. Mass changes of CA0 concrete.

CA0 (#)	**0** (g)	**X** (g)	**(X-0)/0** (%)	**Z** (g)	**(Z-0)/0** (%)	**W** (g)	**(W-0)/0** (%)
1	7729			7208	-6.7		
2	7915						
3	7793	7181	-7.9			7861	0.9
4	7802	7196	-7.8	7286	-6.6		
5	7806	7224	-7.5	7268	-6.9		
6	7841	7192	-8.3				
7	8022	7421	-7.5			8032	0.1
8	7896	7292	-7.6			7861	-0.4
9	7865	7217	-8.2				
AVG	7852	7246	-7.8	7254	-6.7	7918	0.2

Table A.6. Mass changes of CAS concrete.

CAS (#)	**0** (g)	**X** (g)	**(X-0)/0** (%)	**Z** (g)	**(Z-0)/0** (%)	**W** (g)	**(W-0)/0** (%)
1	7883	7219	-8.4				
2	7864	7246	-7.9				
3	7827	7208	-7.9				
4	7883	7220	-8.4				
5	7726	7108	-8.0			7787	0.8
6	7797	7198	-7.7			7868	0.9
7	7843	7203	-8.2			7949	1.4
8	7987	7370	-7.7	7463	-6.6		
9	7797	7196	-7.7	7323	-6.1		
10	7958	7306	-8.2	7404	-7.0		
AVG	7854	7228	-8.0	7397	-6.5	7868	1.0

Table A.7. Mass changes of CAP concrete.

CAP (#)	**0** (g)	**X** (g)	**(X-0)/0** (%)	**Z** (g)	**(Z-0)/0** (%)	**W** (g)	**(W-0)/0** (%)
1	7674	7086	-7.7			7764	1.2
2	7728	7142	-7.6			7823	1.2
3	7727	7071	-8.5			7830	1.3
4	7732	7096	-8.2	7199	-6.9		
5	7704	7103	-7.8	7209	-6.4		
6	7727	7053	-8.7	7157	-7.4		
7	7635	6986	-8.5				
8	7710	7061	-8.4				
9	7756	7063	-8.9				
AVG	7710	7073	-8.3	7188	-6.9	7806	1.2

Table A.8. Mass changes of CAH concrete.

CAH (#)	**0** (g)	**X** (g)	**(X-0)/0** (%)	**Z** (g)	**(Z-0)/0** (%)	**W** (g)	**(W-0)/0** (%)
1	7751	7117	-8.2			7832	1.0
2	7921	7272	-8.2			7975	0.7
3	7810	7116	-8.9			7880	0.9
4	7789	7152	-8.2				
5	7786	7156	-8.1				
6	7827	7128	-8.9				
7	7781	7151	-8.1	7243	-6.9		
8	7848	7219	-8.0	7310	-6.9		
9	7731	7064	-8.6	7161	-7.4		
AVG	7805	7153	-8.4	7238	-7.0	7896	0.9

Table A.9. Mass changes of S00 concrete.

S00 (#)	**0** (g)	**X** (g)	**(X-0)/0** (%)	**Z** (g)	**(Z-0)/0** (%)	**W** (g)	**(W-0)/0** (%)
1	8030	Spalled					
2	8010	Spalled					
3	8125	Spalled					
4	8121	Spalled					
5	8120	Spalled					
6	8110	Spalled					
7	8000	Spalled					
8	8000	Spalled					
9	8000	Spalled					
AVG	8057	-	-	-	-	-	-

Table A.10. Mass changes of S0S concrete.

S0S (#)	**0** (g)	**X** (g)	**(X-0)/0** (%)	**Z** (g)	**(Z-0)/0** (%)	**W** (g)	**(W-0)/0** (%)
1	8183	Spalled					
2	8187	7531	-8.0				
3	8213	7523	-8.4				
4	8240	7546	-8.4	7610	-7.6		
5	8207	7549	-8.0	7624	-7.1		
6	7960	7258	-8.8	7327	-8.0		
7	8080	7416	-8.2			8152	0.9
8	8181	7474	-8.6			8196	0.2
9	7990	7301	-8.6			8052	0.8
AVG	8138	7450	-8.4	7520	-7.6	8133	0.6

Table A.11. Mass changes of S0P concrete.

S0P (#)	**0** (g)	**X** (g)	**(X-0)/0** (%)	**Z** (g)	**(Z-0)/0** (%)	**W** (g)	**(W-0)/0** (%)
1	8216	7523	-8.4				
2	8016	7328	-8.6				
3	7979	7265	-8.9				
4	8016	7402	-7.7			8153	1.7
5	8053	7358	-8.6			8102	0.6
6	8048	7311	-9.2			8070	0.3
7	8133	7424	-8.7	7484	-8.0		
8	8031	7321	-8.8	7374	-8.2		
9	8003	7292	-8.9	7296	-8.8		
AVG	8055	7358	-8.7	7385	-8.3	8108	0.9

Table A.12. Mass changes of S0H concrete.

S0H (#)	**0** (g)	**X** (g)	**(X-0)/0** (%)	**Z** (g)	**(Z-0)/0** (%)	**W** (g)	**(W-0)/0** (%)
1	8116	7415	-8.6				
2	8106	7404	-8.7				
3	8086	7356	-9.0				
4	8086	7395	-8.5			8134	0.6
5	8052	7360	-8.6			8097	0.6
6	8046	7308	-9.2			8077	0.4
7	8105	7399	-8.7	7455	-8.0		
8	8097	7419	-8.4	7478	-7.6		
9	7933	7257	-8.5	7302	-8.0		
AVG	8070	7368	-8.7	7412	-7.9	8103	0.5

Table A.13. Mass changes of SA0 concrete.

SA0 (#)	**0** (g)	**X** (g)	**(X-0)/0** (%)	**Z** (g)	**(Z-0)/0** (%)	**W** (g)	**(W-0)/0** (%)
1	7864	7057	-10.3				
2	7862	7009	-10.8				
3	7820	Spalled					
4	7877	Spalled					
5	7834	7011	-10.5			7838	0.1
6	7776	Spalled					
7	7967	7186	-9.8	7253	-9.0		
8	7935	Spalled					
9	7902	Spalled					
AVG	7871	7066	-10.4	7253	-9.0	7838	0.1

Table A.14. Mass changes of SAS concrete.

SAS (#)	**0** (g)	**X** (g)	**(X-0)/0** (%)	**Z** (g)	**(Z-0)/0** (%)	**W** (g)	**(W-0)/0** (%)
1	7905	7232	-8.5				
2	7832	7175	-8.4			7875	0.5
3	7720	7018	-9.1			7778	0.8
4	7766	7082	-8.8			7812	0.6
5	7754	7070	-8.8				
6	7738	7040	-9.0				
7	7867	7107	-9.7	7242	-7.9		
8	7819	7154	-8.5	7197	-8.0		
9	7797	7079	-9.2	7146	-8.3		
AVG	7800	7106	-8.9	7195	-8.1	7822	0.6

Table A.15. Mass changes of SAP concrete.

SAP (#)	**0** (g)	**X** (g)	**(X-0)/0** (%)	**Z** (g)	**(Z-0)/0** (%)	**W** (g)	**(W-0)/0** (%)
1	7729	7011	-9.3			7829	1.3
2	7672	6971	-9.1			7759	1.1
3	7669	6960	-9.2			7763	1.2
4	7740	7027	-9.2				
5	7681	6978	-9.2				
6	7630	6893	-9.7				
7	7799	7091	-9.1	7166	-8.1		
8	7700	7005	-9.0	7080	-8.1		
9	7641	6903	-9.7	6981	-8.6		
AVG	7696	6982	-9.3	7076	-8.3	7784	1.2

Table A.16. Mass changes of SAH concrete.

SAH (#)	**0** (g)	**X** (g)	**(X-0)/0** (%)	**Z** (g)	**(Z-0)/0** (%)	**W** (g)	**(W-0)/0** (%)
1	7743	7050	-9.0			7840	1.3
2	7715	7031	-8.9			7821	1.4
3	7670	6949	-9.4			7769	1.3
4	7756	7072	-8.8				
5	7737	7047	-8.9				
6	7669	6951	-9.4				
7	7741	7044	-9.0	7122	-8.0		
8	7732	7026	-9.1	7107	-8.1		
9	7691	6970	-9.4	7037	-8.5		
AVG	7717	7016	-9.1	7089	-8.2	7810	1.3

Table A.17. Mass changes of F00 concrete.

F00 (#)	**0** (g)	**X** (g)	**(X-0)/0** (%)	**Z** (g)	**(Z-0)/0** (%)	**W** (g)	**(W-0)/0** (%)
1	8129	Spalled					
2	8137	Spalled					
3	8168	Spalled					
4	8087	Spalled					
5	8065	Spalled					
6	8051	Spalled					
7	8227	Spalled					
8	8225	Spalled					
9	8216	Spalled					
AVG	8145	-	-	-	-	-	-

Table A.18. Mass changes of F0S concrete.

F0S (#)	**0** (g)	**X** (g)	**(X-0)/0** (%)	**Z** (g)	**(Z-0)/0** (%)	**W** (g)	**(W-0)/0** (%)
1	8227	Spalled					
2	8225	Spalled					
3	8216	Spalled					
4	8143	Spalled					
5	8099	Spalled					
6	8276	Spalled					
7	8188	Spalled					
8	8245	Spalled					
9	8205	Spalled					
AVG	8203	-	-	-	-	-	-

Table A.19. Mass changes of F0P concrete.

F0P (#)	**0** (g)	**X** (g)	**(X-0)/0** (%)	**Z** (g)	**(Z-0)/0** (%)	**W** (g)	**(W-0)/0** (%)
1	8082	7522	-6.9				
2	8120	7496	-7.7				
3	8018	7357	-8.2				
4	8013	7450	-7.0	7482	-6.6		
5	8102	7550	-6.8	7585	-6.4		
6	8101	7548	-6.8	7558	-6.7		
7	8122	7522	-7.4			8154	0.4
8	8111	7496	-7.6			8162	0.6
9	8108	7481	-7.7			8178	0.9
AVG	8086	7491	-7.4	7542	-6.6	8165	0.6

Table A.20. Mass changes of F0H concrete.

F0H (#)	**0** (g)	**X** (g)	**(X-0)/0** (%)	**Z** (g)	**(Z-0)/0** (%)	**W** (g)	**(W-0)/0** (%)
1	8129	7533	-7.3				
2	8111	7516	-7.3				
3	8049	7401	-8.1				
4	8115	7534	-7.2	7573	-6.7		
5	8114	7527	-7.2	7568	-6.7		
6	8083	7476	-7.5	7515	-7.0		
7	8135	7570	-6.9			8179	0.5
8	8130	7575	-6.8			8136	0.1
9	8037	7420	-7.7			8068	0.4
AVG	8100	7506	-7.3	7552	-6.8	8128	0.3

Table A.21. Mass changes of FA0 concrete.

FA0 (#)	**0** (g)	**X** (g)	**(X-0)/0** (%)	**Z** (g)	**(Z-0)/0** (%)	**W** (g)	**(W-0)/0** (%)
1	7924	Spalled					
2	7880	Spalled					
3	7762	Spalled					
4	7858	Spalled					
5	7792	Spalled					
6	7877	Spalled					
7	7945	Spalled					
8	7838	Spalled					
9	7769	Spalled					
AVG	7849	-	-	-	-	-	-

Table A.22. Mass changes of FAS concrete.

FAS (#)	**0** (g)	**X** (g)	**(X-0)/0** (%)	**Z** (g)	**(Z-0)/0** (%)	**W** (g)	**(W-0)/0** (%)
1	8010	Spalled					
2	7914	Spalled					
3	7834	Spalled					
4	8034	Spalled					
5	8001	Spalled					
6	7950	Spalled					
7	8009	Spalled					
8	7920	Spalled					
9	7992	Spalled					
AVG	7963	-	-	-	-	-	-

Table A.23. Mass changes of FAP concrete.

FAP (#)	**0** (g)	**X** (g)	**(X-0)/0** (%)	**Z** (g)	**(Z-0)/0** (%)	**W** (g)	**(W-0)/0** (%)
1	7726	7103	-8.1				
2	7664	7032	-8.2				
3	7629	6984	-8.5				
4	7859	7221	-8.1	7278	-7.4		
5	7806	7199	-7.8	7258	-7.0		
6	7698	7039	-8.6	7077	-8.1		
7	7843	7204	-8.1			7904	0.8
8	7825	7170	-8.4			7867	0.5
9	7698	7033	-8.6			7752	0.7
AVG	7750	7109	-8.3	7204	-7.5	7841	0.7

Table A.24. Mass changes of FAH concrete.

FAH (#)	**0** (g)	**X** (g)	**(X-0)/0** (%)	**Z** (g)	**(Z-0)/0** (%)	**W** (g)	**(W-0)/0** (%)
1	7821	7194	-8.0				
2	7837	7246	-7.5				
3	7784	7146	-8.2				
4	7757	7147	-7.9			7849	1.2
5	7773	7154	-8.0			7861	1.1
6	7753	7138	-7.9			7838	1.1
7	7843	7232	-7.8	7271	-7.3		
8	7825	7205	-7.9	7256	-7.3		
9	7720	7114	-7.8	7127	-7.7		
AVG	7790	7175	-7.9	7218	-7.4	7849	1.1

APPENDIX B: SEM IMAGES

In previous chapters SEM images were given in 50000X magnification. In order to see overall morphology same images were given in following figures at lower magnification level.

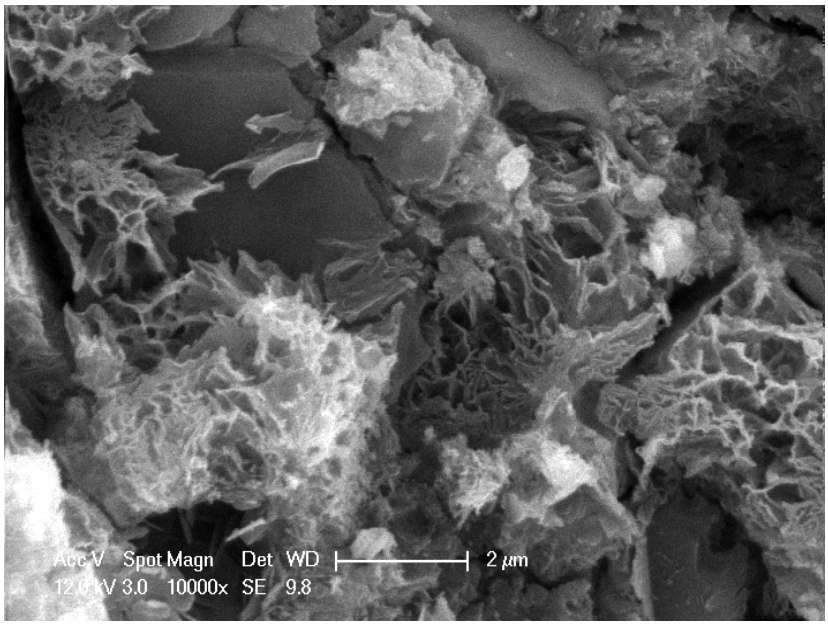

Figure B.1. Figure 4.8.a at lower magnification.

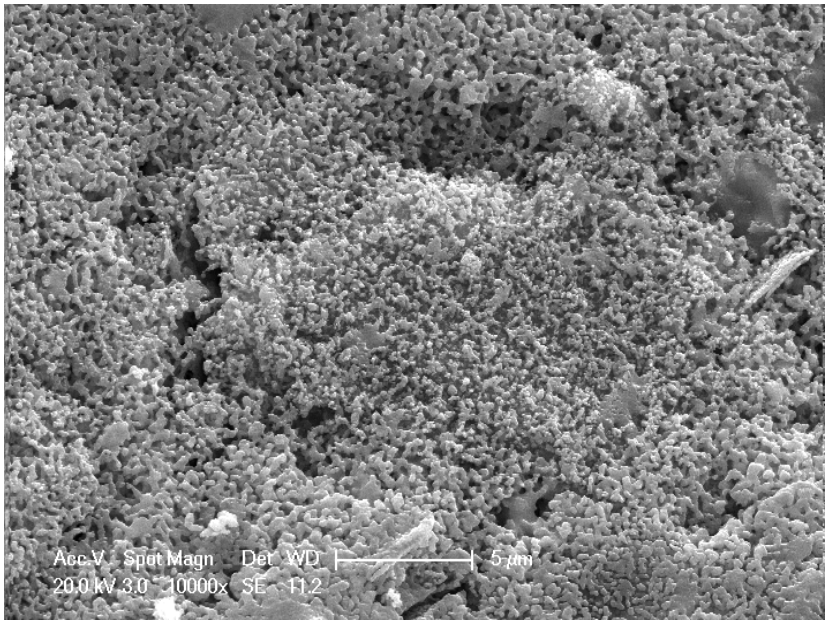

Figure B.2. Figure 4.8.b at lower magnification.

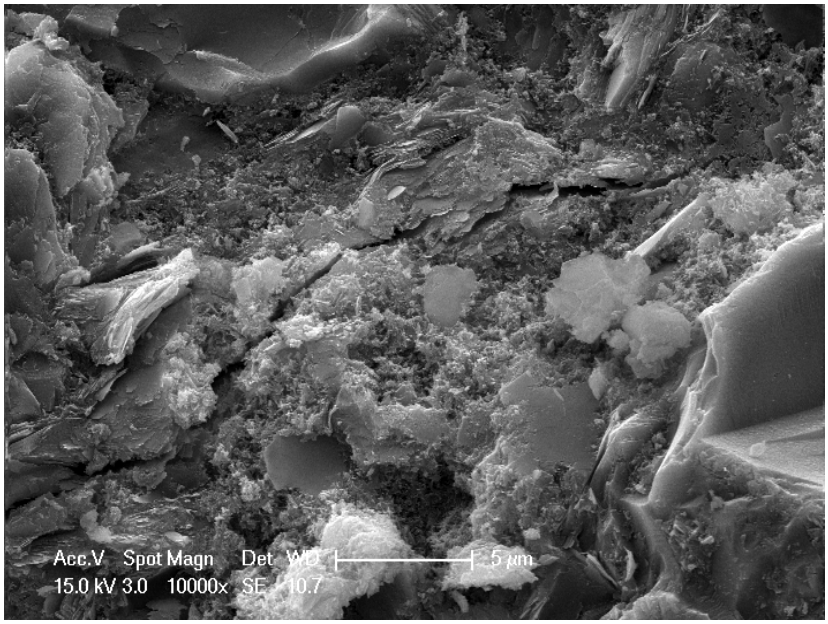

Figure B.3. Figure 4.9.a at lower magnification.

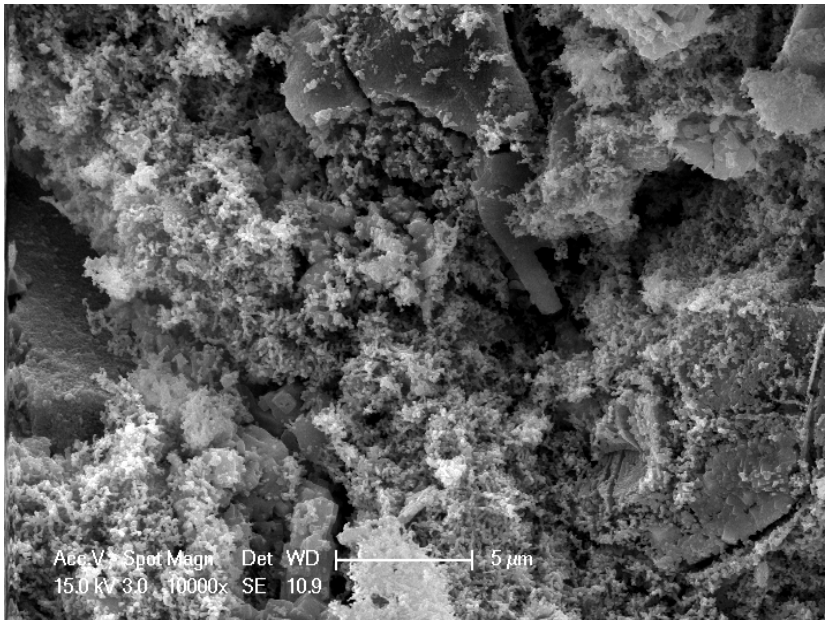

Figure B.4. Figure 4.9.b at lower magnification.

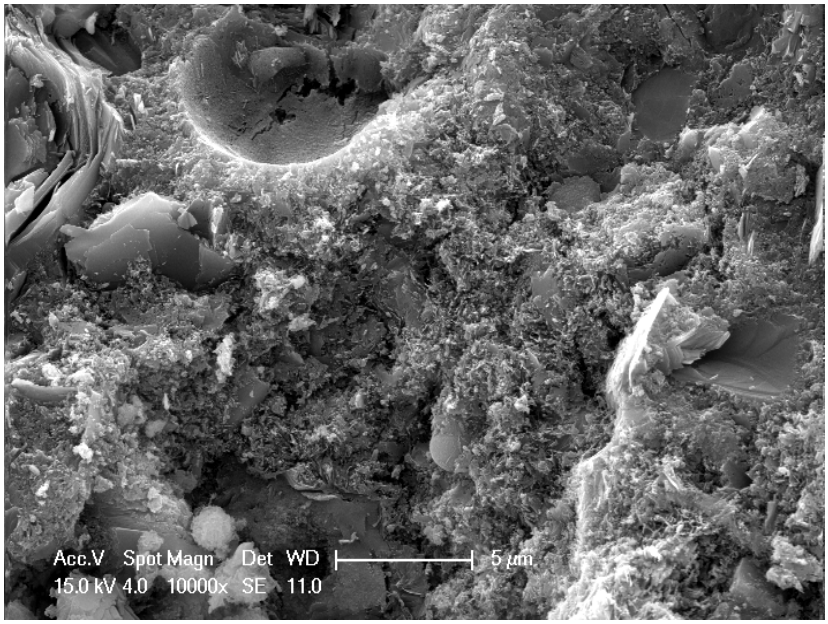

Figure B.5. Figure 4.10.a at lower magnification.

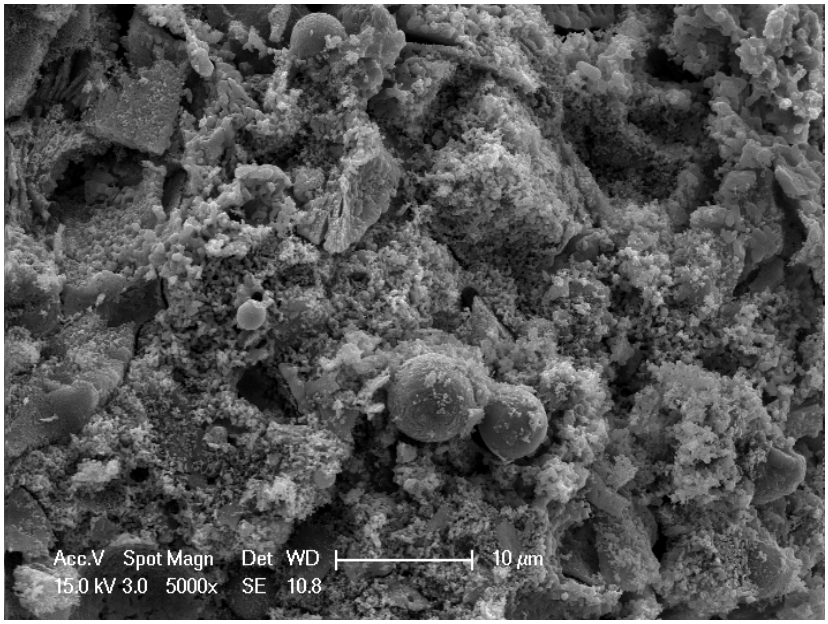

Figure B.6. Figure 4.10.b at lower magnification.

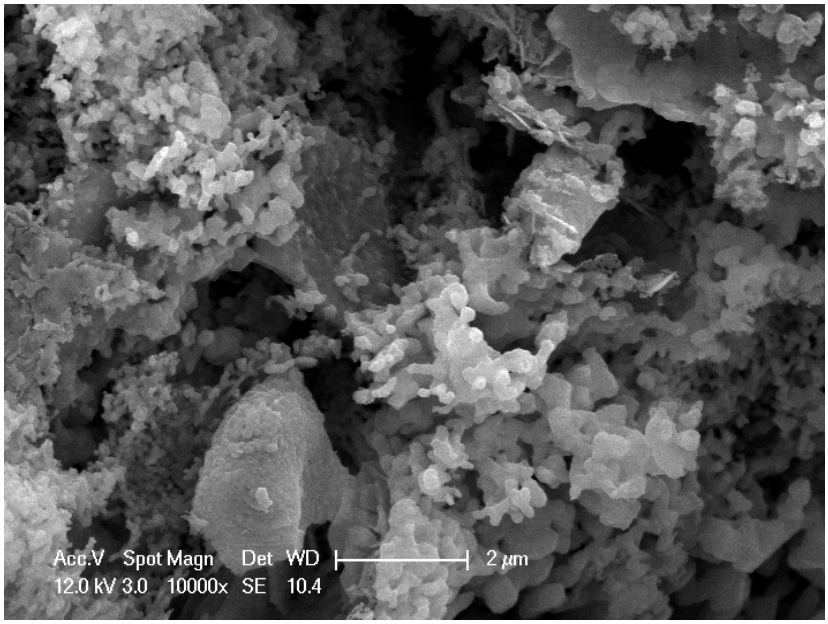

Figure B.7. Figure 4.11.a at lower magnification.

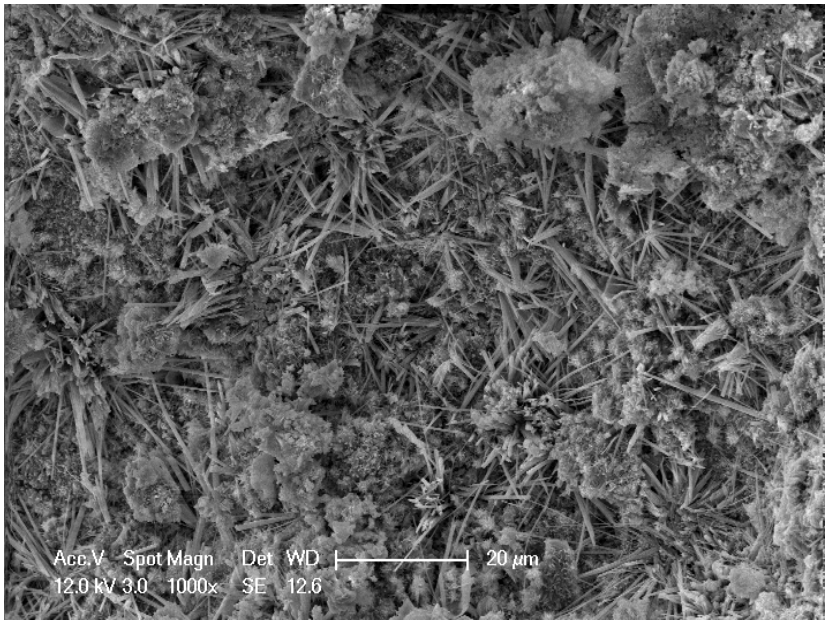

Figure B.8. Figure 4.11.b at lower magnification.

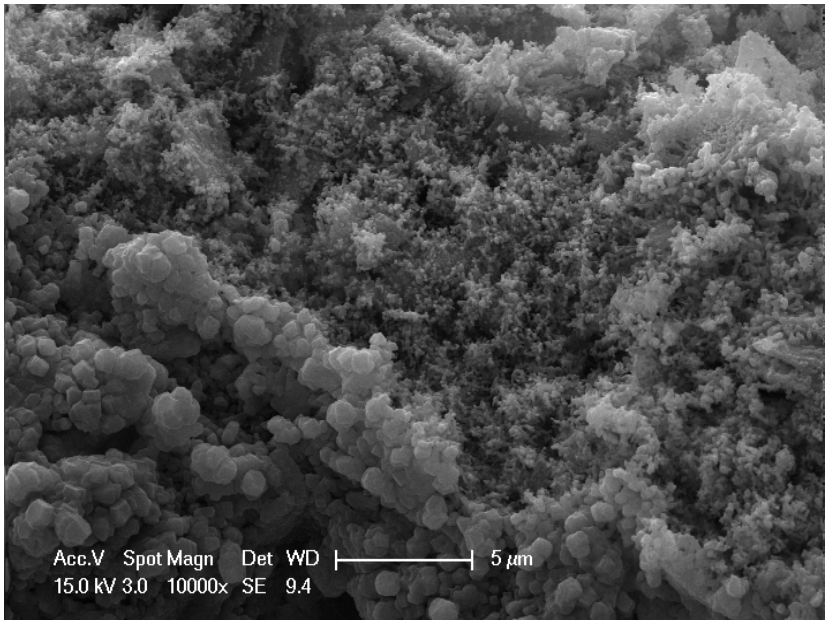

Figure B.9. Figure 4.12.a at lower magnification.

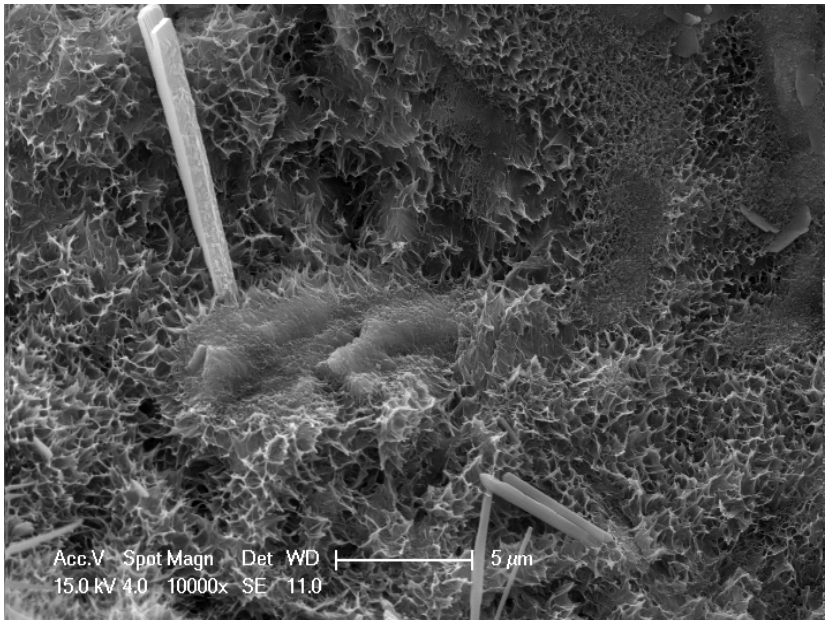

Figure B.10. Figure 4.12.b at lower magnification.

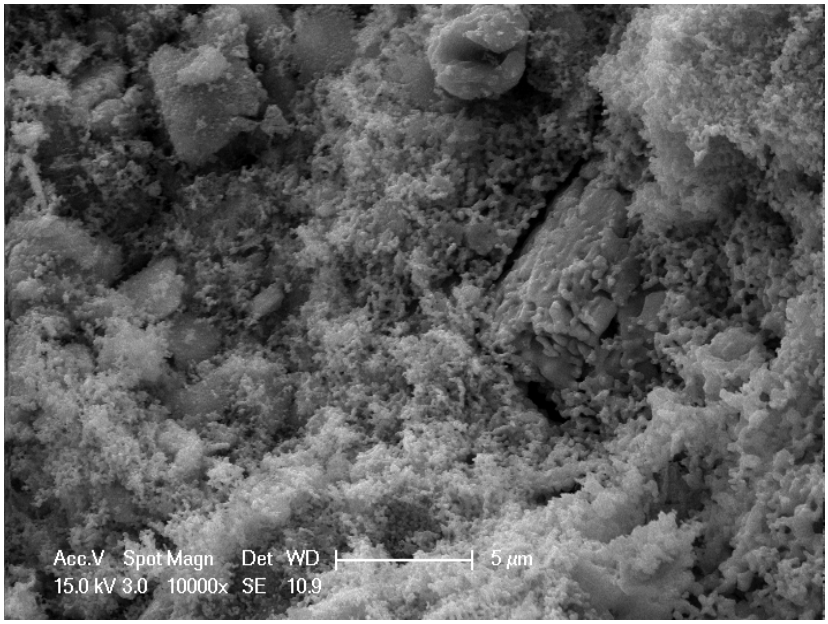

Figure B.11. Figure 4.13.a at lower magnification.

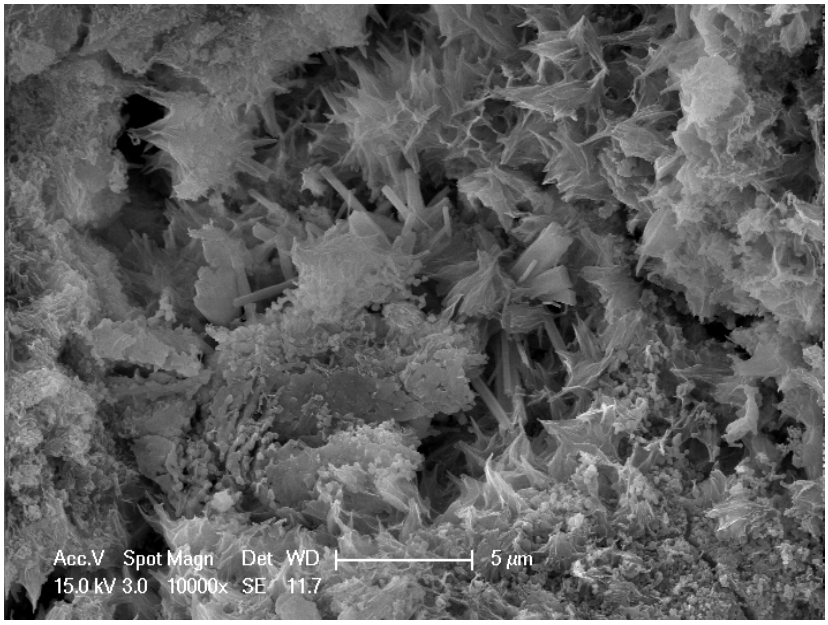

Figure B.12. Figure 4.13.b at lower magnification.

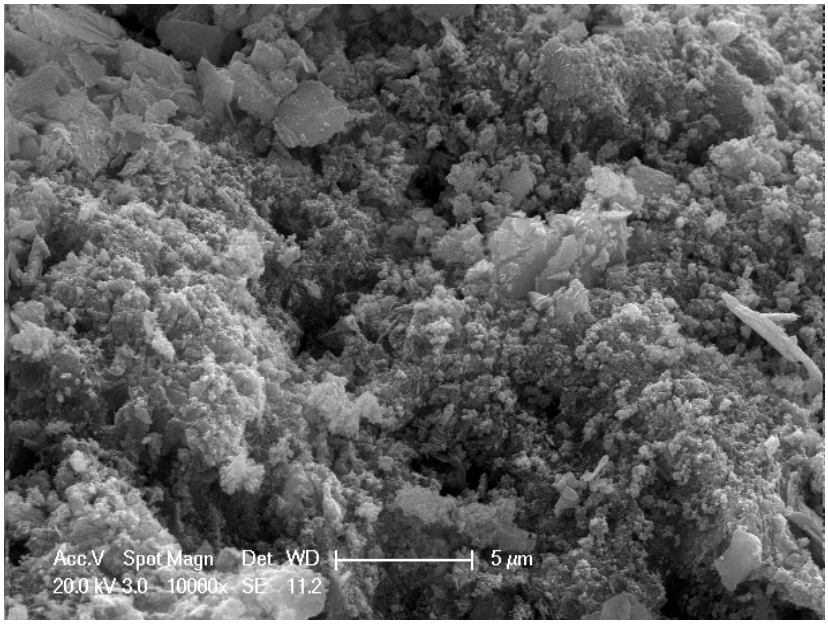

Figure B.13. Figure 4.15.a at lower magnification.

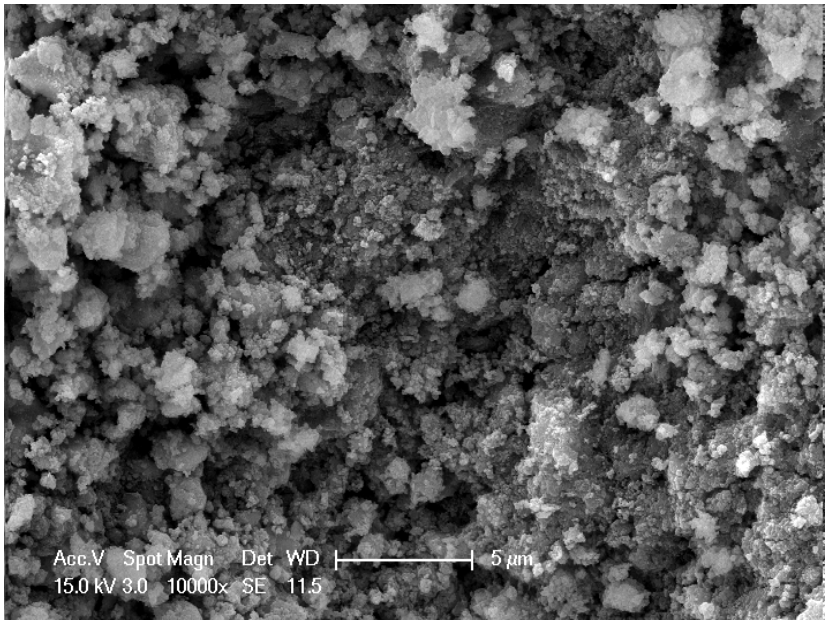

Figure B.14. Figure 4.15.b at lower magnification.

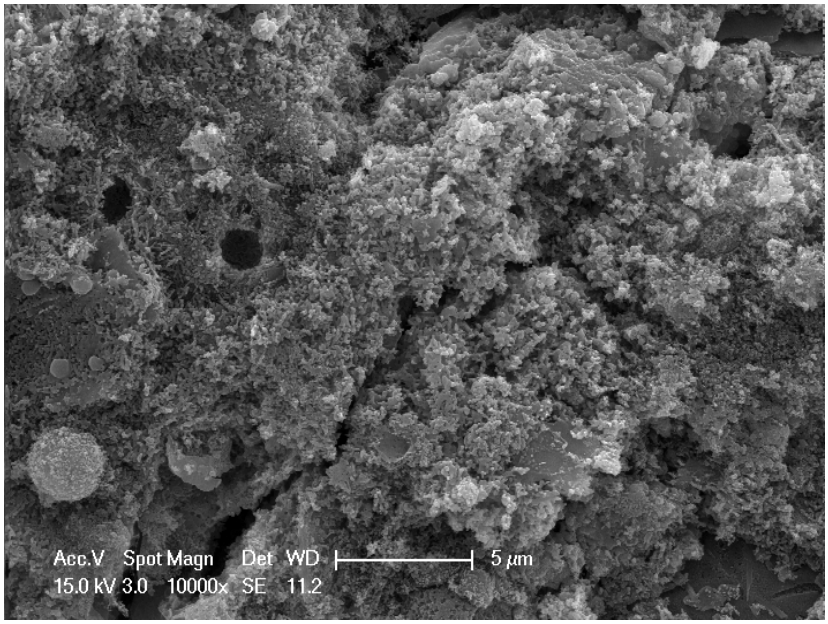

Figure B.15. Figure 4.15.c at lower magnification.

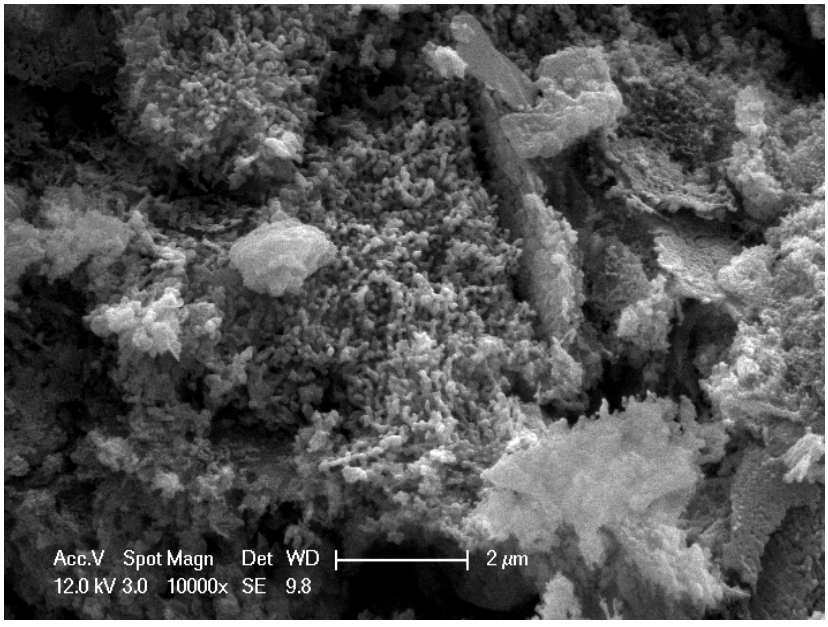

Figure B.16. Figure 4.16.a at lower magnification.

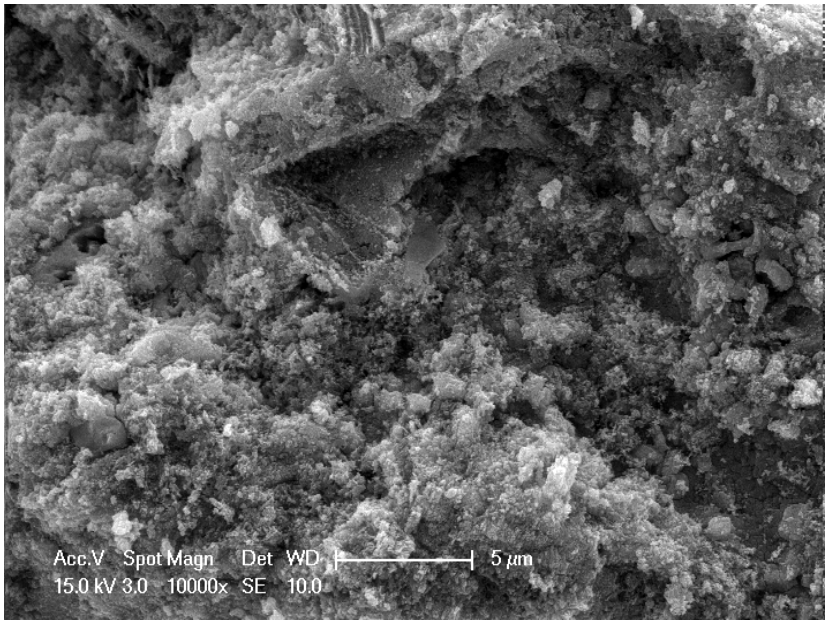

Figure B.17. Figure 4.16.b at lower magnification.

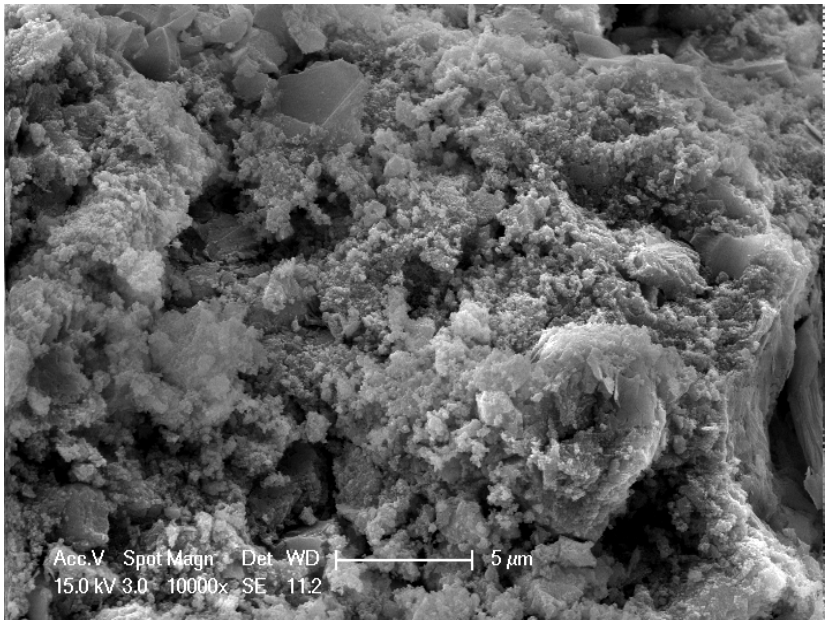

Figure B.18. Figure 4.16.c at lower magnification.

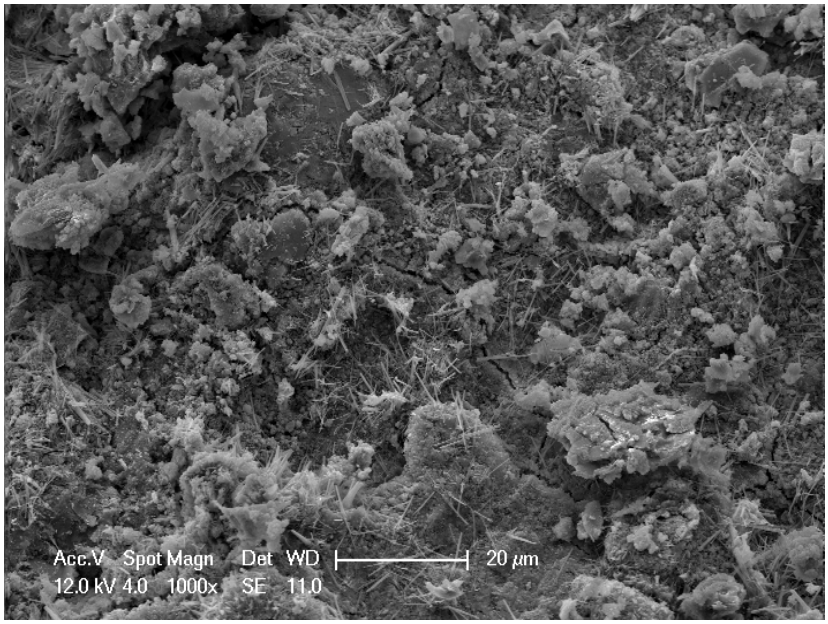

Figure B.19. Figure 4.17.a at lower magnification.

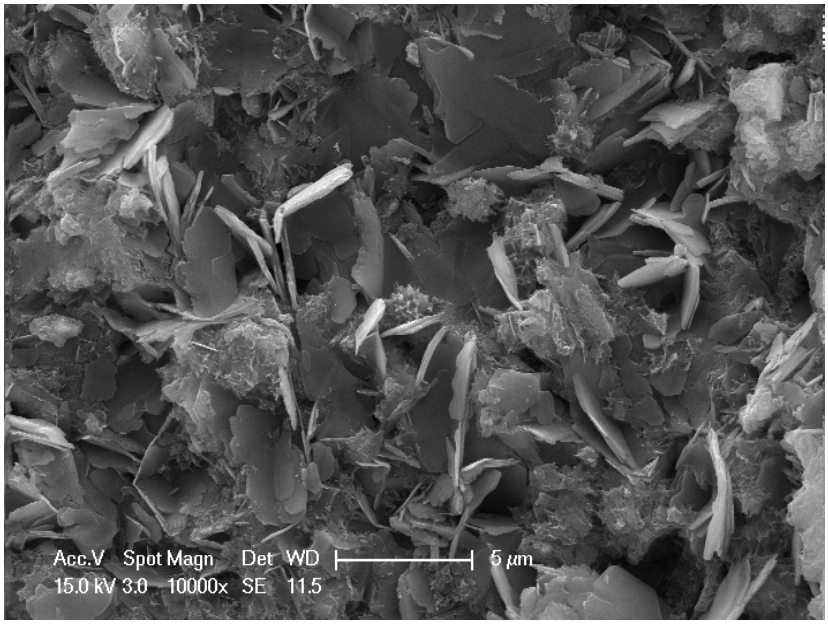

Figure B.20. Figure 4.17.b at lower magnification.

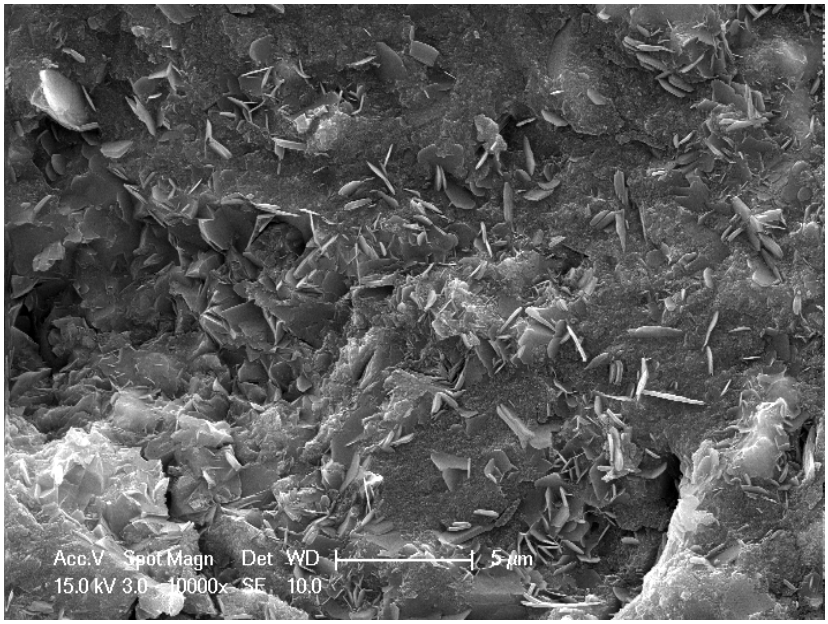

Figure B.21. Figure 4.17.c at lower magnification.

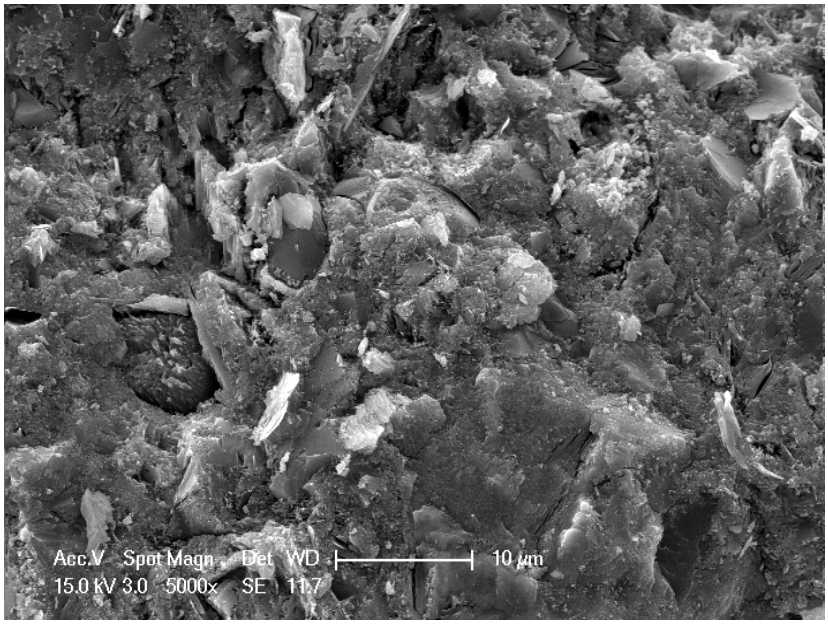

Figure B.22. Figure 5.1.a at lower magnification.

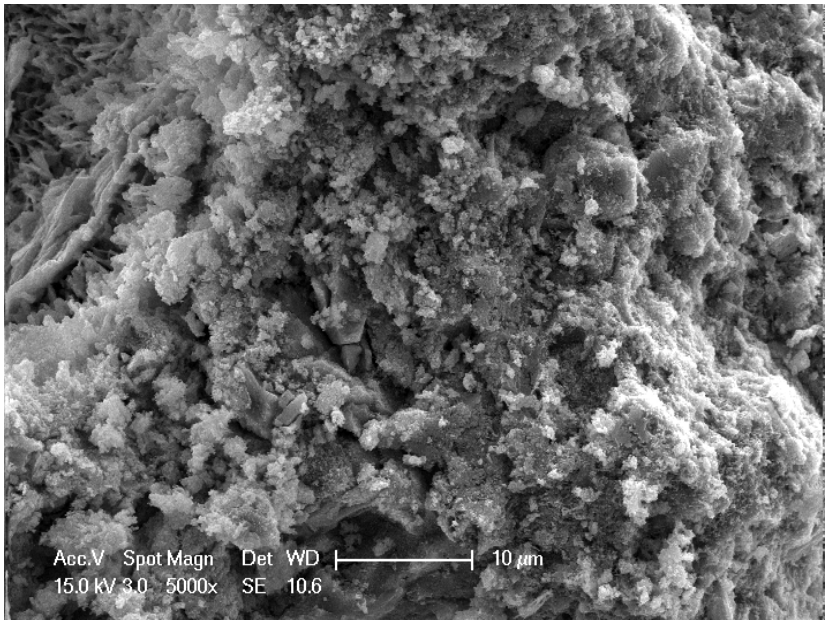

Figure B.23. Figure 5.1.b at lower magnification.

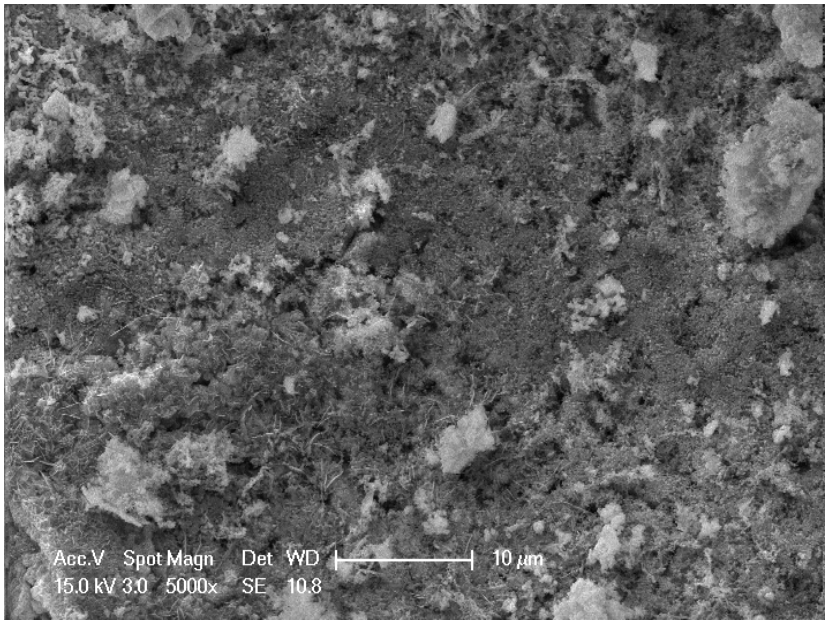

Figure B.24. Figure 5.1.c at lower magnification.

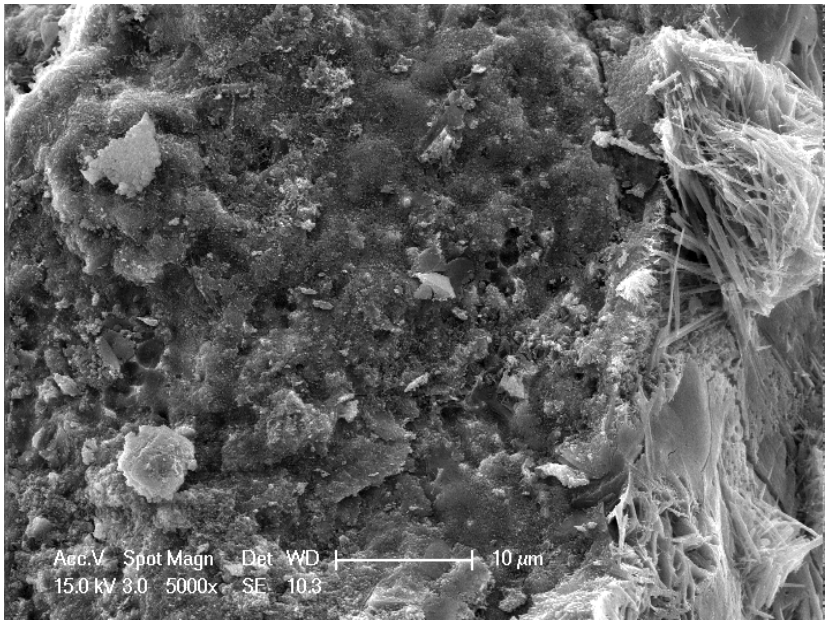

Figure B.25. Figure 5.1.d at lower magnification.

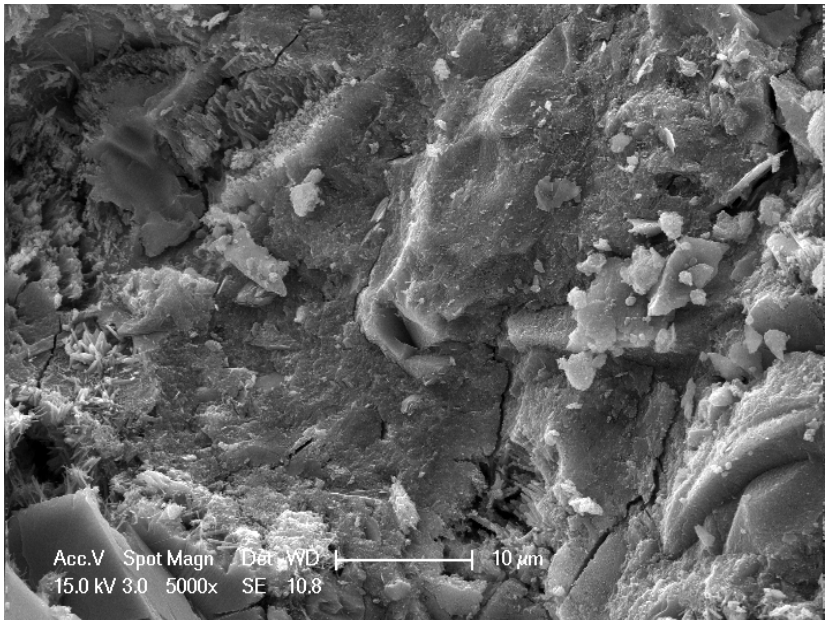

Figure B.26. Figure 5.2.a at lower magnification.

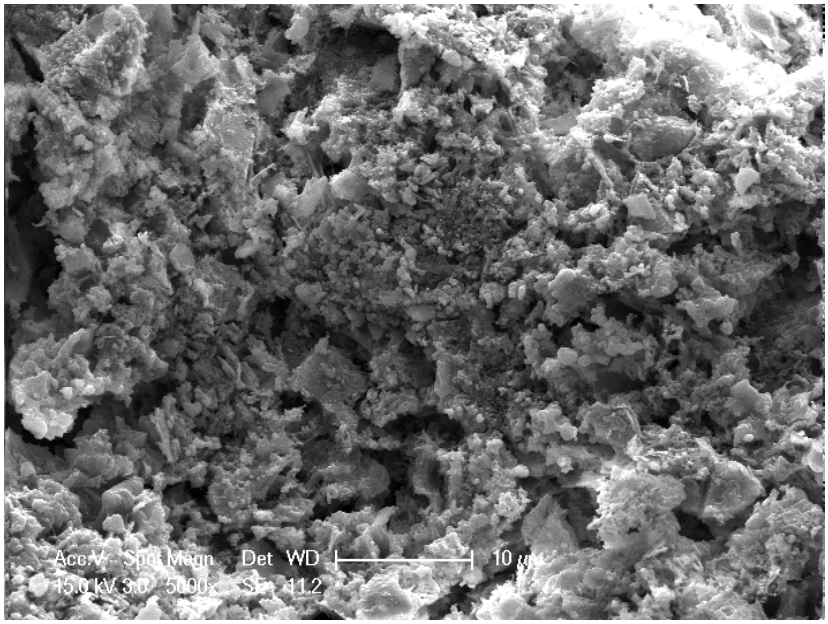

Figure B.27. Figure 5.2.b at lower magnification.

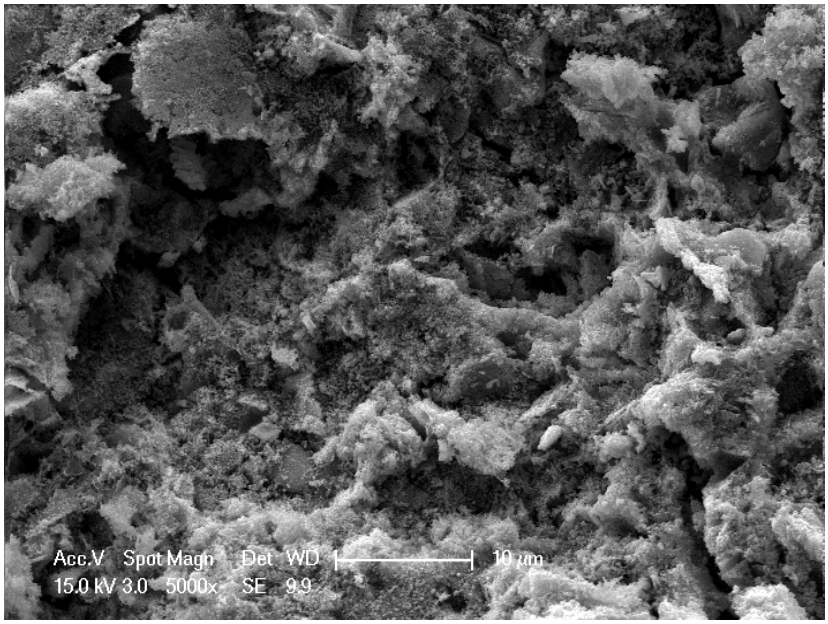

Figure B.28. Figure 5.2.c at lower magnification.

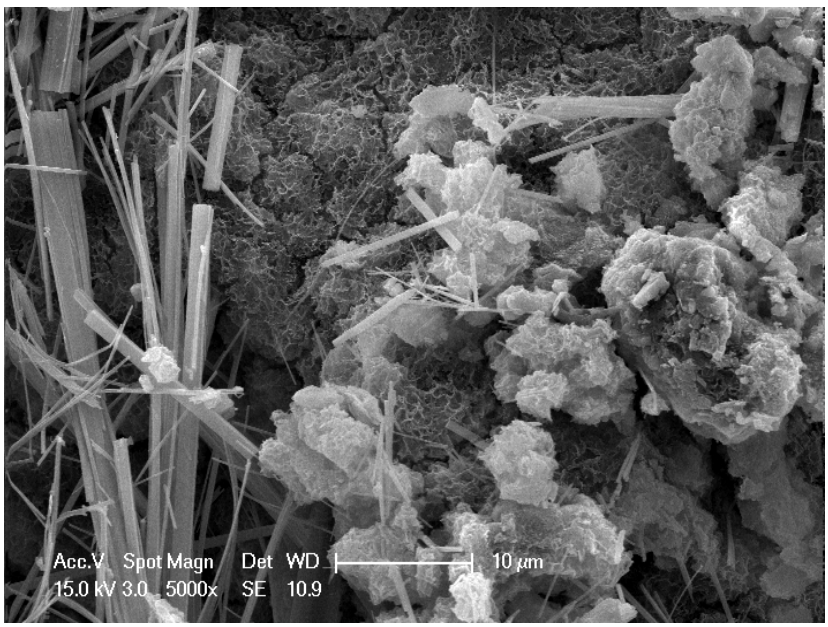

Figure B.29. Figure 5.2.d at lower magnification.

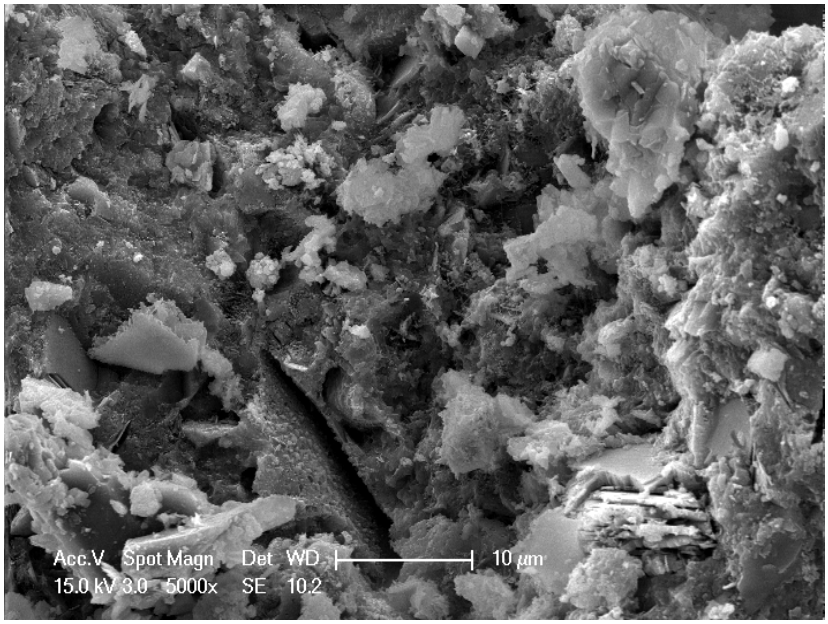

Figure B.30. Figure 5.3.a at lower magnification.

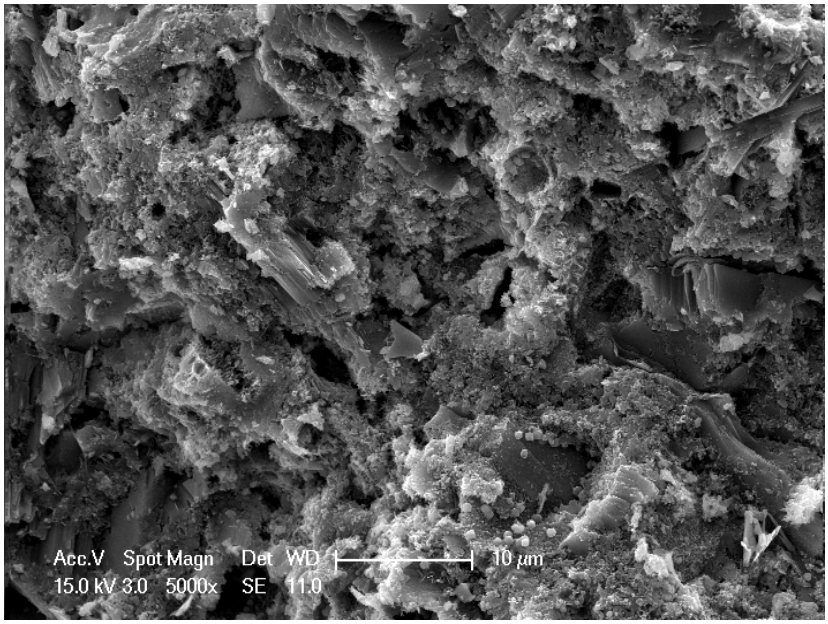

Figure B.31. Figure 5.3.b at lower magnification.

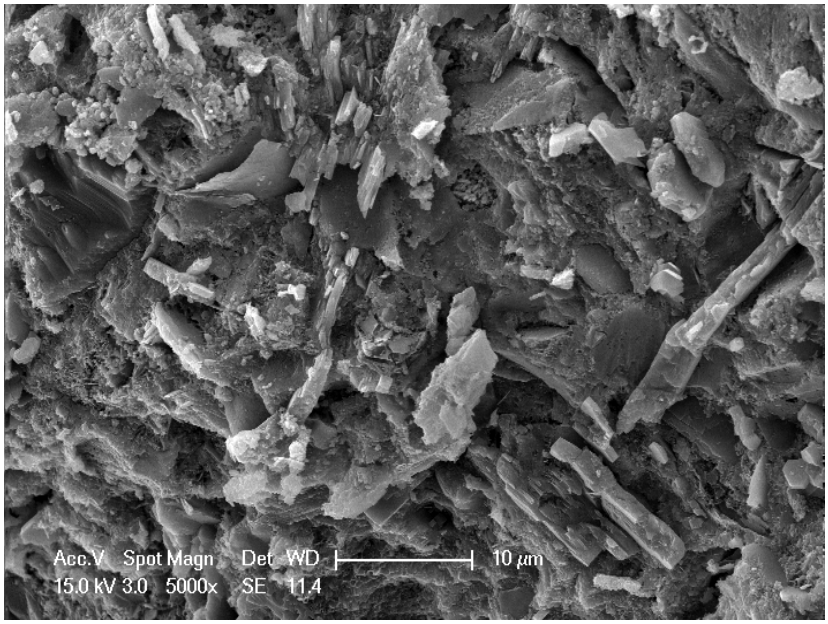

Figure B.32. Figure 5.3.c at lower magnification.

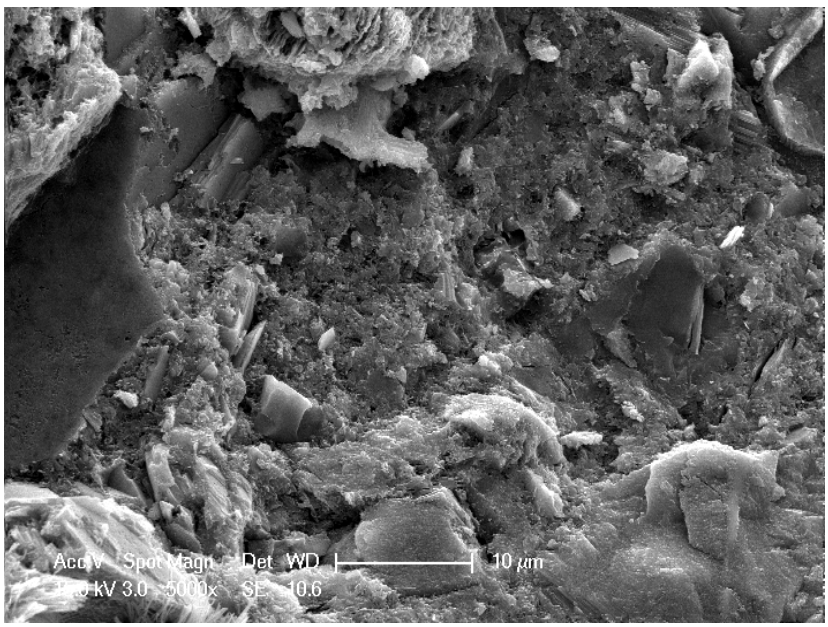

Figure B.33. Figure 5.3.d at lower magnification.

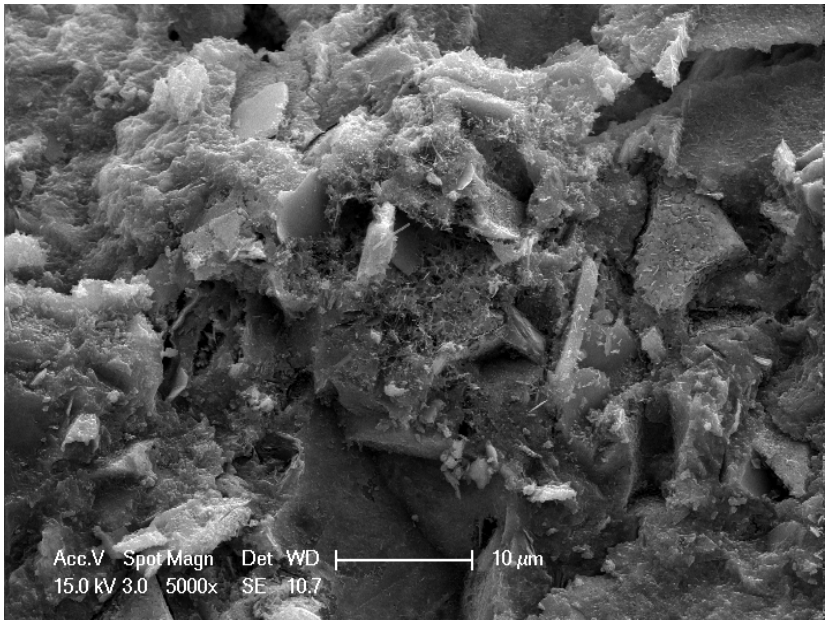

Figure B.34. Figure 5.4.a at lower magnification.

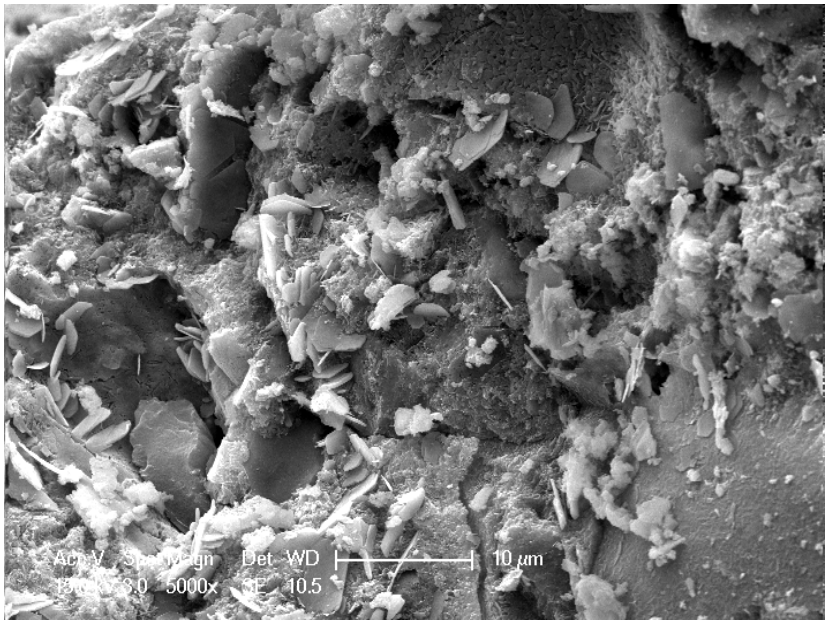

Figure B.35. Figure 5.4.b at lower magnification.

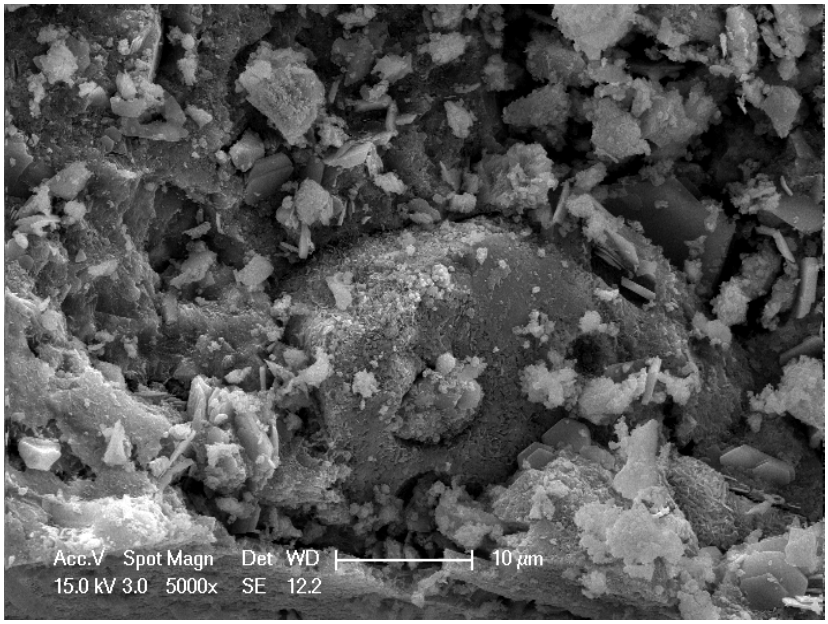

Figure B.36. Figure 5.4.c at lower magnification.

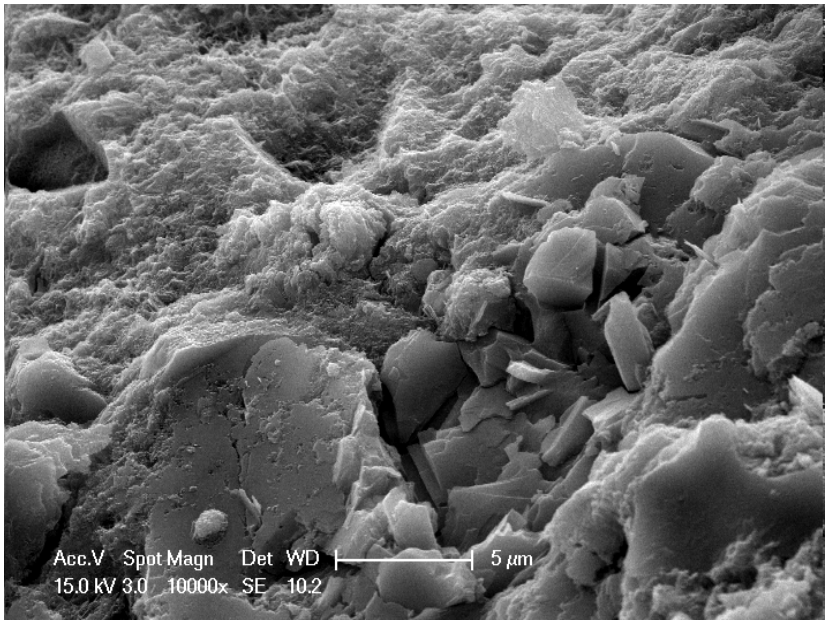

Figure B.37. Figure 5.4.d at lower magnification.

APPENDIX C: TGA DIAGRAMS

TGA and DTA diagrams of samples obtained from CAP, SAP and FAP groups before heating, after cooling, after air re-curing and after water re-curing were given in following figures.

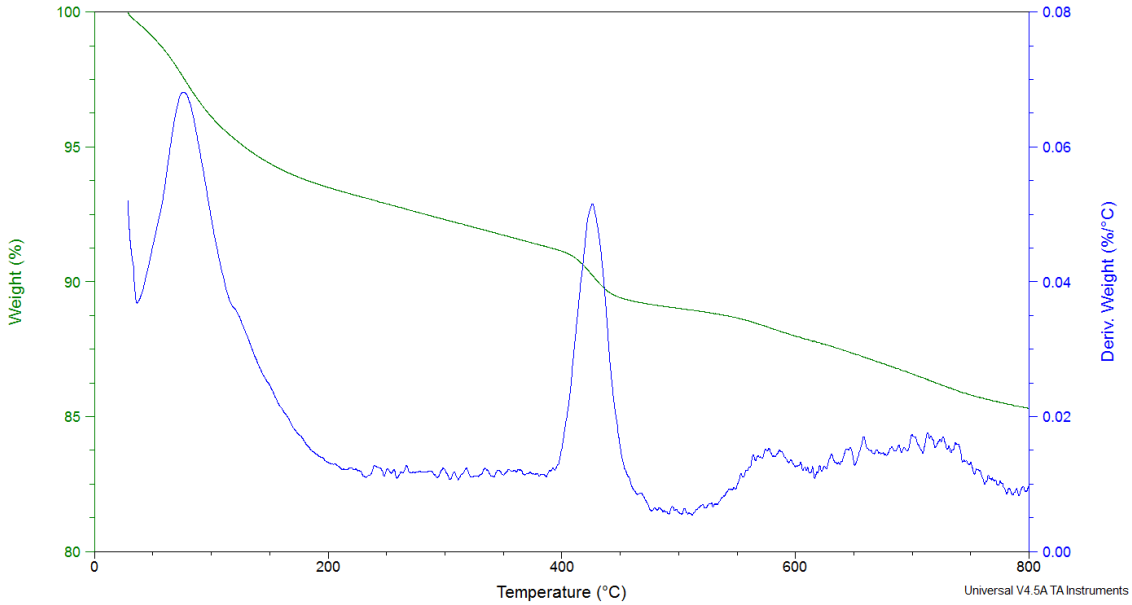

Figure C.1. TGA and DTA diagrams of CAP concrete before heating.

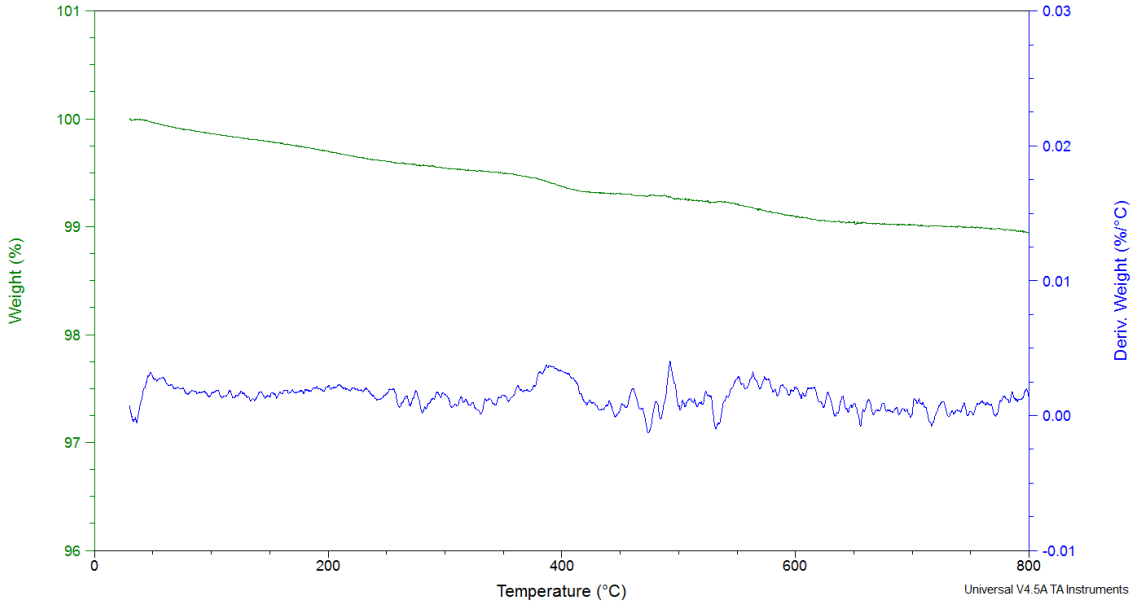

Figure C.2. TGA and DTA diagrams of CAP concrete after cooling (Surface).

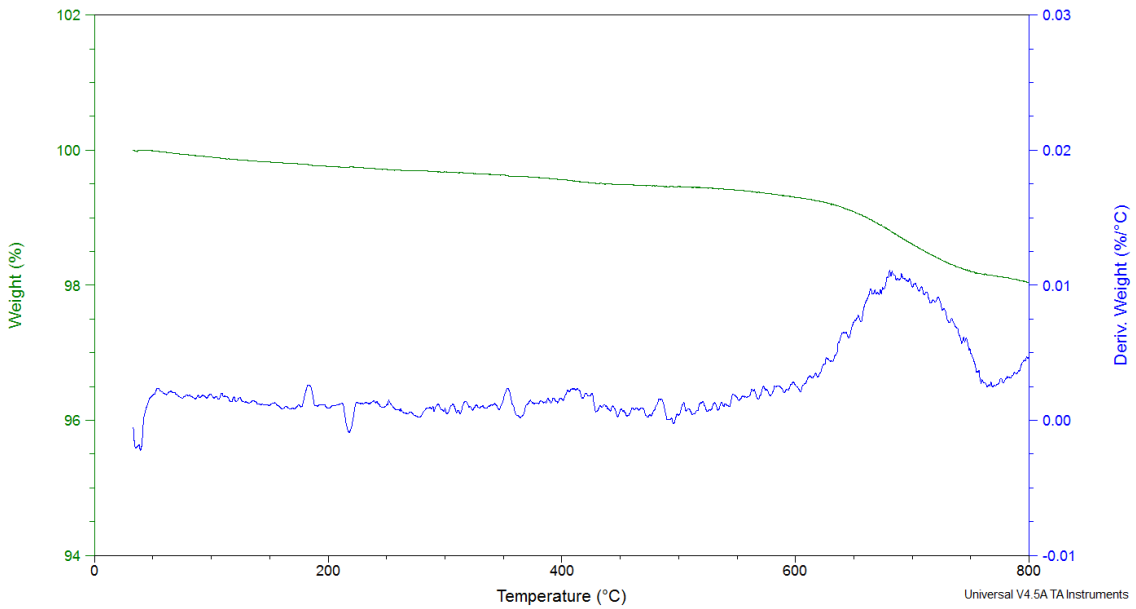

Figure C.3. TGA and DTA diagrams of CAP concrete after cooling (Center).

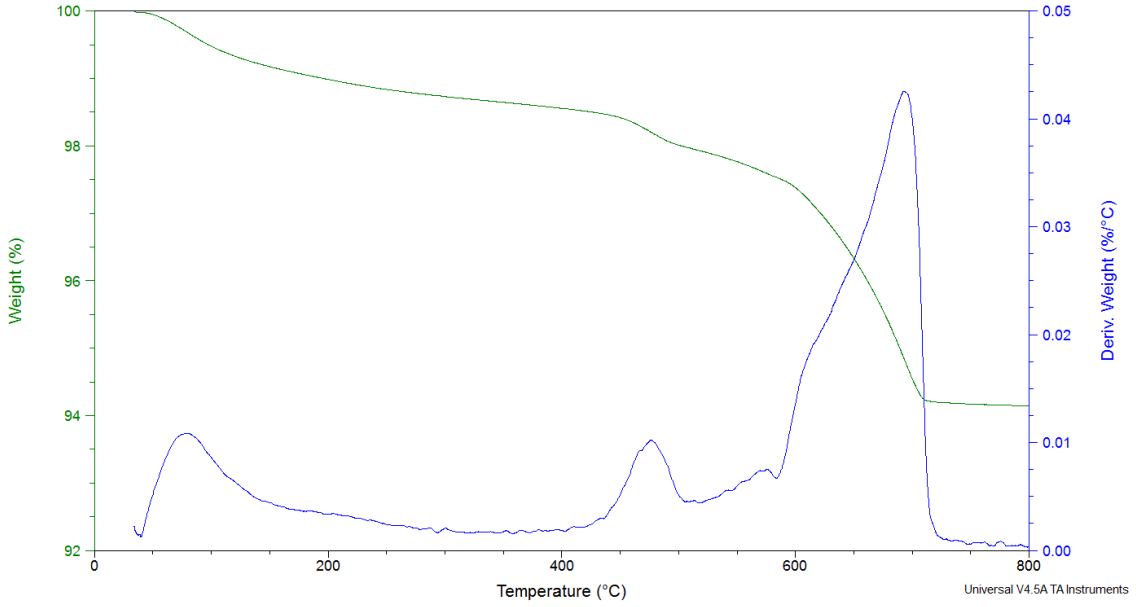

Figure C.4. TGA and DTA diagrams of air re-cured CAP concrete (Surface).

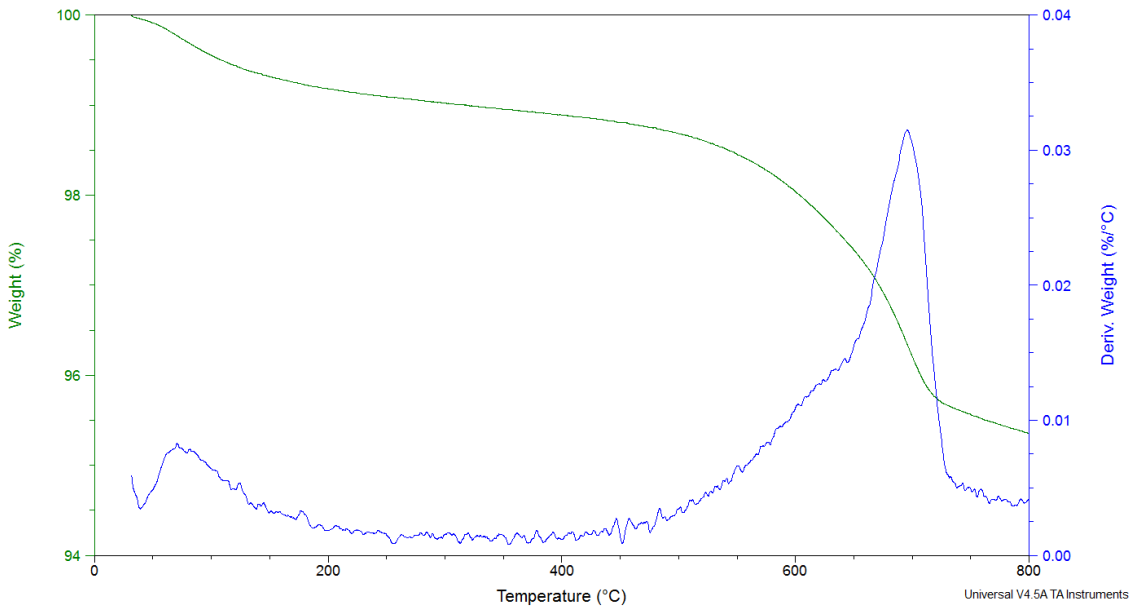

Figure C.5. TGA and DTA diagrams of air re-cured CAP concrete (Center).

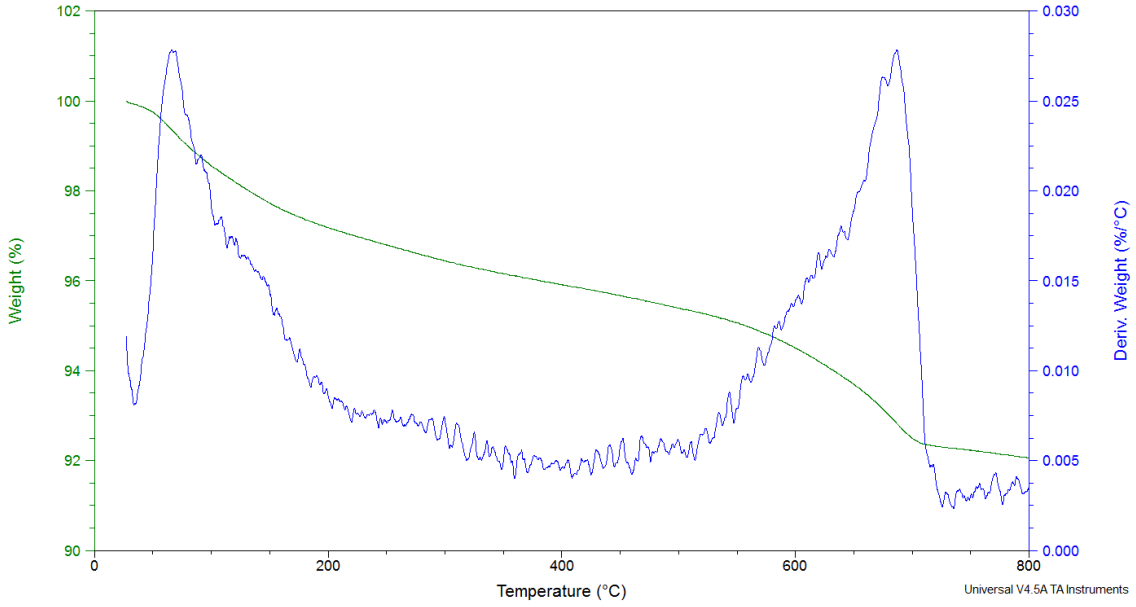

Figure C.6. TGA and DTA diagrams of water re-cured CAP concrete (Surface).

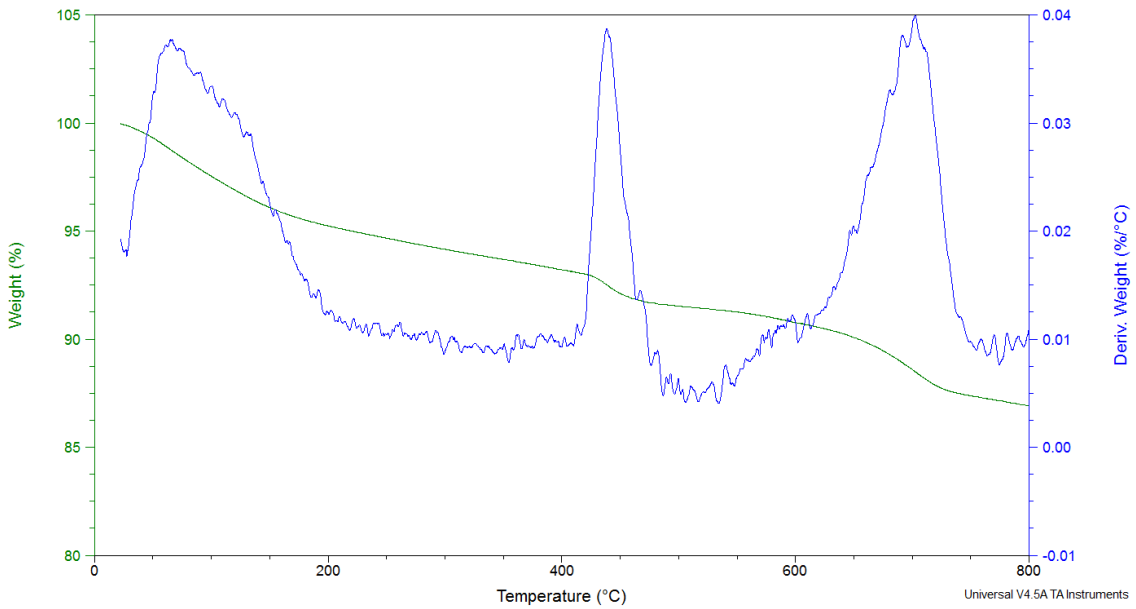

Figure C.7. TGA and DTA diagrams of water re-cured CAP concrete (Center).

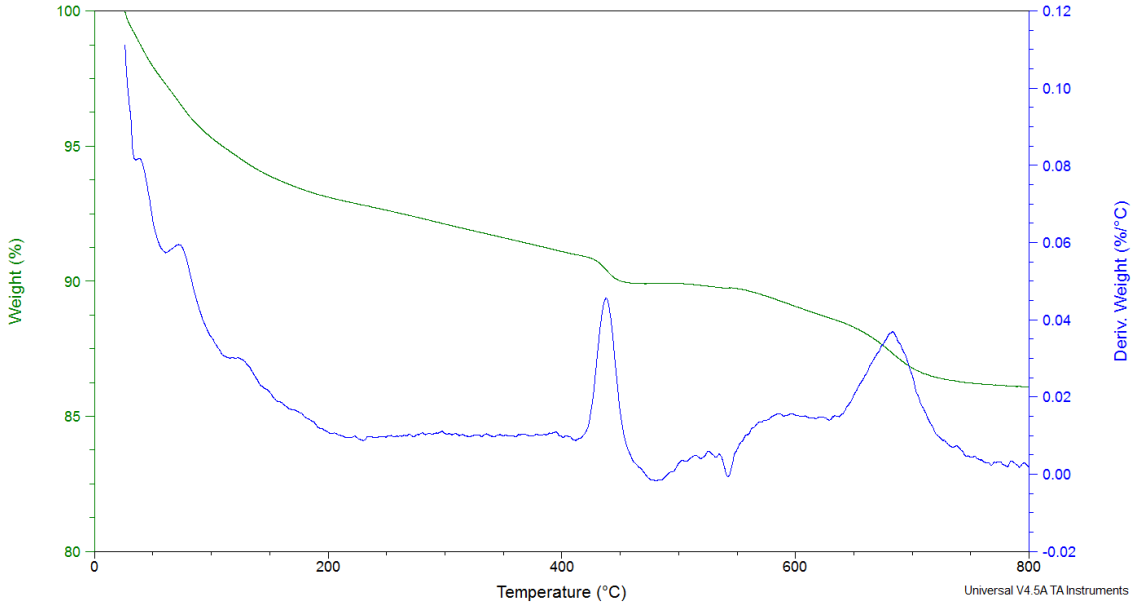

Figure C.8. TGA and DTA diagrams of SAP concrete before heating.

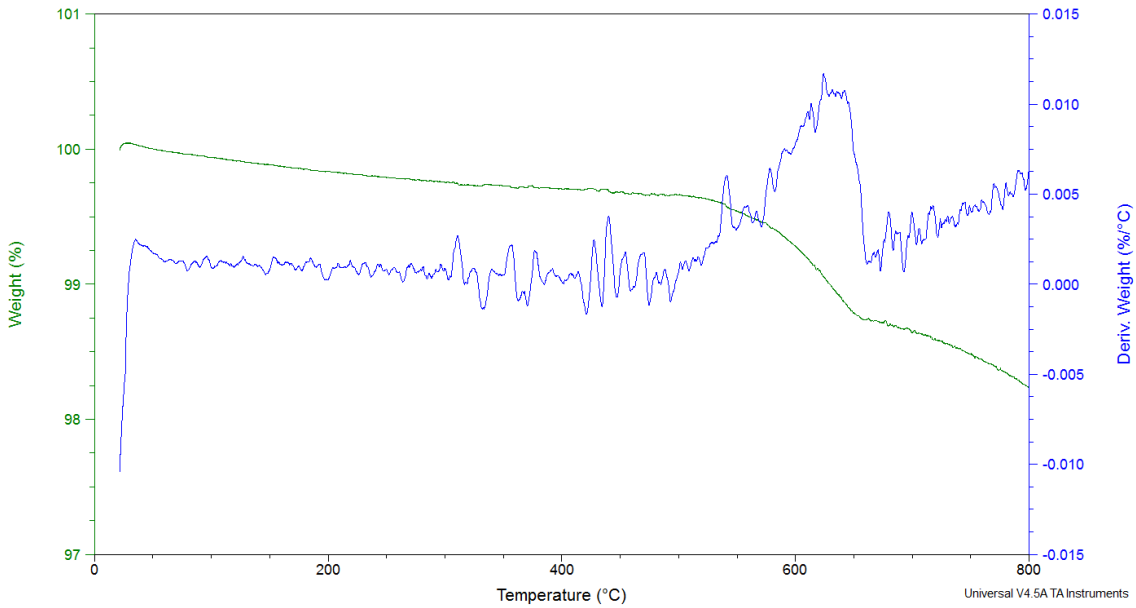

Figure C.9. TGA and DTA diagrams of SAP concrete after cooling (Surface).

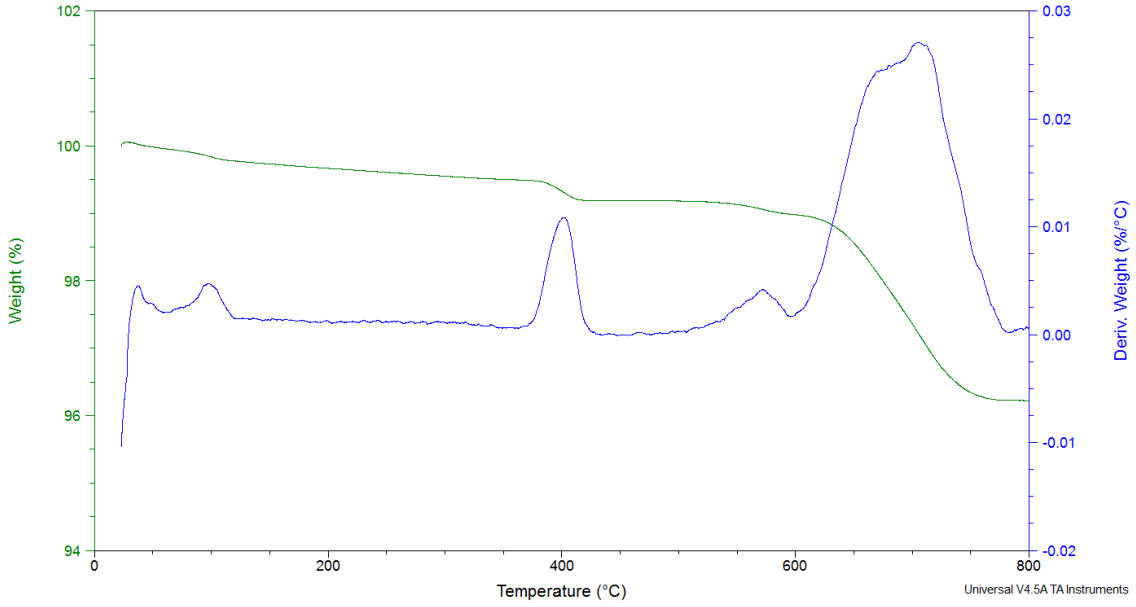

Figure C.10. TGA and DTA diagrams of SAP concrete after cooling (Center).

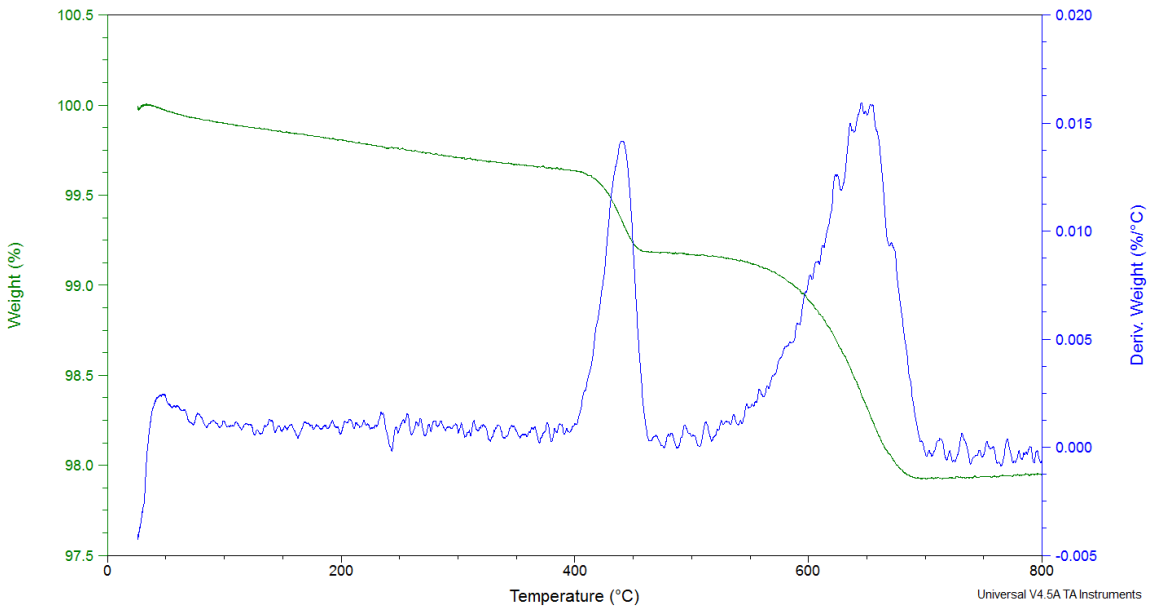

Figure C.11. TGA and DTA diagrams of air re-cured SAP concrete (Surface).

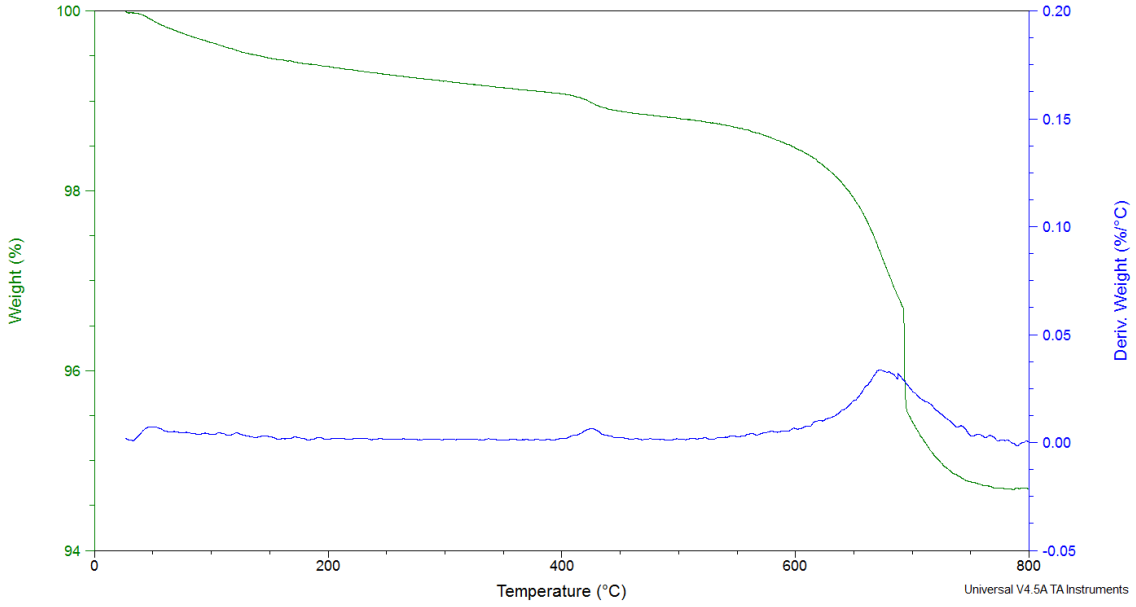

Figure C.12. TGA and DTA diagrams of air re-cured SAP concrete (Center).

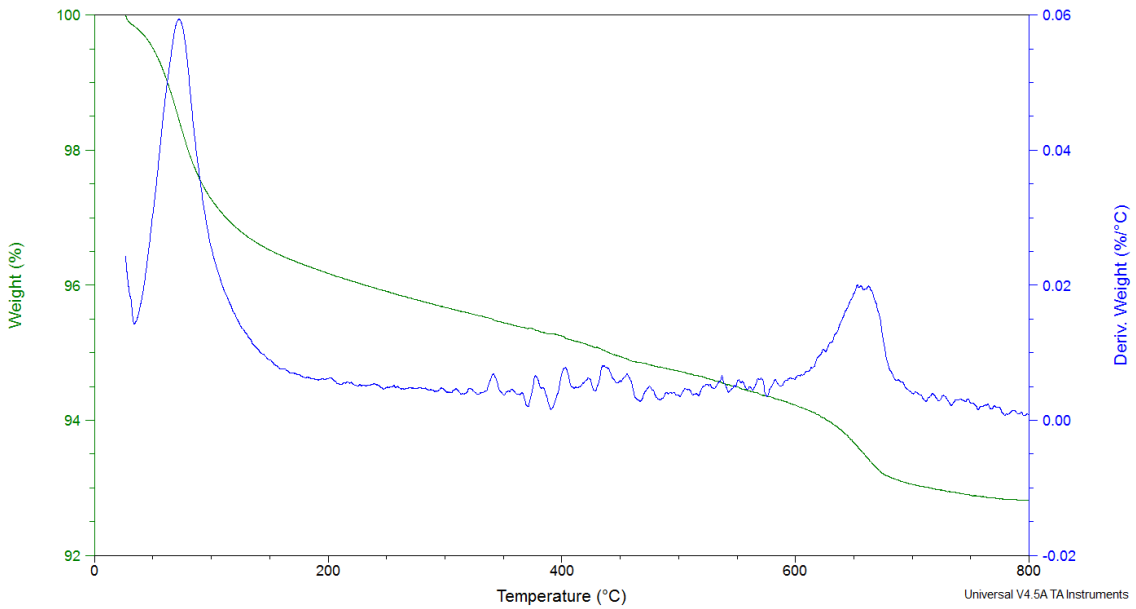

Figure C.13. TGA and DTA diagrams of water re-cured SAP concrete (Surface).

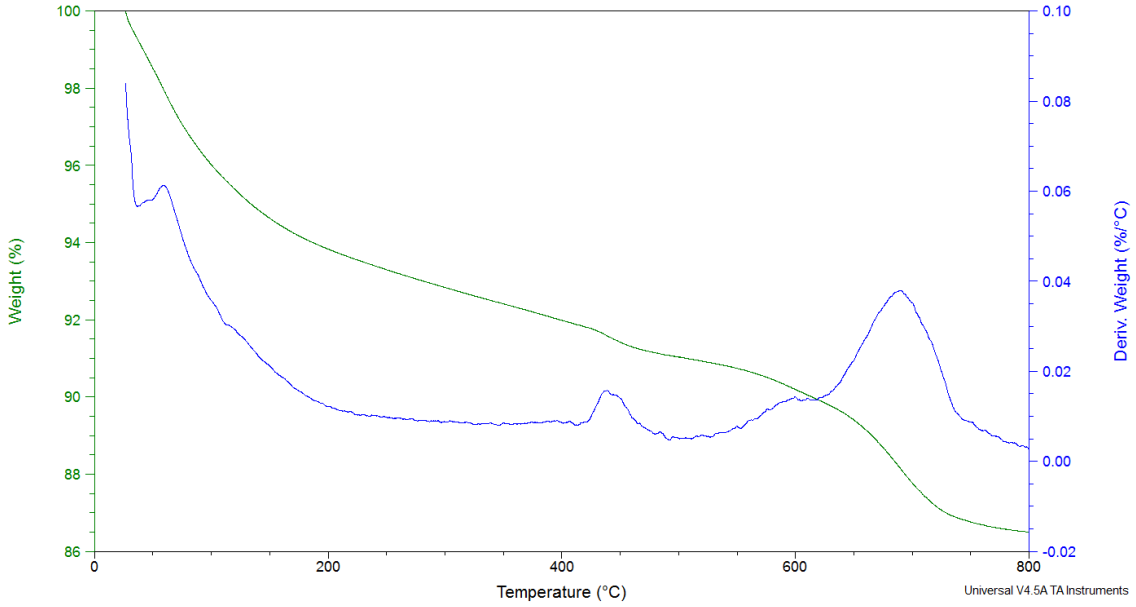

Figure C.14. TGA and DTA diagrams of water re-cured SAP concrete (Center).

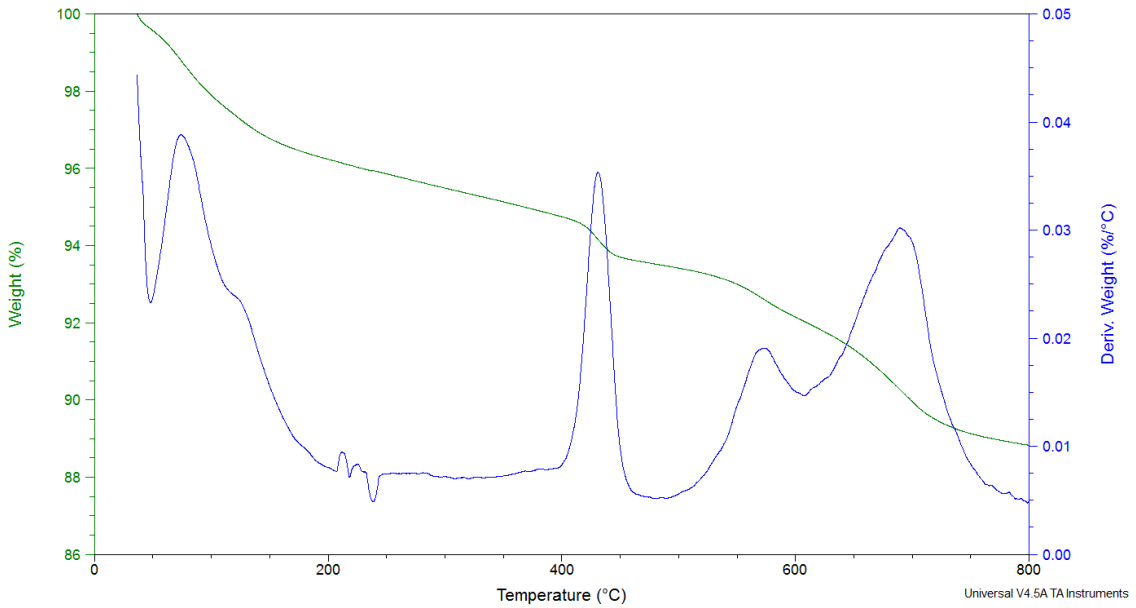

Figure C.15. TGA and DTA diagrams of FAP concrete before heating.

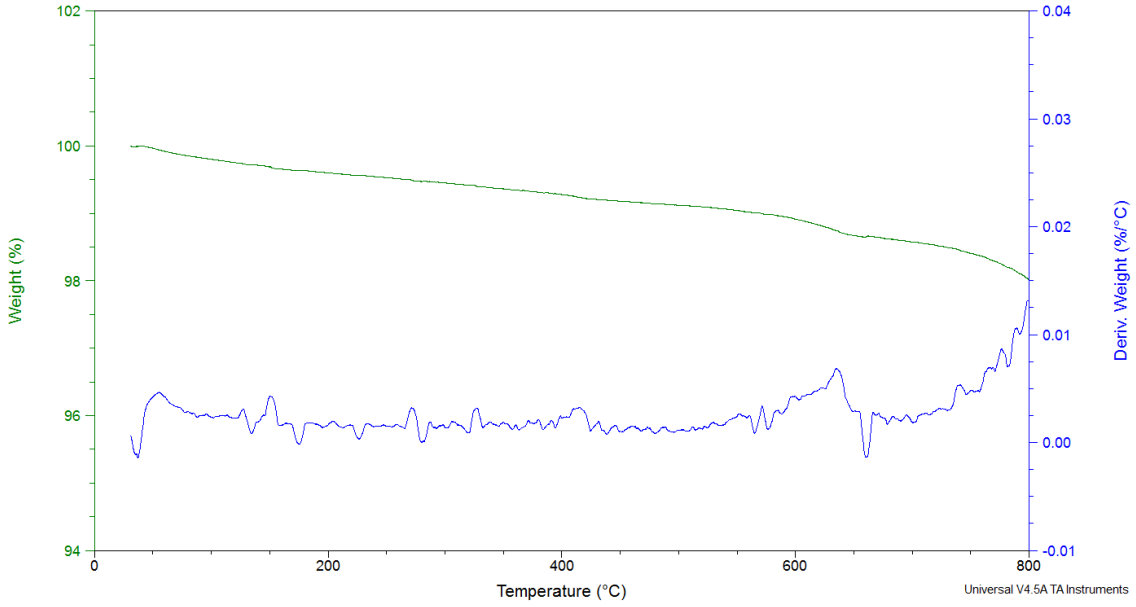

Figure C.16. TGA and DTA diagrams of FAP concrete after cooling (Surface).

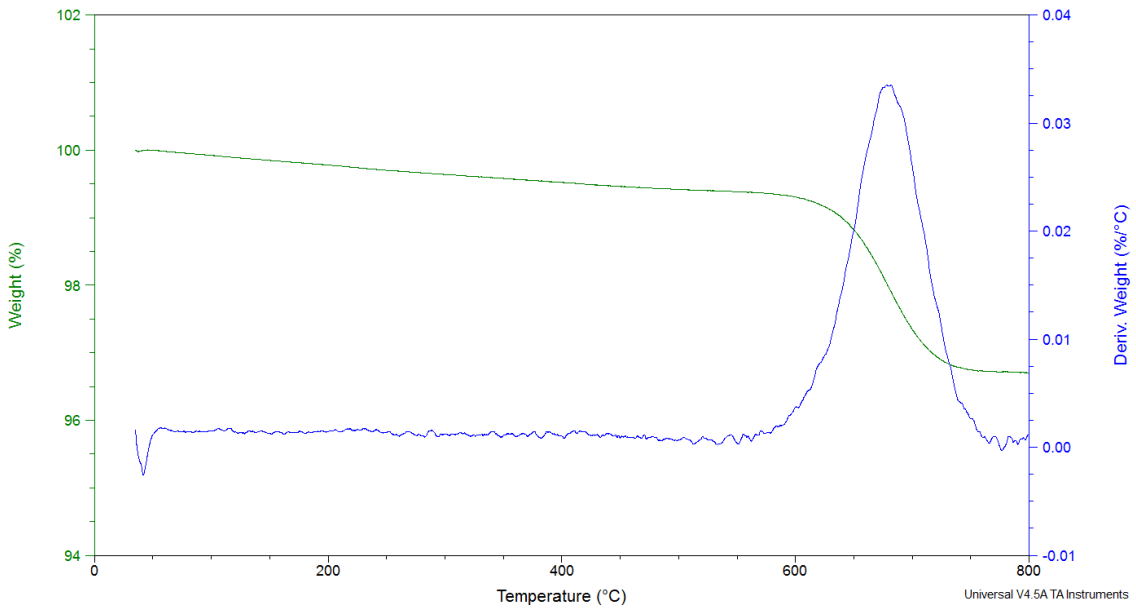

Figure C.17. TGA and DTA diagrams of FAP concrete after cooling (Center).

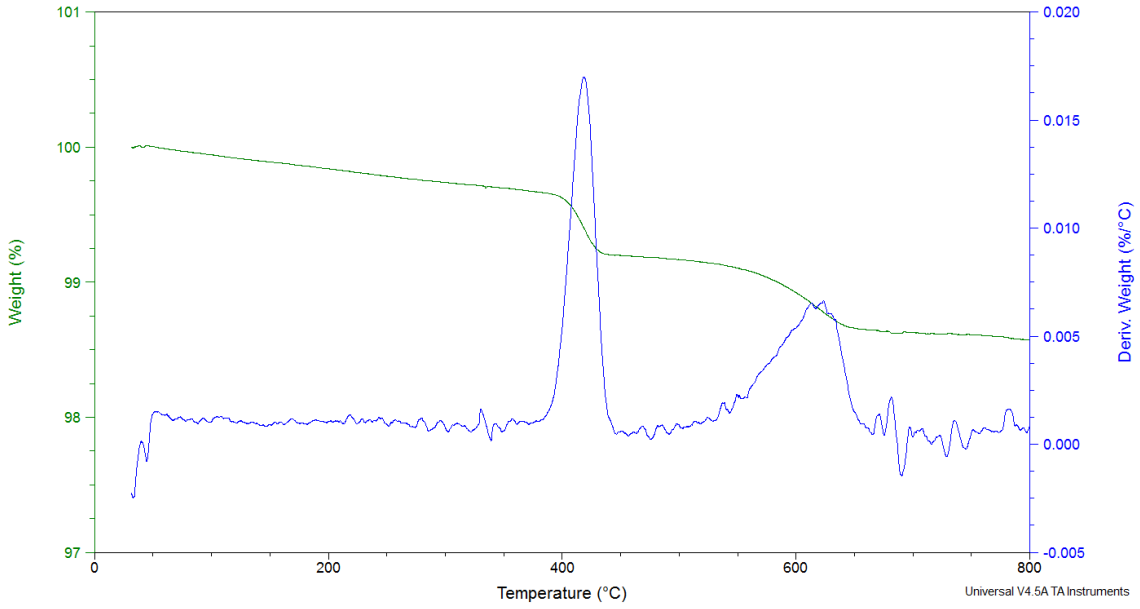

Figure C.18. TGA and DTA diagrams of air re-cured FAP concrete (Surface).

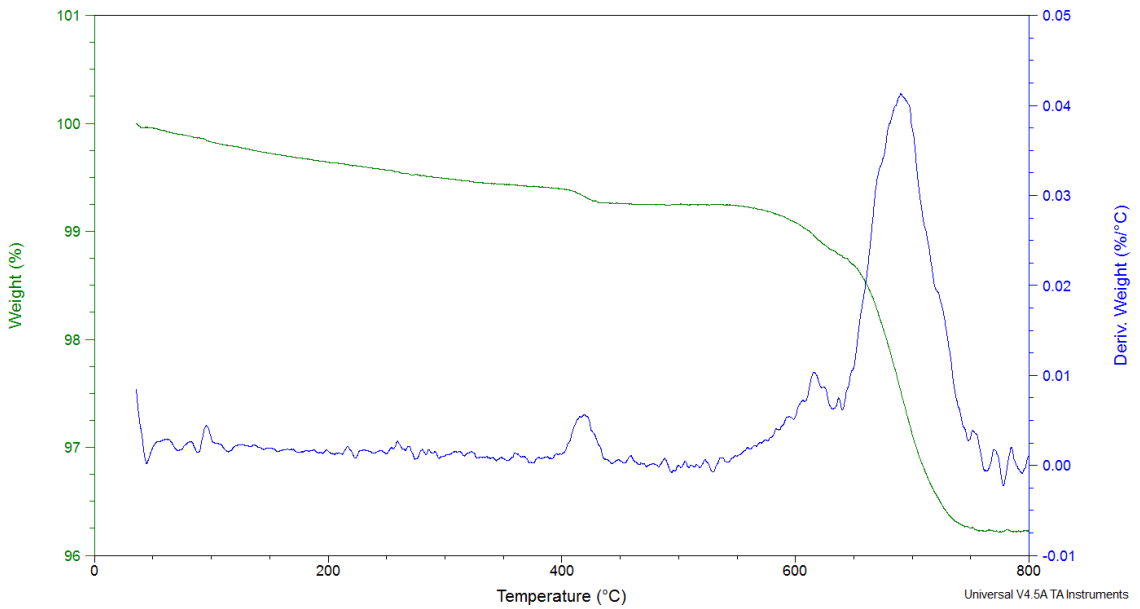

Figure C.19. TGA and DTA diagrams of air re-cured FAP concrete (Center).

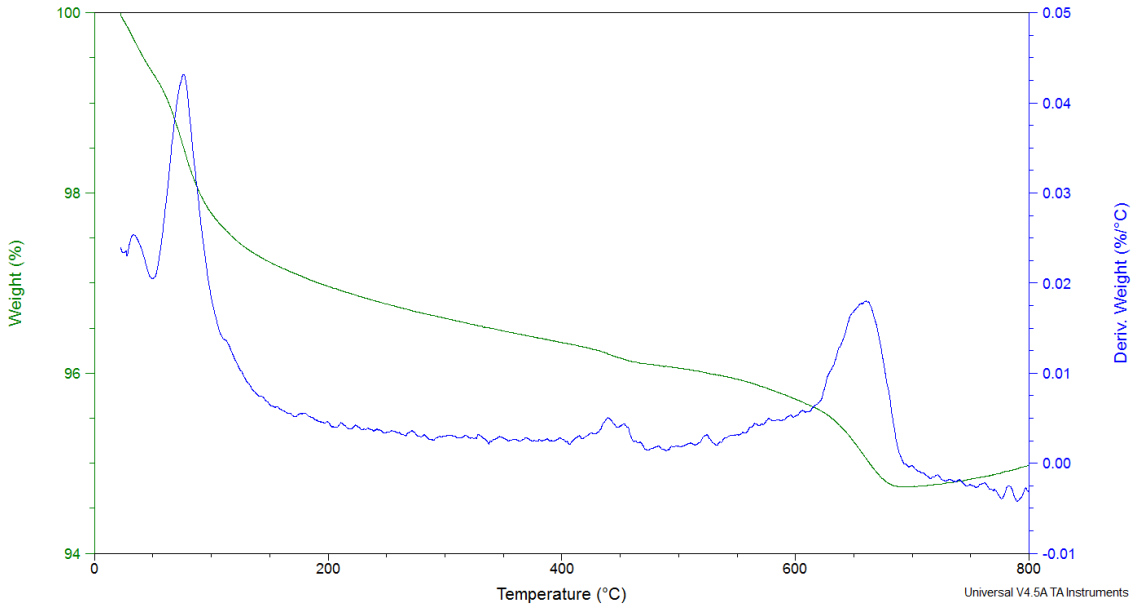

Figure C.20. TGA and DTA diagrams of water re-cured FAP concrete (Surface).

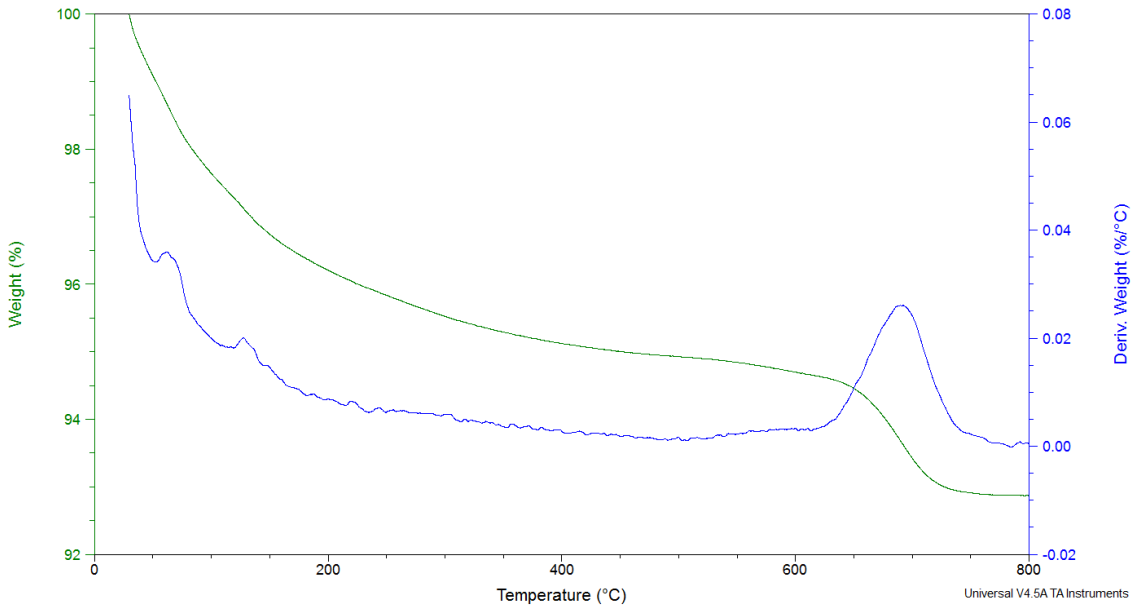

Figure C.21. TGA and DTA diagrams of water re-cured FAP concrete (Center).

APPENDIX D: STRESS & STRAIN DIAGRAMS

Stress and strain diagrams of concrete groups were given in following figures. "0" sign represents the specimen before heating, "X" represents the specimen tested just after cooling. "Z" and "W" represent air re-cured specimen and water re-cured specimen, respectively.

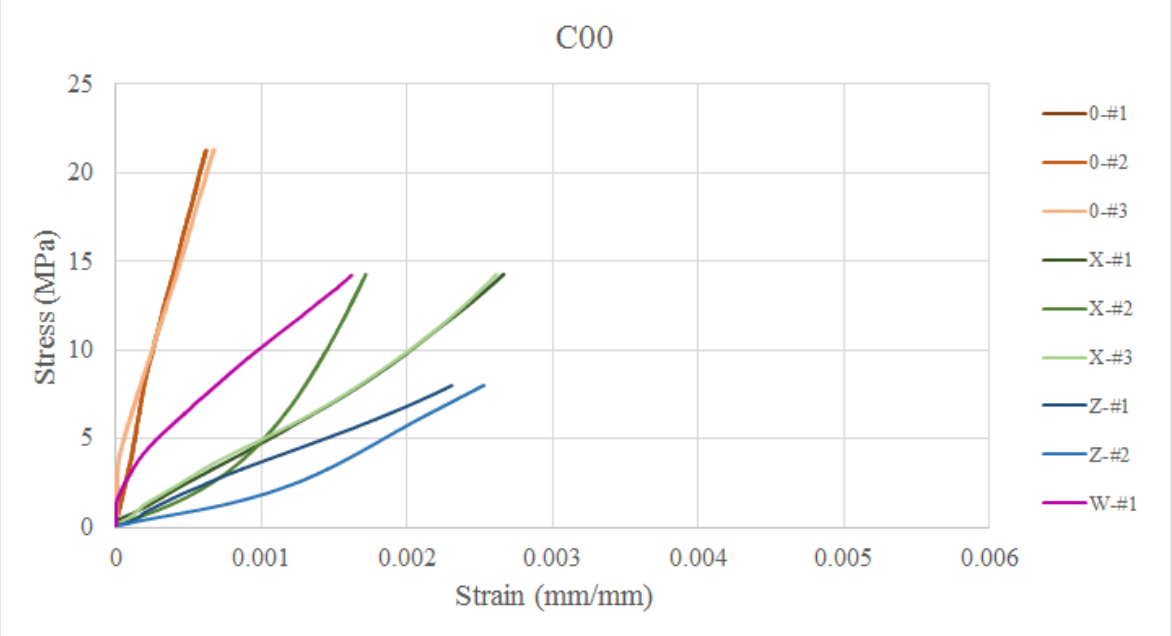

Figure D.1. Stress and strain diagrams of C00 concrete.

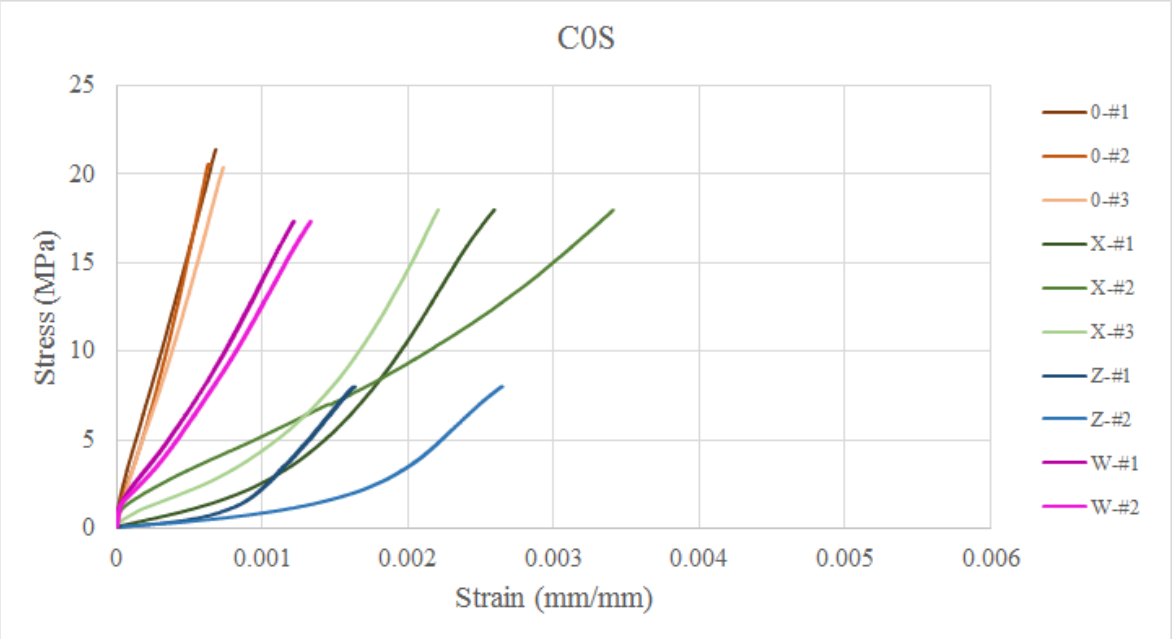

Figure D.2. Stress and strain diagrams of C0S concrete.

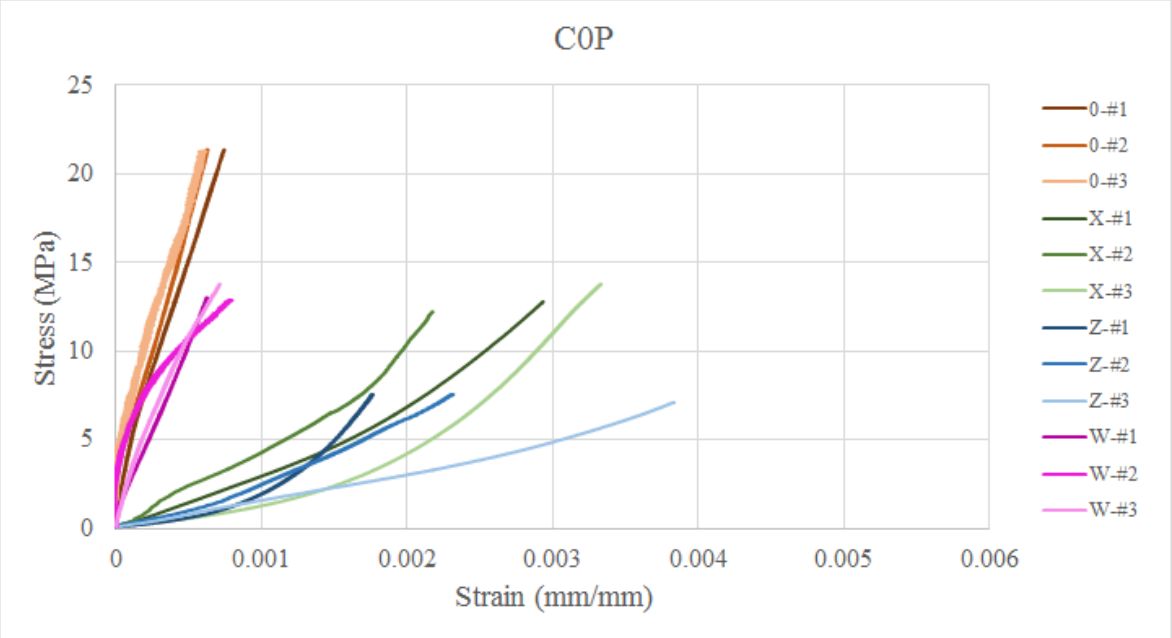

Figure D.3. Stress and strain diagrams of C0P concrete.

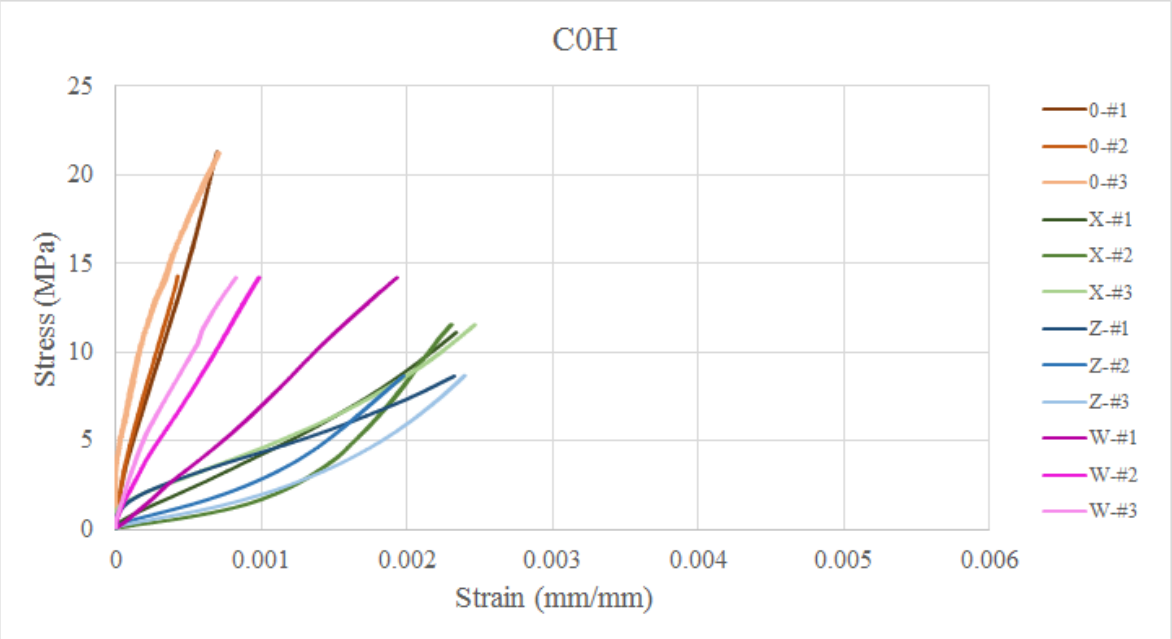

Figure D.4. Stress and strain diagrams of C0H concrete.

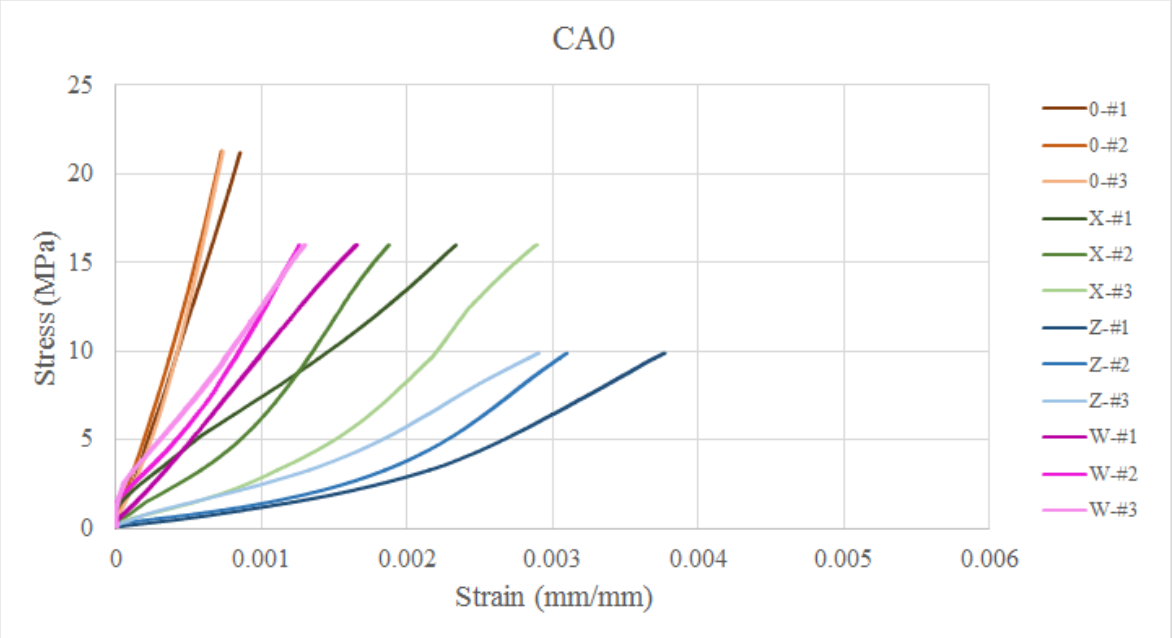

Figure D.5. Stress and strain diagrams of CA0 concrete.

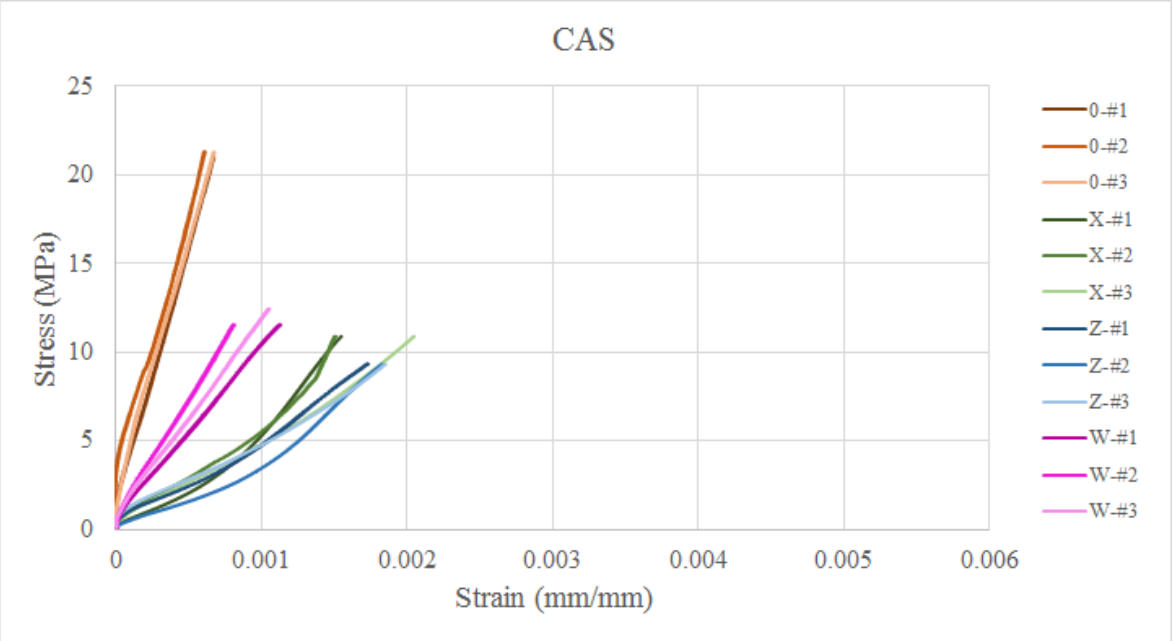

Figure D.6. Stress and strain diagrams of CAS concrete.

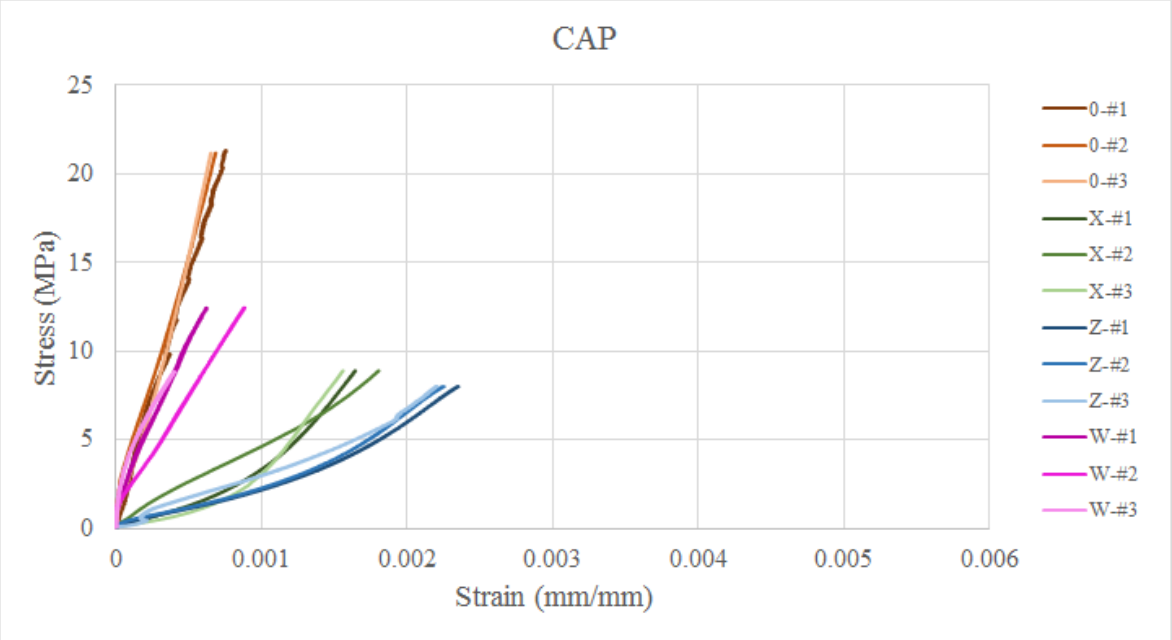

Figure D.7. Stress and strain diagrams of CAP concrete.

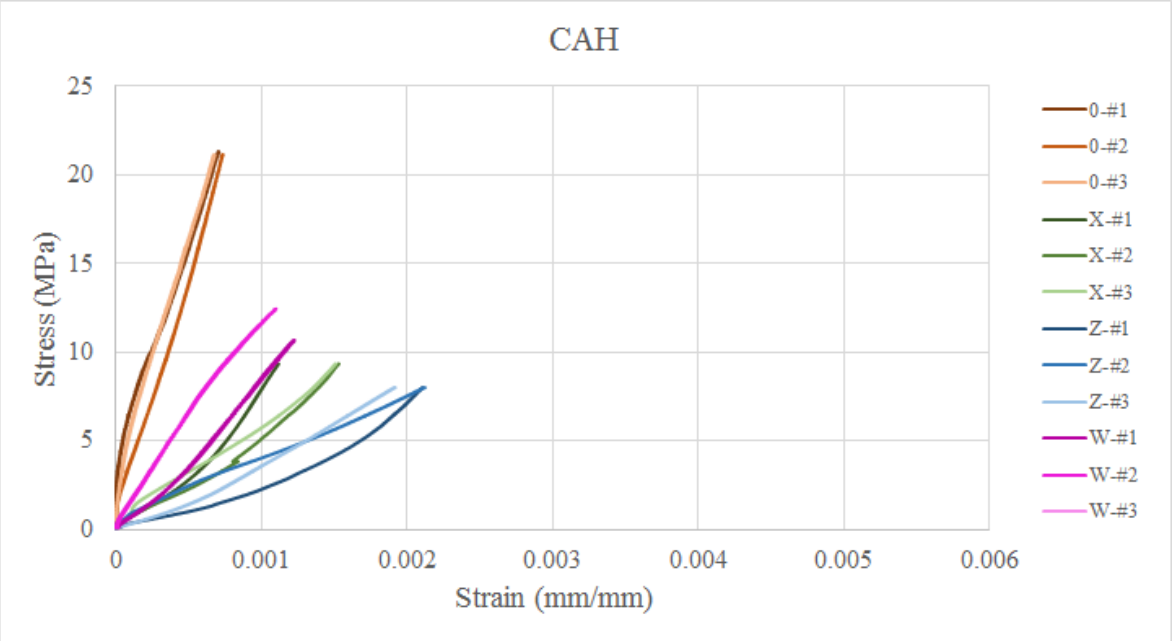

Figure D.8. Stress and strain diagrams of CAH concrete.

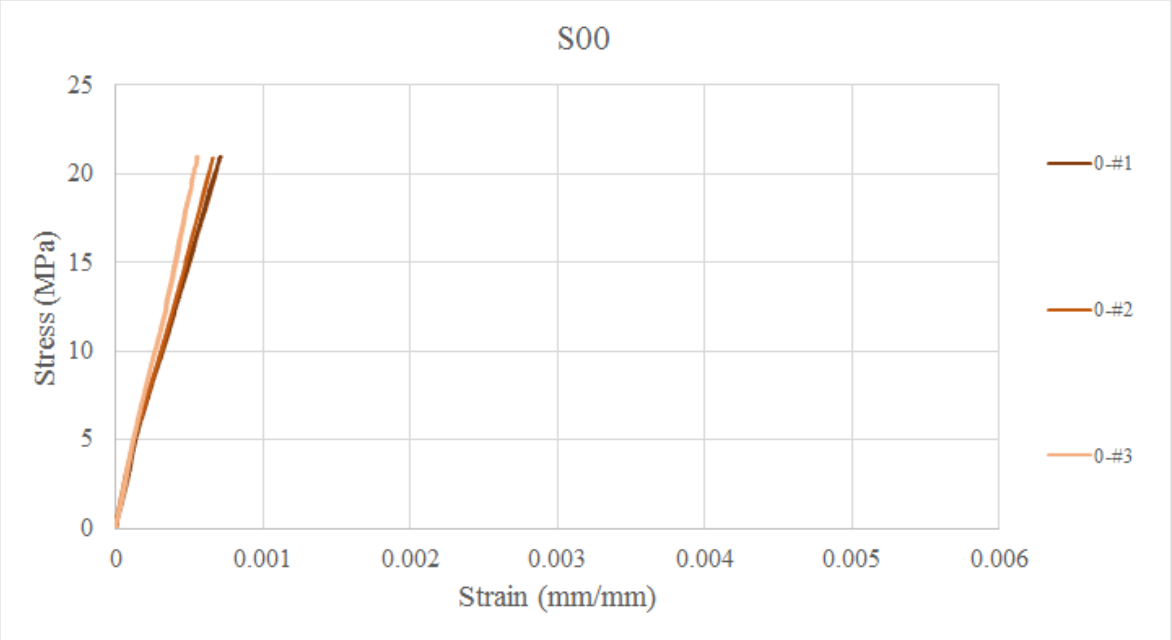

Figure D.9. Stress and strain diagrams of S00 concrete.

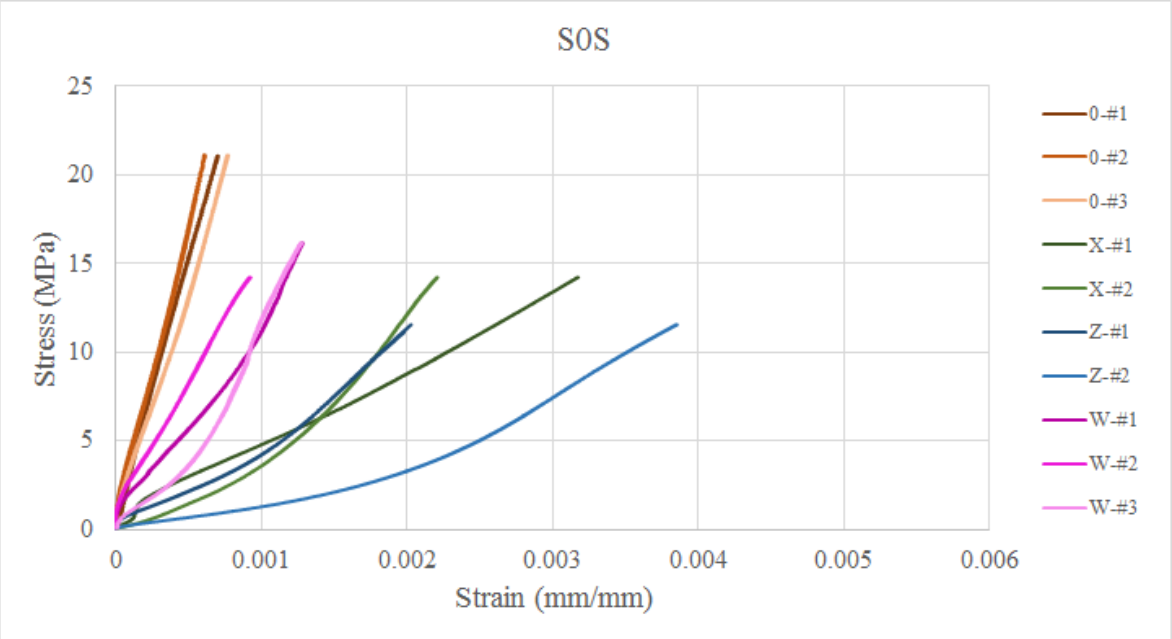

Figure D.10. Stress and strain diagrams of S0S concrete.

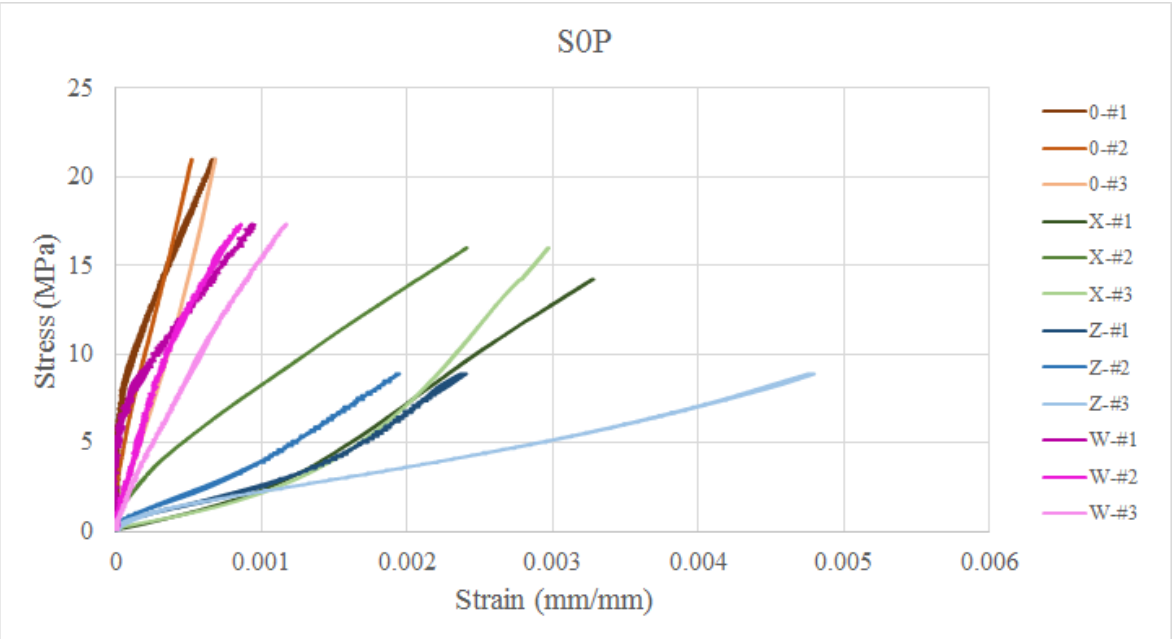

Figure D.11. Stress and strain diagrams of S0P concrete.

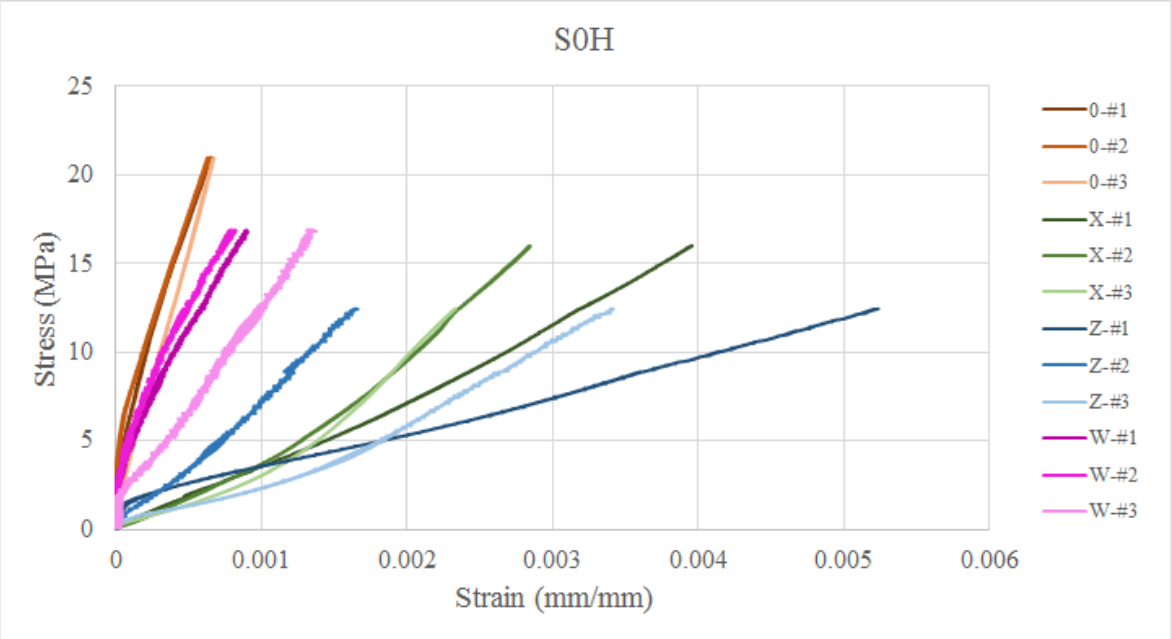

Figure D.12. Stress and strain diagrams of S0H concrete.

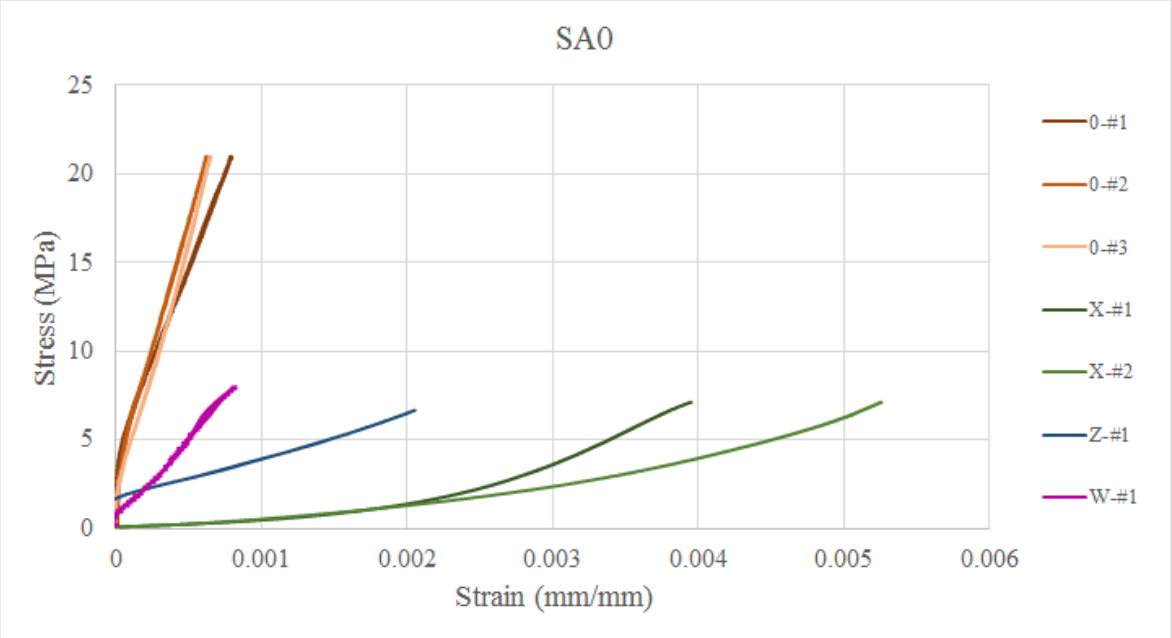

Figure D.13. Stress and strain diagrams of SA0 concrete.

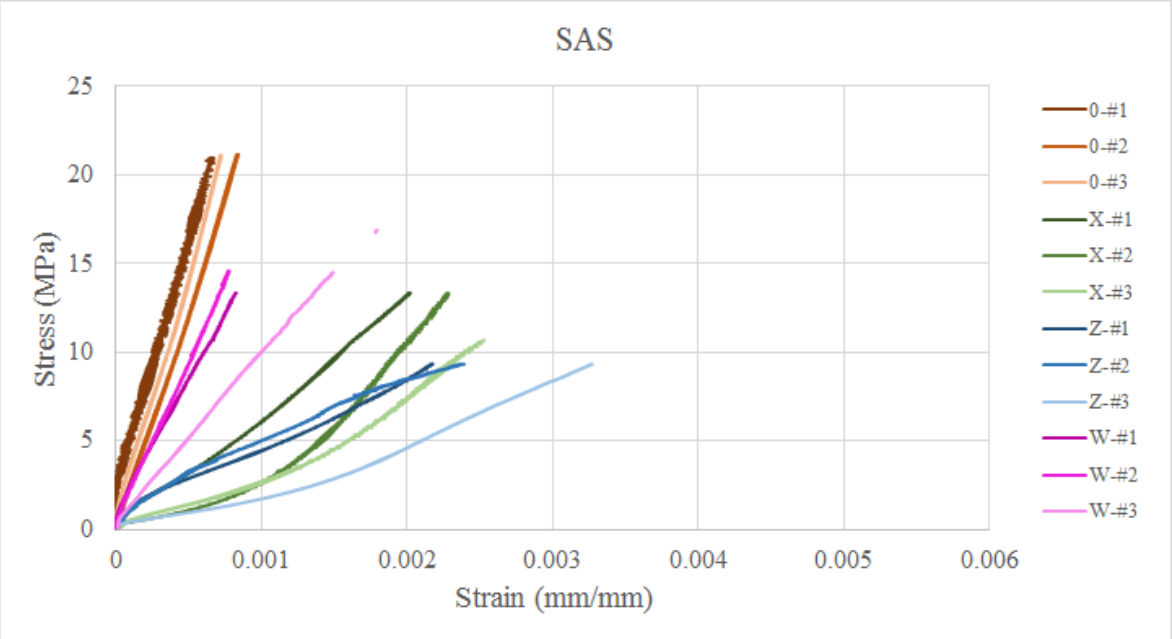

Figure D.14. Stress and strain diagrams of SAS concrete.

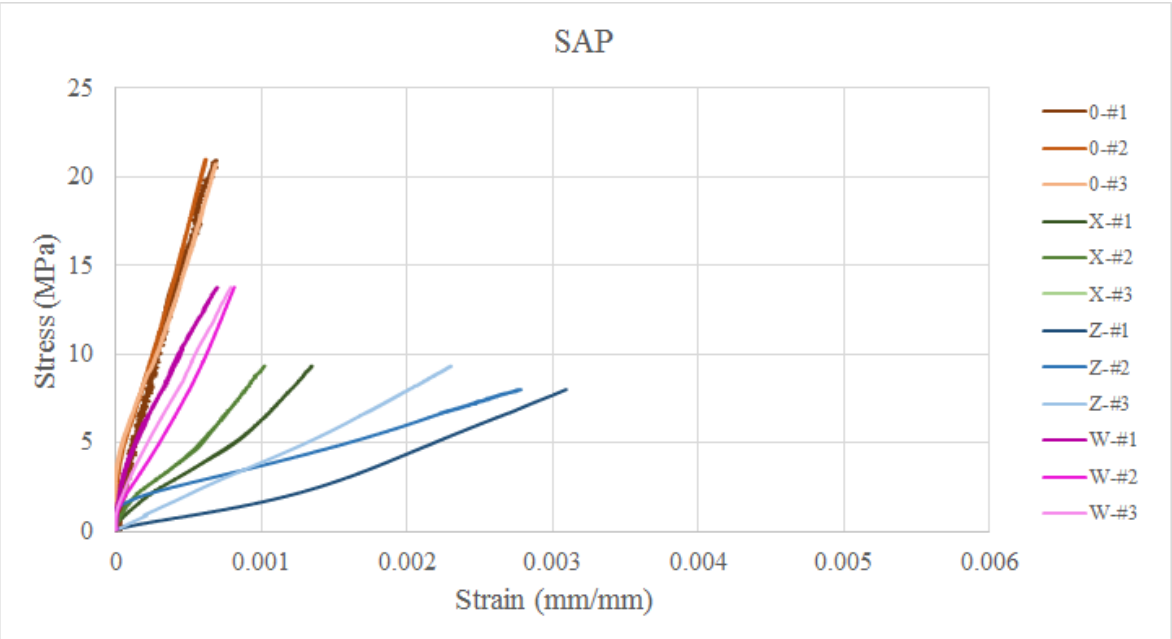

Figure D.15. Stress and strain diagrams of SAP concrete.

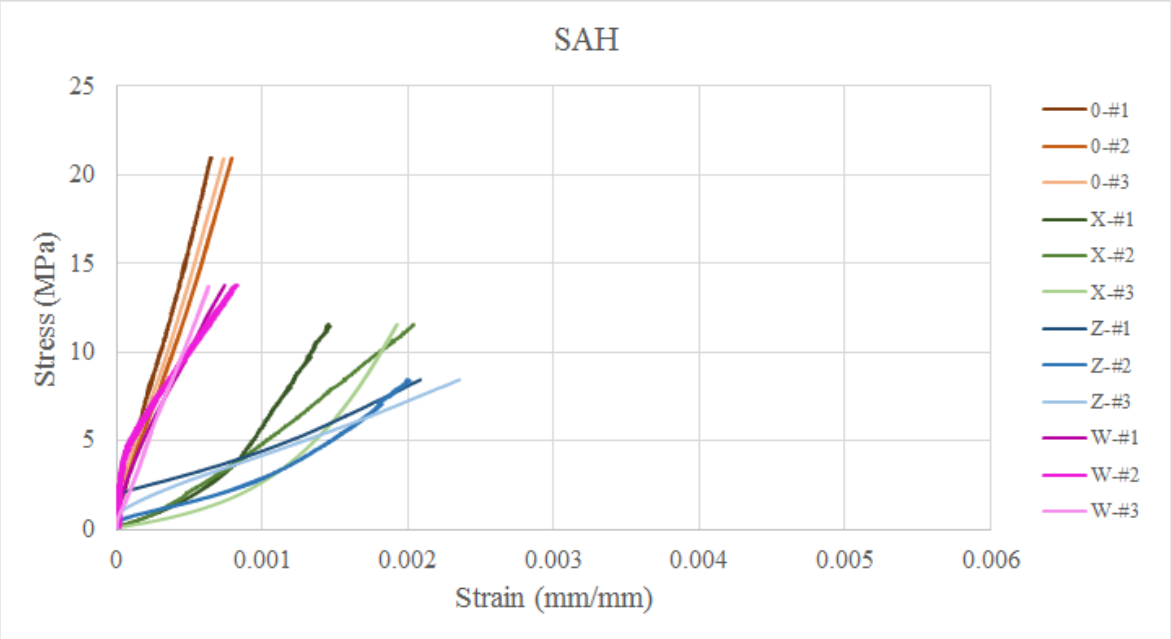

Figure D.16. Stress and strain diagrams of SAH concrete.

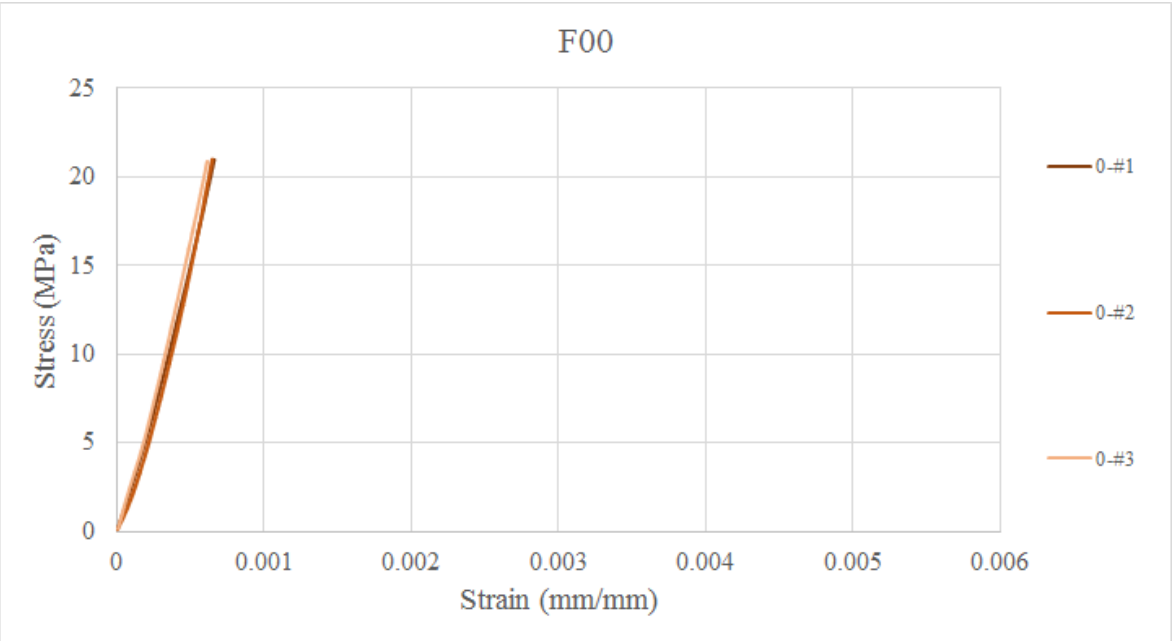

Figure D.17. Stress and strain diagrams of F00 concrete.

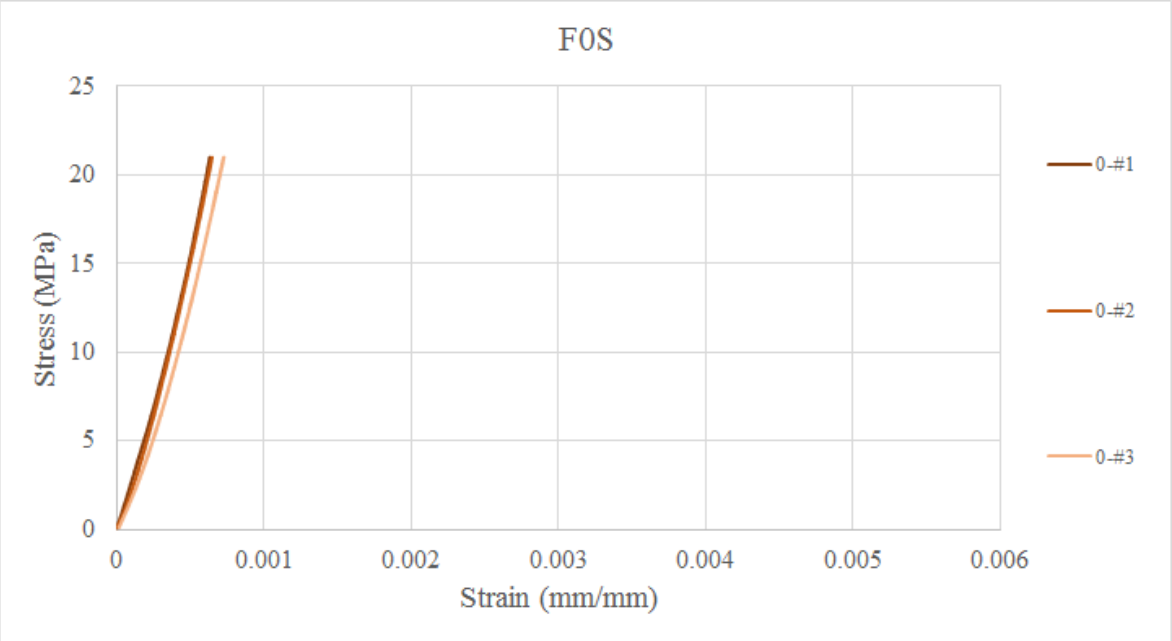

Figure D.18. Stress and strain diagrams of F0S concrete.

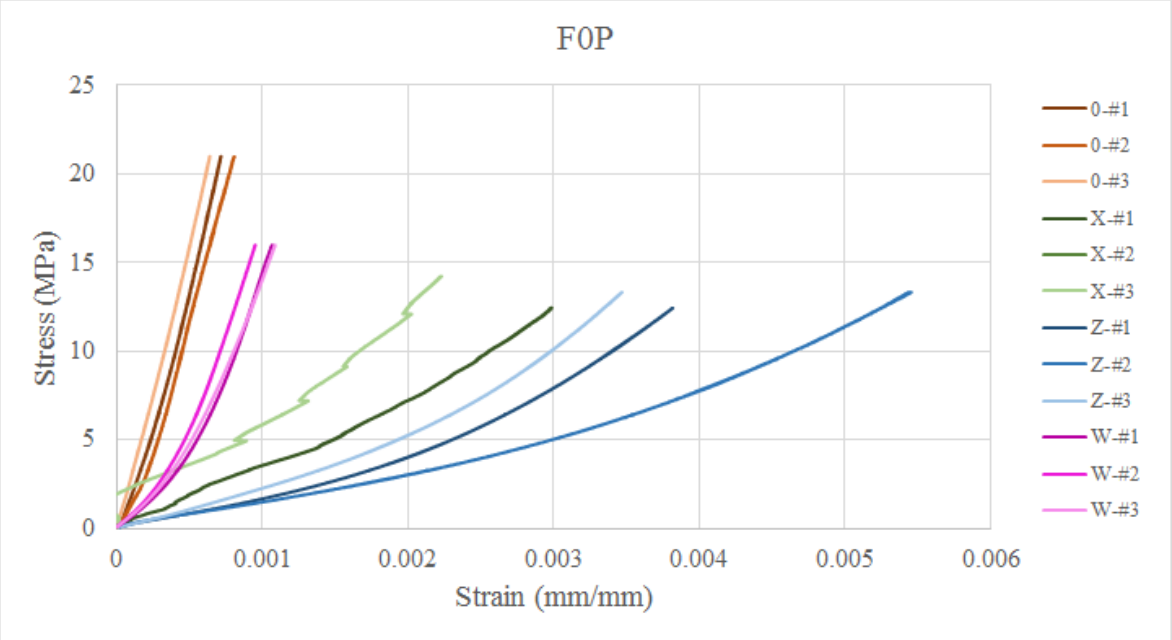

Figure D.19. Stress and strain diagrams of F0P concrete.

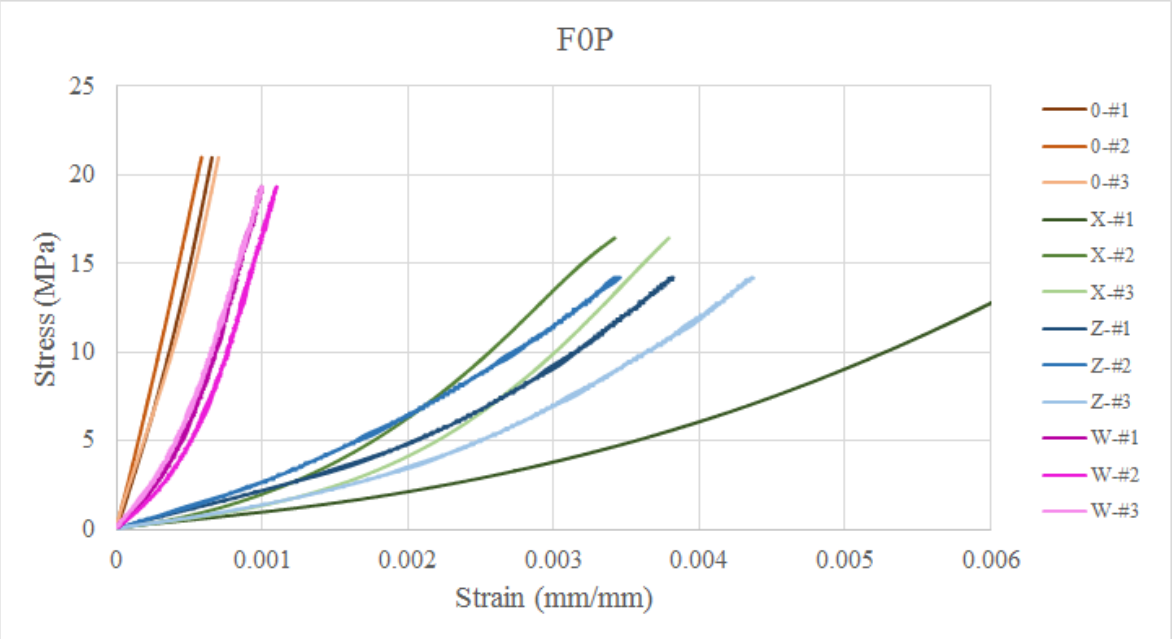

Figure D.20. Stress and strain diagrams of F0H concrete.

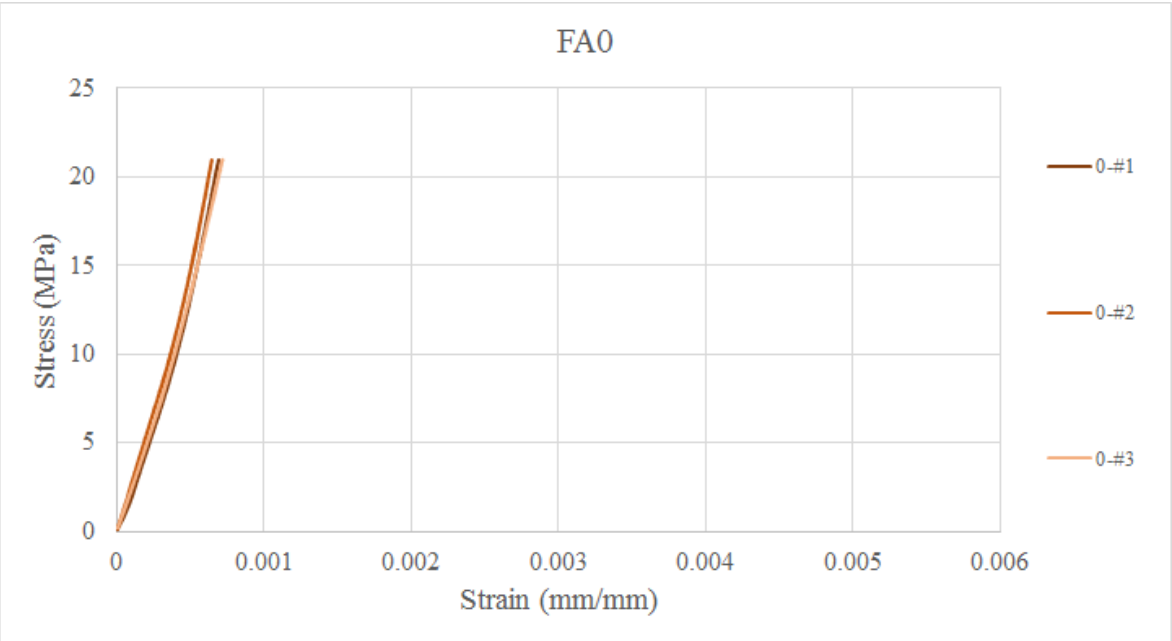

Figure D.21. Stress and strain diagrams of FA0 concrete.

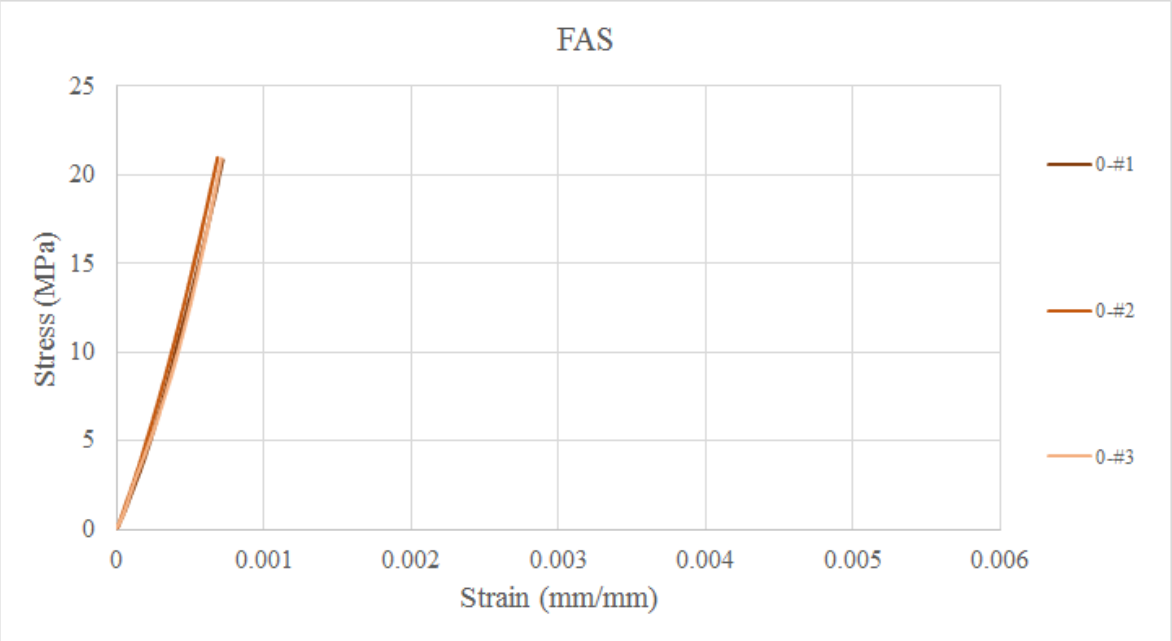

Figure D.22. Stress and strain diagrams of FAS concrete.

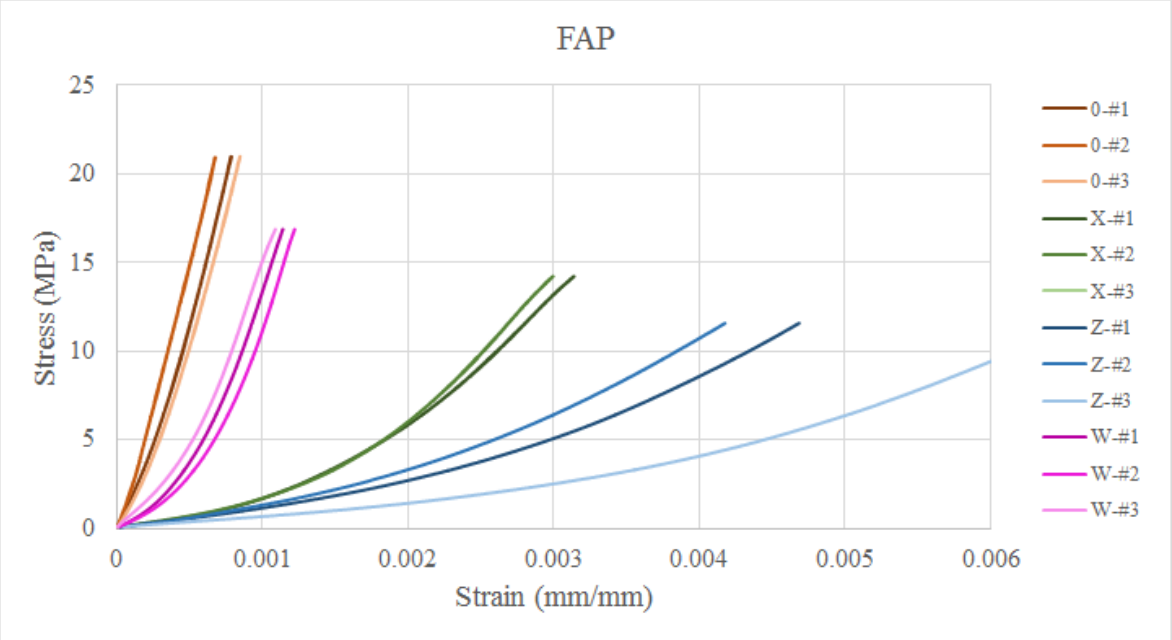

Figure D.23. Stress and strain diagrams of FAP concrete.

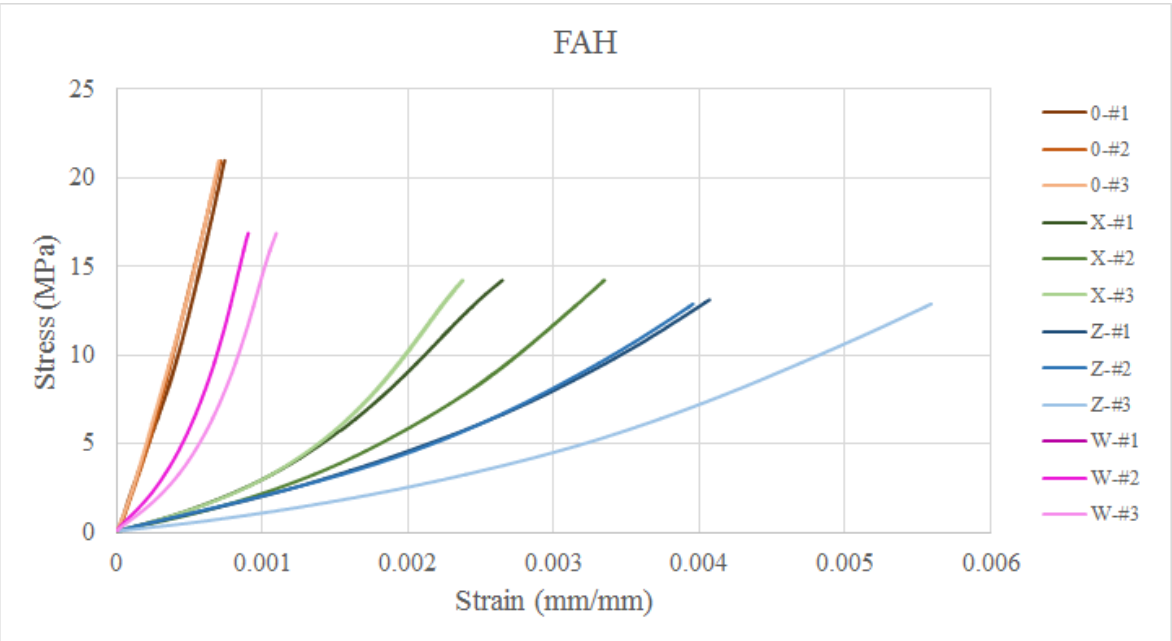

Figure D.24. Stress and strain diagrams of FAH concrete.

APPENDIX E: COMPRESSIVE STRENGTH TABLES

Results of compressive strength test of concrete specimens were given in following tables. "0" sign represents the specimen before heating, "X" represents the specimen tested just after cooling. "Z" and "W" represent air re-cured specimen and water re-cured specimen, respectively.

Table E.1. Compressive strength test results of Portland cement concrete groups before heating.

Group	**Specimen #1 (MPa)**	**Specimen #2 (MPa)**	**Specimen #3 (MPa)**	**Average (MPa)**	**Standard Deviation (MPa)**
C00-0	66.0	66.0	61.5	64.5	2.6
C0S-0	60.5	63.6	61.9	62.0	1.6
C0P-0	57.5	58.9	58.3	58.2	0.7
C0H-0	52.5	57.9	55.9	55.4	2.7
CA0-0	54.5	53.7	56.3	54.8	1.3
CAS-0	55.1	54.2	55.7	55.0	0.7
CAP-0	51.5	51.5	47.1	50.0	2.5
CAH-0	55.6	43.6	50.4	49.8	6.0

Table E.2. Compressive strength test results of Portland cement concrete groups after cooling.

Group	**Specimen #1 (MPa)**	**Specimen #2 (MPa)**	**Specimen #3 (MPa)**	**Average (MPa)**	**Standard Deviation (MPa)**
C00-X	47.6	45.9	38.3	43.9	5.0
C0S-X	48.9	46.5	42.7	46.0	3.1
C0P-X	35.2	38.9	36.5	36.9	1.8
C0H-X	37.4	39.1	33.5	36.7	2.9
CA0-X	34.5	39.3	32.9	35.5	3.3
CAS-X	36.3	33.3	35.2	34.9	1.5
CAP-X	23.7	24.7	27.5	25.3	2.0
CAH-X	27.0	28.4	26.1	27.2	1.2

Table E.3. Compressive strength test results of air re-cured Portland cement concrete groups.

Group	**Specimen #1 (MPa)**	**Specimen #2 (MPa)**	**Specimen #3 (MPa)**	**Average (MPa)**	**Standard Deviation (MPa)**
C00-Z	22.4	23.8	Spalled	23.1	1.0
C0S-Z	30.7	37.6	Spalled	34.2	4.9
C0P-Z	20.1	21.4	16.5	19.3	2.5
C0H-Z	29.5	30.4	24.6	28.2	3.1
CA0-Z	25.8	22.2	23.9	24.0	1.8
CAS-Z	26.4	31.3	25.6	27.7	3.1
CAP-Z	22.4	21.2	18.4	20.7	2.0
CAH-Z	23.4	24.3	17.2	21.7	3.9

Table E.4. Compressive strength test results of water re-cured Portland cement concrete groups.

Group	**Specimen #1 (MPa)**	**Specimen #2 (MPa)**	**Specimen #3 (MPa)**	**Average (MPa)**	**Standard Deviation (MPa)**
C00-W	43.0	Spalled	Spalled	43.0	-
C0S-W	46.7	47.0	Spalled	46.9	0.2
C0P-W	41.0	37.0	35.1	37.7	3.0
C0H-W	40.2	40.8	36.5	39.2	2.3
CA0-W	38.2	40.0	40.3	39.5	1.1
CAS-W	33.2	34.2	33.5	33.6	0.5
CAP-W	31.4	32.3	36.8	33.5	2.9
CAH-W	33.5	38.8	33.5	35.3	3.1

Table E.5. Compressive strength test results of concrete groups incorporating GGBFS before heating.

Group	**Specimen #1 (MPa)**	**Specimen #2 (MPa)**	**Specimen #3 (MPa)**	**Average (MPa)**	**Standard Deviation (MPa)**
S00-0	63.7	63.6	61.8	63.0	1.1
S0S-0	63.5	62.9	55.9	60.8	4.2
S0P-0	67.1	59.1	64.6	63.6	4.1
S0H-0	58.0	62.1	60.4	60.2	2.0
SA0-0	56.8	58.5	55.0	56.8	1.8
SAS-0	50.6	50.2	49.0	49.9	0.8
SAP-0	51.5	48.8	49.9	50.1	1.4
SAH-0	48.1	50.2	47.9	48.7	1.3

Table E.6. Compressive strength test results of concrete groups incorporating GGBFS after cooling.

Group	**Specimen #1 (MPa)**	**Specimen #2 (MPa)**	**Specimen #3 (MPa)**	**Average (MPa)**	**Standard Deviation (MPa)**
S00-X	Spalled	Spalled	Spalled	-	-
S0S-X	44.2	34.7	Spalled	39.4	6.7
S0P-X	46.0	45.0	40.5	43.8	3.0
S0H-X	46.0	46.7	40.9	44.6	3.2
SA0-X	24.3	16.8	Spalled	20.5	5.3
SAS-X	36.9	33.8	32.1	34.2	2.4
SAP-X	29.6	29.5	25.6	28.2	2.3
SAH-X	29.7	31.2	27.8	29.6	1.7

Table E.7. Compressive strength test results of air re-cured concrete groups incorporating GGBFS.

Group	**Specimen #1 (MPa)**	**Specimen #2 (MPa)**	**Specimen #3 (MPa)**	**Average (MPa)**	**Standard Deviation (MPa)**
S00-Z	Spalled	Spalled	Spalled	-	-
S0S-Z	35.0	26.2	33.3	31.5	4.7
S0P-Z	30.1	26.7	29.1	28.7	1.7
S0H-Z	35.5	32.8	29.5	32.6	3.0
SA0-Z	Spalled	21.7	Spalled	21.7	-
SAS-Z	26.6	26.0	29.7	27.4	2.0
SAP-Z	21.8	23.8	18.7	21.4	2.6
SAH-Z	24.4	22.3	21.0	22.6	1.7

Table E.8. Compressive strength test results of water re-cured concrete groups incorporating GGBFS.

Group	**Specimen #1 (MPa)**	**Specimen #2 (MPa)**	**Specimen #3 (MPa)**	**Average (MPa)**	**Standard Deviation (MPa)**
S00-W	Spalled	Spalled	Spalled	-	-
S0S-W	39.6	38.7	37.4	38.6	1.1
S0P-W	49.1	48.2	42.3	46.5	3.7
S0H-W	48.6	48.8	43.4	46.9	3.1
SA0-W	27.0	Spalled	Spalled	27.0	-
SAS-W	37.8	33.8	29.4	33.7	4.2
SAP-W	39.3	38.1	35.9	37.8	1.7
SAH-W	38.9	40.1	35.2	38.1	2.6

Table E.9. Compressive strength test results of concrete groups incorporating PFA before heating.

Group	**Specimen #1 (MPa)**	**Specimen #2 (MPa)**	**Specimen #3 (MPa)**	**Average (MPa)**	**Standard Deviation (MPa)**
F00-0	67.8	70.4	70.2	69.5	1.5
F0S-0	65.9	70.7	71.5	69.4	3.0
F0P-0	74.7	70.4	68.2	71.1	3.3
F0H-0	70.7	67.0	74.3	70.6	3.7
FA0-0	60.6	62.0	61.0	61.2	0.7
FAS-0	64.3	61.3	58.8	61.5	2.8
FAP-0	62.6	59.5	56.1	59.4	3.2
FAH-0	56.1	58.4	61.2	58.6	2.6

Table E.10. Compressive strength test results of concrete groups incorporating PFA after cooling.

Group	**Specimen #1 (MPa)**	**Specimen #2 (MPa)**	**Specimen #3 (MPa)**	**Average (MPa)**	**Standard Deviation (MPa)**
F00-X	Spalled	Spalled	Spalled	-	-
F0S-X	Spalled	Spalled	Spalled	-	-
F0P-X	49.5	45.9	41.1	45.5	4.2
F0H-X	47.4	47.7	37.5	44.2	5.8
FA0-X	Spalled	Spalled	Spalled	-	-
FAS-X	Spalled	Spalled	Spalled	-	-
FAP-X	35.9	35.4	28.6	33.3	4.1
FAH-X	43.9	35.1	38.8	39.3	4.4

Table E.11. Compressive strength test results of air re-cured concrete groups incorporating PFA.

Group	**Specimen #1 (MPa)**	**Specimen #2 (MPa)**	**Specimen #3 (MPa)**	**Average (MPa)**	**Standard Deviation (MPa)**
F00-Z	Spalled	Spalled	Spalled	-	-
F0S-Z	Spalled	Spalled	Spalled	-	-
F0P-Z	34.4	33.8	30.3	32.8	2.3
F0H-Z	44.5	45.2	37.3	42.3	4.4
FA0-Z	Spalled	Spalled	Spalled	-	-
FAS-Z	Spalled	Spalled	Spalled	-	-
FAP-Z	25.7	28.3	22.3	25.4	3.0
FAH-Z	36.9	30.5	28.6	32.0	4.3

Table E.12. Compressive strength test results of water re-cured concrete groups incorporating PFA.

Group	**Specimen #1 (MPa)**	**Specimen #2 (MPa)**	**Specimen #3 (MPa)**	**Average (MPa)**	**Standard Deviation (MPa)**
F00-W	Spalled	Spalled	Spalled	-	-
F0S-W	Spalled	Spalled	Spalled	-	-
F0P-W	50.5	48.3	49.4	49.4	1.1
F0H-W	54.3	52.8	49.8	52.3	2.3
FA0-W	Spalled	Spalled	Spalled	-	-
FAS-W	Spalled	Spalled	Spalled	-	-
FAP-W	41.3	39.6	36.2	39.0	2.6
FAH-W	45.8	44.3	46.1	45.4	0.9

APPENDIX F: MODULUS OF ELASTICITY TABLES

Results of modulus of elasticity test of concrete specimens were given in following tables. "0" sign represents the specimen before heating, "X" represents the specimen tested just after cooling. "Z" and "W" represent air re-cured specimen and water re-cured specimen, respectively.

Table F.1. Modulus of elasticity test results of Portland cement concrete groups before heating.

Group	**Specimen #1 (MPa)**	**Specimen #2 (MPa)**	**Specimen #3 (MPa)**	**Average (MPa)**	**Standard Deviation (MPa)**
C00-0	28914	33989	28027	30310	3217
C0S-0	29875	33023	27125	30008	2951
C0P-0	26777	30093	30058	28976	1904
C0H-0	28244	30932	27046	28741	1990
CA0-0	24773	28512	29413	27566	2460
CAS-0	29242	29666	29202	29370	257
CAP-0	27715	28213	31651	29193	2143
CAH-0	26123	26891	28454	27156	1188

Table F.2. Modulus of elasticity test results of Portland cement concrete groups after cooling.

Group	**Specimen #1 (MPa)**	**Specimen #2 (MPa)**	**Specimen #3 (MPa)**	**Average (MPa)**	**Standard Deviation (MPa)**
C00-X	5799	11001	5862	7554	2985
C0S-X	8103	4757	8147	7002	1945
C0P-X	4512	5241	4810	4854	367
C0H-X	4484	5925	4021	4810	993
CA0-X	6121	8686	5912	6906	1545
CAS-X	7263	6340	4946	6183	1166
CAP-X	5709	4523	6760	5664	1119
CAH-X	8348	5863	5577	6596	1524

Table F.3. Modulus of elasticity test results of air re-cured Portland cement concrete groups.

Group	**Specimen #1 (MPa)**	**Specimen #2 (MPa)**	**Specimen #3 (MPa)**	**Average (MPa)**	**Standard Deviation (MPa)**
C00-Z	3304	3425	Spalled	3365	86
C0S-Z	6454	3615	Spalled	5035	2007
C0P-Z	5021	3401	1772	3398	1625
C0H-Z	3271	4748	4098	4039	740
CA0-Z	3188	3617	3459	3421	217
CAS-Z	5094	5178	4464	4912	390
CAP-Z	3375	3480	3341	3399	72
CAH-Z	3848	3455	4417	3907	484

Table F.4. Modulus of elasticity test results of water re-cured Portland cement concrete groups.

Group	**Specimen #1 (MPa)**	**Specimen #2 (MPa)**	**Specimen #3 (MPa)**	**Average (MPa)**	**Standard Deviation (MPa)**
C00-W	7855	Spalled	Spalled	7855	-
C0S-W	13413	12526	Spalled	12970	627
C0P-W	19509	14629	18876	17671	2654
C0H-W	7482	13587	16417	12495	4566
CA0-W	9760	11516	11135	10804	924
CAS-W	9818	13317	11105	11413	1770
CAP-W	18744	13109	20105	17319	3709
CAH-W	9112	15704	11432	12083	3344

Table F.5. Modulus of elasticity test results of concrete groups incorporating GGBFS before heating.

Group	**Specimen #1 (MPa)**	**Specimen #2 (MPa)**	**Specimen #3 (MPa)**	**Average (MPa)**	**Standard Deviation (MPa)**
S00-0	28533	30059	36670	31754	4325
S0S-0	30039	32292	25721	29351	3339
S0P-0	26661	35856	29296	30604	4735
S0H-0	29354	28860	29601	29272	377
SA0-0	23303	30349	29262	27638	3793
SAS-0	28457	24881	27433	26924	1842
SAP-0	30490	30066	25703	28753	2650
SAH-0	30871	24639	26255	27255	3234

Table F.6. Modulus of elasticity test results of concrete groups incorporating GGBFS after cooling.

Group	**Specimen #1 (MPa)**	**Specimen #2 (MPa)**	**Specimen #3 (MPa)**	**Average (MPa)**	**Standard Deviation (MPa)**
S00-X	Spalled	Spalled	Spalled	-	-
S0S-X	7081	4599	Spalled	5840	1755
S0P-X	4937	6144	5992	5691	657
S0H-X	4002	5871	6045	5306	1133
SA0-X	2183	1451	Spalled	1817	518
SAS-X	6373	6499	4256	5709	1260
SAP-X	6180	8204	Measuring Error	7192	1431
SAH-X	8738	5917	6772	7142	1447

Table F.7. Modulus of elasticity test results of air re-cured concrete groups incorporating GGBFS.

Group	**Specimen #1 (MPa)**	**Specimen #2 (MPa)**	**Specimen #3 (MPa)**	**Average (MPa)**	**Standard Deviation (MPa)**
S00-Z	Spalled	Spalled	Spalled	-	-
S0S-Z	5547	3304	Measuring Error	4426	1586
S0P-Z	3492	4327	1661	3160	1364
S0H-Z	2133	7500	3739	4457	2755
SA0-Z	Spalled	2548	Spalled	2548	-
SAS-Z	3780	3845	2981	3535	481
SAP-Z	2693	2458	3910	3020	779
SAH-Z	3281	3925	3170	3459	408

Table F.8. Modulus of elasticity test results of water re-cured concrete groups incorporating GGBFS.

Group	**Specimen #1 (MPa)**	**Specimen #2 (MPa)**	**Specimen #3 (MPa)**	**Average (MPa)**	**Standard Deviation (MPa)**
S00-W	Spalled	Spalled	Spalled	-	-
S0S-W	11475	14523	13670	13223	1572
S0P-W	15300	20238	14625	16721	3064
S0H-W	16891	19177	11503	15857	3940
SA0-W	9253	Spalled	Spalled	9253	-
SAS-W	15087	18165	9369	14207	4464
SAP-W	18138	15425	15961	16508	1437
SAH-W	17152	14714	21452	17773	3412

Table F.9. Modulus of elasticity test results of concrete groups incorporating PFA before heating.

Group	**Specimen #1 (MPa)**	**Specimen #2 (MPa)**	**Specimen #3 (MPa)**	**Average (MPa)**	**Standard Deviation (MPa)**
F00-0	32122	33773	34568	33488	1248
F0S-0	33128	33560	30209	32299	1823
F0P-0	30809	28638	32843	30763	2103
F0H-0	32195	36013	28923	32377	3549
FA0-0	30875	31934	29380	30730	1283
FAS-0	29789	31046	29441	30092	844
FAP-0	27618	31849	26120	28529	2971
FAH-0	28334	30649	30186	29723	1225

Table F.10. Modulus of elasticity test results of concrete groups incorporating PFA after cooling.

Group	**Specimen #1 (MPa)**	**Specimen #2 (MPa)**	**Specimen #3 (MPa)**	**Average (MPa)**	**Standard Deviation (MPa)**
F00-X	Spalled	Spalled	Spalled	-	-
F0S-X	Spalled	Spalled	Spalled	-	-
F0P-X	4012	Measuring Error	5484	4748	1041
F0H-X	4640	5527	5012	5060	445
FA0-X	Spalled	Spalled	Spalled	-	-
FAS-X	Spalled	Spalled	Spalled	-	-
FAP-X	5242	Measuring Error	5485	5364	172
FAH-X	5860	4490	6498	5616	1026

Table F.11. Modulus of elasticity test results of air re-cured concrete groups incorporating PFA.

Group	**Specimen #1 (MPa)**	**Specimen #2 (MPa)**	**Specimen #3 (MPa)**	**Average (MPa)**	**Standard Deviation (MPa)**
F00-Z	Spalled	Spalled	Spalled	-	-
F0S-Z	Spalled	Spalled	Spalled	-	-
F0P-Z	3388	2454	3901	3248	734
F0H-Z	3784	4230	3505	3840	366
FA0-Z	Spalled	Spalled	Spalled	-	-
FAS-Z	Spalled	Spalled	Spalled	-	-
FAP-Z	2941	3293	2180	2805	569
FAH-Z	3429	3446	2574	3150	499

Table F.12. Modulus of elasticity test results of water re-cured concrete groups incorporating PFA.

Group	**Specimen #1 (MPa)**	**Specimen #2 (MPa)**	**Specimen #3 (MPa)**	**Average (MPa)**	**Standard Deviation (MPa)**
F00-W	Spalled	Spalled	Spalled	-	-
F0S-W	Spalled	Spalled	Spalled	-	-
F0P-W	16217	18132	15720	16690	1274
F0H-W	19736	18044	19407	19062	897
FA0-W	Spalled	Spalled	Spalled	-	-
FAS-W	Spalled	Spalled	Spalled	-	-
FAP-W	16791	15698	16782	16424	628
FAH-W	Measuring Error	19577	16584	18081	2116

APPENDIX G: BPA IMAGES AND GRAPHS

Images used during black pixel analyses (BPA) and graphs obtained after BPA were given in following figures.

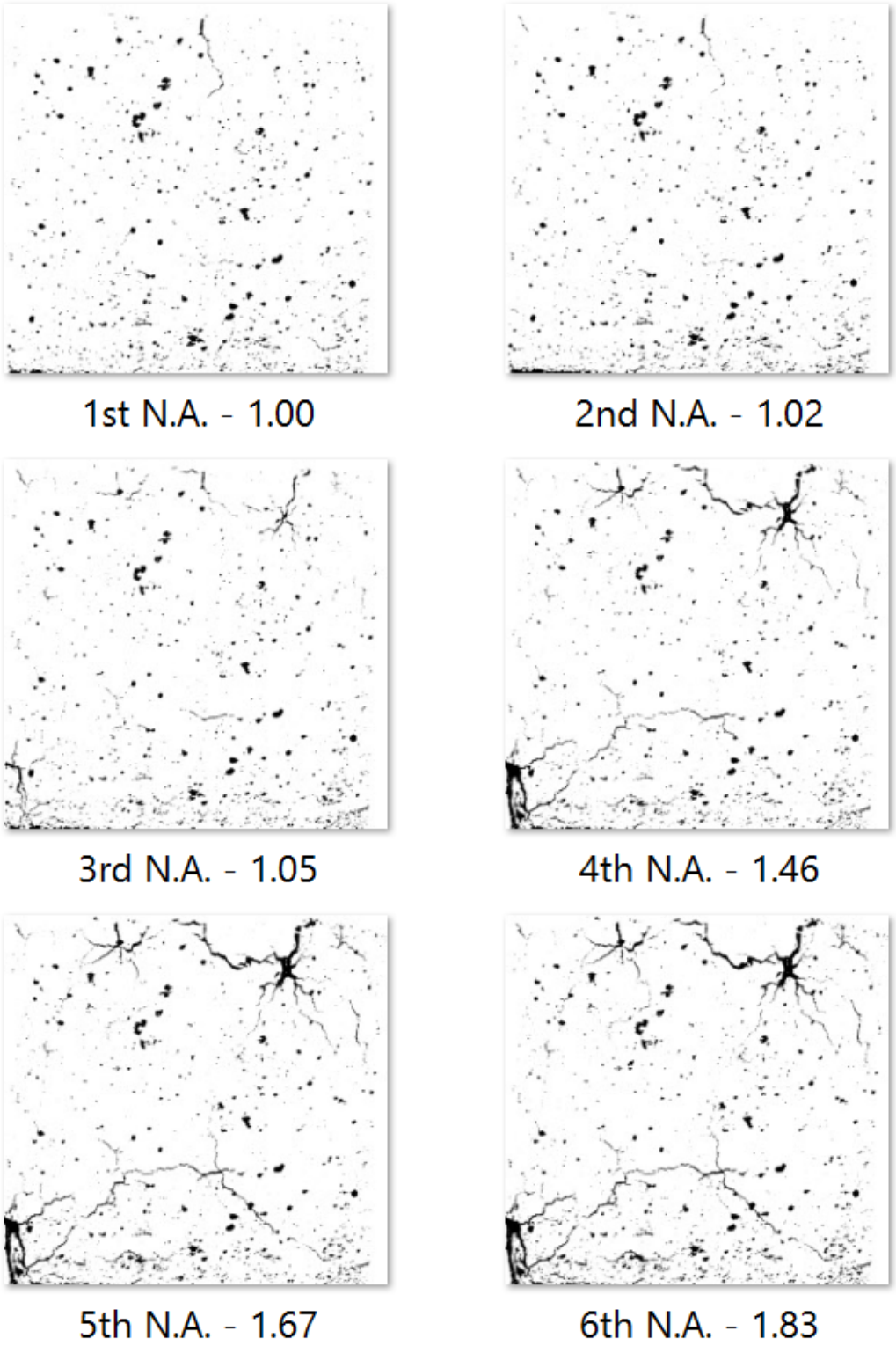

Figure G.1. BPA images of a C0P specimen and corresponding normalized area (N.A.) values.

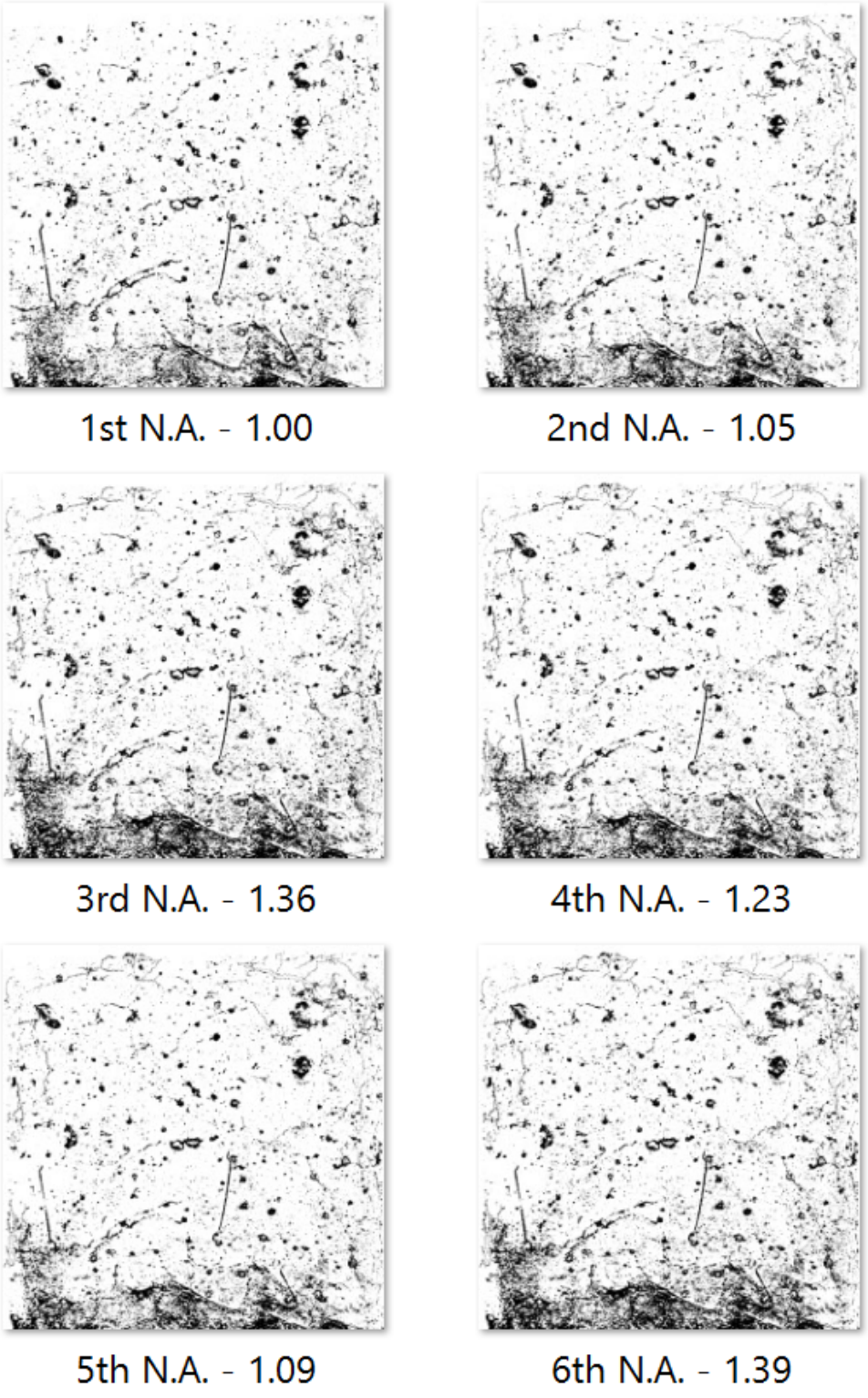

Figure G.2. BPA images of a C0H specimen and corresponding normalized area (N.A.) values.

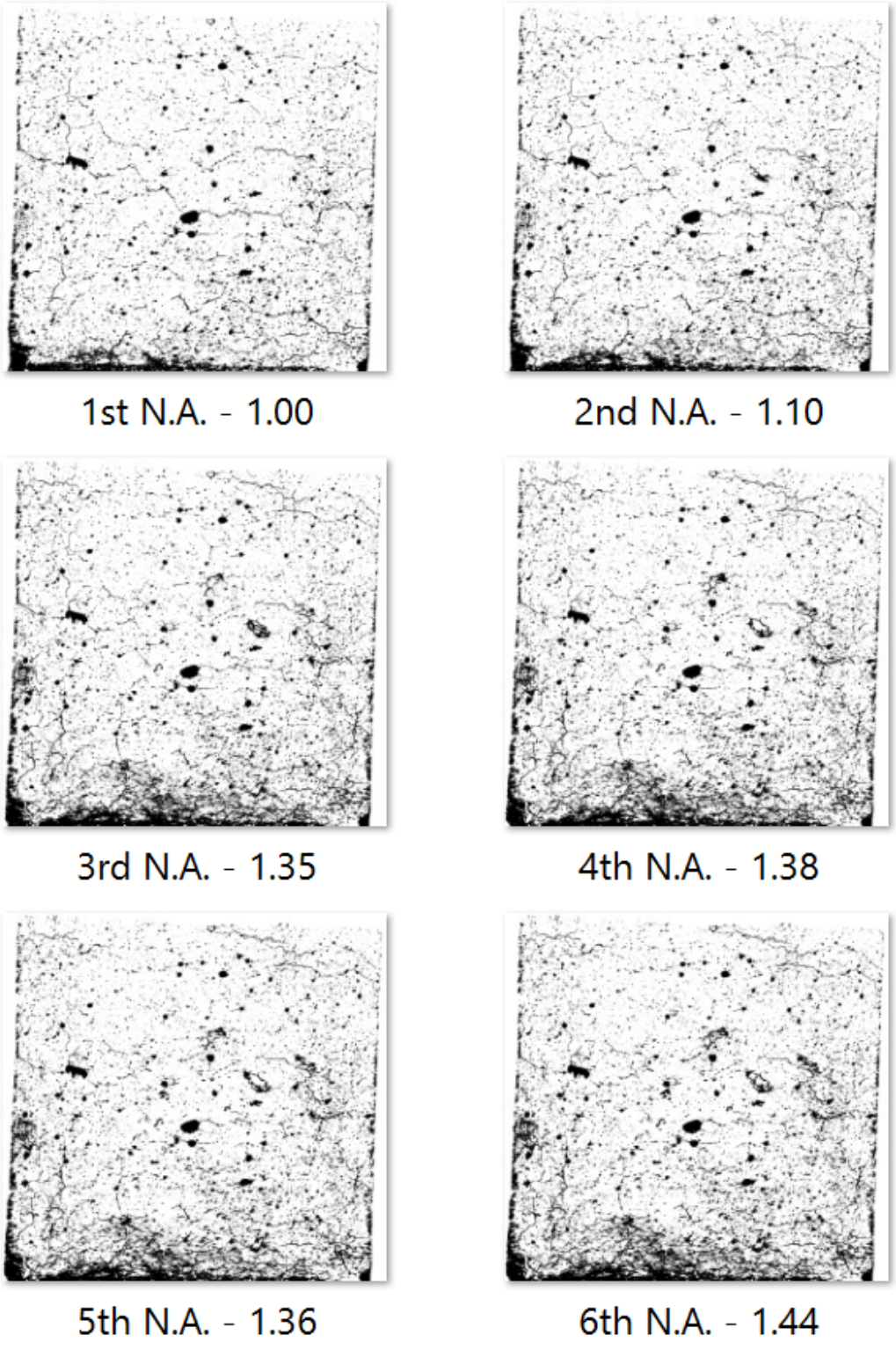

Figure G.3. BPA images of a CA0 specimen and corresponding normalized area (N.A.) values.

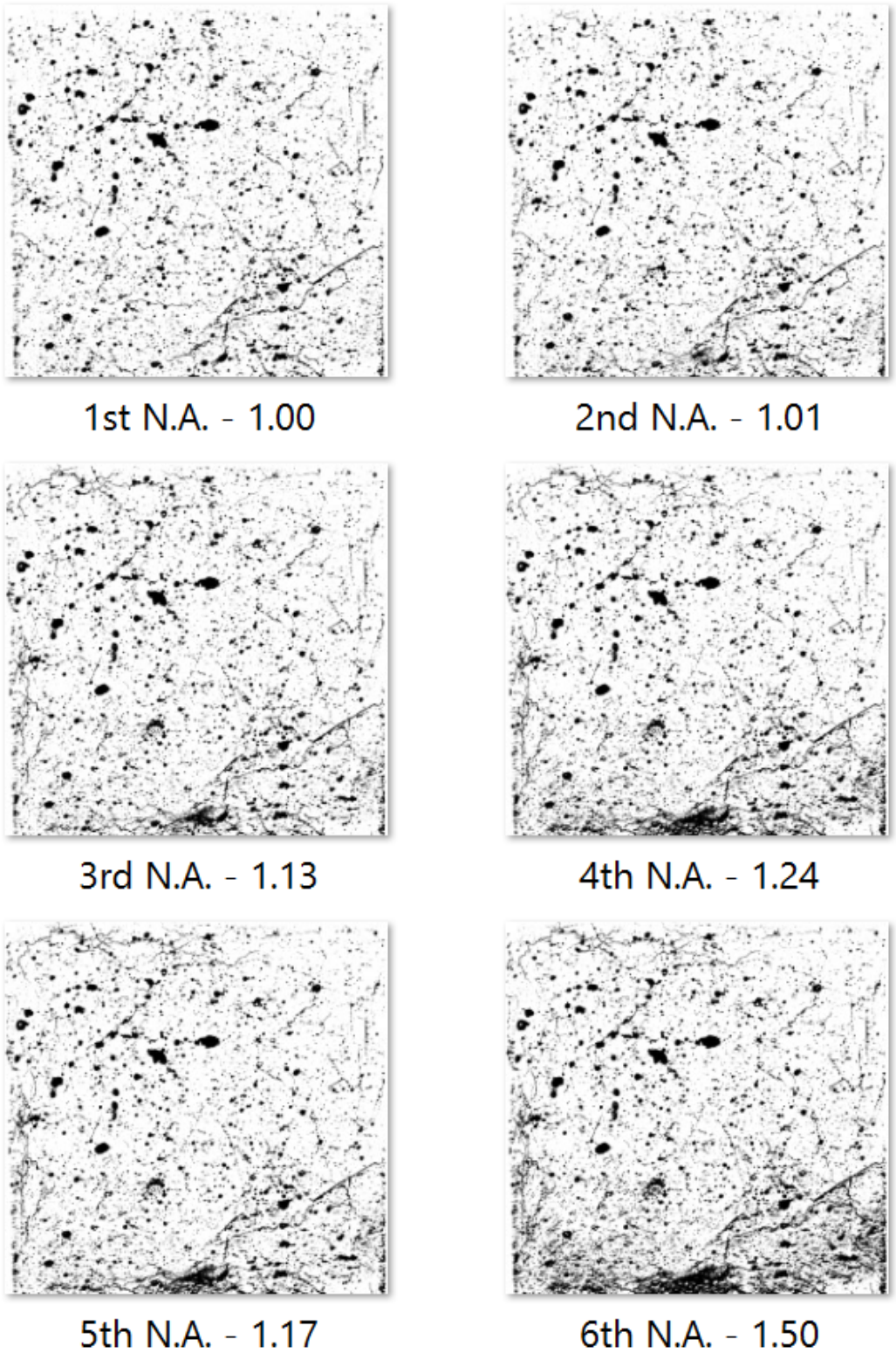

Figure G.4. BPA images of a CAS specimen and corresponding normalized area (N.A.) values.

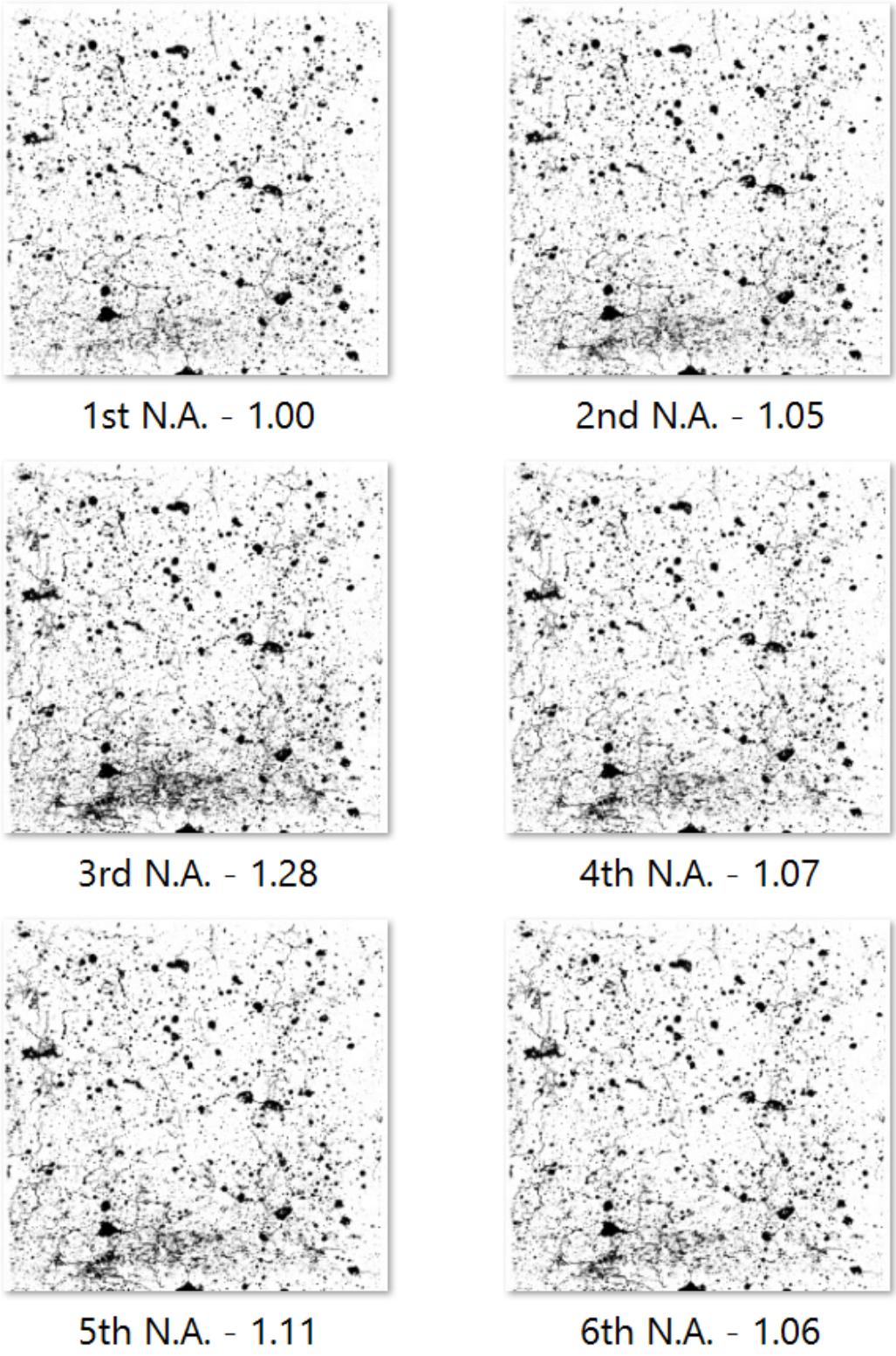

Figure G.5. BPA images of a CAP specimen and corresponding normalized area (N.A.) values.

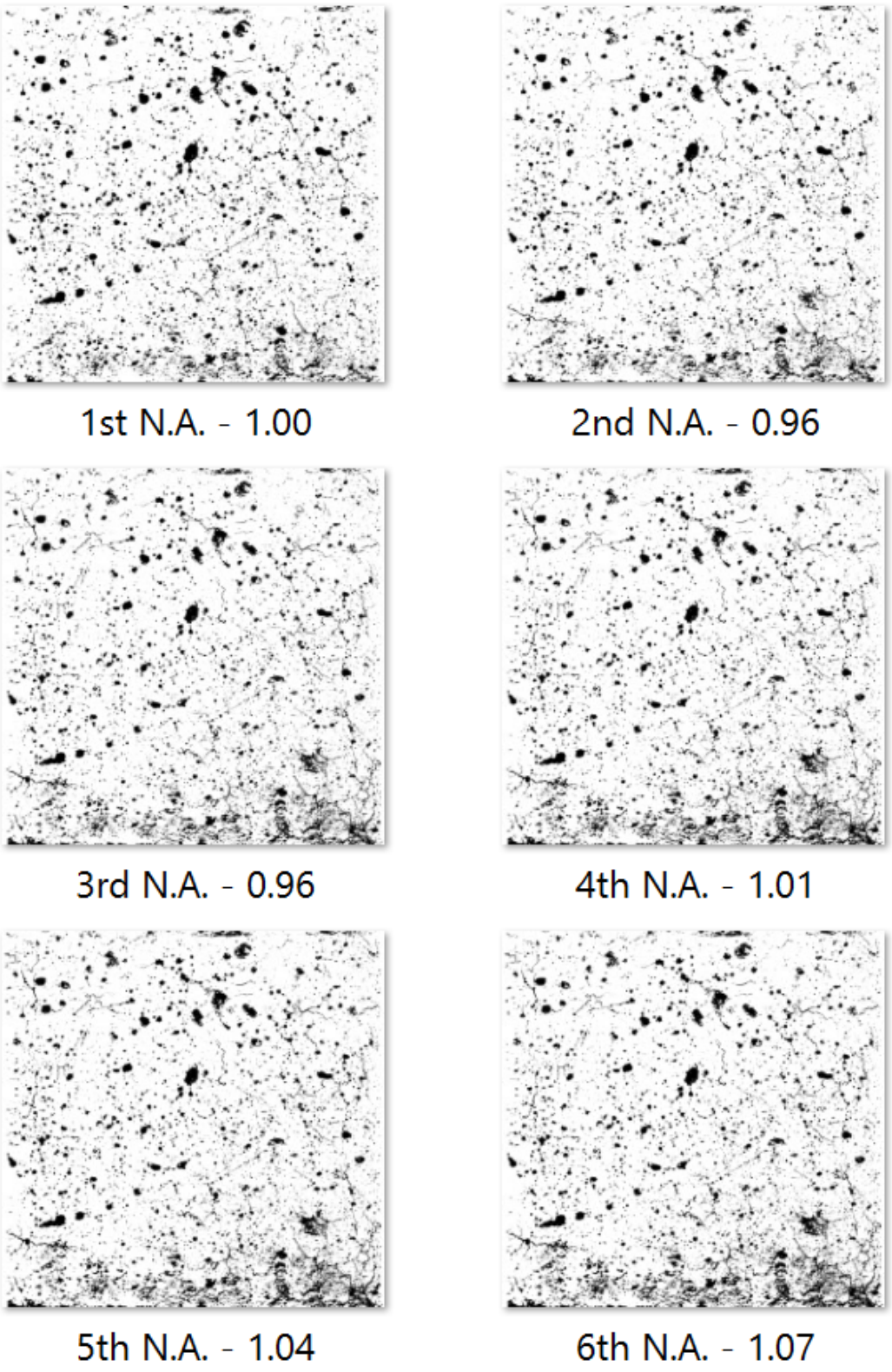

Figure G.6. BPA images of a CAH specimen and corresponding normalized area (N.A.) values.

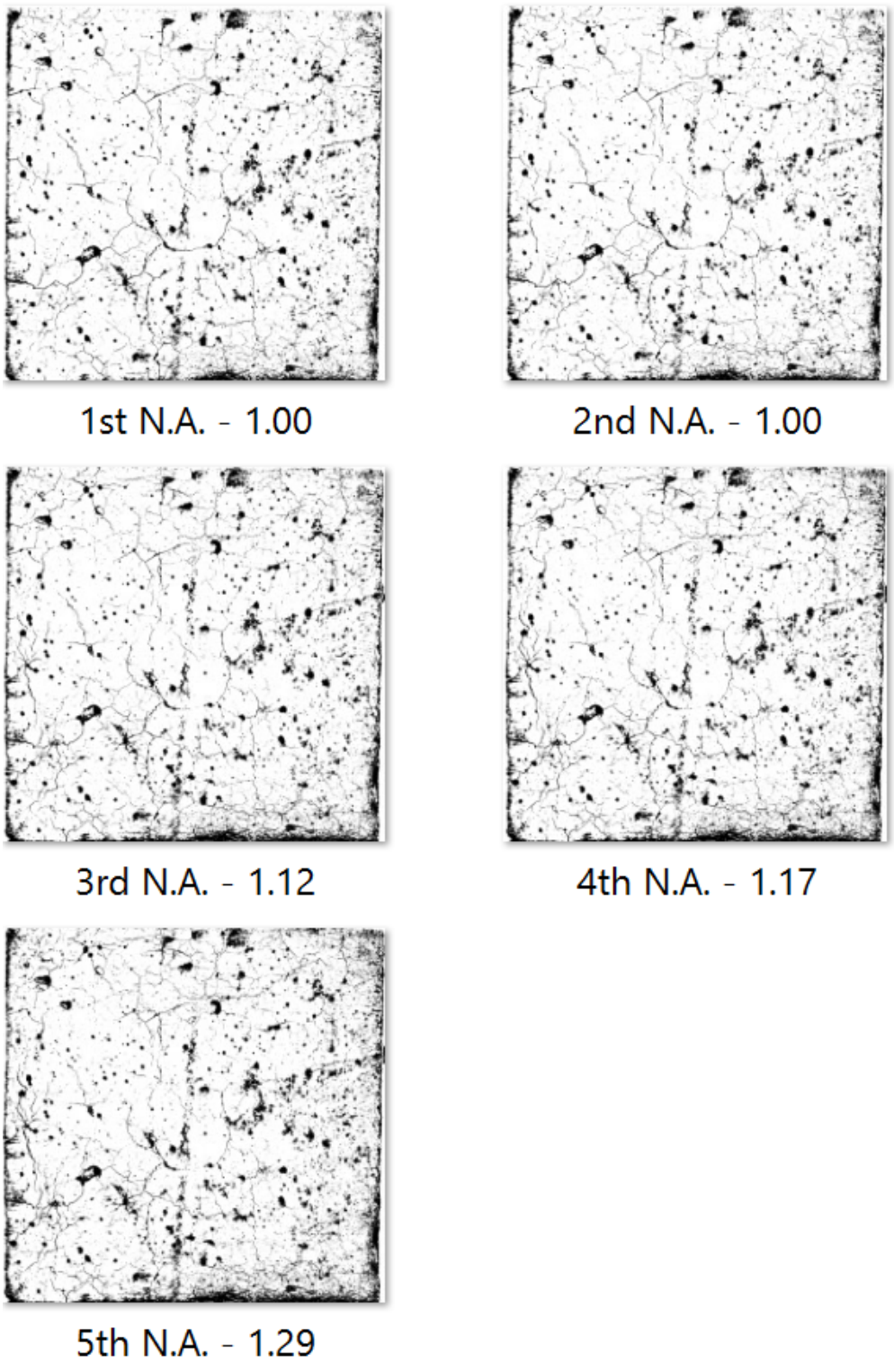

Figure G.7. BPA images of a S0P specimen and corresponding normalized area (N.A.) values.

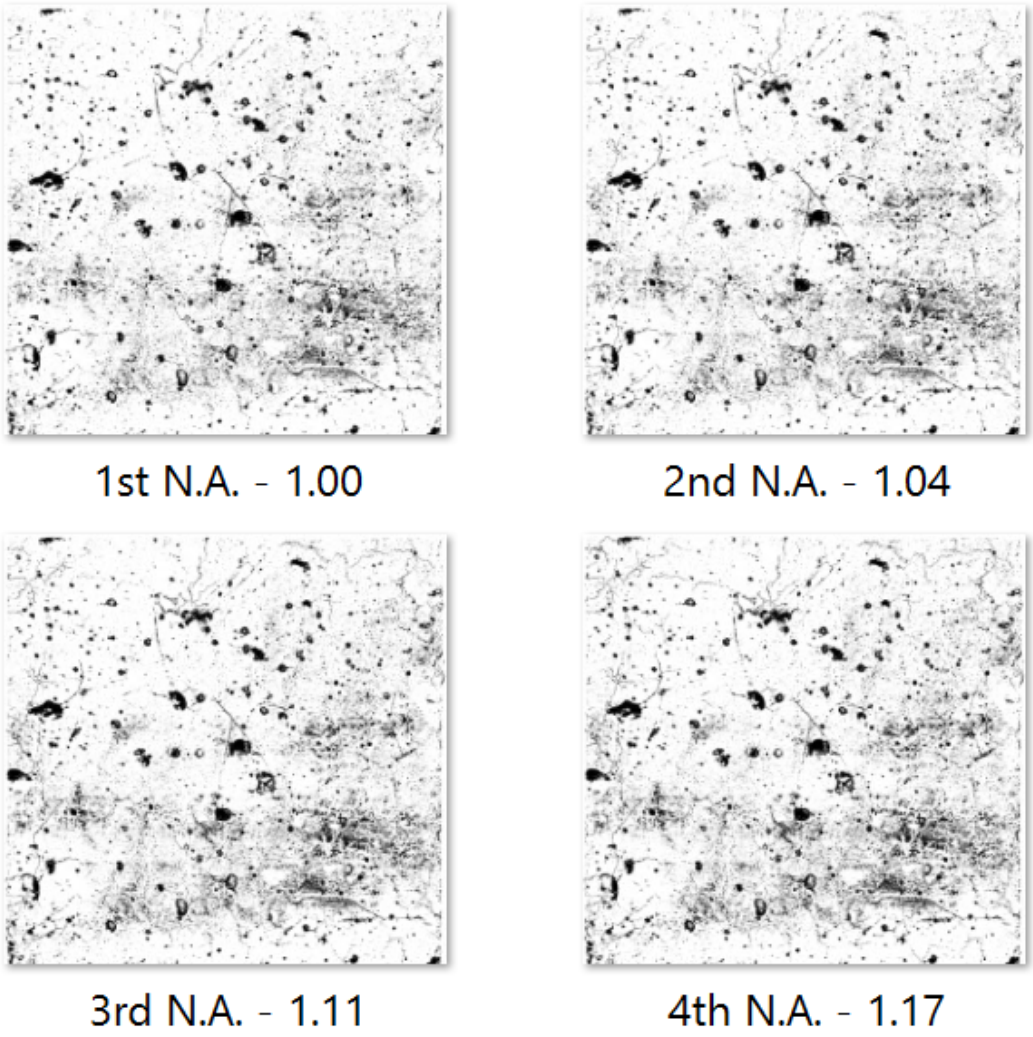

Figure G.8. BPA images of a S0H specimen and corresponding normalized area (N.A.) values.

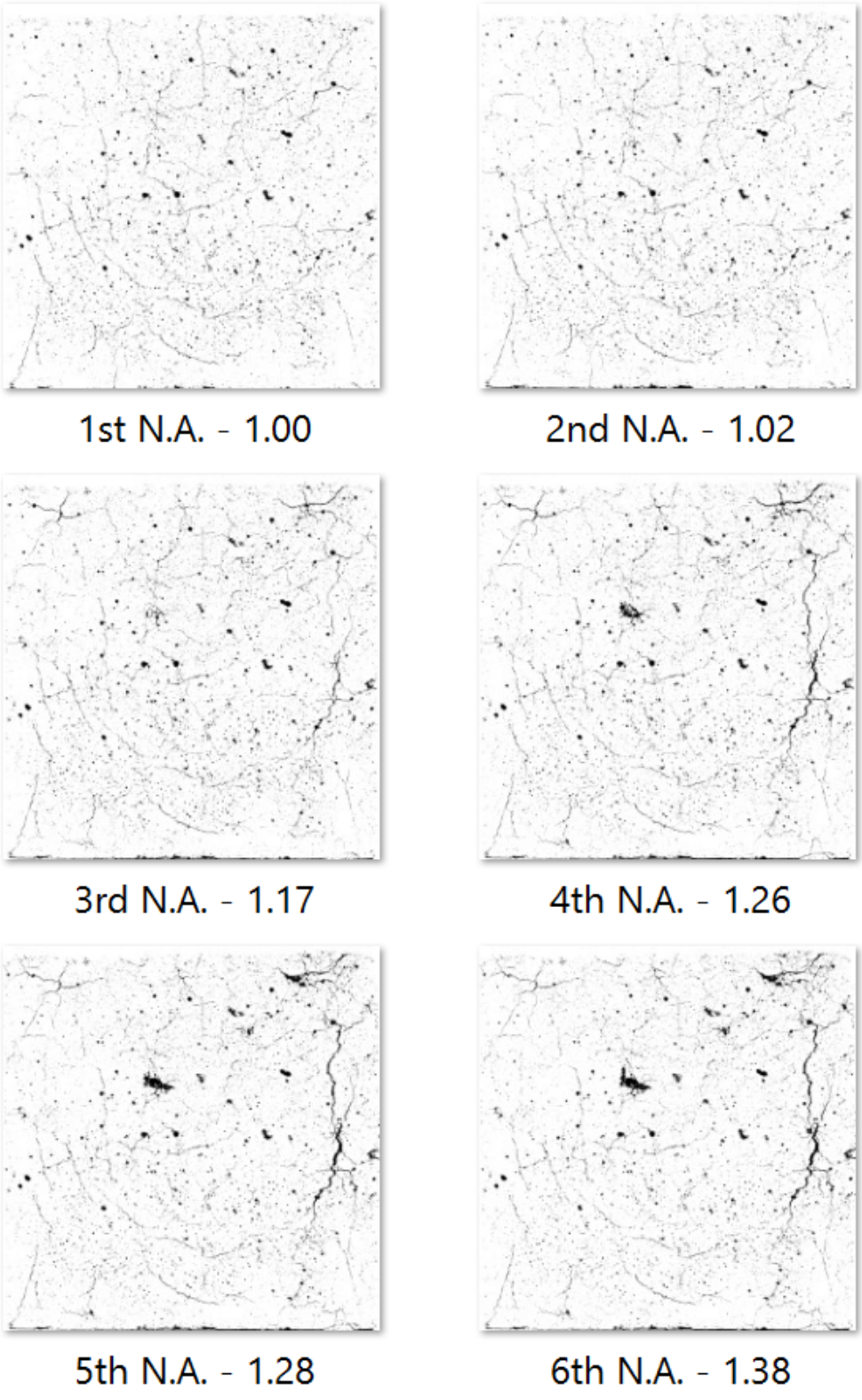

Figure G.9. BPA images of a SAS specimen and corresponding normalized area (N.A.) values.

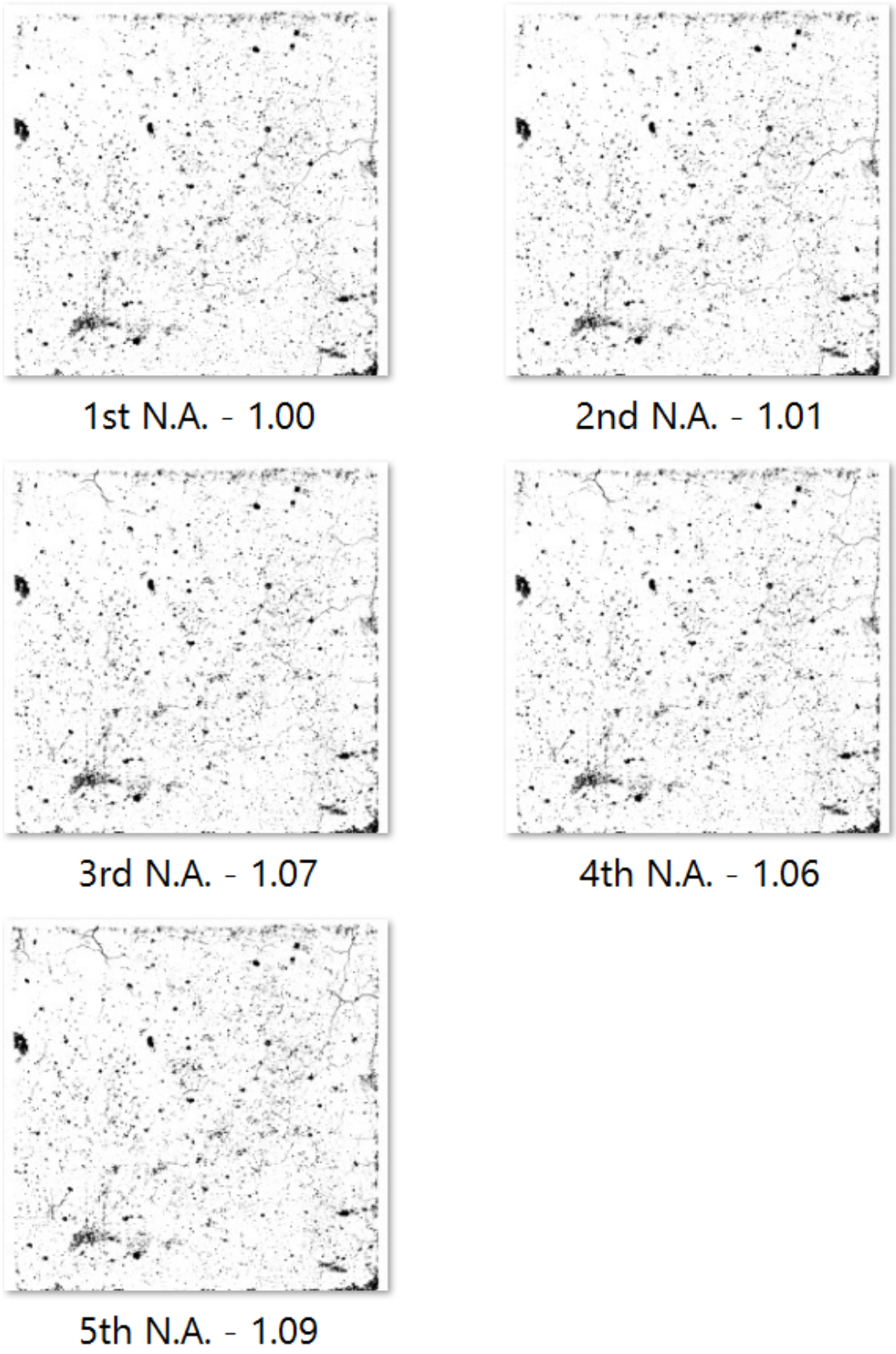

Figure G.10. BPA images of a SAP specimen and corresponding normalized area (N.A.) values.

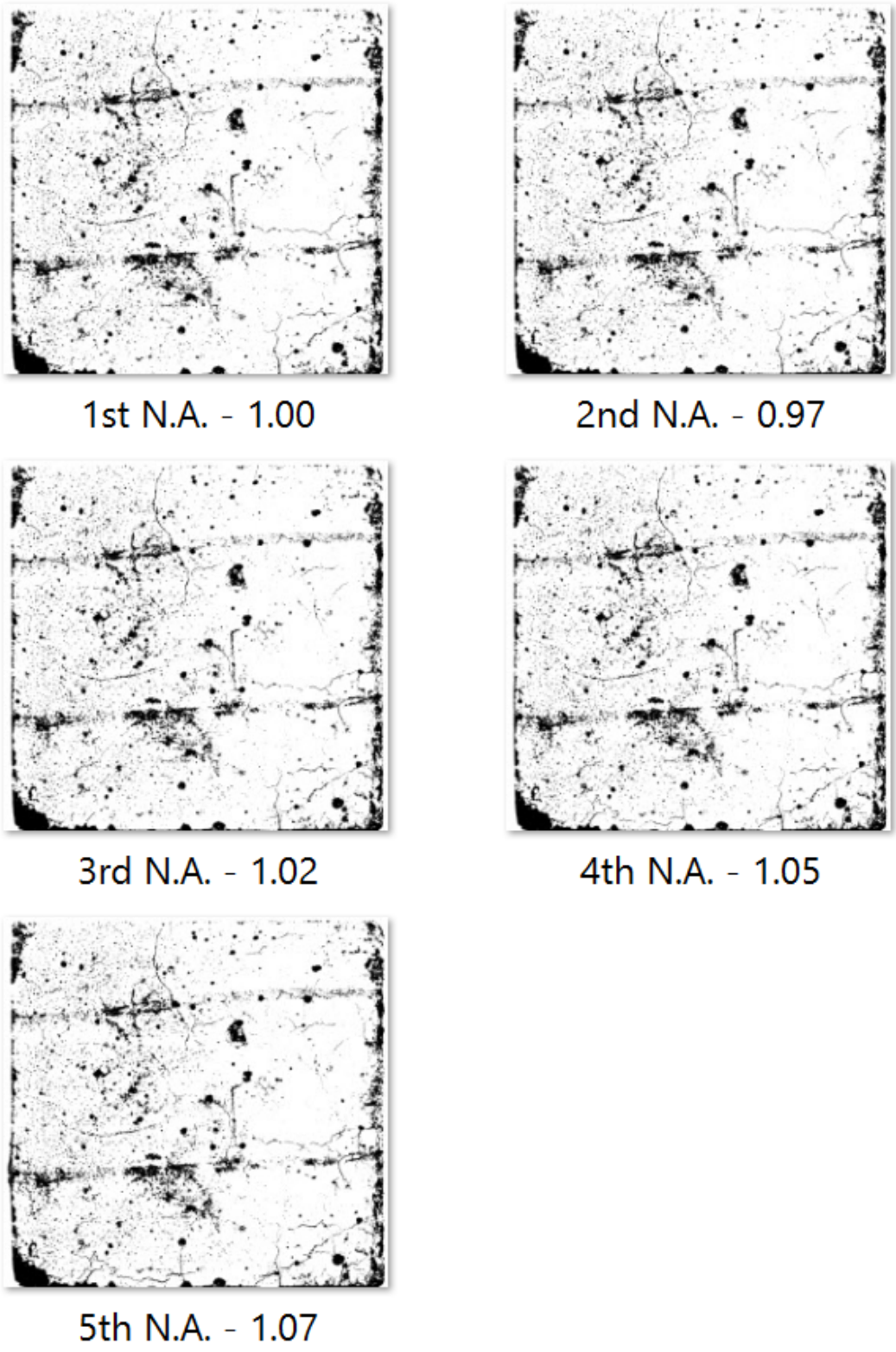

Figure G.11. BPA images of a SAH specimen and corresponding normalized area (N.A.) values.

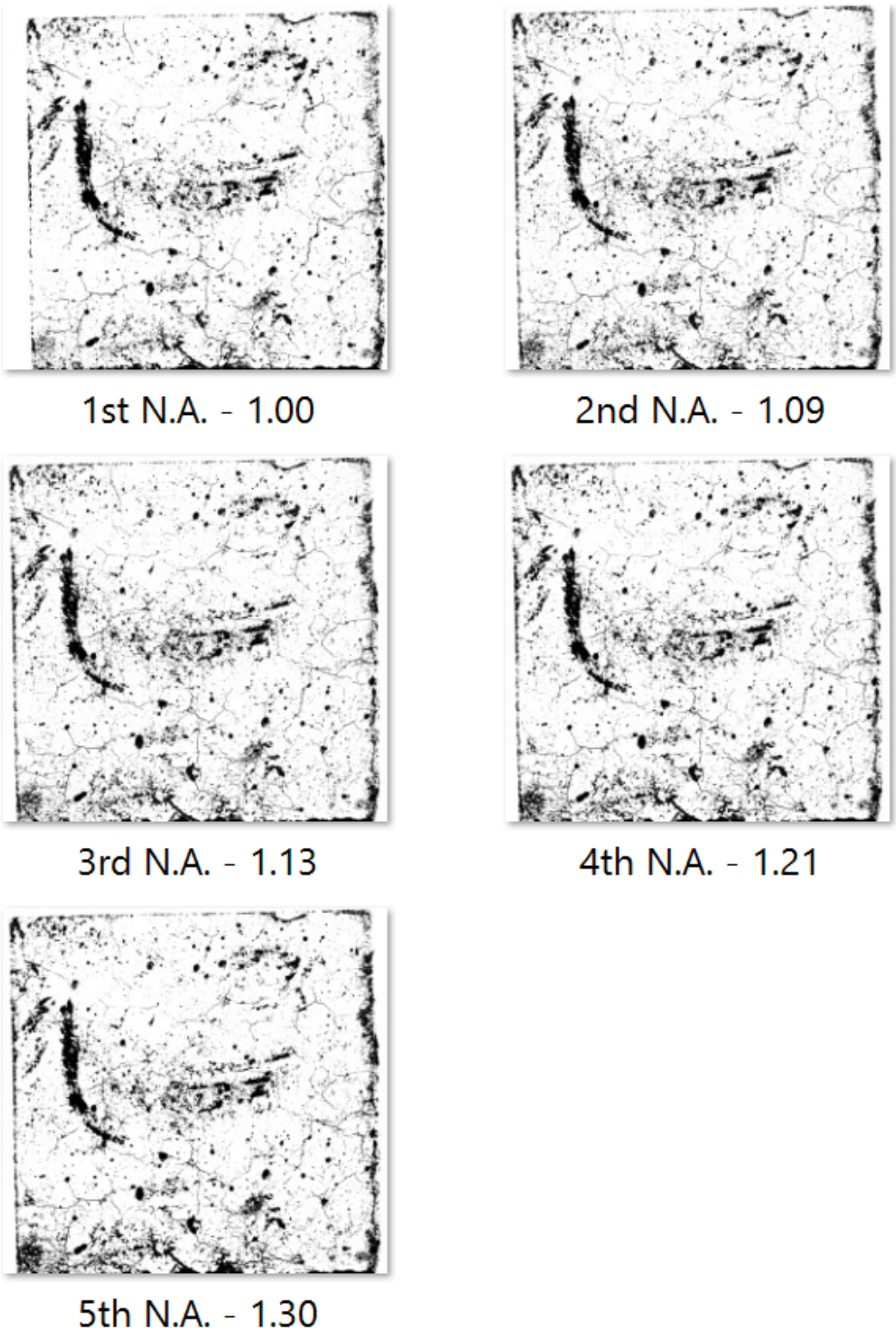

Figure G.12. BPA images of a F0P specimen and corresponding normalized area (N.A.) values.

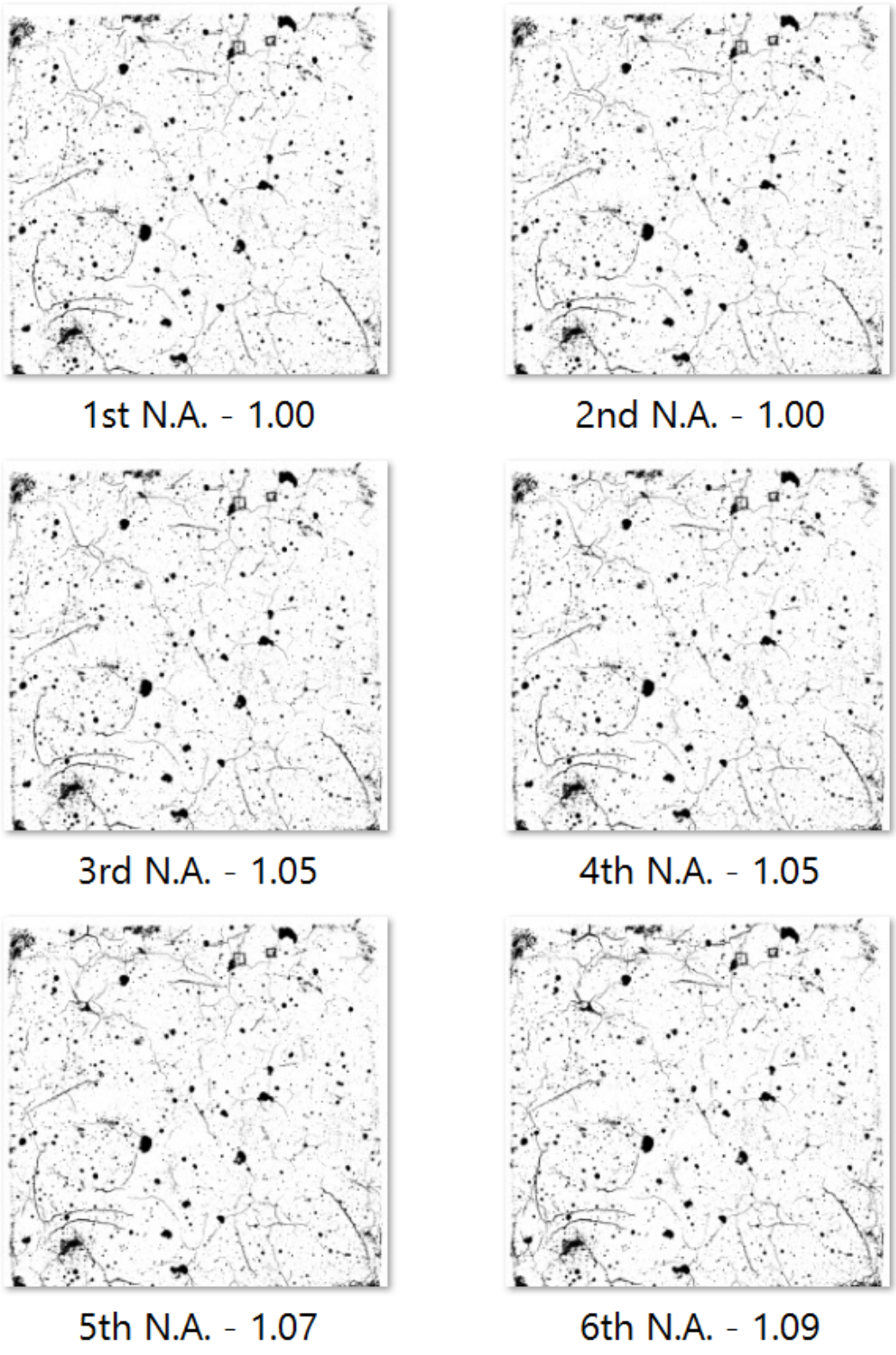

Figure G.13. BPA images of a F0H specimen and corresponding normalized area (N.A.) values.

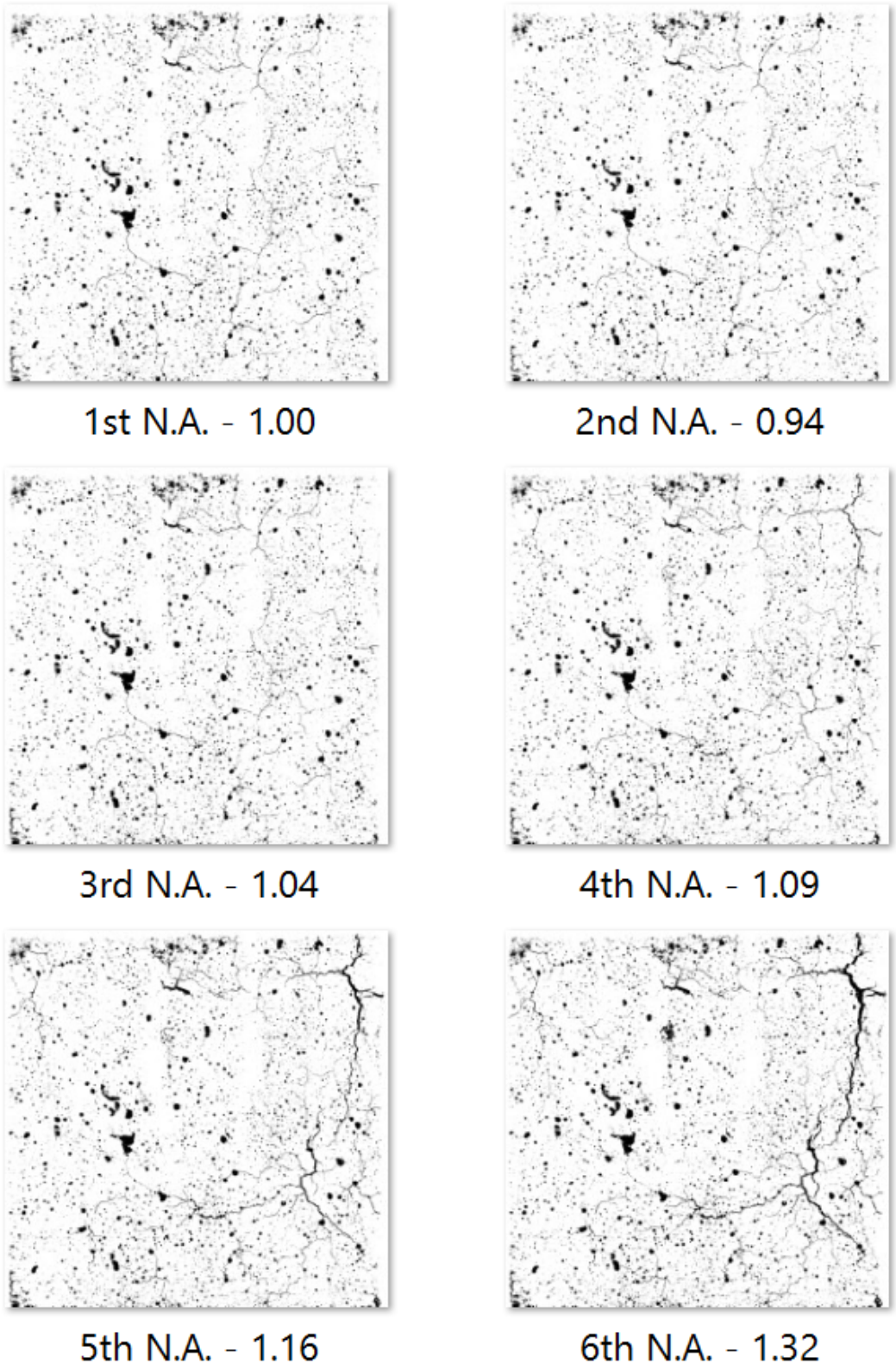

Figure G.14. BPA images of a FAP specimen and corresponding normalized area (N.A.) values.

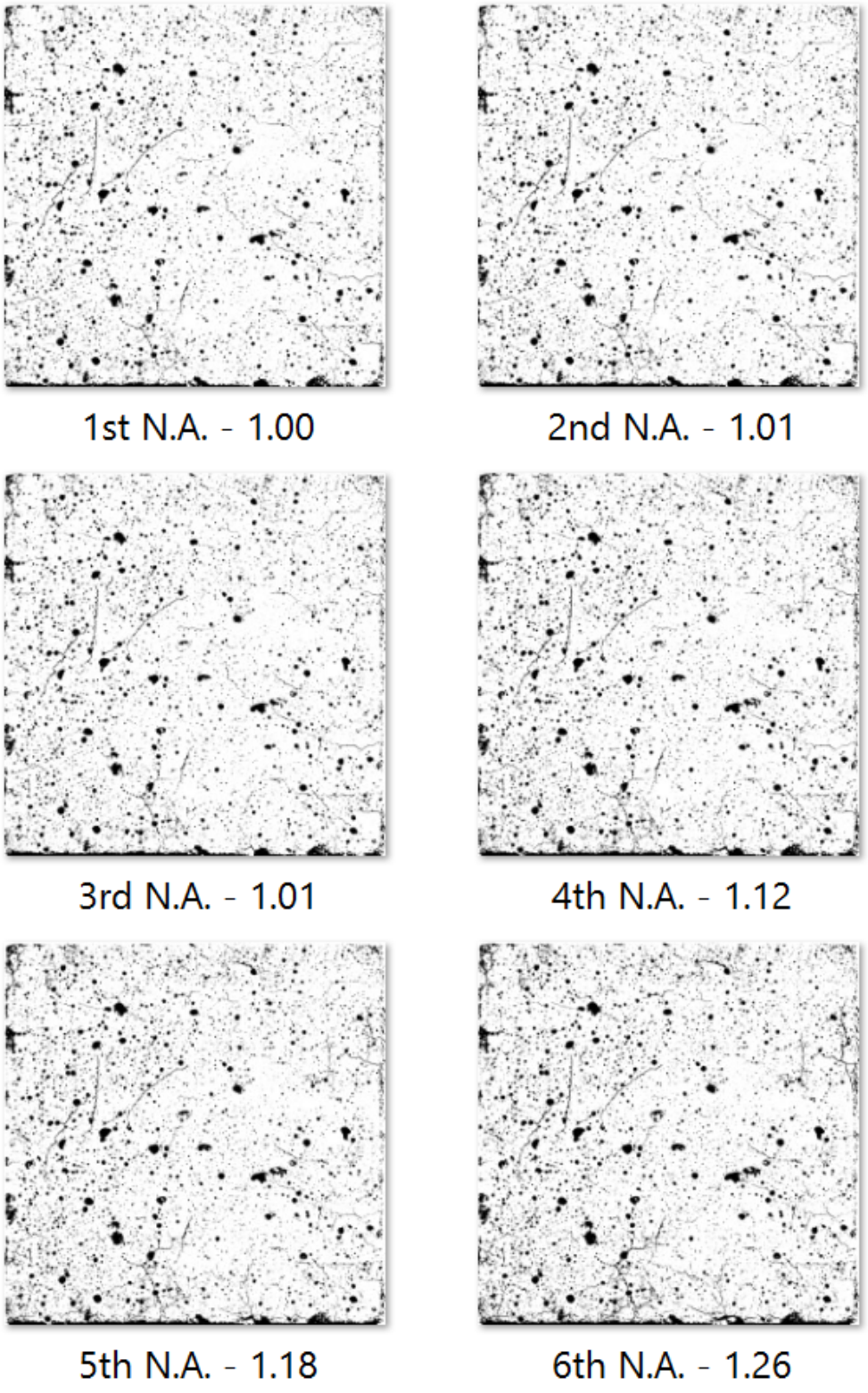

Figure G.15. BPA images of a FAH specimen and corresponding normalized area (N.A.) values.

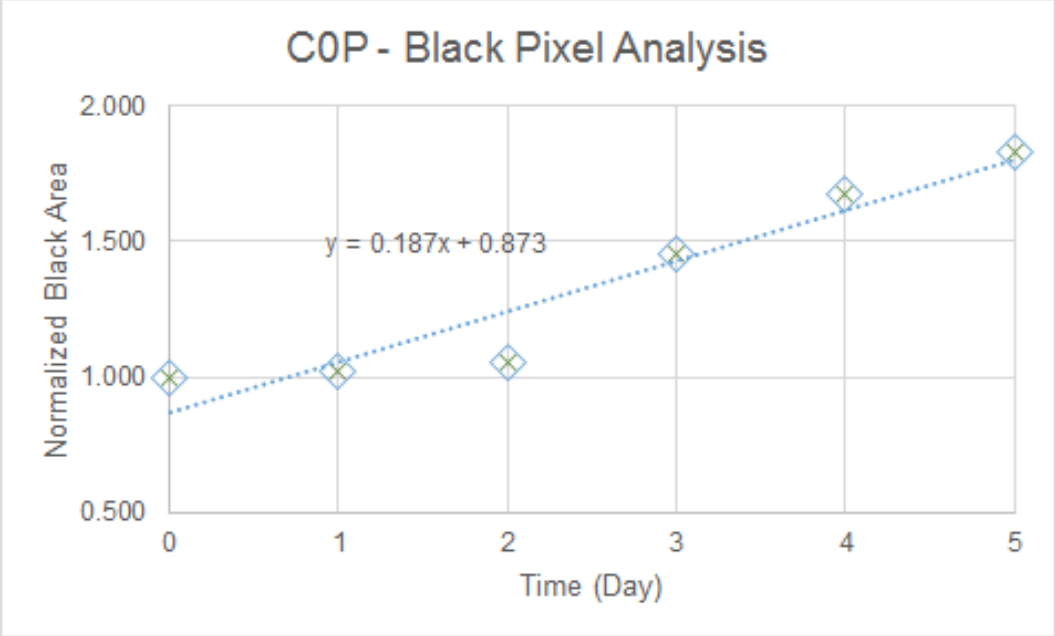

Figure G.16. Graph obtained after BPA on a C0P specimen.

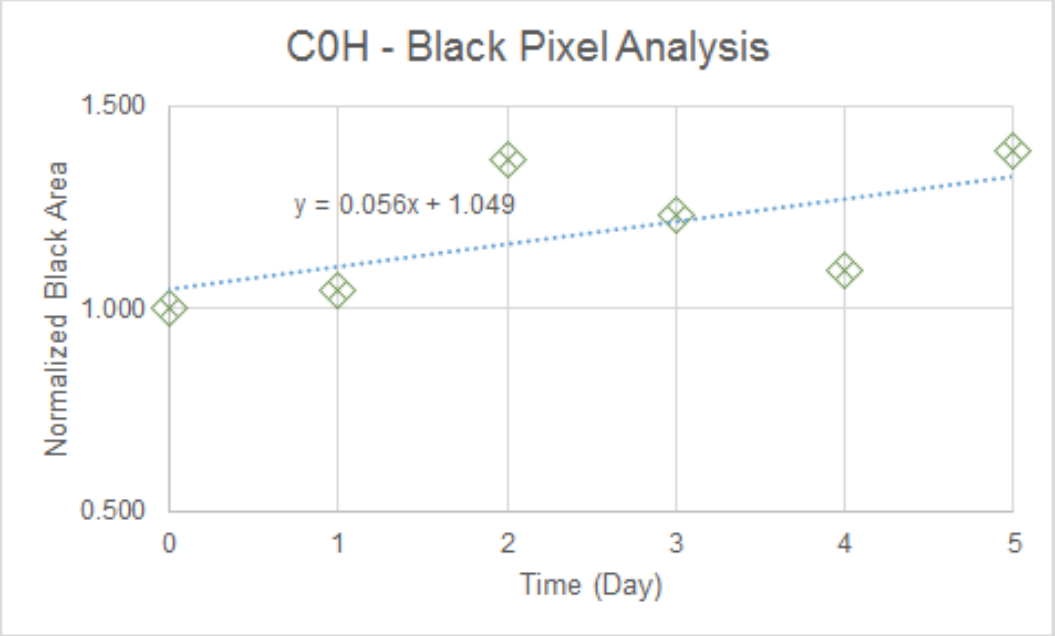

Figure G.17. Graph obtained after BPA on a C0H specimen.

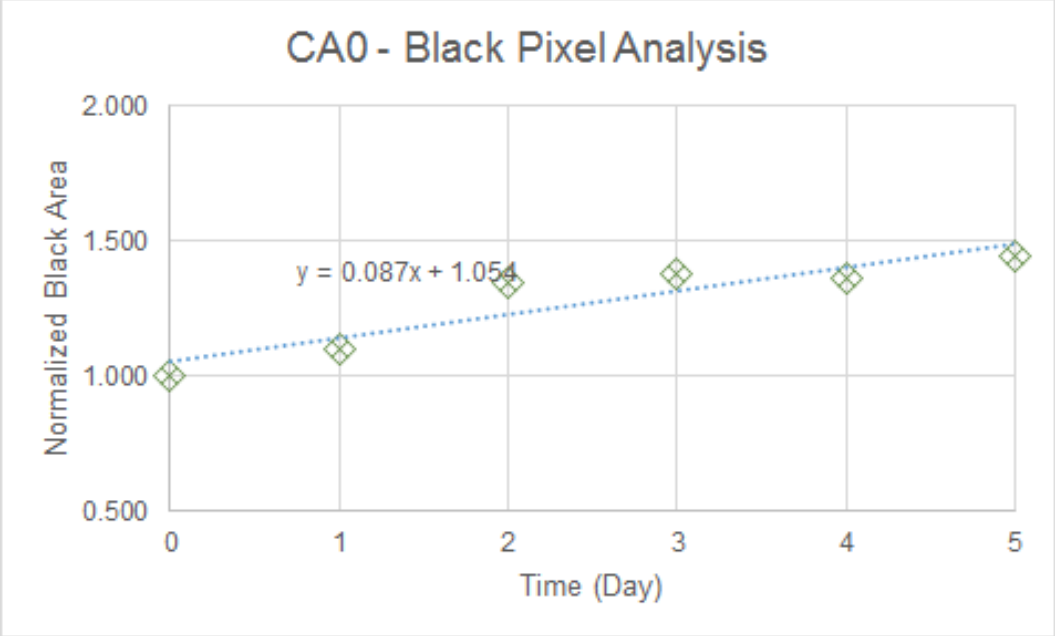

Figure G.18. Graph obtained after BPA on a CA0 specimen.

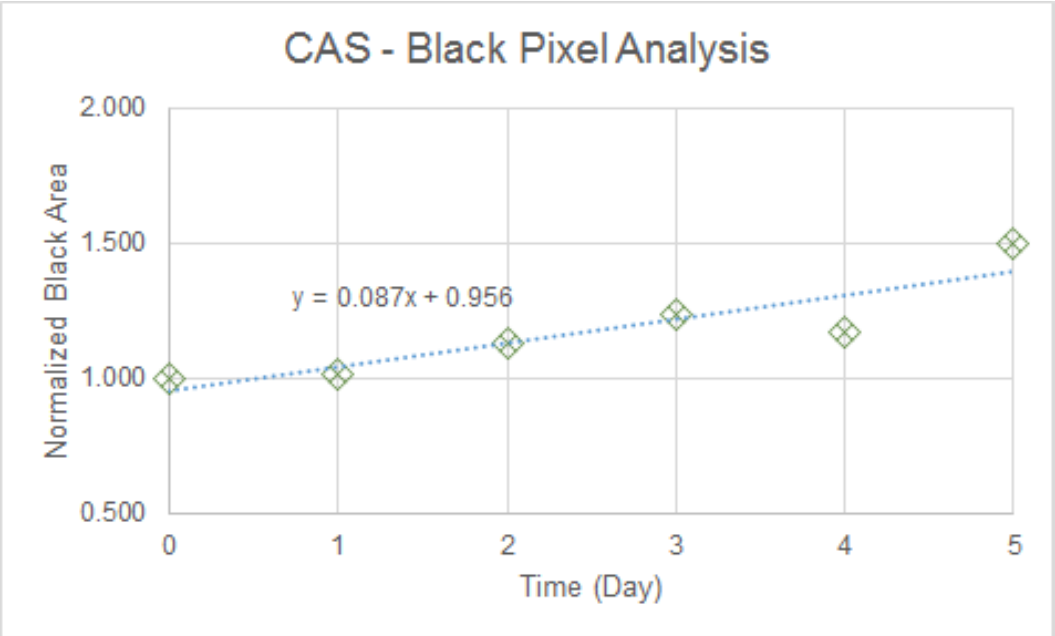

Figure G.19. Graph obtained after BPA on a CAS specimen.

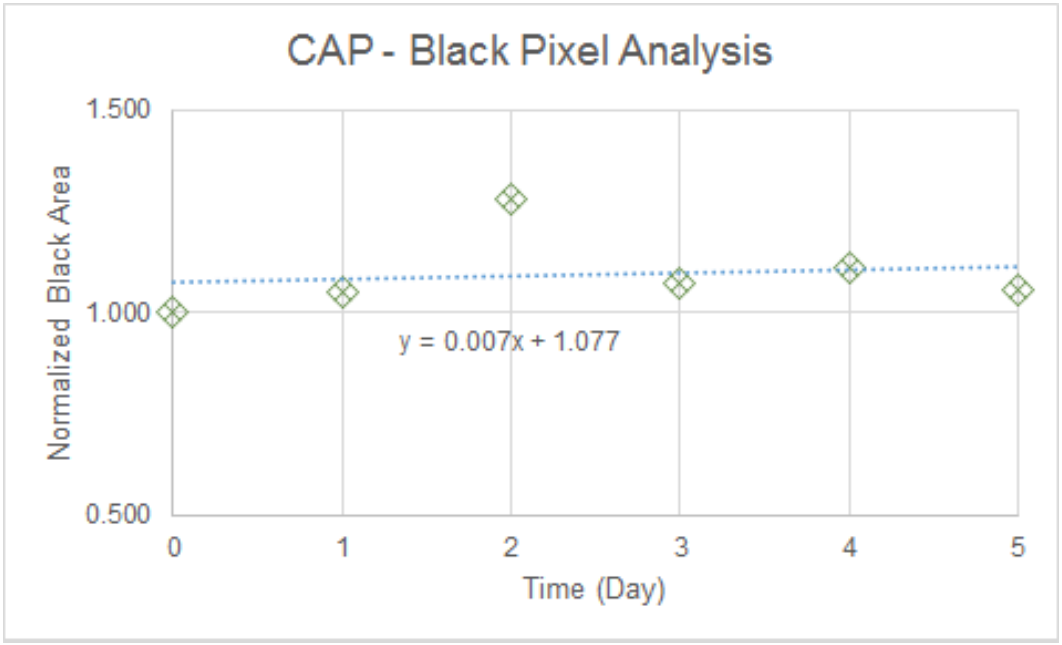

Figure G.20. Graph obtained after BPA on a CAP specimen.

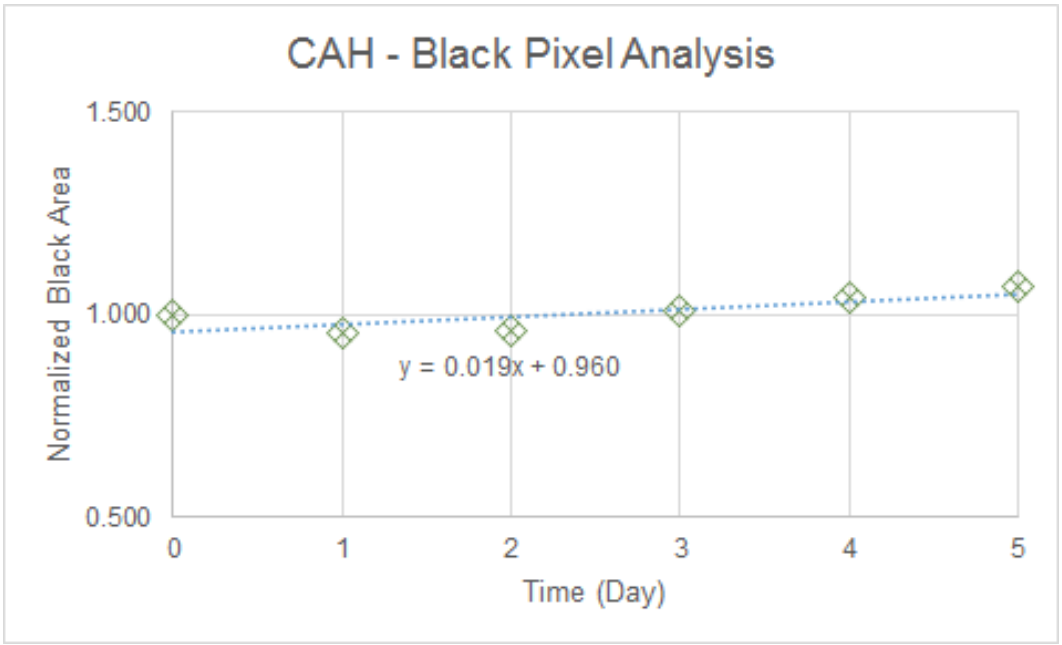

Figure G.21. Graph obtained after BPA on a CAH specimen.

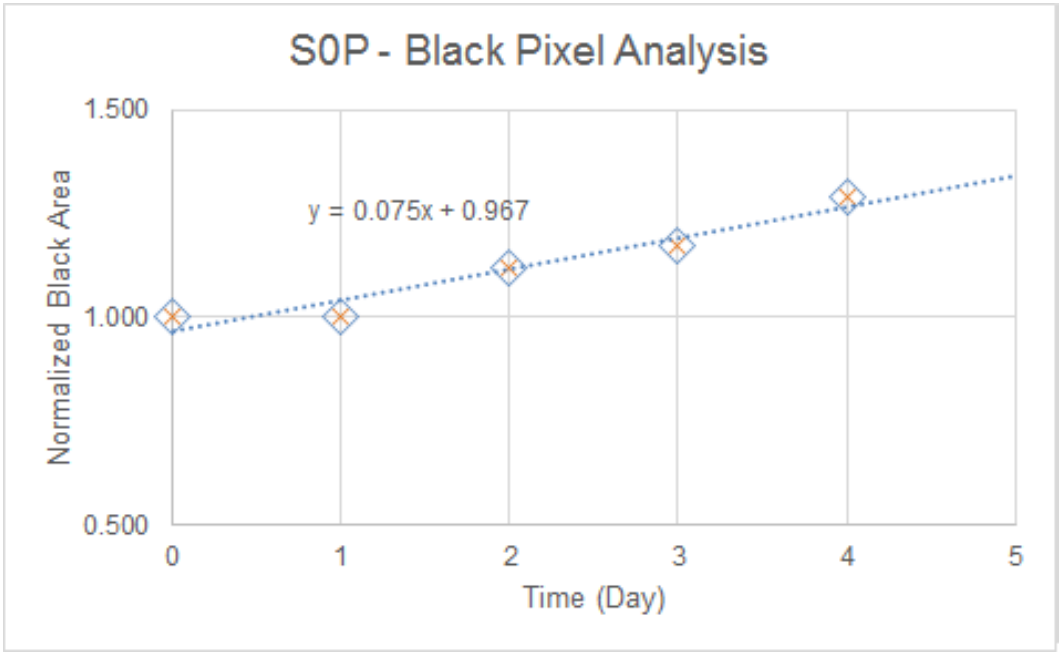

Figure G.22. Graph obtained after BPA on a S0P specimen.

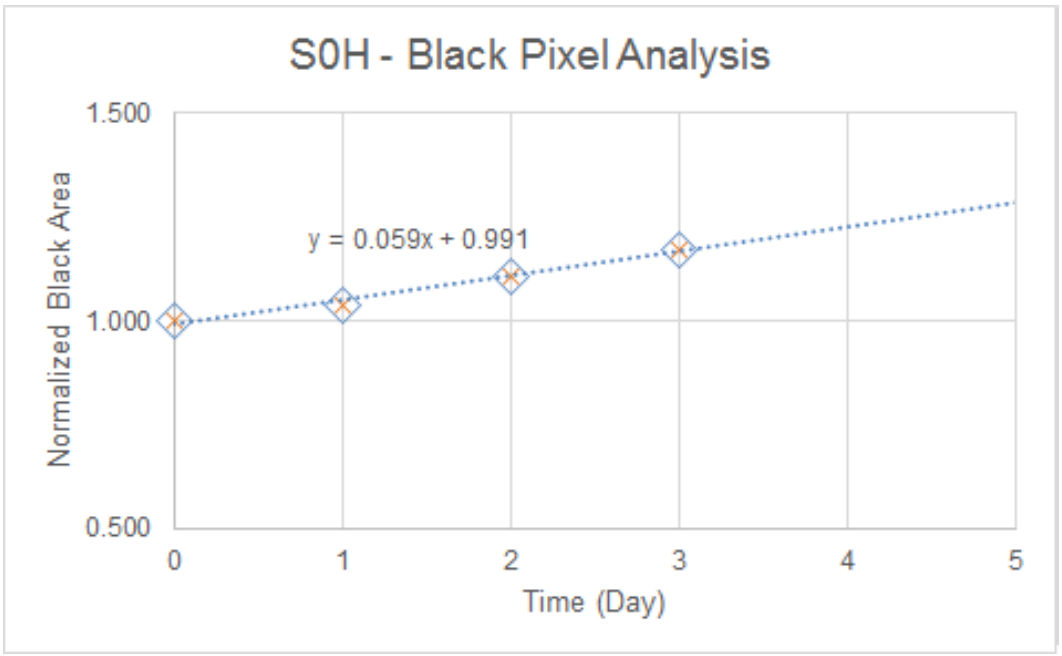

Figure G.23. Graph obtained after BPA on a S0H specimen.

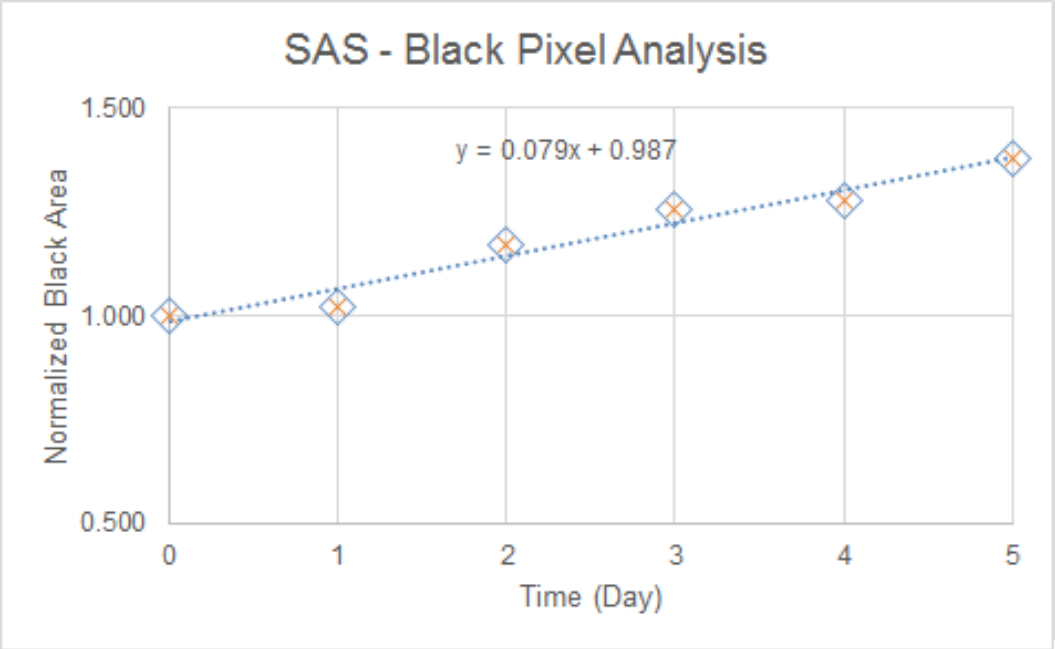

Figure G.24. Graph obtained after BPA on a SAS specimen.

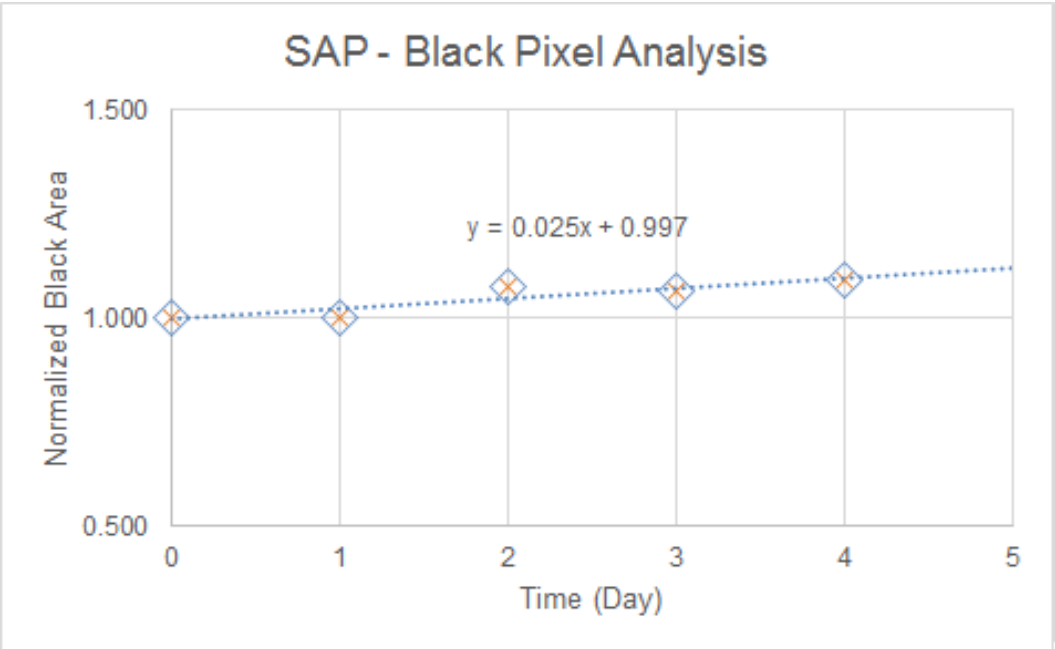

Figure G.25. Graph obtained after BPA on a SAP specimen.

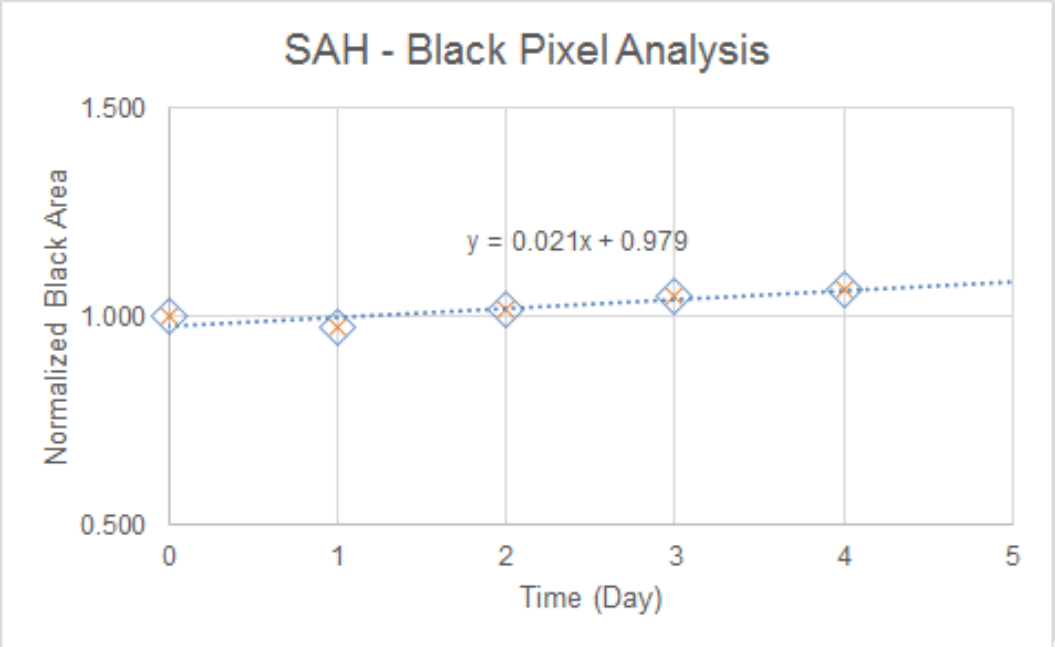

Figure G.26. Graph obtained after BPA on a SAH specimen.

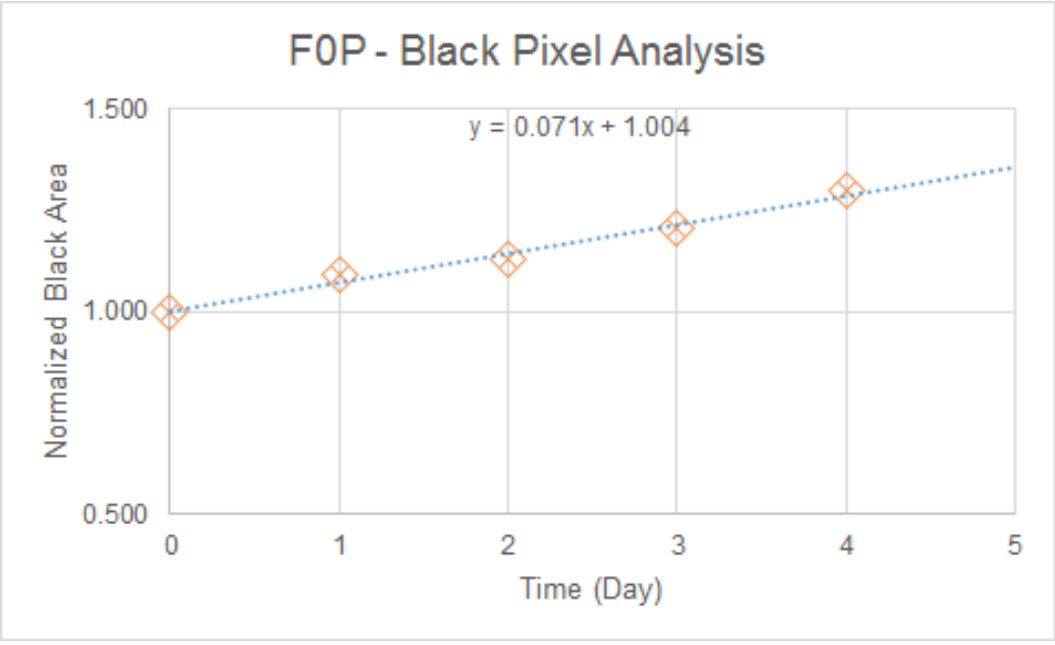

Figure G.27. Graph obtained after BPA on a F0P specimen.

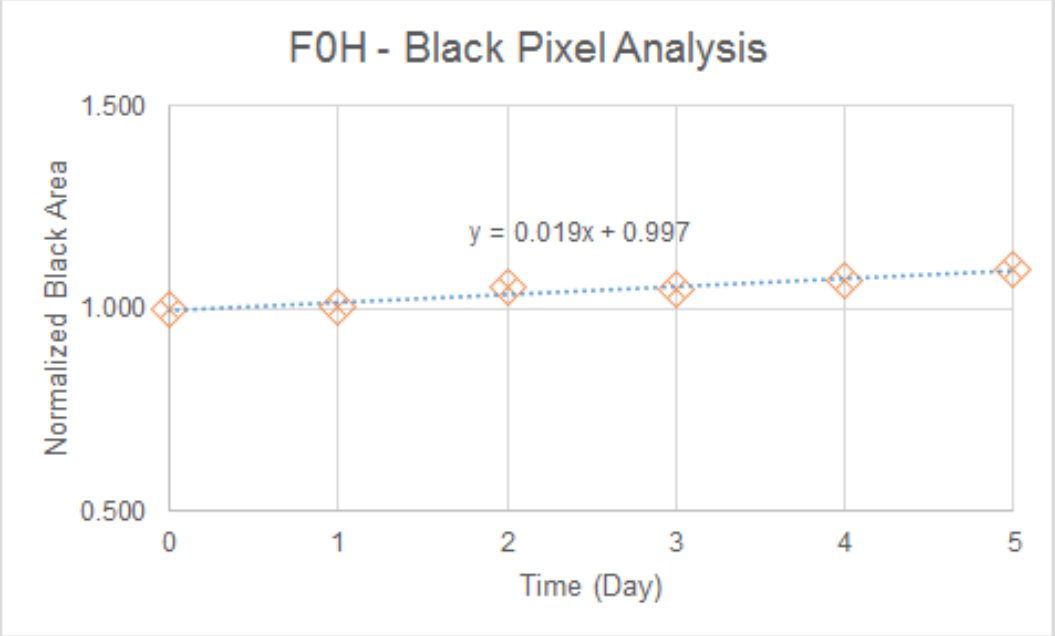

Figure G.28. Graph obtained after BPA on a F0H specimen.

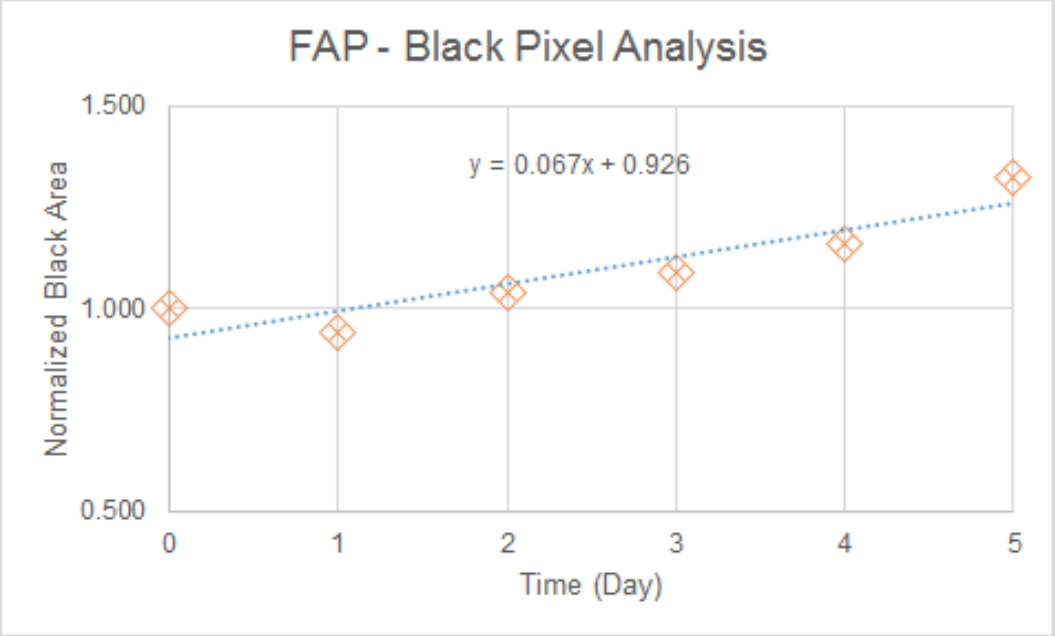

Figure G.29. Graph obtained after BPA on a FAP specimen.

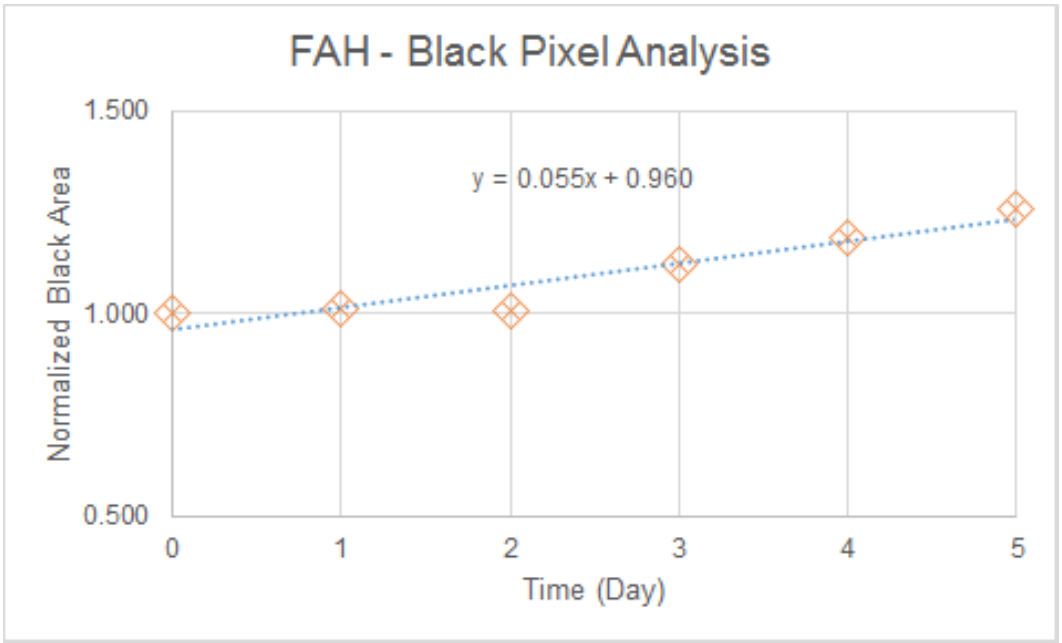

Figure G.30. Graph obtained after BPA on a FAH specimen.